July 2020

SCALING UP THE OXYGENIC PHOTOGRANULE (OPG) WASTEWATER TREATMENT PROCESS

Joseph G. Gitau
University of Massachusetts Amherst

SCALING UP THE OXYGENIC PHOTOGRANULE (OPG) WASTEWATER TREATMENT PROCESS

A Dissertation Presented

by

JOSEPH GITAU GIKONYO

Submitted to the Graduate School of the
University of Massachusetts Amherst in partial fulfilment
of the requirements for the degree of

DOCTOR OF PHILOSOPHY

May 2020

Civil Engineering

SCALING UP THE OXYGENIC PHOTOGRANULE (OPG) WASTEWATER TREATMENT PROCESS

A Dissertation Presented

by

JOSEPH GITAU GIKONYO

Approved as to style and content by:

_____
Chul Park, Co-Chair

_____
John E. Tobiason, Co-Chair

_____
Caitlyn Butler, Member

_____
David Schmidt, Member

_____
Jeeyon Jeong, Member

_____
Mary Fechner, Member

_____
John E. Tobiason, Department Head
Civil and Environmental Engineering Department

DEDICATION

To those who dare in life’s arena, and my loving wife.

ACKNOWLEDGEMENTS

This dissertation has been the product of many people without whose input it would have been difficult if not impossible to undertake. Firstly, I would like to express my sincere gratitude to my advisor Dr, Chul Park for the continuous support and guidance during my Ph.D. study and related research, for his patience, motivation, and immense knowledge. I could not have imagined having a better advisor and mentor for my Ph.D. study. My heartfelt appreciation to Dr. John Tobiason, who has been both my advisor and a dear friend. His constant prodding and ingenious insights on different research agenda, voluminous expertise in engineering practice and profound mentorship facilitated the focused adventure that this scientific journey has been. Thank you for the years of indelible footprints. Together with Dr. Park, your friendship and selfless contribution to my personal and professional development have been invaluable and will forever be appreciated

I would like to express my most profound acknowledgement to the rest of my thesis committee: Dr. Caitlyn Butler, Dr. David Schmidt, Dr. Mary Fechner, and Dr. Jeeyon Jeong for their insightful comments, time dedication, encouragement, resources, but also for the incentives to widen my research from various perspectives. Dr. Park and Dr. Butler have assembled a motley crew of OPG group adventures with whom I have immensely enjoyed this journey. They have also created an atmosphere where discussions and ideas can be curated to contribute towards scientific discourse and practical engineering applications. My sincere thanks for the opportunity to join their teams and access to the laboratory and research facilities. Without their precious support, it would not have been possible to conduct this research.

I am indebted to my fellow labmates Ahmed Abouhend, Abeera Ansari, Andrew Keyser and Arfa Ansari for the camaraderie and stimulating engagements, and for all the fun we have had in the last four years. To Sherrie Webb-Yagodzinski, Patrick Wittbold and the UMASS-WET center team, Kaitlyn Tsuyuki (Dr. Jeong lab) thank you for the technical assistance in the design and execution of the various experiments.

I would like to thank my parents, my brothers and sister, for supporting me throughout this dissertation journey and my life in general. From you, I learnt the founding lessons in life that have gotten me this far. To my dearest wife Coretta Nyambura, thank you for daring greatly every day in this journey. and for unwavering support, encouragement, challenges and distracting me when I got tunnel vision sustained the inspiration for this work

I gratefully acknowledge the funding sources that made my Ph.D. possible. BKT co. Ltd who funded and participated in bridging OPG scale-up endeavors that enabled us to frame research pursuits. The National Science Foundation who through various grants have supported the OPG research and though the PFI program aims to see to full-scale application of the OPG technology.

ABSTRACT

SCALING UP THE OXYGENIC PHOTOGRANULE (OPG) WASTEWATER TREATMENT PROCESS

MAY 2020

JOSEPH G. GIKONYO, B.SC., UNIVERSITY OF NAIROBI

M.S., UNIVERSITY OF MASSACHUSETTS AMHERST

Ph.D., UNIVERSITY OF MASSACHUSETTS AMHERST

Directed by: Professor. Chul Park, Professor. John Tobiason

Photogranular biomass has yet to be utilized at large scale for wastewater treatment despite their potential to lower energy demand due to self-aerating capacity in addition to better process control compared to conventional technologies. An evaluation of critical driving factors affecting scaling up has yet to be undertaken. The current generation of oxygenic photogranules under hydrostatic conditions (a deviation from orthodox conditions creating other granules) limit seeding of larger reactors in time and scale. In addition, evaluating the photosynthetic productivity of granules which exist as closely commingled consortia with tightly coupled production and consumption processes, has yet to be undertaken.

We experimentally evaluate the alternative generation of oxygenic photogranules under hydrodynamic conditions. The photochemical capacity of oxygenic photogranules under variable light conditions was also determined. Concomitantly, we evaluate the effects of light intensity on the performance of reactors of varying scales and the light demand therewith. Finally, granular physical attributes that impact hydrodynamic behaviour and interaction with the bulk fluid due to agitation were assessed.

Oxygenic photogranules were formed only under some combinations of different pressures in 8 days, suggesting a ‘goldilocks zone’ of selection pressure interaction fostering granulation. Rapid generation of multiple granules would ease seeding of reactors higher volume reactors.

OPGs phototrophic capacity was also found to increase with light intensity to a curvilinear maximum beyond which photoinhibition ensues. This implies the existence of light-limited operating conditions below maximal sunlight intensities. Photoelasticity was also observed for granules treated under different light stress with apparent adaptability to abiotic stresses. Moreover, the light dependency is influenced by reactor design and operation, allowing for recovery of the photosynthetic mechanism, and selecting for different microbial dominance. This, in turn, affects different treatment metrics in rectors at a different scale. No linear relationship was observed between reactor performance and increasing light intensity while density, porosity and permeability were found to be in the range of other granular biomass.

No spontaneous granulation has been recorded in conventional wastewater basins. We surmise that this could be due to a mismatch of conditions suppressing potential granulation. Altering the magnitudes of these o could potentially result in the formation of granular aggregates.

TABLE OF CONTENTS

Page

LIST OF TABLES

Table Page

LIST OF FIGURES

Figure Page

CHAPTER 1

PHOTOGRANULES FOR WASTEWATER TREATMENT

1.1 Introduction

Treatment of water and wastewater is critical to safeguarding both public health and the environment. The world health organization estimates that about 2 billion people lack access to basic sanitation.[1] In the history of civilization, wastewater has always been considered filthy [2] and requiring removal from human habitats buttressing a linear ecosystem modelled on a make-use-dispose paradigm.[3] Engineering design of wastewater systems has therefore long been predicated on this 'waste-centered' approach to eliminate the social stigma associated with wastewater.[2] The designs have continually evolved to tackle a range of challenges, including stringent discharge standards, limited space, population growth and distribution, the variability of flows, and limited financing [4] among others.[5–8] The disposal of toxic wastes and emerging contaminants notably induce perturbations in biological wastewater treatment, increasing process risks.[7,9] Moreover, existing wastewater infrastructure has a large environmental footprint to support the separation of solids from the bulk fluid.[5,10,11] The sludge generated and monitoring requirements also incur high disposal [12,13] and labour cost, respectively. High energy use in wastewater treatment, for example, aeration in activated sludge plants accounting for 50-60% of plant energy usage, increases the operational cost.[9,14]

The quantum leap in future wastewater treatment technology will encompass a perspective shift from 'waste centered' to 'resource centered' approaches,[15,16] applying novel biological, physical, and chemical interventions in increasingly fragile

ecosystems.[1,17] Controlling the discharge of untreated wastewater estimated at 80% of the global wastewater volume [18] proffers numerous opportunities in circular economies, including resource recovery and resource savings. For example, the use of granular biomass in wastewater treatment has increased in the recent past, driven by a need for better solid-liquid separation operations, increased functionality, better process control and potential energy savings.[9,14] Granules are self-immobilized biofilms with spheroidal morphologies, dense cores and high settling velocities,[11] which develop with an environmental selection of niche microbes characterized by symbiotic and other relations between keystone communities.[19–21]

Presently, the activated sludge process is widely employed as a wastewater treatment intervention.[22] Physically, activated sludge (AS) manifests in flocs with dimensions of about 50-100 µm [23] with a dominant aerobic bacteria population.[24,25] This grandfather activated sludge process (ASP) is also characterized by poor settleability, high capital and operational cost.[26] Granular sludges, by comparison, tend to have compact spheroidal particles of up to 4.5 mm in diameter.[27,28] In addition to better settleability, higher granular biomass inventory within the reactor negates recycling requirements to decouple hydraulic and solid retention times as in AS basins [29–31] improving operational control and reducing sludge generation.[32] The functional plasticity of granules allowing more biological functions by different microbes in their consortia, is due to diverse redox environments within their structure.[33,34] This versatility allows for compact infrastructure, reducing the need for, and size of, multiple treatment and settling basins as used in AS.[11,27] Granular sludge can reduce wastewater treatment footprints by up to 75% of

existing conventional AS plants.[32,35]

Despite gaining global interest [11,36] and their process versatility,[27] novel granular systems face challenges in commercialization.[37] Granular systems can help reshape the wastewater treatment paradigm [38] if successfully sustained at large scale. Primarily, the granulation mechanism is still not well understood, creating inherent process risks.[32,39] Precise engineering of the granule formation process is thus still not possible [33,34,36] for process optimization. Moreover, granules disintegrate and have unpredictable morphologies [34] impacting process effectiveness. The development of granules does not result in a 100% transformation of the inoculum [35,40] while the initial reactor start-up is slow.[32,37] Additionally, challenges of sustaining the granular system integrity beyond the lab scale [28,41] limit adoption at large scale.

1.2 Oxygenic photogranules (OPGs')

Oxygenic phototrophic granular sludge consists of phototrophic and heterotrophic communities whose symbiotic co-existence allows for aeration-free wastewater treatment (WWT).[28,42–44] The inherent characteristics of these 'natural factories', including oxygen generating capacity, better settleability, higher biomass yield,[28] robustness and resilience, [42] presents a pathway for sustainable WWT, reducing cost and energy, increasing operational effectiveness, and recovery of bioenergy. These spheroidal aggregates develop in the absence of aeration [28,42–45] unlike other bio-granules, such as algal bacterial aggregates and aerobic sludge granules (ASG).[46–48] While ASG can reduce the energy consumption in ASP by up to 60%, [26,32] aeration free OPGs can increase the energy

savings. Increase in OPG sizes results in within-granule stratification, with phototrophs dominantly occupying the outer layer and heterotrophic and nitrifying bacteria their core.[42–44,49] No layering of microbes is observed in smaller granules. At the same time, a maximum oxygen production was reported for granules of 0.5-1 mm.[49] Oxygen generated from photosynthesis by cyanobacteria and green algae is utilized for the oxidation of organic matter and nitrification.[45,50]

In OPGs, filamentous cyanobacteria are a keystone community binding a predominantly organic core [42] via generation of extracellular polymeric substances (EPS) and locomotive entanglement.[42,43] Cyanobacteria of genera *Oscillatoria*, *Microcoleus* [42,45] *Cyanobium* and *Geitlernema* [45] have been reported to dominate their structure. Milferstedt et al. reported that cyanobacterial populations made up 85 (±18)% of OPGs 23rRNA sequence inventory. [42] A higher abundance (8%) of unicellular cyanobacteria *Cyanobium* has also been reported in unsuccessful OPG formation.[45] In addition, characterization of OPG ecology has identified the presence of microalgae, *Scenedesmus*, and bacteria, *Lysobacter* and *Sediminibacterium*.[42,45] Similar to activated sludge biome, aerobic bacteria that oxidize organics and ammonia [28,44,45] additionally colonize the OPGs ecosystem. Moreover, while process alterations to induce denitrification are necessary for ASP, these microbes can inhabit anoxic regions of large OPGs >3mm.[45,49] This diverse ecosystem confers functional versatility to OPGs for application in wastewater treatment through the exchange of substrates requiring different biological transformations.[33,37,51]

1.3 Scaling up photogranular wastewater treatment

The full realization of OPG-based wastewater treatment's benefits can be achieved by proofing of technology and adoption at large scale.[52–54] Mature anaerobic and aerobic granular technologies have been adopted in large-scale wastewater treatment applications.[36,40] Successful photogranular reactors, on the other hand, have been reported in small scale lab applications.[28,46,50,55] These reactors were operated as sequencing batch reactors (SBR) and continuous flow reactors [47] and had above 70% removal of both chemical oxygen demand (COD) and nutrients. While bench-scale OPG reactors have exhibited successful performance,[28,44] pilot-scale reactors have had limited success.[41] The failure in pilot-scale OPG reactors was characterized by decreased oxygen generation, loss of granular structure and community changeover to suspended algal culture. Loss of their cyanobacterial structural backbone could be responsible for the observed granule disintegration, consequent deterioration of biomass settleability and decreased treatment effectiveness.[41]

The granulation process has been attributed to numerous mechanisms.[27,33,34] Various selection pressures resulting from substrates availability, hydraulic loading, shear stress, symbiotic prevalence, aeration, and photon energy have all been enumerated, claimed and disavowed as the causes of granulation in various studies.[33,56–58] It can be argued that the process of granulation, ubiquitous and occurring under different environments,[11,59] is fundamentally a nature and nurture response to applied stresses in relation to each other and with varying degrees of interaction with the biome. The stresses, including shear,[60–62] chemical elements,[46,51,62–65] and selective settling [61,66,67] in turn, induce socialism of the

biota which aggregate on and with existing particulate matter.[33,34,68] The physical-chemical processes of particle aggregation (organic and inorganic) have been well documented and relate to changes in particle-particle interactions and changes in surface chemistry.[68–71] Motility of microbes and their entanglement, as is the case with filamentous cyanobacteria in OPGs,[34,43,72] enhances this bio-aggregation process. Understanding the relative contributions of these abiotic stresses in relation to each other is essential to facilitate the engineering of large-scale sustainable OPG systems.

Scaling up of OPG systems raises various queries, including the four addressed in the following chapters of this dissertation. Firstly, *how can we achieve the rapid generation of sufficient OPG biomass to seed large reactors*? Optimal seeding density has been reported as essential for effective OPG reactor operation [73] with a 40-60 hydrostatic OPGs/L of reactor volume. Various inoculum sources, incubation conditions and periods have been reported in generating phototrophic granules. For algal-bacterial aggregates reported in various studies,[46–48,55,66,74–78] light intensity in the range of 40-300 µmol m^{-2} s^{-1}, aeration and mixing were provided to incubated samples of pure and mixed culture consortia (Table 1- 1). Multiple granular aggregates consisting of algal-bacterial symbiotic communities were obtained in all cases in 7 to 30 days.

On the other hand, other studies[28,42,43,45,50,79] have reported use of activated sludge inoculum to generate OPGs hydrostatically in closed vials with 150 µmol m^{-2} s^{-1} of light and no mixing. Each hydrostatic incubation generated a single granule per vial in 7 to 30 days.[43,44] A large-scale hydrostatic cultivation set-up would be necessary to seed high

volume OPG basins with a reported optimal seeding density of 40 granules per 1 L volume.[28] The scale in area and time required for the generation of hydrostatic granular biomass would, therefore, hinder both initial and subsequent start-ups. Authors have also reported propagation of OPGs in reactor operation seeded with hydrostatic granules. [28,73] OPGs, therefore, persist in disparate shear environments including with shear-induced selection pressure similar to other granules.[60–62] Substrates feast and famine pressure, on the other hand, stem from sequencing batch operation of OPG reactors [28] and batch inocula in hydrostatic cultivation. Moreover, feast and famine conditions of light substrate arise with operational photoperiodicity and transition of granules within the reactor due to mixing.[80] The granulation process and selection pressures promoting granule formation and function are ubiquitous; therefore, we *hypothesize* that the formation of seed OPGs from activated sludge inoculum should also occur directly under hydrodynamic conditions.

Table 1- 1: Literature reported light and mixing conditions for the successful cultivation of photogranules. Light intensity values converted using 1KLux=20PAR approximation.

Study	Light Intensity used	Agitation
Hende et al., 2014	100-174 µmol m^{-2} s^{-1}	200 rpm
Godos et al., 2014	10000lux (135 µmol m^{-2} s^{-1})	300 rpm
Lee et al., 2014	120±10 µmol m^{-2} s^{-1}	0.2 L/min, 250rpm
Tiron et al., 2015	235 µmol m^{-2} s^{-1}	150rpm mixing
Wang et al., 2015	74-15±5 µmol m^{-2} s^{-1}	200rpm
Huang et al.,2015	1932 µmol m^{-2} s^{-1}	2cm/s
Tang et al., 2016	6000 lux (120 µmol m^{-2} s^{-1})	0-1 L/s
Arcila et al., 2016	200 µmol m^{-2} s^{-1}	10 rpm (0.2m/s)
Ahmad et al., 2017	900-1100lux (20 µmol m^{-2} s^{-1})	0.5cm/s
Stauch-White et al., 2017	10000 lux (180 µmol m^{-2} s^{-1})	-
Liu et al., 2017	6000±200lux (120 µmol m^{-2} s^{-1})	0.58/1.17/1.76 cm/s
Zhang et al., 2017	121±7.3 µmol m^{-2} s^{-1}	4L/s
Milferstedt et al., 2017	10000 lux (180 µmol m^{-2} s^{-1})	-
Zhao et al., 2018	7200 lux (144 µmol m^{-2} s^{-1})	0.55 cm/s
He et al., 2018	Sunlight (window facing south)	5cm/s,200 rpm
Kuo-Dahab et al., 2018	160-200 µmol m^{-2} s^{-1})	-

In large-scale systems, the use of aeration to initiate granulation would render the OPG bioreactors operationally similar to existing AS basins which are also exposed to natural light and have aeration.[30] However, no record of spontaneous generation of algal-bacterial granular biomass beyond activated sludge flocs has been reported. The communities within the activated sludge process are predominantly bacteria and few phototrophs.[42,81] This can be attributed to the scale of selection pressures at play, limiting both significant increases in phototrophs and granular aggregation. Moreover, adding energy-intensive aeration, which constitutes the highest energy use for AS treatment plants,[28,82] to the algal-bacterial process would negatively impact its sustainability.

We likewise *hypothesized* that phototrophic granulation occurs within a 'goldilocks zone' due to the interaction of chemical energies (organic and nutrient loading), shear pressure,

and critical light energy in varying magnitudes (Figure 1- 1). These alternative methods for generation of OPGs that differ from published protocols [2,4,26,31,49] are examined in Chapter 2. The hydrodynamic cultivation can potentially enable the generation of multiple OPGs to seed large reactors. Optimizing the interaction of selection pressures can additionally facilitate the direct conversion of inocula into OPGs in large reactors negating seeding requirements.

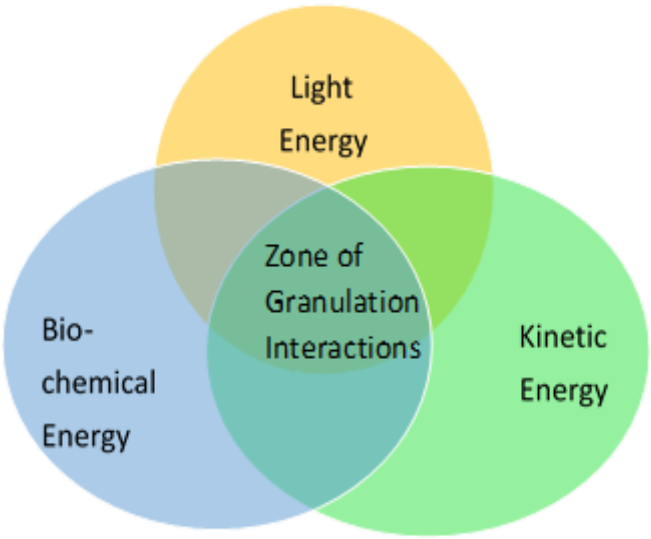

Figure 1- 1: Energy interaction for OPG granulation. The zone of interaction presents potential conditions where the interaction of different abiotic stresses promote granular biotic responses**.**

Secondly, *how much light is suitable for optimal OPG photosynthesis*? The photogranular wastewater treatment process is reliant on the biological generation of oxygen.[51,83,84] The culpable photosynthetic process is correlated to the quality and quantity of light,[85–87] which significantly impacts photochemical production. The generation of oxygen is also limited by the OPGs' photosynthetic clades composition and their adaptation to light.[88,89] Light spectrum distribution (quality) depends on the light source [90,91] and phototrophs

have evolved different mechanisms to utilize light available in their niche optimally.[92–96] It was reported that the light spectrum fit to active photosynthetic radiation was critical to photo productivity.[97,98] Some light sources and especially sunlight emits radiation such as UV that can have deleterious impacts on cyanobacteria photoactivity.[99–104] Nevertheless, phototrophs have evolved various protection mechanisms to survive these adverse and variable light conditions.[88,105,106] For example, *Synechococcus spp.* are reported to have adequate spectra acclimation with highly correlated photophysiological responses including pigment concentrations, cyclic electron flows and growth rates.[98]

The sensitivity of microbial phototrophic productivity to light intensity (quantity) varies curvilinearly [87,88] with regions of light and electron transport limitation. Low light can limit the photosynthetic generation of oxygen, while high light can induce photodamage [85,87,88]. In scaling up the OPG wastewater treatment process, light can be supplied via artificial or natural sources. While artificial light sources are more amenable to controls, natural light varies seasonally and diurnally with an average maximum of 2000 μmol m^{-2} s^{-1} at full sun.[107–109] This high intensity has been reported to cause photoinhibition in most phototrophs. [87,110] From the variability of photosynthetic activity with light intensity, we *postulate* the existence of optimal light conditions for OPG phototrophic activity balancing photon capture and electron transport rates.[80,88,111,112] This phenomenon is examined in Chapter 3. Determination of optimum conditions would facilitate precise engineering of OPG infrastructure utilizing either natural or artificial light sources.

Moreover, the functional versatility of OPGs due to a commingled microbial community results in concurrent consumption and generation of substrates (Figure 1- 2). Oxygen generated via photosynthesis is utilized by heterotrophic and nitrifying bacteria for the oxidation of organic matter and ammonia, respectively, from the bulk wastewater [28,42,43,49] or utilized for phototrophic respiration.[113] Carbon dioxide dissolved in wastewater or generated from organic oxidation is, in turn, utilized by the phototrophs. These substrates can also be transferred between the close microbial associations within the OPGs or into and out of the bulk fluid (Figure 1- 2). The classical monitoring of a single photosynthetic marker (O_2 or C) [113–115] within the bulk fluid. This approach can result in the erroneous estimation of curvilinear photoproduction with increasing light intensity. This can further compromise the design parameters of the OPG system, even with optimal light conditions. The photochemical capacity of OPGs was, therefore estimated using a modified approach.

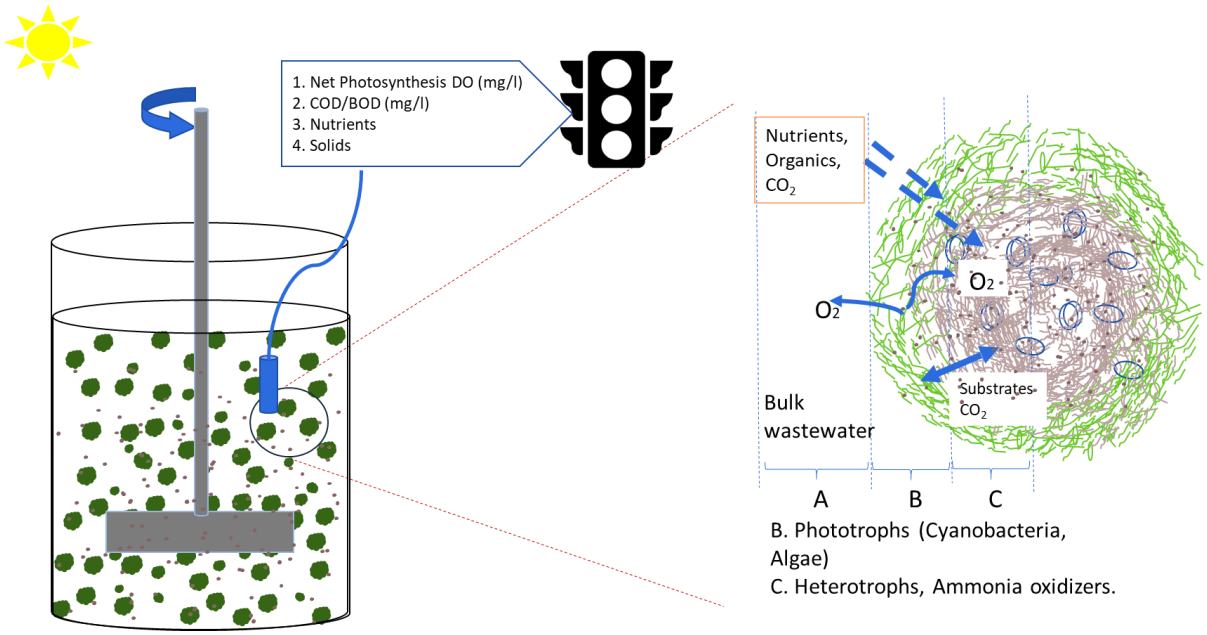

Figure 1- 2: Schematic showing an OPG reactor with monitoring of wastewater treatment parameters. The side panel shows the transfer of various substrates into and out of single granule.

Thirdly, *how is light utilized in reactors of different scales*? As opposed to other bio-granules which develop in aerated upflow reactors,[116,117] photo-granules require light for functional and structural integrity. Maintaining the microscale balance for light-based systems with macro flows in full-scale operation requires accelerating the co-processes of photosynthesis and respiration. [74] The light reliant primary process, photosynthesis, hinges on the effectiveness and efficiency of light utility.[80] This, in turn, is dependent on the reactor hydrodynamic ecosystem, the concentration of phototrophs in granules,[80] and the quality and quantity of light.[95,111] This light-dependent aeration capacity impacts the effectiveness and capacity of wastewater treatment in OPG systems. Light provided at the surface of a reactor attenuates in the water column with increasing depth and turbidity.[118–120] Reactor depth varies with design size and operational volume while the turbidity changes with biomass growth, particle sizes, and influent particle concentration.[120,121] These factors, in addition to agitation, amend the interaction of phototrophs embedded in the granules with light (light exposure frequency). Moreover, high exposure frequency at photoinhibition irradiances can impair OPG function, while low intensity can limit the generation of essential oxygen. The impacts of these interrelated factors on the utility of light within OPG reactors is examined in Chapter 4.

Finally, *what are the magnitudes of OPGs physical parameters affecting their behaviour within the reactor ecosystem*? The OPG manifestation and functional integrity are anchored on the presence of eukaryotic and prokaryotic phototrophs and heterotrophic

bacteria.[28,42,43,45,122,123] In addition, their diverse microbial consortia include ciliates and flagellates [24] colonizing the granular biome. Critically, the system must achieve an equilibrium between granular growth rates ($\mu_{granules}$) and growth of microbes ($\mu_{microbes}$) while phototrophic and heterotrophic biomass balance is needed for granular functional integrity. The growth rate of phototrophs, slower than that of aerobic heterotrophic bacteria,[124] can limit the system scale and capacity and is also rate-limiting for growth of OPG sizes. Environmental stresses within the reactor can cause microbial predominance within the system to shift temporally and spatially.[125,126] The phenotypic parameters, including shape, sizes, behaviour, growth and other biochemical properties of these microbial populations, determine the physiology of the OPGs. The environmental stresses such as shear also modify the resulting granular formations by attrition and aggregating influences.[56] The hydrodynamic behaviour of granules within the reactors is contingent on their physical parameters influencing their interactions with bulk fluid.[68,127] These parameters, including density, porosity and permeability, are enumerated in Chapter 5 for both static and reactor derived OPGs. We *hypothesize* that OPGs have varying densities and porosities based on assorted sizes. Agitation operations determine the frequency and duration [128–130] of granular exposure to the light zone, while resultant shear stresses influence the formation,[60,62,65,131] the size and shape of granules.[60,132] Reactor design, in turn, influences both the quantity and of light available as 'light area' and system capacity while its operation determines the light utility and success of OPG WWT operations.

Sustaining OPGs system at large scale can, therefore, be a conduit for a resource-centric wastewater treatment paradigm building upon the gains made with large scale ASG technology.[26,27,38] This fosters adopting reuse and recycling strategies of resources in wastewater as opposed to disposal.[3] The potential resource savings from OPG systems include significant energy and financial savings while reducing infrastructure footprint.[27,38] Moreover, OPGs have been reported to have up to 3 times higher biomass yields (g COD/g COD) compared to activated sludge systems alluding to harnessing of light energy and CO_2.[28] These higher yields can foster energy resource recovery via anaerobic digestion of biomass.[44,133] The OPG systems can be engineered for enhanced nutrients recovery from wastewater, which can then be reapplied into the ecosystem closing the nutrient loop.[51,80,134] The framework to achieve this is anchored on ensuring the adequate and sustainable generation of OPG consortia and optimizing light provision and utility for effective and efficient reactor function.

1.4 Bibliography

1 Sanitation. https://www.who.int/news-room/fact-sheets/detail/sanitation (accessed 26 Nov2019).

2 Lofrano G, Brown J. Wastewater management through the ages: A history of mankind. *Sci Total Environ* 2010; **408**: 5254–5264.

3 Jørgensen S, Pedersen LJT. The Circular Rather than the Linear Economy. In: *RESTART Sustainable Business Model Innovation*. Springer International Publishing: Cham, 2018, pp 103–120.

4 Massoud MA, Tarhini A, Nasr JA. Decentralized approaches to wastewater treatment and management: Applicability in developing countries. *J Environ Manage* 2009; **90**: 652–659.

5 Muga HE, Mihelcic JR. Sustainability of wastewater treatment technologies. *J Environ Manage* 2008; **88**: 437–447.

6 Boller M. Small wastewater treatment plants — A challenge to wastewater engineers. *Water Sci Technol* 1997; **35**: 1–12.

7 Angelakis AN, Snyder SA. Wastewater Treatment and Reuse: Past, Present, and Future. *Water* 2015; **7**: 4887–4895.

8 Carey RO, Migliaccio KW. Contribution of Wastewater Treatment Plant Effluents to Nutrient Dynamics in Aquatic Systems: A Review. *Environ Manage* 2009; **44**: 205–217.

9 Gu Y, Li Y, Li X, Luo P, Wang H, Wang X *et al.* Energy Self-sufficient Wastewater Treatment Plants: Feasibilities and Challenges. *Energy Procedia* 2017; **105**: 3741–3751.

10 Neyens E, Baeyens J, Dewil R, De heyder B. Advanced sludge treatment affects extracellular polymeric substances to improve activated sludge dewatering. *J Hazard Mater* 2004; **106**: 83–92.

11 Milferstedt K, Hamelin J, Park C, Jung J, Hwang Y, Cho S-K *et al.* Biogranules applied in environmental engineering. *Int J Hydrog Energy* 2017; **42**: 27801–27811.

12 Kalderis D, Aivalioti M, Gidarakos E. Options for sustainable sewage sludge management in small wastewater treatment plants on islands: The case of Crete. *Desalination* 2010; **260**: 211–217.

13 Hau KC, Sculli D. Costs of disposal of sewage sludge: a case study. *Eng Costs Prod Econ* 1991; **21**: 133–141.

14 Barroso Soares R. Comparative Analysis of the Energy Consumption of Different Wastewater Treatment Plants. *Int J Archit Arts Appl* 2017; **3**: 79.

15 Rittmann BE, McCarty PL. *Environmental Biotechnology: Principles and Applications*. Tata McGraw Hill Education Private Limited, 2012Google-Books-ID: qM43AwAAQBAJ.

16 June 2015 WEF-WV-. WEF - Water Volumes - June 2015. http://wef.org/resources/publications/all-magazines/water-environment-technology/wet-issues/water-environment--technology2/wet-magazine---june-2015/water-volumes---june-2015/ (accessed 28 Jan2019).

17 Water & Wastewater Report | ASCE. https://www.asce.org/water_and_wastewater_report/ (accessed 7 Jan2019).

18 The Reuse Opportunity. Int. Water Assoc. https://iwa-network.org/publications/the-reuse-opportunity/ (accessed 26 Nov2019).

19 Alphenaar A. ANAEROBIC GRANULAR SLUDGE: 1994; : 214.

20 Bathe S, Kreuk MK de, McSwain BS, Schwarzenbeck N. *Aerobic Granular Sludge*. IWA Publishing, 2005.

21 Tiron O, Bumbac C, Patroescu IV, Badescu VR, Postolache C. Granular activated algae for wastewater treatment. *Water Sci Technol J Int Assoc Water Pollut Res* 2015; **71**: 832–839.

22 Henze M (ed.). *Biological wastewater treatment: principles, modelling and design*. IWA Pub: London, 2008.

23 Knocke WR. Density of activated sludge solids. *Water Res* 1992; **26**: 1559–1561.

24 Oyserman BO, Martirano JM, Wipperfurth S, Owen BR, Noguera DR, McMahon KD. Community Assembly and Ecology of Activated Sludge under Photosynthetic Feast–Famine Conditions. *Environ Sci Technol* 2017; **51**: 3165–3175.

25 Seviour R, Nielsen PH. *Microbial Ecology of Activated Sludge*. IWA Publishing, 2010.

26 Niermans R, Giesen A, Loosdrecht M van, Buin B de. Full-scale Experiences with Aerobic Granular Biomass Technology for Treatment of Urban and Industrial Wastewater. *Proc Water Environ Fed* 2014; **2014**: 2347–2357.

27 Giesen A, van Loosdrecht M, Robertson S, de Buin B. Aerobic Granular Biomass Technology: further innovation, system development and design optimisation. 2015. doi:info:doi/10.2175/193864715819539641.

28 Abouhend AS, McNair A, Kuo-Dahab WC, Watt C, Butler CS, Milferstedt K *et al.* The Oxygenic Photogranule Process for Aeration-Free Wastewater Treatment. *Environ Sci Technol* 2018; **52**: 3503–3511.

29 Lee DJ, Chen GW, Liao YC, Hsieh CC. On the free-settling test for estimating activated sludge floc density. *Water Res* 1996; **30**: 541–550.

30 Amanatidou E, Samiotis G, Trikoilidou E, Pekridis G, Taousanidis N. Evaluating sedimentation problems in activated sludge treatment plants operating at complete sludge retention time. *Water Res* 2015; **69**: 20–29.

31 Mancell-Egala WASK, Kinnear DJ, Jones KL, De Clippeleir H, Takács I, Murthy SN. Limit of stokesian settling concentration characterizes sludge settling velocity. *Water Res* 2016; **90**: 100–110.

32 Sarma SJ, Tay JH. Aerobic granulation for future wastewater treatment technology: challenges ahead. *Environ Sci Water Res Technol* 2017; **4**: 9–15.

33 Nancharaiah YV, Kiran Kumar Reddy G. Aerobic granular sludge technology: Mechanisms of granulation and biotechnological applications. *Bioresour Technol* 2018; **247**: 1128–1143.

34 Sarma SJ, Tay JH, Chu A. Finding Knowledge Gaps in Aerobic Granulation Technology. *Trends Biotechnol* 2017; **35**: 66–78.

35 Giesen A, Loosdrecht M van, Pronk M, Robertson S, Thompson A. Aerobic Granular Biomass Technology: recent performance data, lessons learnt and retrofitting conventional treatment infrastructure. *Proc Water Environ Fed* 2016; **2016**: 1913–1923.

36 Liu Y, Tay J-H. State of the art of biogranulation technology for wastewater treatment. *Biotechnol Adv* 2004; **22**: 533–563.

37 Zhang Q, Hu J, Lee D-J. Aerobic granular processes: Current research trends. *Bioresour Technol* 2016; **210**: 74–80.

38 Andreas Giesen, Andrew Thompson. Aerobic Granular Biomass: Setting The New Standard For Cost-Effective, Energy Efficient And Sustainable Wastewater Treatment | Request PDF. https://www.royalhaskoningdhv.com/nereda. 2012.https://www.researchgate.net/publication/323005503_Aerobic_Granular_Biomass_Setting_The_New_Standard_For_Cost-Effective_Energy_Efficient_And_Sustainable_Wastewater_Treatment (accessed 18 Mar2020).

39 Liu Y, Xu H-L, Show K-Y, Tay J-H. Anaerobic granulation technology for wastewater treatment. *World J Microbiol Biotechnol* 2002; **18**: 99–113.

40 Sengar A, Basheer F, Aziz A, Farooqi IH. Aerobic granulation technology: Laboratory studies to full scale practices. *J Clean Prod* 2018; **197**: 616–632.

41 McNair A. Pilot Reactor Operation of the Oxygenic Photogranule (OPG) Wastewater Treatment Process. *Environ Water Resour Eng Masters Proj* 2017.https://scholarworks.umass.edu/cee ewre/83.

42 Milferstedt K, Kuo-Dahab WC, Butler CS, Hamelin J, Abouhend AS, Stauch-White K *et al.* The importance of filamentous cyanobacteria in the development of oxygenic photogranules. *Sci Rep* 2017; **7**: 17944.

43 Kuo-Dahab WC, Stauch-White K, Butler CS, Gikonyo GJ, Carbajal-González B, Ivanova A *et al.* Investigation of the Fate and Dynamics of Extracellular Polymeric Substances (EPS) during Sludge-Based Photogranulation under Hydrostatic Conditions. *Environ Sci Technol* 2018; **52**: 10462–10471.

44 Park C, Dolan S (deceased). Patent Algal Sludge Granule OPG Jan 2019. 2019; : 11.

45 Stauch-White K, Srinivasan VN, Camilla Kuo-Dahab W, Park C, Butler CS. The role of inorganic nitrogen in successful formation of granular biofilms for wastewater treatment that support cyanobacteria and bacteria. *AMB Express* 2017; **7**. doi:10.1186/s13568-017-0444-8.

46 He Q, Chen L, Zhang S, Chen R, Wang H, Zhang W *et al.* Natural sunlight induced rapid formation of water-born algal-bacterial granules in an aerobic bacterial granular photo-sequencing batch reactor. *J Hazard Mater* 2018; **359**: 222–230.

47 Ahmad JSM, Cai W, Zhao Z, Zhang Z, Shimizu K, Lei Z *et al.* Stability of algal-bacterial granules in continuous-flow reactors to treat varying strength domestic wastewater. *Bioresour Technol* 2017; **244**: 225–233.

48 Lee CS, Oh H-S, Oh H-M, Kim H-S, Ahn C-Y. Two-phase photoperiodic cultivation of algal–bacterial consortia for high biomass production and efficient nutrient removal from municipal wastewater. *Bioresour Technol* 2016; **200**: 867–875.

49 Abouhend AS, Milferstedt K, Hamelin J, Ansari AA, Butler C, Carbajal-González BI *et al.* Growth Progression of Oxygenic Photogranules and Its Impact on Bioactivity for Aeration-Free Wastewater Treatment. *Environ Sci Technol* 2019. doi:10.1021/acs.est.9b04745.

50 Hann M. Factors Impacting the Cultivation, Structure, and Oxygen Profiles of Oxygenic Photogranules for Aeration-Free Wastewater Treatment. *Environ Water Resour Eng Masters Proj* 2018.https://scholarworks.umass.edu/cee_ewre/90.

51 Lee Y-J, Lei Z. Microalgal-bacterial aggregates for wastewater treatment: A mini-review. *Bioresour Technol Rep* 2019; : 100199.

52 Beck D. Technology development life cycle processes. 2013 doi:10.2172/1089868.

53 Caetano M, Araujo CS, Amaral DC, Guerrini FM. Open innovation and technology development process: the gap on partnership adoption from a case study perspective. *Prod Manag Dev* 2011; **9**: 111–120.

54 Sheasley WD. Leading the Technology Development Process. *Res-Technol Manag* 2016.https://www.tandfonline.com/doi/abs/10.1080/08956308.1999.11671284 (accessed 5 Dec2018).

55 Liu L, Fan H, Liu Y, Liu C, Huang X. Development of algae-bacteria granular consortia in photo-sequencing batch reactor. *Bioresour Technol* 2017; **232**: 64–71.

56 Liu Y, Tay J-H. The essential role of hydrodynamic shear force in the formation of biofilm and granular sludge. *Water Res* 2002; **36**: 1653–1665.

57 Zhou D, Niu S, Xiong Y, Yang Y, Dong S. Microbial selection pressure is not a prerequisite for granulation: Dynamic granulation and microbial community study in a complete mixing bioreactor. *Bioresour Technol* 2014; **161**: 102–108.

58 Yuanyuan Z, Xuehong Z, Wenjie Z. Research Advances in Anammox Granular Sludge. In: *Proceedings of the AASRI International Conference on Industrial Electronics and Applications (2015)*. Atlantis Press: London, UK, 2015 doi:10.2991/iea-15.2015.113.

59 Uetake J, Tanaka S, Segawa T, Takeuchi N, Nagatsuka N, Motoyama H *et al*. Microbial community variation in cryoconite granules on Qaanaaq Glacier, NW Greenland. *FEMS Microbiol Ecol* 2016; **92**. doi:10.1093/femsec/fiw127.

60 Tay J-H, Liu Q-S, Liu Y. The effects of shear force on the formation, structure and metabolism of aerobic granules. *Appl Microbiol Biotechnol* 2001; **57**: 227–233.

61 Liu Y-Q, Tay J-H. Fast formation of aerobic granules by combining strong hydraulic selection pressure with overstressed organic loading rate. *Water Res* 2015; **80**: 256–266.

62 Bindhu B k., Madhu G. Selection pressure theory for aerobic granulation – an overview. *Int J Environ Waste Manag* 2014; **13**: 317–329.

63 Arcila JS, Buitrón G. Influence of solar irradiance levels on the formation of microalgae-bacteria aggregates for municipal wastewater treatment. *Algal Res* 2017; **27**: 190–197.

64 Kang AJ, Munz G, Yuan Q. Influence of pH control on material characteristics, bacterial community composition and BNR performance of mature aerobic granules. *Process Saf Environ Prot* 2019; **124**: 158–166.

65 Qin L, Tay J-H, Liu Y. Selection pressure is a driving force of aerobic granulation in sequencing batch reactors. *Process Biochem* 2004; **39**: 579–584.

66 Arcila JS, Buitrón G. Microalgae–bacteria aggregates: effect of the hydraulic retention time on the municipal wastewater treatment, biomass settleability and methane potential. *J Chem Technol Biotechnol* 2016; **91**: 2862–2870.

67 Trebuch LM, Oyserman BO, Janssen M, Wijffels RH, Vet LEM, Fernandes TV. Impact of hydraulic retention time on community assembly and function of photogranules for wastewater treatment. *Water Res* 2020; **173**: 115506.

68 Elimelech M, Gregory J, Jia X. *Particle Deposition and Aggregation: Measurement, Modelling and Simulation*. Butterworth-Heinemann, 2013.

69 Gregory J. Monitoring particle aggregation processes. *Adv Colloid Interface Sci* 2009; **147**–**148**: 109–123.

70 Amin S, Barnett GV, Pathak JA, Roberts CJ, Sarangapani PS. Protein aggregation, particle formation, characterization & rheology. *Curr Opin Colloid Interface Sci* 2014; **19**: 438–449.

71 Philo J, Arakawa T. Mechanisms of Protein Aggregation. *Curr Pharm Biotechnol* 2009; **10**: 348–351.

72 Gao D, Liu L, Liang H, Wu W-M. Aerobic granular sludge: characterization, mechanism of granulation and application to wastewater treatment. *Crit Rev Biotechnol* 2011; **31**: 137–152.

73 Ansari AA, Abouhend AS, Park C. Effects of seeding density on photogranulation and the start-up of the oxygenic photogranule process for aeration-free wastewater treatment. *Algal Res* 2019; **40**: 101495.

74 Ji X, Jiang M, Zhang J, Jiang X, Zheng Z. The interactions of algae-bacteria symbiotic system and its effects on nutrients removal from synthetic wastewater. *Bioresour Technol* 2018; **247**: 44–50.

75 Zhang B, Lens PNL, Shi W, Zhang R, Zhang Z, Guo Y *et al.* Enhancement of aerobic granulation and nutrient removal by an algal–bacterial consortium in a lab-scale photobioreactor. *Chem Eng J* 2018; **334**: 2373–2382.

76 Valigore JM, Gostomski PA, Wareham DG, O'Sullivan AD. Effects of hydraulic and solids retention times on productivity and settleability of microbial (microalgal-bacterial) biomass grown on primary treated wastewater as a biofuel feedstock. *Water Res* 2012; **46**: 2957–2964.

77 Van Den Hende S, Carré E, Cocaud E, Beelen V, Boon N, Vervaeren H. Treatment of industrial wastewaters by microalgal bacterial flocs in sequencing batch reactors. *Bioresour Technol* 2014; **161**: 245–254.

78 Zhao Z, Yang X, Cai W, Lei Z, Shimizu K, Zhang Z *et al.* Response of algal-bacterial granular system to low carbon wastewater: Focus on granular stability, nutrients removal and accumulation. *Bioresour Technol* 2018; **268**: 221–229.

79 Park C, Dolan S (deceased). Algal-Sludge Granule for Wastewater Treatment and Bioenergy Feedstock Generation. 2015.https://patentscope.wipo.int/search/en/detail.jsf?docId=WO2015112654 (accessed 7 Jan2019).

80 González-Camejo J, Viruela A, Ruano MV, Barat R, Seco A, Ferrer J. Effect of light intensity, light duration and photoperiods in the performance of an outdoor photobioreactor for urban wastewater treatment. *Algal Res* 2019; **40**: 101511.

81 Gonzalez-Martinez A, Sihvonen M, Muñoz-Palazon B, Rodriguez-Sanchez A, Mikola A, Vahala R. Microbial ecology of full-scale wastewater treatment systems in the Polar Arctic Circle: Archaea, Bacteria and Fungi. *Sci Rep* 2018; **8**. doi:10.1038/s41598-018-20633-5.

82 Managing Energy Costs in Wastewater Treatment Plants - Madison Gas and Electric - Madison, Wisconsin. https://www.mge.com/saving-energy/business/bea/article_detail.htm?nid=%202431 (accessed 4 Oct2018).

83 Falkowski PG, Raven JA. *Aquatic Photosynthesis*. Princeton University Press, 2007.

84 Geider RJ, Osborne BA. *Algal Photosynthesis*. 1992http://public.eblib.com/choice/publicfullrecord.aspx?p=3084381 (accessed 14 Dec2018).

85 da C. A. Alves PL, Magalhães ACN, Barja PR. The Phenomenon of Photoinhibition of Photosynthesis and Its Importance in Reforestation. *Bot Rev* 2002; **68**: 193–208.

86 Krause-Jensen D, Sand-Jensen K. Light attenuation and photosynthesis of aquatic plant communities. *Limnol Oceanogr* 1998; **43**: 396–407.

87 Powles SB. Photoinhibition of Photosynthesis Induced by Visible Light. *Annu Rev Plant Physiol* 1984; **35**: 15–44.

88 Giacometti GM, Morosinotto T. Photoinhibition and Photoprotection in Plants, Algae, and Cyanobacteria. In: Lennarz WJ, Lane MD (eds). *Encyclopedia of Biological Chemistry*. Academic Press: Waltham, 2013, pp 482–487.

89 Beardall J, Raven JA. Cyanobacteria vs green algae: which group has the edge? *J Exp Bot* 2017; **68**: 3697–3699.

90 Gigahertz-Optik. Basics of Light Measurement » Gigahertz-Optik. No-date.https://www.gigahertz-optik.de/en-us/basics-light-measurement/ (accessed 20 Sep2018).

91 LRC. How can full-spectrum light sources be compared? | Full-Spectrum Light Sources | Lighting Answers | NLPIP. Light. Res. CenterRPI. 2018.https://www.lrc.rpi.edu/programs/nlpip/lightinganswers/fullspectrum/comparisons.asp (accessed 20 Sep2018).

92 Kalaji HM, Carpentier R, Allakhverdiev SI, Bosa K. Fluorescence parameters as early indicators of light stress in barley. *J Photochem Photobiol B* 2012; **112**: 1–6.

93 Massa GD, Kim H-H, Wheeler RM, Mitchell CA. Plant Productivity in Response to LED Lighting. *HortScience* 2008; **43**: 1951–1956.

94 Parkin TB, Brock TD. The effects of light quality on the growth of phototrophic bacteria in lakes. *Arch Microbiol* 1980; **125**: 19–27.

95 Smith H. Light Quality, Photoperception, and Plant Strategy. *Annu Rev Plant Physiol* 1982; **33**: 481–518.

96 Son K-H, Lee J-H, Oh Y, Kim D, Oh M-M, In B-C. Growth and Bioactive Compound Synthesis in Cultivated Lettuce Subject to Light-quality Changes. *HortScience* 2017; **52**: 584–591.

97 Urrestarazu M, Nájera C, Gea M del M. Effect of the Spectral Quality and Intensity of Light-emitting Diodes on Several Horticultural Crops. *HortScience* 2016; **51**: 268–271.

98 Bernstein HC, Konopka A, Melnicki MR, Hill EA, Kucek LA, Zhang S *et al.* Effect of mono- and dichromatic light quality on growth rates and photosynthetic performance of Synechococcus sp. PCC 7002. *Front Microbiol* 2014; **5**. doi:10.3389/fmicb.2014.00488.

99 Castenholz RW, Garcia-Pichel F. Cyanobacterial Responses to UV Radiation. In: Whitton BA (ed). *Ecology of Cyanobacteria II*. Springer Netherlands: Dordrecht, 2012, pp 481–499.

100 Cullen JJ, Neale PJ. Ultraviolet radiation, ozone depletion, and marine photosynthesis. *Photosynth Res* 1994; **39**: 303–320.

101 Helbling EW, Villafañe V, Ferrario M, Holm-Hansen O. Impact of natural ultraviolet radiation on rates of photosynthesis and on specific marine phytoplankton species. *Mar Ecol Prog Ser* 1992; **80**: 89–100.

102 Kataria S, Jajoo A, Guruprasad KN. Impact of increasing Ultraviolet-B (UV-B) radiation on photosynthetic processes. *J Photochem Photobiol B* 2014; **137**: 55–66.

103 Szilárd A, Sass L, Deák Z, Vass I. The sensitivity of Photosystem II to damage by UV-B radiation depends on the oxidation state of the water-splitting complex. *Biochim Biophys Acta BBA - Bioenerg* 2007; **1767**: 876–882.

104 Schuurmans RM, van Alphen P, Schuurmans JM, Matthijs HCP, Hellingwerf KJ. Comparison of the Photosynthetic Yield of Cyanobacteria and Green Algae: Different Methods Give Different Answers. *PLOS ONE* 2015; **10**: e0139061.

105 Pattanaik B, Schumann R, Karsten U. Effects of Ultraviolet Radiation on Cyanobacteria and their Protective Mechanisms. *Algae Cyanobacteria Extreme Environ* 2007; : 29–45.

106 Xu C, Sullivan JH. Reviewing the Technical Designs for Experiments with Ultraviolet-B Radiation and Impact on Photosynthesis, DNA and Secondary Metabolism. *J Integr Plant Biol* 2010; **52**: 377–387.

107 Arrow Electronics. LED application in agricultural lighting can efficiently increase crop yields. Arrow.com. 2017.https://www.arrow.com/en/research-and-events/articles/agriculture-lighting (accessed 26 Sep2018).

108 S P, Sa K, A P. Characteristics of Photosynthetic Active Radiation (PAR) Through Statistical Analysis at Larnaca, Cyprus. *SM J Biom Biostat* 2017; **2**: 1–16.

109 Li-Cor. Principles of radiation measurement. .;No date.https://www.licor.com/env/pdf/light/Rad_Meas.pdf (accessed 21 Aug2017).

110 Barber J, Andersson B. Too much of a good thing: light can be bad for photosynthesis. *Trends Biochem Sci* 1992; **17**: 61–66.

111 Zhang B, Guo Y, Lens PNL, Zhang Z, Shi W, Cui F *et al.* Effect of light intensity on the characteristics of algal-bacterial granular sludge and the role of N-acyl-homoserine lactone in the granulation. *Sci Total Environ* 2018. doi:10.1016/j.scitotenv.2018.12.250.

112 Grant C, Louda J. Microalgal pigment ratios in relation to light intensity: implications for chemotaxonomy. *Aquat Biol* 2010; **11**: 127–138.

113 Bouman HA, Platt T, Doblin M, Figueiras FG, Gudmundsson K, Gudfinnsson HG *et al.* Photosynthesis–irradiance parameters of marine phytoplankton: synthesis of a global data set. 2018; : 16.

114 Ralph PJ, Gademann R. Rapid light curves: A powerful tool to assess photosynthetic activity. *Aquat Bot* 2005; **82**: 222–237.

115 Figueroa FL. Relations between electron transport rates determined by pulse amplitude modulated chlorophyll fluorescence and oxygen evolution in macroalgae under different light conditions. *Photosynth Res* 2003; **75**: 259–275.

116 Zhang C, Sun S, Liu X, Wan C, Lee D-J. Influence of operational conditions on the stability of aerobic granules from the perspective of quorum sensing. *Environ Sci Pollut Res* 2017; **24**: 7640–7649.

117 Mishima K, Nakamura M. Self-Immobilization of Aerobic Activated Sludge–A Pilot Study of the Aerobic Upflow Sludge Blanket Process in Municipal Sewage Treatment. *Water Sci Technol* 1991; **23**: 981–990.

118 Gallegos CL, Moore KA. Factors contributing to water-column light attenuation. 2000.http://repository.si.edu//handle/10088/18204 (accessed 26 Sep2018).

119 Brito AC, Newton A. Measuring Light Attenuation in Shallow Coastal Systems. *J Ecosyst Ecography* 2013; **03**. doi:10.4172/2157-7625.1000122.

120 Curtis TP, Mara DD, Dixo NGH, Silva SA. Light penetration in waste stabilization ponds. *Water Res* 1994; **28**: 1031–1038.

121 Pearsall WH, Ullyott P. Light Penetration into Fresh Water: I. a Thermionic Potentiometer for Measuring Light Intensity with Photo-Electric Cells. *J Exp Biol* 1933; **10**: 293–305.

122 Arcila JS, Buitrón G. Microalgae–bacteria aggregates: effect of the hydraulic retention time on the municipal wastewater treatment, biomass settleability and methane potential. *J Chem Technol Biotechnol* 2016; **91**: 2862–2870.

123 Alam MA, Vandamme D, Chun W, Zhao X, Foubert I, Wang Z *et al.* Bioflocculation as an innovative harvesting strategy for microalgae. *Rev Environ Sci Biotechnol* 2016; **15**: 573–583.

124 Lee CS, Lee S-A, Ko S-R, Oh H-M, Ahn C-Y. Effects of photoperiod on nutrient removal, biomass production, and algal-bacterial population dynamics in lab-scale photobioreactors treating municipal wastewater. *Water Res* 2015; **68**: 680–691.

125 Guedes da Silva L, Tomás-Martínez S, Wahl A, van Loosdrecht M. *The environment selects: Modeling energy allocation in microbial communities under dynamic environments*. 2019 doi:10.1101/689174.

126 Elias S, Banin E. Multi-species biofilms: living with friendly neighbors. *FEMS Microbiol Rev* 2012; **36**: 990–1004.

127 Datt C, Elfring GJ. Dynamics and rheology of particles in shear-thinning fluids. *J Non-Newton Fluid Mech* 2018; **262**: 107–114.

128 Hall SM. Chapter 6 - Blending and Agitation. In: Hall SM (ed). *Rules of Thumb for Chemical Engineers (Sixth Edition)*. Elsevier, 2018, pp 99–124.

129 Jirout T, Rieger F. Impeller design for mixing of suspensions. *Chem Eng Res Des* 2011; **89**: 1144–1151.

130 Edward L. Paul, Atiemo-Obeng VA, Kresta SM (eds.). *Handbook of industrial mixing: science and practice*. Wiley-Interscience: Hoboken, N.J, 2004.

131 B K B, G M. Influence of three selection pressures on aerobic granulation in sequencing batch reactor. *Indian J Chem Technol IJCT* 2016; **22**: 241–247.

132 Yu W, Gregory J, Campos L, Li G. The role of mixing conditions on floc growth, breakage and re-growth. *Chem Eng J* 2011; **171**: 425–430.

133 Seynhaeve L. Anaerobic digestion of algal-sludge granules. 2014.

134 Delgadillo-Mirquez L, Lopes F, Taidi B, Pareau D. Nitrogen and phosphate removal from wastewater with a mixed microalgae and bacteria culture. *Biotechnol Rep* 2016; **11**: 18–26.

CHAPTER 2

HYDRODYNAMIC GENERATION OF OXYGENIC PHOTOGRANULES

2.1 Abstract

Oxygenic photogranules (OPGs) are a promising biotechnology for wastewater treatment with self-aerating potential. The current generation of OPGs occurs under hydrostatic conditions in contrast to other reported bioaggregates. We investigated the cultivation of OPGs under hydrodynamic conditions achieving granulation in 8 days. Different inoculum concentrations, light intensities and shear conditions were applied for the granulation. Dilute samples under low-light (LL), medium-light (ML), and high-light (HL) conditions exhibited granulation. Low shear conditions G-11 s^{-1} promoted granulation under all light conditions with highly dilute inoculum (x4 dilution), and only in LL for x2 inoculum dilution. A shear rate of G-39 s^{-1} resulted in granulation under all light conditions with all dilute inocula. On the other hand, a high shear rate (G-73 s^{-1}) did not result in identifiable granular assemblages other than in LL samples coupled with low biomass concentration (x4 dilutions). Loose aggregates were formed in ML dilute samples with this high shear. This disparity indicates that OPG granulation and associated phototrophic enrichment ensues only with favourable interaction of the various selection pressures applied. Moreover, granulation improved settleability of biomass, resulting in low settling volume indices (SVI) and increases of mean particle sizes. However, decreasing values of singular SVI indices were insufficient in characterizing

successful hydrodynamic granulation. The SVI5/SVI30 ratio was hence applied with a decrease and convergence of the ratio observed for granulating samples.

2.2 Introduction

Phototrophs harness solar energy to power synthesis of biomolecules constituting the basic production system for the biosphere.[1] Phototrophic microbes are often integrated into different architectural assemblages in their environmental niches.[2] While these assemblages can have deleterious environmental impacts [3] and cause infrastructure damage,[4,5] others can be beneficially utilized for anthropogenic applications, such as photogranular wastewater treatment.[6–9]

Granular sludge consists of self-immobilized microbial consortia with high density, compact cores, and spheroidal profiles. Each granule is effectively a 'micro-reactor' in which biochemical transformations occur. The granules' compact structure can also withstand high-strength wastewater and shock loadings.[10,11] These characteristics facilitate higher retention of biomass giving cost and space savings [12] in wastewater treatment operations compared to conventional activated sludge (CAS) plants.[13]

Anaerobic granules consist of co-operative methanogenic, acetogenic, and various hydrolytic fermentative trophic groups.[12] Aerobic granules, on the other hand, have a microbial consortium comprising aerobic heterotrophic bacteria and nitrifying bacteria on their outer layers with facultative, anaerobic bacteria in their cores.[14] While the apparent disparity in microbial dominance between the above granules is dependent on

environmental niche occupied, microbial colonialization evolves along a spatial gradient, resulting in generic layered granular structures. These self-immobilized granular bioaggregates can thus be considered supraspecific homologs,[15] similar in structure and differing only in microbial species dominance.

Oxygenic photogranules (OPG) reported by different investigators [16–21] bear semblance to this ubiquitous granular morphology. The microbial community in the OPGs consists of motile filamentous cyanobacteria (MFC) and algae species dominating the phototrophic outer layer with light exposure while non-phototrophic bacteria dominate the inner core.[17,19] Unlike other granules reported,[22–27] OPGs have been cultivated and applied in reactors under light without supplemental aeration.[8,17–19] Presently the protocol for the generation of OPGs involves inoculating activated sludge in small glass vials with light energy under hydrostatic conditions.[17–19] The setup usually results in the generation of a single OPG aggregate in each vial that can subsequently be introduced into a reactor for wastewater treatment.[8]

Selection pressures reported to enhance the formation of other granules [22,23,28–31] can also be inferred for OPGs. Hydraulic selection pressure (HSP) can be inferred from reported sequencing batch reactor (SBR) operation of OPG reactors, with a 10 min settling period [8] effectively retaining only rapidly settling biomass. It has been reported that long settling times induced minimal HSP and hence did not promote the propagation of aerobic granules, while too short settling times (<3 min) resulted in washout of microbes and small granules hence no granulation.[28] Therefore, for successful granulation, the rate of

removal of unsettled granules via HSP control should consider their growth rate ($\mu_{granules}$) to ensure retention of juvenile granules and sufficient biomass for functionality.

Feast and famine selection pressure is inherent in SBR operations that have a Feed-React-Settle-Decant routine and have also been reported as necessary to granulation.[32] Granular systems, including reported OPG reactors [8] at various scales are inevitably operated in this scheme.[13,33,34] SBR operation results in the creation of substrate diffusion gradients into the granular matrix [35] with convective mass transport also distributing substrates in bulk fluid and into the granules through their porous structure.[36–38] Furthermore, the OPG reactor was configured with operational cycling of dark and light periods creating feast and famine conditions for a 'light-substrate'.[8] For OPGs developed under hydrostatic batch conditions, famine conditions persisting initially in activated sludge inoculum are followed by a feast state due to biomass decay.[17,18] In these conditions, bioaggregation, or compaction of activated sludge inoculum, was promoted and light-induced phototrophic enrichment resulted in OPG development.[17–19]

The presence of shear in granular systems emanates from applied agitation by aeration or mechanical mixers and serves to suspend the biomass, distributing dissolved bulk substrate flux and 'shaping' the granules. Investigators reported that shear is essential for not only granular formation and shape but also sizing granules, with higher shear resulting in smaller and more spherical aggregates.[39,40] The shear force also increases hydrophobicity and particle density while aiding in initiating and enhancing collision of

bridging particles in the fluid media.[41] Agitation in OPG reactors not only has similar influences but also critically facilitates the interaction of the granules with the light source. Light supplied at the surface of reactors penetrates the fluid media and decays per Beer-Lamberts law.[42] The turbidity and colour [43] in the reactor bulk matrix limits light penetration necessitating the suspension of OPG granules to 'see' light substrate.[44] For cyanobacteria which form the structural backbone of OPGs,[17] growth is strongly correlated to light intensity and weakly to carbon assimilation in a growth optimization strategy.[45] Similar to other phototrophs, the oxygen production in the phototrophic outer layer of OPGs, potentially varies linearly with light intensity under low light to saturation [46–48] with potential photoinhibition at high light intensities.[49] Mixing is therefore essential to ensure optimal interaction of OPGs with light to sustain granular functional and structural integrity.

The ubiquity of granulation and selection pressures promoting granule formation and function led to a hypothesis that the formation of seed OPGs from activated sludge inoculum should also occur directly under hydrodynamic conditions. The present protocol for the generation of seed OPG involves cultivation under hydrostatic conditions. Attempts to form OPGs without aeration and using only activated sludge under hydrodynamic conditions have not been reported. We likewise hypothesized that phototrophic granulation occurs within a 'goldilocks zone' due to the interaction of chemical energies (organic and nutrient loading), shear pressure, and critical light energy in varying magnitudes. This study aims to examine these two hypotheses by conducting matrices of batch experiments with varying energy flows. If successful, the formation of

OPGs from activated sludge under hydrodynamic conditions would be potentially a preferred seeding protocol to hydrostatic cultivation by reducing the time for photogranulation. Nevertheless, the work associated with the second hypothesis may explain why photogranules, and potentially other microbial granules, would still occur under limited sets of environmental conditions.

2.3 Materials and methods

2.3.1 Experimental set-up

A jar test rig mixer (Phipps & Bird Model 7790-302, six paddle stirrer) was used to induce mixing in batch reactors. The mixer's variable speed drives were calibrated to run at speeds of 20, 50 and 80 rpm for each experimental set. The paddle blade impellers used had an impeller diameter (d) of 5 cm, width 2.9 cm and were set at a clearance of 5 cm from the vessel bottom. Cylindrical clear glass jars (1 L) were used for the experiment with an operating volume of 800 mL. Previously described methodology [50] was applied to determine the theoretical shear stress resulting from mixing in the batch reactors. The 20, 50 and 80 rpm mixing speeds induced shear stresses of 0.01 N m^{-2} (velocity gradient, G: 11 s^{-1}), 0.04 N m^{-2} (G: 39 s^{-1}), and 0.07 N m^{-2} (G: 73 s^{-1}), respectively. The experimental set was operated under different light intensities of 6.5±1, 12.7±1 and 25±1 Klux, using 9 W LEDs (EcoSmart, daylight- 5000 K) with a luminosity of 840 Lumens, equivalent to photosynthetic flux densities (PPFD) of 117, 216, and 450 µmol m^{-2} s^{-1} respectively [51]. These light conditions corresponding to LL, ML, and HL, respectively, were provided continuously for a duration of 8 days.

2.3.2 Reactor seeding

Grab samples of activated sludge were collected from a local wastewater treatment plant (WWTP).[18] The facility employs an activated sludge system with mechanical aeration. The activated sludge inoculum sourced from the WWTP had a mixed liquor suspended solids (MLSS) concentration of 2500-3000 mg/L. An activated sludge volume of 30 L was collected for each batch. This volume was split into three sets which were then diluted with deionized water giving x4, x2 and x1 dilute inocula. The volumes were continuously mixed to maintain homogeneity. The batch reactors were then seeded and capped to reduce both evaporation and atmospheric interaction. Duplicate batch reactors were operated for each condition as set out in (Table 2- 1) below.

Table 2- 1: Experimental set-up with combinations of different conditions utilized for hydrodynamic OPG cultivation.

Mixing/Light intensity	20 rpm (0.01 N m^{-2})	50 rpm (0.04 N m^{-2})	80 rpm (0.07 N m^{-2})
6.4 Klux (LL) (117 µmol m^{-2} s^{-1})	x4, x2, and x1 dilution in duplicates	x4, x2, and x1 dilution in duplicates	x4, x2, and x1 dilution in duplicates
12.7 Klux (ML) (216 µmol m^{-2} s^{-1})	x4, x2, and x1 dilution in duplicates	x4, x2, and x1 dilution in duplicates	x4, x2, and x1 dilution in duplicates
25 Klux (HL) (450 µmol m^{-2} s^{-1})	x4, x2, and x1 dilution in duplicates	x4, x2, and x1 dilution in duplicates	x4, x2, and x1 dilution in duplicates

2.3.3 Analytical methods

Total and volatile suspended solids (TSS, VSS) were quantified following standard methods (2540D).[52] The characterization of chlorophylls' *a*, *b*, *c* pigments in the reactors biomass followed Standard Methods 10200H.[52] Soluble fractions obtained as 0.45 μm filtrate were used to determine chemical oxygen demand (COD) according to standard methods (5220D).[52] The sludge volume index (SVI) was determined following standard methods (2710D) [52] at 5 min (SVI5) and 30 min (SVI30) settling time. The dissolved oxygen (DO) and pH of the samples were measured using a portable DO meter (Extech 407510A) and a benchtop pH meter (Corning 320). The light intensity was measured using a Li-Cor L-193S spherical underwater sensor (LI-Cor science) [53] for baseline ambient illumination and an EasyView^{TM} 30 light meter (Extech instruments) to calibrate reactor surface illumination.

2.3.4 Microscopy

We periodically collected samples (5 mL) in Petri dishes and obtained high-resolution images for image analysis. Image pro®v10 software (MEDIA CYBERNETICS) was utilized to characterize the images for particle sizes and number. A Weibull distribution was used to describe the particle size distribution.[54] Additionally, we collected samples for light microscopy (EVOS FL Color AMEFC-4300), which was conducted using bright field and epifluorescence (RFP light cube-532 excitation/590 Emission) to characterize changing morphology and microbial composition.[55–57] Potential cyanobacterial enrichment expected with OPG granulation results in yellow-orange fluorescence [58] due to their phycoerythrin pigment.

2.3.5 Statistical analysis

Minitab (Minitab v.17) and Excel (2010) software were applied for all statistical analysis, including particle size derivation of mean and median (D_{50}) measures. The significance of the results was determined at the 0.05 probability level ($P < 0.05$). A metric, SVI 5/SVI 30 ratio, was used to describe temporal settleability [59] of samples. A general linear model (least squares) was fit to the SVI ratio data for days 6 and 8 of the cultivation and subjected to ANOVA OriginPro (OriginLab v.2020) analysis of means and variances. Pearson correlation was used to evaluate the correlation between variables.

2.4 Results

2.4.1 Evolution of particle sizes

An increase of the consortia particle concentration around the mean sizes was observed under all conditions with 20 rpm agitation (Table 2- 2). The mean particle sizes for x4 and x2 dilution sets changed from an average of 0.08 mm (±0.001) and 0.06 mm (±0.006) both to 0.15 mm (±0.004), while the mean size of x1 sets increased from an average of 0.06 mm (±0.006) to 0.11 mm (±0.004). This increase in mean particle size was also accompanied by positively skewed distributions (Figure 2- 1-a,b,c). Initial sludge flocs for the 20 rpm set had median diameter (d_{50}) of 0.15 mm (±0.003), which increased to a median size of 0.22 mm (±0.009), 0.20 mm (±0.02), and 0.19 mm (±0.007) for x4, x2, x1 dilution sets, respectively (Table 2- 2).

For 50 rpm sets, the mean particle size exhibited decreases for x4 and x1 inoculum dilutions and an increase for the x2 dilution samples. The mean particle size decreased from 0.16 mm (±0.019) to an average mean size of 0.14 mm (±0.019) (Table 2- 2) for the x4 dilution sets. The mean particle size for x2 dilutions increased from 0.13 mm (± 0.008) to 0.15 mm (±0.008), while those of undiluted samples (x1 dilution) decreased from 0.11 mm (±0.006) to a mean size of 0.10 mm (±0.01) (Table 2- 2). The mean particle size was observed to shift towards smaller sizes for the 50 rpm ensemble (Figure 2- 1-[*d,e,f*]). The median size for the 50 rpm ensemble also decreased from an average d_{50} of 0.23 mm (±0.014) on day 0 to 0.20 mm (±0.019), 0.22 mm (±0.008) and 0.18 mm (±0.008) for the x4, x2 and x1 dilutions under all light conditions respectively (Table 2-2). The decrease in mean and median particle sizes suggests shear-induced particle attrition.[60]

Table 2- 2*:* Statistical summary of particle size distribution characteristics from hydrodynamic OPG batches. Duplicate experimental sets with the standard deviation of ensemble indicated and all dimensions in mm.

Mixing (rpm)	Dilution factor		N	Mean (mm)	Standard Deviation	Mode (mm)	Median (D50) (mm)
	4	Day 0	2727	0.08	0.06	0.04	0.16
		Day 8 (6.4 KLux)	2134	0.15	0.13	0.04	0.22
		Day 8 (12.7 KLux)	6502	0.14	0.13	0.04	0.22
		Day 8 (25 KLux)	2132	0.16	0.16	0.04	0.23
	2	Day 0	59	0.06	0.05	0.04	0.15
20		Day 8 (6.4 KLux)	2820	0.13	0.13	0.05	0.19
		Day 8 (12.7 KLux)	3996	0.18	0.23	0.05	0.22
		Day 8 (25 KLux)	2820	0.14	0.14	0.05	0.20
	1	Day 0	19	0.06	0.03	0.04	0.15
		Day 8 (6.4 KLux)	723	0.11	0.08	0.04	0.18
		Day 8 (12.7 KLux)	859	0.13	0.11	0.05	0.20
		Day 8 (25 KLux)	1255	0.12	0.10	0.05	0.20
	4	Day 0	2446	0.16	0.14	0.06	0.24
		Day 8 (6.4 KLux)	9032	0.11	0.09	0.04	0.19
		Day 8 (12.7 KLux)	8779	0.15	0.14	0.04	0.19
		Day 8 (25 KLux)	9183	0.15	0.11	0.04	0.23
	2	Day 0	296	0.13	0.08	0.06	0.24
50		Day 8 (6.4 KLux)	8779	0.15	0.14	0.04	0.22
		Day 8 (12.7 KLux)	7310	0.16	0.15	0.04	0.23
		Day 8 (25 KLux)	9161	0.14	0.14	0.04	0.21
	1	Day 0	42	0.11	0.06	0.06	0.21
		Day 8 (6.4 KLux)	102	0.11	0.08	0.04	0.19
		Day 8 (12.7 KLux)	37	0.09	0.08	0.05	0.17
		Day 8 (25 KLux)	172	0.10	0.08	0.04	0.18
	4	Day 0	285	0.12	0.05	0.06	0.24
		Day 8 (6.4 KLux)	4096	0.13	0.11	0.04	0.20
		Day 8 (12.7 KLux)	5125	0.14	0.12	0.04	0.21
		Day 8 (25 KLux)	1303	0.09	0.08	0.04	0.17
	2	Day 0	285	0.12	0.05	0.06	0.22
80		Day 8 (6.4 KLux)	1899	0.11	0.10	0.04	0.18
		Day 8 (12.7 KLux)	322	0.09	0.07	0.04	0.18
		Day 8 (25 KLux)	170	0.09	0.05	0.04	0.18
	1	Day 0	42	0.11	0.06	0.06	0.21
		Day 8 (6.4 KLux)	185	0.10	0.07	0.04	0.18
		Day 8 (12.7 KLux)	26	0.07	0.04	0.04	0.17
		Day 8 (25 KLux)	17	0.07	0.05	0.04	0.16

The 80 rpm ensemble had an average initial mean particle size of 0.12 mm (± 0.002). This mean was conserved at 0.12 mm (±0.026) for x4 dilution while decreasing to an average 0.10 mm (± 0.008) and 0.08 mm (± 0.018) for x2 and x1 dilutions, respectively (Table 2- 2). The median particle size for the 80 rpm set on day 0 was, on average, 0.22 mm (±0.017). This decreased to an average d_{50} of 0.19 mm (±0.020) for x4 dilutions, 0.18 mm (±0.003) for x2 dilution and 0.17 mm (± 0.007) for x1 dilution. Compared to day 0 samples, most 80 rpm sets experienced a shift towards smaller particle size distribution (Figure 2- 1-[*g,h,i*]).

Shear has been widely documented as an essential driver [28–30,60] for bio-aggregation and formation of granules due to resultant particle-particle interactions.[40] Shear stress can result in both particle adherence and disintegration and is responsible for granular smoothing via abrasion similar to that experienced by sediments in benthal zones.[40] The overall decrease in both mean and median size for the 50 rpm and 80 rpm ensemble can be attributed to particle breakage and detachment resulting from higher mixing induced particle-particle collisions.[40,60] However, the positive skews observed in some 50 and 80 rpm sets (Figure 2- 1-[*d, i*]) indicate an increase in the concentration of larger particle sizes. This increase and observed OPGs in 50 rpm and 80 rpm (6.4 KLux, x4 dilution) samples, suggests a microbially driven aggregation withstanding the shear limitations,[62,63] hence the smaller size decrease compared to x2 and x1 dilution sets from day 0 mean size (Table 2- 2).

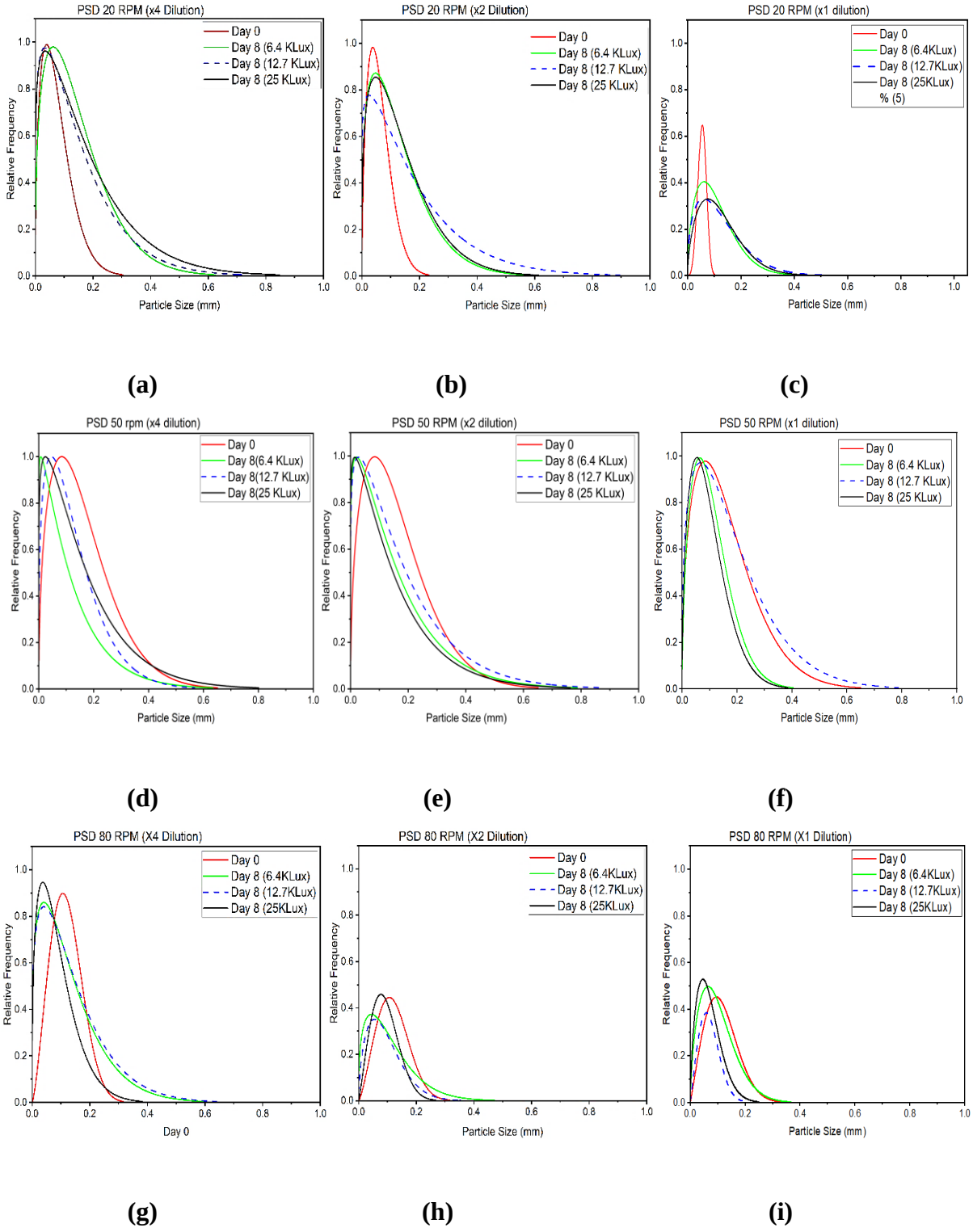

Figure 2- 1: Particle size distribution (Weibull distribution) showing the relative frequency of number of particles of each size to total number of particles within the sample (n>235) (a),(b),(c) 20 RPM (d),(e),(f) 50 RPM (g),(h),(i) 80 RPM.

2.4.2 Settleability

Aggregation of inorganic and organic particles altering the physical properties of solid flocs fosters their separation from the water via Stokesian settling mechanics.[64] Bioaggregation results in higher settling velocities (zone or hindered) compared to that of discrete particles. The ease of solids separation in wastewater treatment, as measured by the sludge volume index (SVI), is often used as an operational signal on the effectiveness of a treatment process.[65–68] SVI is expressed as the volume occupied by the mass of settled biomass, for example, in 5 minutes (SVI5) or 30 minutes (SVI30). Low SVI values characterize rapidly settling solids. Well settled activated sludge systems have SVI30 values of roughly 150 mL/g and higher values are indicative of bulking sludge.[69–72] The undiluted initial activated sludge inoculum for all experimental sets had an average SVI5 of 221 mL/g (Figure 2- 2) and an SVI30 of 219 mL/g (Figure 2- 3).

OPGs have a reported average SVI30 of 53 mL/g,[8] while aerobic granules have a reported average SVI5 of 88 mL/g [73–75] and algal bacterial granules an average SVI5 of 47.5 mL/g.[22] Initial SVI5 values for the sludge inoculum were on average 798 mL/g and 432 mL/g and SVI30 values of 235 mL/g and 246 mL/g for x4 and x2 dilutions, respectively (Figure 2- 2, Figure 2- 3). The increase of SVI5 with dilution suggests poor settleability reflecting the relative difference of solids concentration in the initial samples after dilution. Dilution-induced reduction in inter-particle interaction diminishes flocculant (Type II) and hindered (Type III) settling effects of activated sludge.[36] A decline in both SVI5 (Figure 2- 2) and SVI30 (Figure 2- 3) indices were observed for dilute inoculum sets under most mixing and light conditions over the experimental period.

The SVIs for x4 dilution (6.4 KLux) under all mixing conditions decreased to <100 ml/g comparable to values reported for other granule aggregates. This result suggests the progression of granulation within the reactors under these conditions. In contrast, the SVI5 of undiluted samples changed marginally over the same period (Figure 2- 2). Moreover, the SVI30s of undiluted sets also decreased (Figure 2- 3) other than in 20 rpm-6.4 Klux and 12.7 Klux samples (Figure 2- 3-a). While low SVIs are surrogates for aggregation, this later result alludes to the incongruity of using a single SVI index to predict the success of granulation.

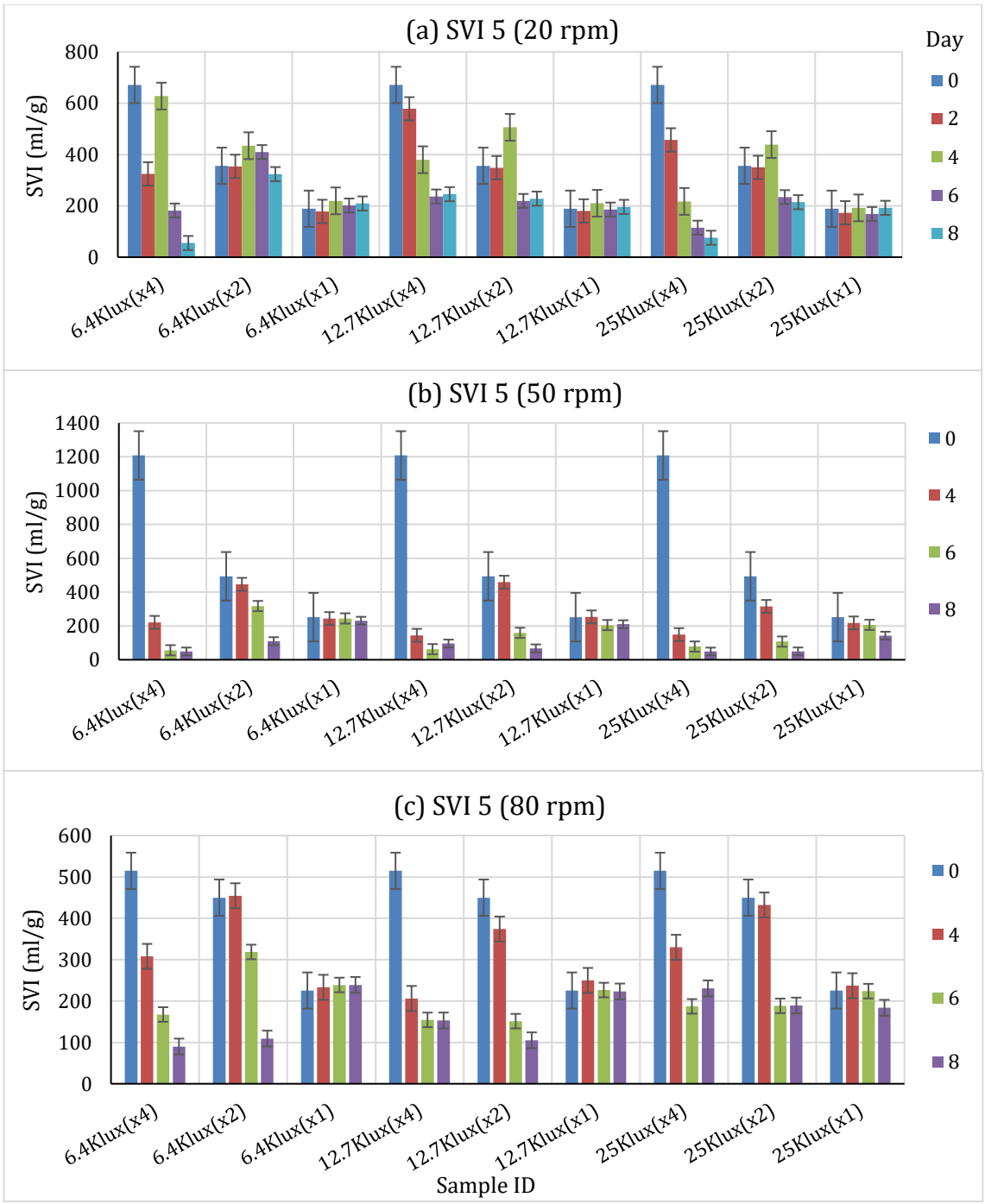

Figure 2- 2: SVI 5 (mL/g) values for a) 20 rpm b) 50 rpm c) 80 rpm over the experimental period from day 0 to day 8. Different vertical scales used to reflect the disparity of SVI5 magnitudes. Error bars represent the standard error of duplicate averages for each condition.

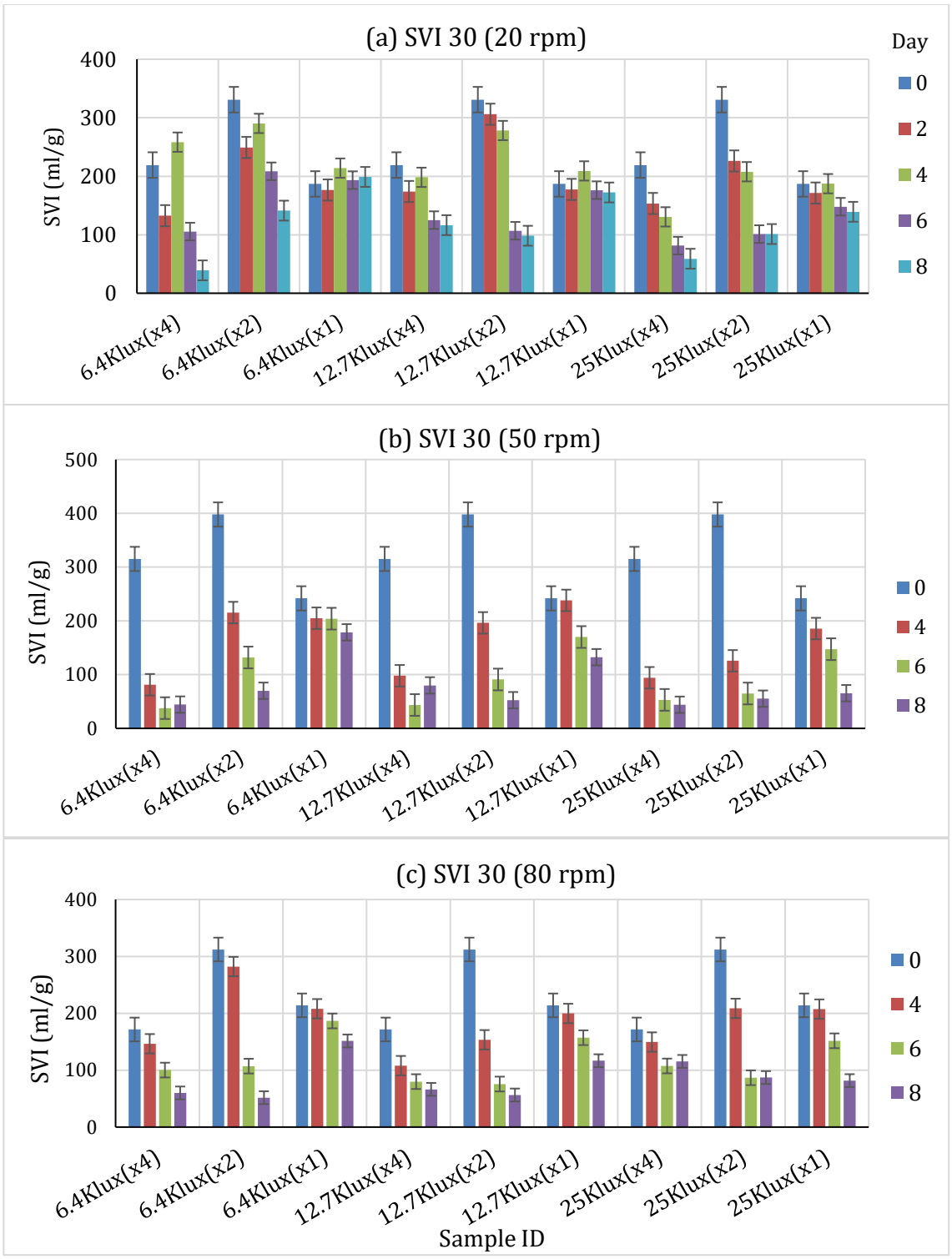

Figure 2- 3*:* SVI 30 (mL/g) values for a) 20 rpm b) 50 rpm c) 80 rpm over the experimental period from day 0 to day 8. Different vertical scales used to reflect the disparity of SVI30 magnitudes. Error bars represent the standard error of duplicate averages for each condition.

A temporal increase in settling velocities translates to both decrease and convergence of the ratio of SVI 5/SVI 30.[59] We hence applied this ratio as a characteristic metric for granulation. The SVI5/SVI30 ratio decreased for x4 dilution samples under all mixing and light conditions (Figure 2- 4), with 50 rpm sets having the highest decrease (70%) between days 0 and 8 (Figure 2- 4-b) alluding to improved settleability consistent with granulation (Figure 2- 5-b). This decrease in 50 rpm sets corresponds to low terminal SVI5 of 49 mL/g, 96 mL/g, and 48 mL/g for 6.4 KLux, 12.7 KLux and 25 KLux, respectively, a strong indication of granulation (Figure 2- 2 -b). An increase in the SVI5/SVI30 ratio for x2 dilution samples under all light conditions for 20 rpm sets was observed, suggesting deteriorating settleability (Figure 2- 4-a) and no granules formed (Figure 2- 5-a). In contrast, the SVI5/SVI30 ratio for x2 dilution sets with 50 rpm and 80 rpm decreased by day 8 after an initial increase other than in 80 rpm (25 KLux) sample which levelled off (Figure 2- 4-b,c). This trend suggests potential bio aggregation (Figure 2- 5-[b, c]) after an initial acclimation period to shear stress. Undiluted sets under different light and mixing conditions had increasing or unchanging SVI5/SVI30 over the batch period, indicating no sign of improved settleability (Figure 2- 4). This trend contrasts with the decrease in SVI5 observed for some sets (50 rpm,x1 dilution-Figure 2- 4-b) indicating that increased settling velocities cannot be sole proxies for successful granulation (Figure 2- 5).

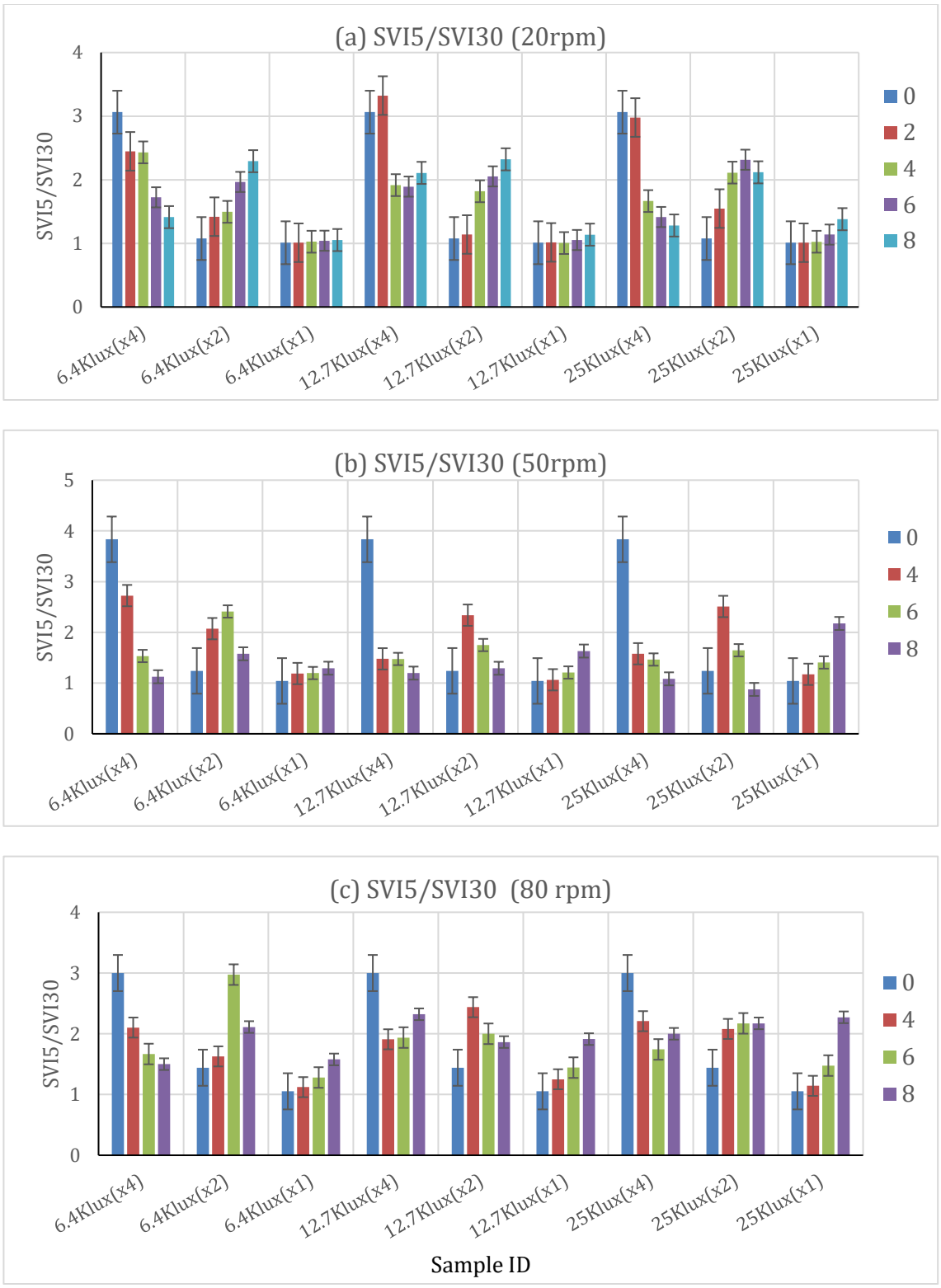

Figure 2- 4: SVI5/SVI30 ratio a) 20 rpm b) 50 rpm c) 80 rpm over the experimental period from day 0 to day 8. Error bars represent the standard error of each averaged ratio for each condition.

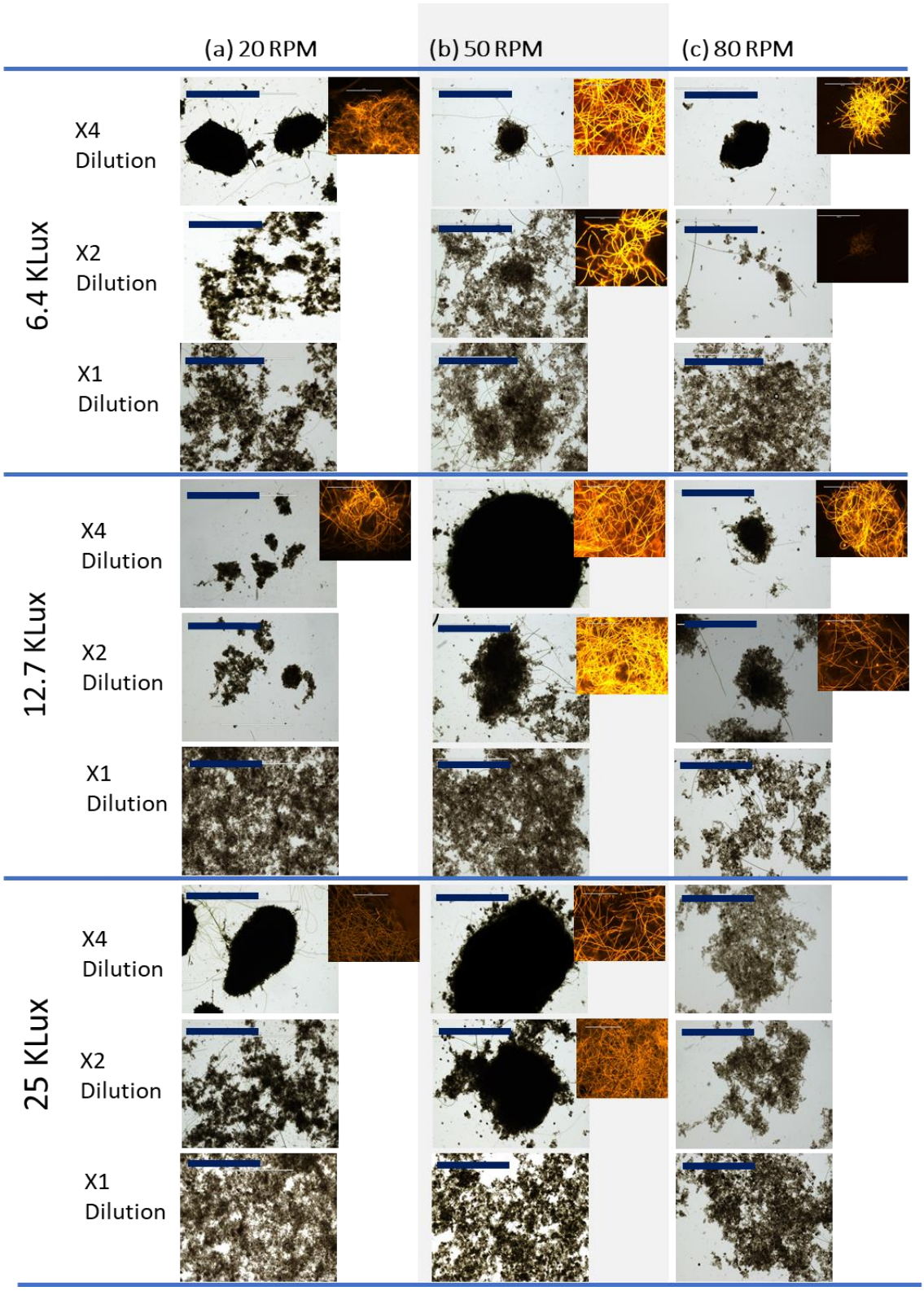

Figure 2- 5: Brightfield images of grab samples on day 8 under different experimental conditions. Insets (Not to scale) show phycocyanin auto-fluorescence. Scale bars are 2000µm.

A general linear model (GLM),[76] was fit to the day 6 and day 8 SVI5/SVI30 data (Table 2- 3) for experimental conditions. The model results indicated statistically significant effects ($p<0.05$) of the three parameters, light, mixing, and dilution, applied to the SVI ratio (SVI5/SVI30) with an R^2 of 76% and 70% for day 6 and day 8, respectively suggesting interdependence in their influence on the SVI ratios. The model parameters also indicate a better fit on day 6 compared to day 8. The R^2 (adjusted) indicates 62% improvement of the model due to added variables on day 6 and decreases to 52% on day 8. However, the lower R^2 (predicted) values indicate potential model overfit attributable to some operational conditions utilized. This result suggests that variability of the experimental conditions impacts the SVIs ratio metric. For example, continued illumination from day 6 can alter the phototrophic composition of biomass impacting the settleability and granulation. Some sample sets had increases in mean particle size, e.g. in undiluted samples under 20 rpm (Table 2- 2), without a corresponding decrease in the SVI5/SVI30 ratio (Figure 2- 4-a). This trend suggests that the size increase had minimal impact on the settleability due to the morphology of the aggregates formed.

Table 2- 3: General linear model fit parameters for SVI5/SVI30 ratios.

SVI day	**Std. Dev**	**P**	**R^2**	**R^2(adj)**	**PRESS**	**R^2(pred)**
Day 6	0.28	2.365E-5	76.02%	62.16%	7.46	50.96%
Day 8	0.35	3.346E-7	69.75%	52.28%	9.93	44.49%

2.4.3 Phototrophic enrichment

Granulation of hydrostatic OPGs was characterized by phototrophic development.[18,19] Similarly, we observed a color change of sludge inoculum from brown to green, implying phototrophic enrichment with particle size changes (Figure 2- 1) in some experimental sets from day 4 of the experiments. Ultimately, the observed phototrophic enrichment in the hydrodynamic batches occurred along with granular development in some sets (Figure 2- 5) and decreasing SVI5/SVI30 ratios (Figure 2- 4). Granulation was observed in x4 dilution samples under all mixing and light conditions except in 25 Klux 80 rpm sets. This granulating sets also presented a decreasing and converging SVI ratio index (Figure 2- 4-a) Granules were also observed in x2 dilution samples with 20 rpm (6.4 Klux) and with 50 rpm under all irradiances (Figure 2- 5-b). The photogranules' outer surface was dominated by motile filamentous cyanobacteria forming an interwoven mat-like structure [17] (Figure 2- 6), bearing morphological similarity to OPGs cultivated under hydrostatic conditions.[17,18]

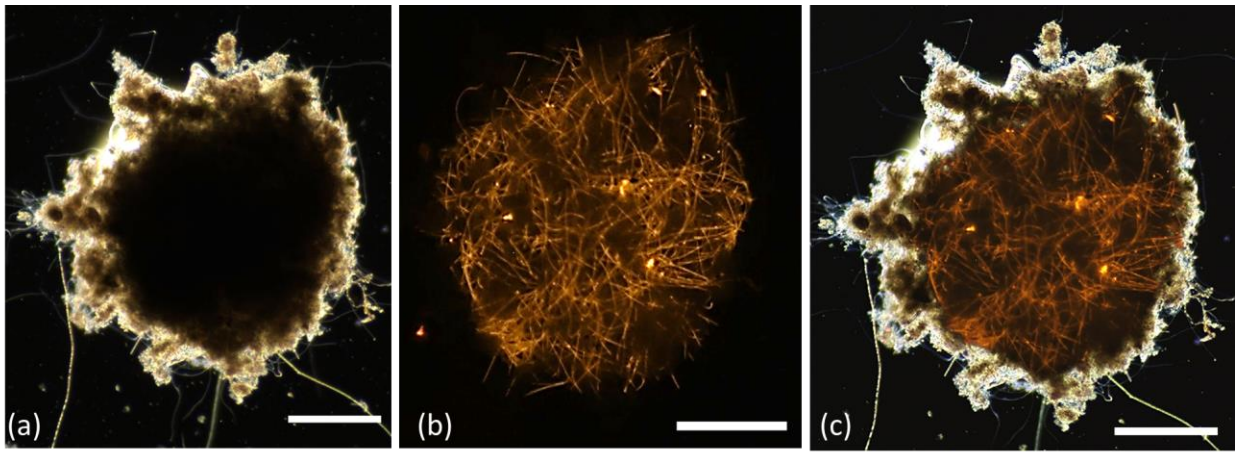

Figure 2- 6: Oxygenic photogranules generated under 20 rpm mixing with 6.4 KLux and x4 dilution. (a) Brightfield image (BF), (b) Cyanobacterial red fluorescence protein (RFP) auto-fluorescence, and (c) BF and RFP superimposed image. The scale bars are 500 µm.

The observed size increase (Figure 2- 1), improving SVI ratio indices (Figure 2- 4-a) and granular development (Figure 2- 5, Figure 2- 6) in 20 rpm x4 dilution sets mirrored that reported for hydrostatic cultivation of OPGs.[24] The development was characterized by an initial decay phase with decreasing DO levels (Figure 2- 7-a) followed by a stage of phototrophic bloom with a color change from brown to green and increase of all chlorophyll pigments to day 4 (Figure 2- 8-[a, b]), Figure 2- 9-a). Thereafter, the trend of chlorophyll *a* concentration for 20 rpm and x4 dilution under all light conditions had a plateau phase between day 4 and 6 (Figure 2- 8-a) while both chlorophyll *b* and chlorophyll *c* decreased. Between days 6 and 8, an increase in both chlorophyll *a* and *b* concentration along with a marginal change in the chlorophyll *c* concentrations was observed.

The period after day-4 was also characterized by increased DO levels, suggesting photosynthetic oxygenation (Figure 2- 7-a). The other 20 rpm ensemble sets had similar initial chlorophyll trend (Figure 2- 8-[a,b], Figure 2- 9-a) with samples under 25 KLux having the highest chlorophyll *a* peak for each dilution cluster by day-4 (Figure 2- 8-a). A subsequent increase of chlorophyll *a* (Figure 2- 8-a) concentrations ensued between days 4 and 6. This increase was accompanied by a decrease of both chlorophyll *b* (Figure 2- 8-b) and chlorophyll *c* concentrations except for 25 Klux sample concentrations which increased (Figure 2- 9-a). This trend was followed by an increase in chlorophyll pigments concentration after cultivation day 6 to the end of the experiment (Figure 2- 8-[a,b], Figure 2- 9-a). Correlation coefficients for chlorophyll trends were r=0.77 and 0.46

between chlorophylls *a and b* and chlorophyll *a and c*, respectively. Chlorophyll *b* and *c* had a correlation coefficient of r=0.62.

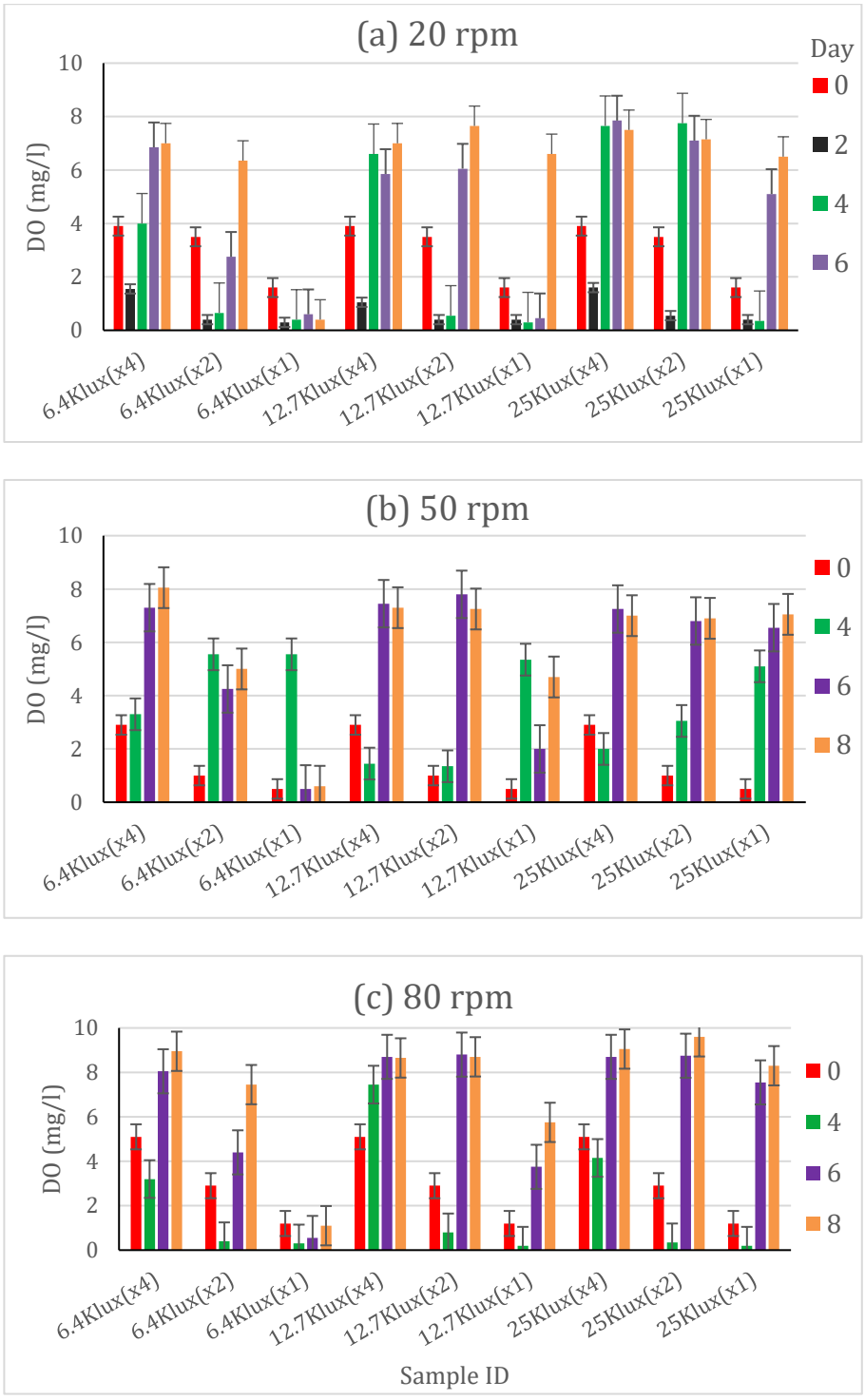

Figure 2- 7: Plots of dissolved oxygen concentrations (mg/l) under a) 20 rpm, b) 50 rpm, c) 80 rpm mixing. Error bars show the standard error of averaged duplicate readings.

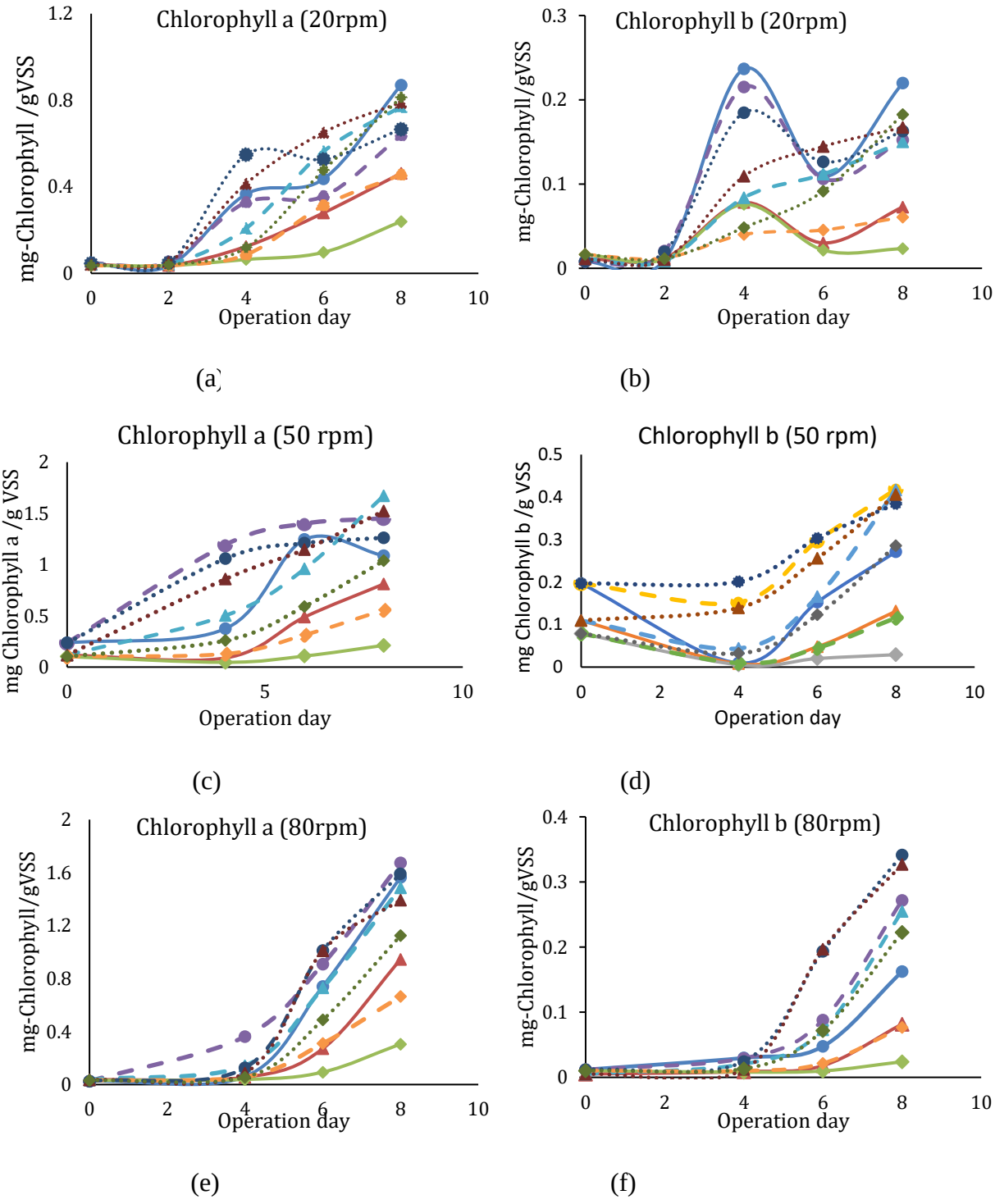

Figure 2- 8: Chlorophyll a and Chlorophyll b concentrations (a) and (b) 20 rpm (c) and (d) 50 rpm (e) and (f) 80 rpm. The (Solid─) lines represent samples under 6.4 KLux, (Dashed ---) lines 12.7 Klux, and (Dotted……) lines 25 KLux irradiances. The symbol (○) represents x4 dilution, (Δ) x2 dilution, and (◊) x1 dilution sets.

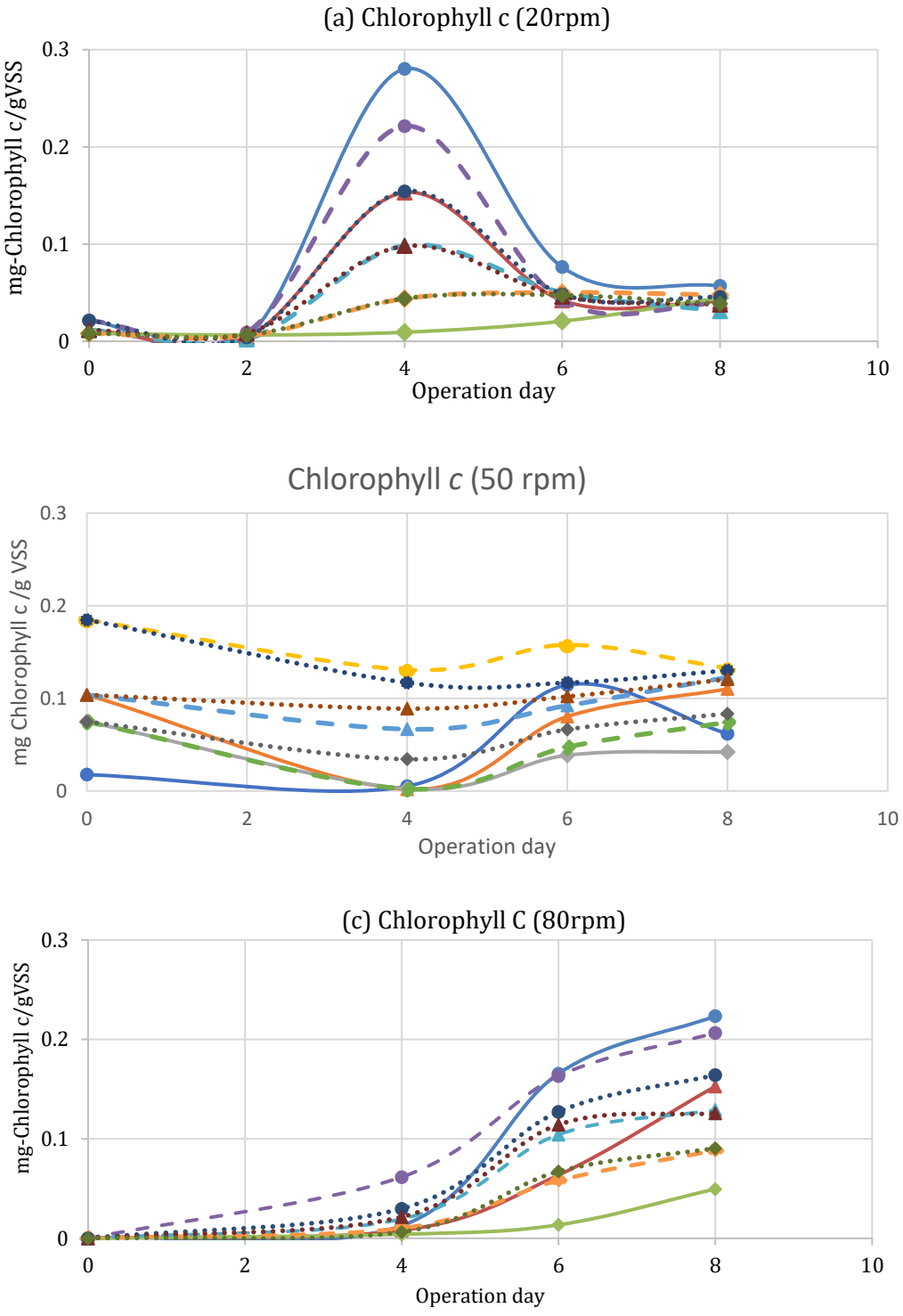

Figure 2- 9: Chlorophyll c concentrations with mgChl-b/gVSS. (a) 20 rpm (b) 50 rpm (c) 80 rpm. (Solid─) lines are 6.4 Klux samples, (Dashed ---) lines are 12.7 Klux samples and (Dotted……) lines are 25 Klux samples. (○) represents x4 dilution, (Δ) x2 Dilution, and (◊) x1 Dilution sets.

For sets under 50 rpm agitation, a general increase in chlorophyll *a* concentration (Figure 2- 8-c) was accompanied by marginal changes in both chlorophyll *b* (Figure 2- 8-d), and chlorophyll *c* (Figure 2- 9-b) concentrations by day 4. Only x4 dilution sets under 12.7 and 25 Klux, followed a DO troughing trend to day 4 (Figure 2- 7) with persistent DO increase observed it the other 50 rpm sets. The chlorophyll *a* pigment concentration (Figure 2- 8-c) increased beyond day 4 to the end of the experiment. The chlorophyll *a* pigment concentration increased with dilution from x1 to x4 up to day 6 in all inoculum concentrations. This increase can be ascribed to elevated light energy interactions per particle concentration from higher agitation. Similarly, chlorophyll *b* concentrations increased after day 4 other than in 6.4 KLux (x1) sets (Figure 2- 8-d). The chlorophyll *c* concentrations for most sets decreased to day 4, increased to day 6, and remained constant upto day 8. The chlorophyll *c* concentrations for x4 dilution (6.4 KLux,12.7 KLux) sets decreased to day 8 (Figure 2- 9-b). The chlorophyll *a* trend had a positive correlation (r=0.64) with chlorophyll *b* and was negatively correlated to chlorophyll *c* (r= -0.11) in the 50 rpm sets.

The 50 rpm chlorophyll *a* and *b* concentration trends were positively correlated (r=0.94 and 0.35, respectively) with those of 20 rpm sets. A strongly negative correlation (r= -0.74) of chlorophyll *c* trends, was observed between the two mixing ensembles. In contrast to 20 rpm sets, the phototrophic enrichment in 50 rpm ensemble occurred in tandem with a decrease in the median and mean particle sizes for x4 and x1 dilutions (Table 2- 2). Under the 80 rpm sets, an increase of chlorophyll *a* pigment concentration (Figure 2- 8-e) was observed over the experimental period. Samples under 12.7 KLux (x4

dilution) had increasing chlorophyll *c* concentration (Figure 2- 9-c), while other chlorophyll *b* and *c* pigment concentrations remained relatively constant by day 4. An increase in chlorophyll *b* and *c* pigment concentrations occurred beyond day 4 to the end of the experiment. Sets with x4 dilution had the highest chlorophyll *a* peak for all irradiances, congruent to increase or marginal decrease of mean particle sizes (Table 2- 2) and low SVI5 indices (Figure 2- 2-c).

For the 80 rpm ensemble, trends in chlorophyll *a* concentration were strongly correlated to that of both the chlorophyll *b* and *c*, accessory pigments associated with eukaryotic phototrophs [77–79] with an average r=0.97. Chlorophyll *b* and *c* had a slightly lower correlation with r=0.91. The correlation coefficients of 80 rpm chlorophyll *a* concentration trends were r= 0.93 and 0.89 with 20 rpm and 50 rpm ensembles, respectively. Lower correlations were also observed for chlorophyll *b* (r=0.53,0.76) and (r=0.1,-0.07) chlorophyll *c* between 80-20 rpm and 80-50 rpm, respectively. The positive correlation is consistent with observed overall phototrophic enrichment in all ensembles (Figure 2- 8, Figure 2- 9). The low and negative correlations for chlorophyll *a* and *c* reflect environmental influences on phototrophic microbial selection.[77,79]

An increase in the chlorophyll *a/b* ratio coupled with a decrease in the chlorophyll *b* and *c* concentration would suggest cyanobacterial enrichment.[18] Conversely, a decrease in chlorophyll *a/b* ratio with increasing chlorophyll *b* and *c* concentration alludes to a decline in phototrophic microbial communities without chlorophyll *b* and *c* pigments, such as cyanobacteria.[79] For the 20 rpm ensemble, the ratio increased from day 0 to day

2, other than in x4 dilution sets, followed by a decrease to day 4, subsequently increasing by day-6 (Figure 2- 10-a). The ensemble average peak chlorophyll a/b ratio on day 6 was 5.2 (±1.8) which is higher than the reported 2.2 average for algae.[18]

On the other hand, the chlorophyll *a/b* ratio under 50 rpm (Figure 2- 10-b) increased to day 4 for the entire ensemble. A concurrent decrease in chlorophyll *c* pigments (Figure 2- 9-b) suggest a decline in phototrophic microbes with chlorophyll *c* light-harvesting pigments [80]. Beyond day 4, a general decreasing trend in the chlorophyll *a/b* ratio for 50 rpm sets ensued to day 6. The decrease in the ratio corresponded to increasing chlorophyll *b* and *c* pigments (Figure 2- 8-d, Figure 2- 9-b). For 80 rpm sets (Figure 2- 10-c), the chlorophyll *a/b* ratio increased or changed marginally for most sets to day 4, other than for 12.7 KLux (x4 dilution) sets whose ratio increased six-fold to 12. Further, chlorophyll *a/b* ratio of this 12.7 Klux (x4 dilution) and 25 KLux (x2 dilution) sets decreased to day 6, while that of other sets increased in the same period with an average peak of 10.2 (±3.8). The ratios of all 80 rpm sets except in x1 dilution (6.4 KLux) decreased to day 8 (Figure 2- 10-c). This ratio decline mirrored observed trends under 50 rpm sets beyond day 4 (Figure 2- 10-b) but not in most 20 rpm ensemble sets (Figure 2- 10-a). The decline can be attributed to higher light energy flow as a result of mixing, dilution and light intensity inducing phototrophic stress [45,49]. Moreover, the better linear model fit on day 6 compared to day 8 (Table 2- 3) is potentially due to the influence of algae enrichment seen with the decrease of chlorophyll a/b along with an increase in chlorophyll *b* (Figure 2- 10, Figure 2- 8) affecting settleability in all sets.

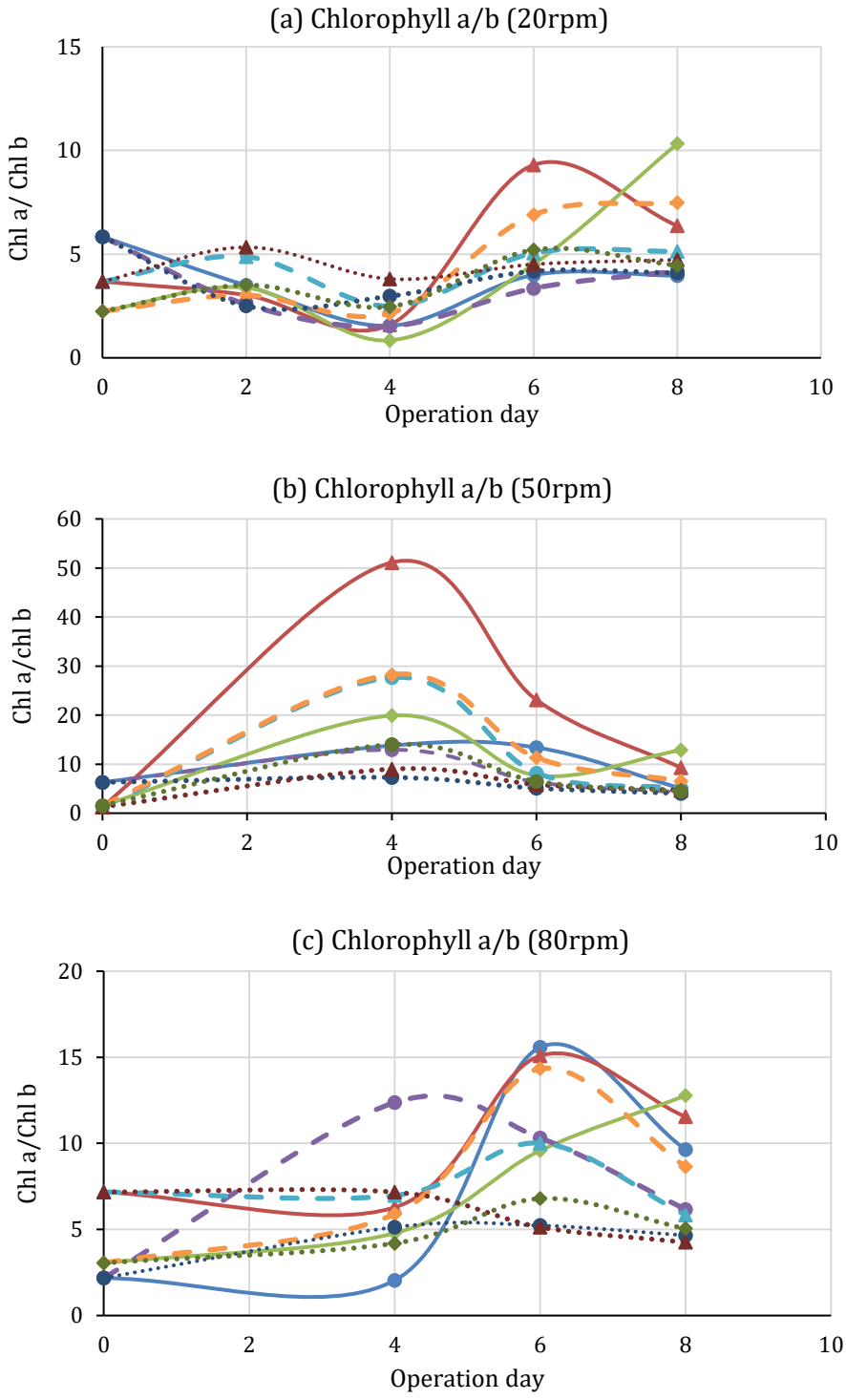

Figure 2- 10: Chlorophyll a/b ratios (a) 20 rpm (b) 50 rpm (c) 80 rpm. Different x-axis scales used due to substantially different chlorophyll a/b ranges among the mixing speed. (Solid─) lines are 6.4 KLux irradiance samples, (Dashed ---) lines are 12.7 KLux samples and (Dotted……) lines are 25 KLux samples. (○) represents x4 dilution, (Δ) x2 Dilution, (◊) x1 Dilution sets.

2.5 Discussion

Current research on granule-based wastewater treatment focuses on understanding granules operational and functional characteristics to improve their engineering application.[41,59,81,82] For photogranular biomass, photosynthesis, the keystone process, proffers additional functional complexity due to its elasticity to variability in quantity and quality of light.[1,26,46,83,84] The phototrophic microbes are also essential for either granular structure such as in algal-bacterial aggregation with aeration [22–25] or both the structure and function for self-aerated processes -OPG.[8,17,18,21] In the latter, maintaining functional integrity involves balancing the photosynthetic rate generating oxygen and the microbial consortia respiration rates consuming oxygen for COD removal and ammonia oxidation.

We examined the potential for hydrodynamic granulation of oxygenic photogranules (OPGs) from activated sludge inoculum. While different combinations of conditions were examined, the batch sets having 20 rpm and 50 rpm mixing, combined with x4 and x2 dilute activated sludge inoculum with different light conditions tested were found to be amenable for rapid (less than 8 days) formation of OPGs (Figure 2- 5). The higher mixing speed 80 rpm (73 s^{-1}) formed granules only with x4 dilute inoculum and 6.4 Klux light conditions (Figure 2- 5-b). In addition, no OPGs were observed in the undiluted inoculum (Figure 2- 5), which had increasing SVI ratio indices (Figure 2- 4). These variable experimental outputs indicate a granulation promoting confluence of diverse magnitudes of applied variables.

OPGs can hence be said to develop due to the favourable interaction of kinetic, biochemical, and light energies in various proportions. OPG granulation, on the one hand, occurs under negligible kinetic energy (i.e., hydrostatic photogranulation) [17–19] but also occurs in the shear ecosystem in reactors (i.e., reactor operation).[8,21] This study showed that high agitation rates (i.e., 80 rpm) resulted in a decline of particle sizes (Figure 2- 1-[g-i], Table 2- 2) and curtailed aggregation in contrast to the lower agitation rates (50 rpm; 20 rpm) as seen with the increasing trend of SVI ratios (Figure 2- 4-c). However, when combined with low light intensity 6.4 KLux and x4 dilution, OPGs were formed at this high shear. The 50 rpm sets, resulted in granulation under a broader range of dilutions and light intensities (Figure 2- 4-b, Figure 2- 5).

Agitation of OPG reactors induces shear on the fluid and particle matrices of inocula. The mean shear rates determined for this hydrodynamic OPGs cultivation study were 11 s^{-1}, 39 s^{-1} and 73 s^{-1} for the 20 rpm, 50 rpm, and 80 rpm respectively [50]. Various investigators have reported on the importance of shear as a selection pressure for granular formation.[31,39,60] Hydrodynamic forces distribute the mass flux within the reactor and initiate particle-particle interaction with induced shear sculpting the resultant three-dimensional structure.[40] Moreover, the increase in hydrophobicity induced by strong shear is essential for the initial cell to cell contact as it reduces the surface free Gibbs energy of the cells resulting in their separation from the liquid phase.[31,40,75]

The SVI5/SVI30 ratio (Figure 2- 4) and PSD trends indicate sustained aggregation of biomass in the lower shear rate (20 rpm and 50 rpm) conditions compared to the high

shear rate 80 rpm sets (Table 2- 2). Propagation of OPGs has been reported in reactor operations with a calculated shear rate of 38 s^{-1} [8] comparable to 50 rpm conditions. This similarity suggests an ideal shear threshold for granulation for the substrate conditions investigated. Low shear potentially favors the persistence of any particle interactions due to minimal particle attrition. Moreover, while OPGs were formed in other dilutions, no identifiable granules were observed in undiluted sets. Increasing solids concentration distorts the viscosity of the bulk fluid transforming its rheology from a Newtonian dominated flow into a particle-particle interaction flow suspension.[87,88] In addition, higher solid fractions necessitate higher shear stress for solvent shearing.[87]

High agitation in reactors, 80 rpm, resulted in a calculated eddy length scale of 117 µm smaller than the observed mean ensemble size of 117 µm and median particle size of 220 µm in the inoculum (Table 2- 2). A higher viscosity in undiluted samples results in higher shear stress on particles if eddy length scales are equal to or smaller than sizes of biomass [62] decreasing particle sizes. In addition, enhanced particle collisions and dissipation of kinetic energy limited the aggregation in this ensemble and decreased the bulk consortia size.[60] The granulation under 80 rpm mixing can be attributed to the ecology resistance to dominant particle interactions and shear stress,[62] especially with dilution (Figure 2- 5). An eddy length of 160 µm was determined for 50 rpm samples with a mean inoculum particle size of 132 µm and a median of 220 µm. On the other hand, the 20 rpm set had an eddy length scale [89] of 296 µm compared to the inoculum mean size of 72 µm and median 153 µm (Table 2- 2). The higher length scales of shear energy dissipation

compared to mean sizes and a reduced particle-particle collision could explain the observed persistent aggregation in the 20-50 rpm ensembles (Figure 2- 5).

Environmental microbial selection within the granular ecosystem is also dependent on the magnitude and balance of system energy.[86] Microbes have been reported to have different tolerance to shear due to their structure, morphology, and metabolism.[62] Algae have the highest shear tolerance compared to both cyanobacteria and dinoflagellates,[62] which may explain the persistence of algae under the 80 rpm agitation, with undiluted samples and lack of cyanobacteria. This algal persistence is seen with high chlorophyll *a,b* concentrations (Figure 2- 8-[e,f]) and decreasing chlorophyll *a/b* ratios (Figure 2- 10-c). Shear stress can lead to reduced growth rate, cell mortality, cell lysis,[62,63] and can have a detrimental effect on carbon and nitrogen fixation in cyanobacteria.[90] Fragments of filamentous cyanobacteria were observed in 80 rpm agitation batch set potentially due to shear-induced shredding of filamentous microbes limiting granulation.[17,40,90] This shear resistance variability can explain the decrease in chlorophyll *a/b* ratio for both 50 rpm and the 80 rpm (Figure 2- 4) reactors observed after day-6 despite increasing chlorophyll *a* and *b* concentrations. The decrease in any cyanobacteria populations, primarily due to high shear could have diminished their contribution to overall chlorophyll *a* concentration.

For OPGs, the light substrate provides essential photon energy for the photosynthetic transformation of substrates. The motility and entanglement of filamentous cyanobacteria have been postulated to be responsible for OPG development.[18] In the batch operation

adopted, light substrate utility is a function of both dilution and agitation as well as light intensity provided. Phototrophic enrichment had a high sensitivity to increasing light intensity (Figure 2- 8 to Figure 2- 10). Inoculum dilution allows for penetration of light, increasing light-biomass interaction compared to undiluted sets at the same mixing speed. The change in mean sizes had a high positive correlation to the light intensity ($r>0.85$) across all mixing speeds and dilution ($r>0.92$). Granulation was observed preferentially for the dilute sets characterized by a higher increase in both mean sizes and positive skew for 20 rpm agitation (Figure 2- 1-a/b). In addition, a higher mixing speed increases the incidence of light exposure at the same light intensity. The proportion of phototrophic enrichment increased with both the dilution and mixing speed (Figure 2- 8 to Figure 2- 10). Moreover, the concurrent granulation of OPGs with this enrichment in dilute samples, suggest ideal magnitudes for light substrate interaction necessary to induce the development of OPGs.

However, no OPGs were formed in high shear-light substrate conditions, e.g., 80 rpm-25 Klux and x4 dilution (Figure 2- 5). The high energy inflow from high agitation and light intensity were found to favor microalgae growth (Figure 2- 8- [e,f]) due to their higher resistance to both shear [62] and high-intensity light.[49] The lack of granulation can potentially be due to photoinhibition [49] and shear-induced granular limitation.[62] In the conditions evaluated, undiluted inoculum samples did not form granules despite OPG granulation being observed in hydrostatic conditions with undiluted AS inoculum and about 10 KLux light intensity.[17–19] Similarly, natural light and agitation present with

concentrated biomass in activated sludge aeration basins do not propagate phototrophic enrichment essential for OPG granules.[17]

Feast and famine selection pressure has been reported as requisite for granulation [28–31] with famine in the activated sludge inoculum at the start of the experiment consistent with operations of the AS reactors in steady state.[95] Biomass decay (Figure 2- 7) and resulting feast conditions support the growth of phototrophic biomass in both hydrodynamic and hydrostatic cultivation of OPGs.[18] This sequential feast-famine conditions in OPG granulation also induces selection pressures for microbial aggregation forming granules.[16,29,31]

Despite the different morphologies of biomass solids, both activated sludge and granular biomass systems employ similar inputs, namely, agitation, a wastewater stream, and a microbial consortium. In conventional activated sludge operations for wastewater treatment, no spontaneous granule formation has been reported to date. However, altered operational conditions have resulted in the formation of granular biomass using activated sludge inoculum.[17–19,74,85] Moreover, similar inputs exist in other environments, such as in waterways, where niche colonization takes the morphology of mats and biofilms.[2] Thus despite the prevalence of analogous conditions, the form and interactions of those conditions select for enhancement of different phenotypes.[86] It is thus evident that both operational conditions and some eco-physiology response are culpable for granulation.

The growth of polyphosphate accumulating organisms (PAOs) has been reported to be due to environmental selection of phenotypic characteristics that optimize energy allocation within the ecosystem.[86] For activated sludge, the interaction of kinetic and biochemical energy determines its existence as either flocs or granular biomass by promoting corresponding phenotypic characteristics. Filamentous bacteria, such as *Thiothrix*, also present in aerobic granules, form the structural backbones of AS flocs.[96,97] In large quantities, they can, however, cause bulking, compromising liquid-solid separation.[70] In AGS, these filamentous microbes are integral to the resultant spherical structure.[40,98]

Similarly, granulation, a ubiquitous phenomenon, occurs due to the interaction of macro inputs, energy, that coupled with biological responses result in the formation of granules. Results presented indicate the existence of multiple granulation frontiers with different combinations of macro energy inputs. The various ensembles of energy can be presented as a ‘zone of granulation interactions (Figure 2- 11). When these ‘goldilocks conditions’ are achieved, a bio-structural response ensues favouring spheroidal structures and enhancing selection of aggregating characteristics of cyanobacteria.

We propose that particle-particle attachment coupled with ecological associations as microbes seek a survival niche [98–100] occurs at the onset of granulation. This initial aggregation is compounded by increasing sizes of the micro flocs due to microbial growth, particle adherence, and filamentous entanglement.[18,40] Thereafter, microbial translocation and dominance in response to persisting environmental conditions seem to

occur in tandem with granular growth. Current approaches seek to identify discrete environmental conditions within this granulation enabling zone.[11] This research indicates the existence of a wide array of 'granulating' conditions. A systems-based broad perspective, such as conditional flux-based analysis,[86] can be used to identify the trade-offs for operational conditions selecting for granulation characteristics. Further research is necessary to develop appropriate formalism and to identify similarities in the biological response of different granules morphologies.

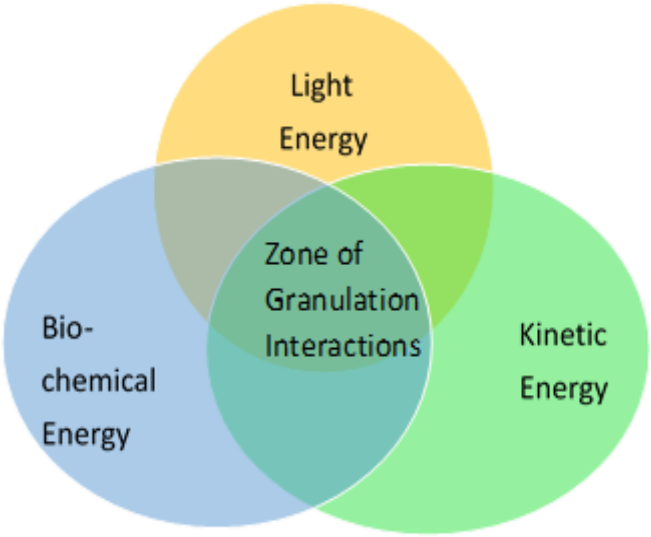

Figure 2- 11: Energy interaction for OPG granulation. The zone of interaction presents potential conditions where the interaction of different abiotic stresses promote granular biotic responses**.**

2.6 Bibliography

1. Barber, J. & Andersson, B. Too much of a good thing: light can be bad for photosynthesis. *Trends Biochem. Sci.* **17**, 61–66 (1992).

2. Donlan, R. M. Biofilms: Microbial Life on Surfaces. *Emerg. Infect. Dis.* **8**, 881–890 (2002).

3. Anderson, D. M., Glibert, P. M. & Burkholder, J. M. Harmful algal blooms and eutrophication: Nutrient sources, composition, and consequences. *Estuaries* **25**, 704–726 (2002).

4. Jensen, H., Biggs, C. A. & Karunakaran, E. The importance of sewer biofilms. *Wiley Interdiscip. Rev. Water* **3**, 487–494 (2016).

5. Ellison, C. K. *et al.* Obstruction of pilus retraction stimulates bacterial surface sensing. *Science* **358**, 535–538 (2017).

6. Liu, X.-W., Yu, H.-Q., Ni, B.-J. & Sheng, G.-P. Characterization, Modeling and Application of Aerobic Granular Sludge for Wastewater Treatment. in *Biotechnology in China I* 275–303 (Springer, Berlin, Heidelberg, 2009). doi:10.1007/10_2008_29.

7. Jasmine, D. A., Malarmathi, K. B., Daniel, S. K. & Malathi, S. Natural Algal-Based Processes as Smart Approach for Wastewater Treatment. *Smart Mater. Wastewater Appl.* 379–398 (2016).

8. Abouhend, A. S. *et al.* The Oxygenic Photogranule Process for Aeration-Free Wastewater Treatment. *Environ. Sci. Technol.* **52**, 3503–3511 (2018).

9. Cheremisinoff, N. P. *Handbook of Water and Wastewater Treatment Technologies*. (Butterworth-Heinemann, 2001).

10. Adav, S. S., Lee, D.-J., Show, K.-Y. & Tay, J.-H. Aerobic granular sludge: Recent advances. *Biotechnol. Adv.* **26**, 411–423 (2008).

11. Zhang, Q., Hu, J. & Lee, D.-J. Aerobic granular processes: Current research trends. *Bioresour. Technol.* **210**, 74–80 (2016).

12. McHugh, S., O'Reilly, C., Mahony, T., Colleran, E. & O'Flaherty, V. Anaerobic Granular Sludge Bioreactor Technology. *Rev. Environ. Sci. Biotechnol.* **2**, 225–245 (2003).

13. Noppeney, R. About the Nereda Wastewater Treatment Process. https://www.royalhaskoningdhv.com/en-gb/nereda/nereda-wastewater-treatment%20technology (2018).

14. Gao, D., Liu, L., Liang, H. & Wu, W.-M. Aerobic granular sludge: characterization, mechanism of granulation and application to wastewater treatment. *Crit. Rev. Biotechnol.* **31**, 137–152 (2011).

15. Haszprunar, G. The types of homology and their significance for evolutionary biology and phylogenetics. *J. Evol. Biol.* **5**, 13–24 (1992).

16. Abouhend, A., Butler, C., El-Moselhy, K. & Park, C. The Oxygenic Photogranule (OPG) for Aeration-free and Energy-Recovery Wastewater Treatment Process. in *Proceedings of the Water Environment Federation* vol. 2016 1–8 (2016).

17. Milferstedt, K. *et al.* The importance of filamentous cyanobacteria in the development of oxygenic photogranules. *Sci. Rep.* **7**, 17944 (2017).

18. Kuo-Dahab, W. C. *et al.* Investigation of the Fate and Dynamics of Extracellular Polymeric Substances (EPS) during Sludge-Based Photogranulation under Hydrostatic Conditions. *Environ. Sci. Technol.* **52**, 10462–10471 (2018).

19. Stauch-White, K., Srinivasan, V. N., Camilla Kuo-Dahab, W., Park, C. & Butler, C. S. The role of inorganic nitrogen in successful formation of granular biofilms for wastewater treatment that support cyanobacteria and bacteria. *AMB Express* **7**, (2017).

20. Ansari, A., Abouhend, A. S. & Park, C. (in minor revision) Effects of seeding density on photogranulation and the start-up of the oxygenic photogranule process for aeration-free wastewater treatment. *Algal Res.*

21. Park, C. & Dolan, S. (deceased). Patent Algal Sludge Granule OPG Jan 2019. 11 (2019).

22. Ahmad, J. S. M. *et al.* Stability of algal-bacterial granules in continuous-flow reactors to treat varying strength domestic wastewater. *Bioresour. Technol.* **244**, 225–233 (2017).

23. He, Q. *et al.* Natural sunlight induced rapid formation of water-born algal-bacterial granules in an aerobic bacterial granular photo-sequencing batch reactor. *J. Hazard. Mater.* **359**, 222–230 (2018).

24. Lee, C. S., Oh, H.-S., Oh, H.-M., Kim, H.-S. & Ahn, C.-Y. Two-phase photoperiodic cultivation of algal–bacterial consortia for high biomass production and efficient nutrient removal from municipal wastewater. *Bioresour. Technol.* **200**, 867–875 (2016).

25. Zhang, B. *et al.* Enhancement of aerobic granulation and nutrient removal by an algal–bacterial consortium in a lab-scale photobioreactor. *Chem. Eng. J.* **334**, 2373–2382 (2018).

26. Arcila, J. S. & Buitrón, G. Influence of solar irradiance levels on the formation of microalgae-bacteria aggregates for municipal wastewater treatment. *Algal Res.* **27**, 190–197 (2017).

27. Arcila, J. S. & Buitrón, G. Microalgae–bacteria aggregates: effect of the hydraulic retention time on the municipal wastewater treatment, biomass settleability and methane potential. *J. Chem. Technol. Biotechnol.* **91**, 2862–2870 (2016).

28. Liu, Y.-Q. & Tay, J.-H. Fast formation of aerobic granules by combining strong hydraulic selection pressure with overstressed organic loading rate. *Water Res.* **80**, 256–266 (2015).

29. B K, B. & G, M. Influence of three selection pressures on aerobic granulation in sequencing batch reactor. *Indian J. Chem. Technol. IJCT* **22**, 241–247 (2016).

30. Qin, L., Tay, J.-H. & Liu, Y. Selection pressure is a driving force of aerobic granulation in sequencing batch reactors. *Process Biochem.* **39**, 579–584 (2004).

31. Bindhu, B. k. & Madhu, G. Selection pressure theory for aerobic granulation – an overview. *Int. J. Environ. Waste Manag.* **13**, 317–329 (2014).

32. Zhang, C., Sun, S., Liu, X., Wan, C. & Lee, D.-J. Influence of operational conditions on the stability of aerobic granules from the perspective of quorum sensing. *Environ. Sci. Pollut. Res.* **24**, 7640–7649 (2017).

33. Wood-Black, F. Considerations for Scale-Up – Moving from the Bench to the Pilot Plant to Full Production. in *Academia and Industrial Pilot Plant Operations and Safety* vol. 1163 37–45 (American Chemical Society, 2014).

34. Isanta, E. *et al.* Long term operation of a granular sequencing batch reactor at pilot scale treating a low-strength wastewater. *Chem. Eng. J.* **198**–**199**, 163–170 (2012).

35. Li, Y. & Liu, Y. Diffusion of substrate and oxygen in aerobic granule. *Biochem. Eng. J.* **27**, 45–52 (2005).

36. Wilén, B.-M., Liébana, R., Persson, F., Modin, O. & Hermansson, M. The mechanisms of granulation of activated sludge in wastewater treatment, its optimization, and impact on effluent quality. *Appl. Microbiol. Biotechnol.* **102**, 5005–5020 (2018).

37. Meyer, R. L., Saunders, A. M., Zeng, R. J., Keller, J. & Blackall, L. L. Microscale structure and function of anaerobic—aerobic granules containing glycogen accumulating organisms. *FEMS Microbiol. Ecol.* **45**, 253–261 (2003).

38. Etterer, T. & Wilderer, P. A. Generation and properties of aerobic granular sludge. *Water Sci. Technol.* **43**, 19–26 (2001).

39. Chen, Y., Jiang, W., Liang, D. T. & Tay, J. H. Structure and stability of aerobic granules cultivated under different shear force in sequencing batch reactors. *Appl. Microbiol. Biotechnol.* **76**, 1199–1208 (2007).

40. Liu, Y. & Tay, J.-H. The essential role of hydrodynamic shear force in the formation of biofilm and granular sludge. *Water Res.* **36**, 1653–1665 (2002).

41. Sengar, A., Basheer, F., Aziz, A. & Farooqi, I. H. Aerobic granulation technology: Laboratory studies to full scale practices. *J. Clean. Prod.* **197**, 616–632 (2018).

42. Brito, A. C. & Newton, A. Measuring Light Attenuation in Shallow Coastal Systems. *J. Ecosyst. Ecography* **03**, (2013).

43. Gallegos, C. L. & Moore, K. A. Factors contributing to water-column light attenuation. (2000).

44. Krause-Jensen, D. & Sand-Jensen, K. Light attenuation and photosynthesis of aquatic plant communities. *Limnol. Oceanogr.* **43**, 396–407 (1998).

45. Jahn, M. *et al.* Growth of Cyanobacteria Is Constrained by the Abundance of Light and Carbon Assimilation Proteins. *Cell Rep.* **25**, 478-486.e8 (2018).

46. Kirk, J. T. *Light and Photosynthesis in Aquatic Ecosystems*. (Cambridge University Press, 1994).

47. Falkowski, P. G. & Raven, J. A. *Aquatic Photosynthesis*. (Princeton University Press, 2007).

48. Kirilovsky, D. Photoprotection in cyanobacteria: the orange carotenoid protein (OCP)-related non-photochemical-quenching mechanism. *Photosynth. Res.* **93**, 7 (2007).

49. Giacometti, G. M. & Morosinotto, T. Photoinhibition and Photoprotection in Plants, Algae, and Cyanobacteria. in *Encyclopedia of Biological Chemistry* (eds. Lennarz, W. J. & Lane, M. D.) 482–487 (Academic Press, 2013). doi:10.1016/B978-0-12-378630-2.00229-2.

50. Furukawa, H. *et al.* Correlation of Power Consumption for Several Kinds of Mixing Impellers. *Int. J. Chem. Eng.* **2012**, 1–6 (2012).

51. Li-Cor. Principles of radiation measurement. (.;No date).

52. ALPHA. *Standard Methods for the Examination of Water and Wastewater*. (ALPHA,AWWA,WEF, 2012).

53. Assemany, P. P. *et al.* Algae/bacteria consortium in high rate ponds: Influence of solar radiation on the phytoplankton community. *Ecol. Eng.* **77**, 154–162 (2015).

54. Esmaeelnejad, L., Siavashi, F., Seyedmohammadi, J. & Shabanpour, M. The best mathematical models describing particle size distribution of soils. *Model. Earth Syst. Environ.* **2**, 1–11 (2016).

55. Campbell, D., Hurry, V., Clarke, A. K., Gustafsson, P. & Öquist, G. Chlorophyll Fluorescence Analysis of Cyanobacterial Photosynthesis and Acclimation. *Microbiol Mol Biol Rev* **62**, 667–683 (1998).

56. Cohen, S. E., Erb, M. L., Pogliano, J. & Golden, S. S. Best practices for fluorescence microscopy of the cyanobacterial circadian clock. *Methods Enzymol.* **551**, 211–221 (2015).

57. Carreira, C., Staal, M., Middelboe, M. & Brussaard, C. P. D. Autofluorescence imaging system to discriminate and quantify the distribution of benthic cyanobacteria and diatoms: Imaging benthic photoautotrophs. *Limnol. Oceanogr. Methods* **13**, e10016 (2015).

58. Ansari, A. A., Abouhend, A. S. & Park, C. Effects of seeding density on photogranulation and the start-up of the oxygenic photogranule process for aeration-free wastewater treatment. *Algal Res.* **40**, 101495 (2019).

59. Sarma, S. J. & Tay, J. H. Aerobic granulation for future wastewater treatment technology: challenges ahead. *Environ. Sci. Water Res. Technol.* **4**, 9–15 (2017).

60. Tay, J.-H., Liu, Q.-S. & Liu, Y. The effects of shear force on the formation, structure and metabolism of aerobic granules. *Appl. Microbiol. Biotechnol.* **57**, 227–233 (2001).

61. Hogg, R. Issues in Particle Size Analysis. *KONA Powder Part. J.* **26**, 81–93 (2008).

62. Wang, C. & Lan, C. Q. Effects of shear stress on microalgae - A review. *Biotechnol. Adv.* **36**, 986–1002 (2018).

63. Michels, M. H. A., van der Goot, A. J., Norsker, N.-H. & Wijffels, R. H. Effects of shear stress on the microalgae Chaetoceros muelleri. *Bioprocess Biosyst. Eng.* **33**, 921–927 (2010).

64. Mancell-Egala, W. A. S. K. *et al.* Limit of stokesian settling concentration characterizes sludge settling velocity. *Water Res.* **90**, 100–110 (2016).

65. Sezgin, M. Variation of sludge volume index with activated sludge characteristics. *Water Res.* **16**, 83–88 (1982).

66. Bye, C. M. & Dold, P. L. Sludge volume index settleability measures: effect of solids characteristics and test parameters. *Water Environ. Res.* **70**, 87–93 (1998).

67. Snyder, R. & Wyant, D. Training manual for wastewater treatment plant operators. 105.

68. Randall, C. W., Barnard, J. L. & Stensel, H. D. *Design and Retrofit of Wastewater Treatment Plants for Biological Nutritient Removal*. (CRC Press, 1998).

69. Pronk, M. *et al.* Full scale performance of the aerobic granular sludge process for sewage treatment. *Water Res.* **84**, 207–217 (2015).

70. Mesquita, D. P., Amaral, A. L. & Ferreira, E. C. Identifying different types of bulking in an activated sludge system through quantitative image analysis. *Chemosphere* **85**, 643–652 (2011).

71. Amanatidou, E., Samiotis, G., Trikoilidou, E., Pekridis, G. & Taousanidis, N. Evaluating sedimentation problems in activated sludge treatment plants operating at complete sludge retention time. *Water Res.* **69**, 20–29 (2015).

72. Li, Z. *et al.* Population balance modeling of activated sludge flocculation: Investigating the influence of Extracellular Polymeric Substances (EPS) content and zeta potential on flocculation dynamics. *Sep. Purif. Technol.* **162**, 91–100 (2016).

73. Deng, S., Wang, L. & Su, H. Role and influence of extracellular polymeric substances on the preparation of aerobic granular sludge. *J. Environ. Manage.* **173**, 49–54 (2016).

74. Derlon, N., Wagner, J., da Costa, R. H. R. & Morgenroth, E. Formation of aerobic granules for the treatment of real and low-strength municipal wastewater using a sequencing batch reactor operated at constant volume. *Water Res.* **105**, 341–350 (2016).

75. Zhu, L., Zhou, J., Yu, H. & Xu, X. Optimization of hydraulic shear parameters and reactor configuration in the aerobic granular sludge process. *Environ. Technol.* **36**, 1605–1611 (2015).

76. Chopra, S., Thampy, T., Leahy, J., Caplin, A. & LeCun, Y. Factor Graphs for Relational Regression. 14.

77. Kuczynska, P., Jemiola-Rzeminska, M. & Strzalka, K. Photosynthetic Pigments in Diatoms. *Mar. Drugs* **13**, 5847–5881 (2015).

78. Jeffrey, S. W. Photosynthetic pigments of the phytoplankton of some coral reef waters1: pigments of coral reef waters. *Limnol. Oceanogr.* **13**, 350–355 (1968).

79. Golterman, H. . Chapter 13 Algae and their Pigments. in *Physiological Limnology: An Approach to the Physiology of Lake Ecosystems* vol. 2 233–247 (Elsevier, 1975).

80. Green, B. & Parson, W. W. *Light-Harvesting Antennas in Photosynthesis*. (Springer Science & Business Media, 2003).

81. Yuanyuan, Z., Xuehong, Z. & Wenjie, Z. Research Advances in Anammox Granular Sludge. in *Proceedings of the AASRI International Conference on Industrial Electronics and Applications (2015)* (Atlantis Press, 2015). doi:10.2991/iea-15.2015.113.

82. Sarma, S. J., Tay, J. H. & Chu, A. Finding Knowledge Gaps in Aerobic Granulation Technology. *Trends Biotechnol.* **35**, 66–78 (2017).

83. Cory, R. M., Ward, C. P., Crump, B. C. & Kling, G. W. Sunlight controls water column processing of carbon in arctic fresh waters. *Science* **345**, 925–928 (2014).

84. Haigh, J. D., Winning, A. R., Toumi, R. & Harder, J. W. An influence of solar spectral variations on radiative forcing of climate. *Nature* **467**, 696–699 (2010).

85. Barr, J. J., Cook, A. E. & Bond, P. L. Granule Formation Mechanisms within an Aerobic Wastewater System for Phosphorus Removal. *Appl Env. Microbiol* **76**, 7588–7597 (2010).

86. Guedes da Silva, L., Tomás-Martínez, S., Wahl, A. & van Loosdrecht, M. *The environment selects: Modeling energy allocation in microbial communities under dynamic environments*. (2019). doi:10.1101/689174.

87. The influence of particles on suspension rheology:: Anton Paar Wiki. *Anton Paar* https://wiki.anton-paar.com/en/the-influence-of-particles-on-suspension-rheology/.

88. Ford, T. F. Viscosity-concentration and fluidity-concentration relationships for suspensions of spherical particles in newtonian liquids. *J. Phys. Chem.* **64**, 1168–1174 (1960).

89. Doran, P. M. Mixing. in *Bioprocess Engineering Principles* 255–332 (Elsevier, 2013). doi:10.1016/B978-0-12-220851-5.00008-3.

90. Moisander, P. H., Hench, J. L., Kononen, K. & Paerl, H. W. Small-scale shear effects on heterocystous cyanobacteria. *Limnol. Oceanogr.* **47**, 108–119 (2002).

91. Mikkelsen, L. H. The shear sensitivity of activated sludge: Relations to filterability, rheology and surface chemistry. *Colloids Surf. Physicochem. Eng. Asp.* **182**, 1–14 (2001).

92. Ratkovich, N. *et al.* Activated sludge rheology: A critical review on data collection and modelling. *Water Res.* **47**, 463–482 (2013).

93. Tixier, N., Guibaud, G. & Baudu, M. Determination of some rheological parameters for the characterization of activated sludge. *Bioresour. Technol.* **90**, 215–220 (2003).

94. Liu, Y. & Tay, J.-H. State of the art of biogranulation technology for wastewater treatment. *Biotechnol. Adv.* **22**, 533–563 (2004).

95. Jørgensen, S. E. & Fath, B. D. Steady-State Models. in *Developments in Environmental Modelling* vol. 23 159–174 (Elsevier, 2011).

96. Richard, M., Brown, S. & Collins, F., CO. Activated Sludge Microbiology Problems and Their Control. in 21 (2003).

97. Xia, J., Ye, L., Ren, H. & Zhang, X.-X. Microbial community structure and function in aerobic granular sludge. *Appl. Microbiol. Biotechnol.* **102**, 3967–3979 (2018).

98. Gao, D., Liu, L., Liang, H. & Wu, W. *Aerobic Granular Sludge: Characterization, Mechanism of Granulation and Application to Wastewater Treatment*. vol. 31 (2010).

99. Rickard, A. H., Gilbert, P., High, N. J., Kolenbrander, P. E. & Handley, P. S. Bacterial coaggregation: an integral process in the development of multi-species biofilms. *Trends Microbiol.* **11**, 94–100 (2003).

100. Spormann, A. M. Physiology of Microbes in Biofilms. in *Bacterial Biofilms* (ed. Romeo, T.) 17–36 (Springer Berlin Heidelberg, 2008). doi:10.1007/978-3-540-75418-3_2.

CHAPTER 3

IN VIVO EVALUATION OF OXYGENIC PHOTOGRANULES' PHOTOSYNTHETIC CAPACITY BY PULSE AMPLITUDE MODULATION AND PHOTOTROPHIC-IRRADIANCE CURVES

3.1 Abstract

The commingled microbial moiety of oxygenic photogranules (OPGs) facilitates aeration-free wastewater treatment. Embedded in an EPS matrix, microbial producers and consumers of oxygen occupying granular niches exchange substrates amongst and with the bulk fluid. An assessment of the OPG's phototrophic potential or functional capacity may require combining different photoactivity signals. We determined the photochemical capacity of OPGs grown at different light intensities. High light (HL) adapted OPGs exhibited higher photosynthetic capacity using both photosynthetic oxygen evolution (POE) and chlorophyll fluorescence (rapid light curves-RLC) signals compared to low light (LL) adapted OPGs. POE rates were higher than the relative electron transport rates from RLCs while the correlation coefficients (κ) between the two were lower than reported values for pure cyanobacteria and algae cultures. These lower coefficients reflect the enhanced contribution from different photosynthetic clades with a variety of light-harvesting pigments present in OPGs. The saturation irradiances before the onset of photoinhibition were 1000 μmol m^{-2} s^{-1} and 1200 μmol m^{-2} s^{-1} for POE evaluation and 478 μmol m^{-2} s^{-1},611μmol m^{-2} s^{-1} for RLC with LL and HL, respectively. Moreover, HL adapted samples had higher non-photochemical quenching rates which allude to the OPG's photo-elastic potential. OPGs showed higher resilience to pH stress than temperature shocks. In an OPG reactor, the photochemical activity is influenced by the granular size, granular ecology, and reactor operation metrics related to mixing such as self-shading, light intensity, photoperiods, and reactor depth.

3.2 Introduction

Light energy powers the bulk of primary production in the biosphere with phototrophs transforming this energy into chemical energy [1] for utility at different trophic levels. This light energy is harvested by a moiety of light-harvesting complexes (LHCs) comprising photoreceptors and associated protein complexes.[2] These tetrapyrrole receptors include chlorophyll and phycobilisomes pigments with the latter only present in cyanobacteria [3,4] while chlorophylls are found in all phototrophs.[2,3,5] The absorbed energy is transferred to reaction centers (II) and (I) protein complexes through a specialized chain of intermediary biomolecules and redox reactions to power carbon assimilation in the Calvin-Benson cycle.[1] Phototrophic autotrophs have developed adaptations to variability in light quantity and quality [6–8] in their environmental niches, such as leaf angles in higher plants and buoyancy regulation in algae and cyanobacteria [9–11] optimizing their photo-interaction.

For emerging granular based wastewater systems, a consortium of microbes coexists in different associations within the granular ecosystem.[12–14] These biospheres are micro-reactors exchanging substrates within their matrix [14,15] and beyond their structural boundary with the bulk fluid.[14] This exchange is a function of granular physical properties such as porosity and permeability affecting advective and diffusive mass transfer.[16,17] These granular properties are in turn a result of the microbial composition, their spatial distribution in the granule morphology [18] and interactions with environmental stresses.[19]

Photogranules such as oxygenic photogranules (OPGs) have a phototrophic outer layer,[18,20] where an oxygen-evolving complex in the photosystem II (PSII) undertakes photooxidation of water via the KOKs cycle [21,22] producing oxygen. This self-aeration property reduces the high energy demand and cost associated with conventional wastewater treatment.[12,14,18,23] The dissolved oxygen can diffuse into the bulk fluid outside the granular boundary or into the granular core where aerobic oxidation of ammonia and organics by nitrifying and heterotrophic bacteria proliferating in the aerobic zone [18,24] occurs. Mature OPGs with diameters >3 mm have anaerobic or anoxic conditions within their stratified core.[18] In this zone, denitrification occurs, converting nitrate to nitrogen gas.[24] Similarly, nutrients and organic substrates with a concentration gradient between the bulk wastewater and granular environment diffuse into the granular matrix.

Current practices for estimating phototrophic activity involve the use of photosynthetic irradiance (P-I) relations and rapid light curves (RLC).[25,26] The P-I or photosynthesis response curve relates phototrophic activity as oxygen generated or carbon (^{14}C) consumed in the ordinate over an increasing light intensity abscissa.[11,26] Inherent limitations of these approaches include their low sensitivity to low O_2 concentrations and differential uptake of $^{14}C/^{12}C$.[27] RLC, on the other hand, utilizes the fluorescence characteristics of chlorophyll light-harvesting complexes.[28] Incident pulses of amplitude modulated (PAM) light results in oxidation of reduced reaction centers (RC) and quenching of the incident energy.[29] The consumption of incident light energy in the ensuing photosynthetic activity constitutes photochemical quenching (qP). Fully oxidized and closed reaction centers reemit excess incident energy via pigment fluorescence or as heat in non-photochemical quenching (NPQ).[30,31]

Fluorescence and non-fluorescence quenching are part of the photoprotective suite of mechanisms,[9,31] that enable phototrophs to dissipate excess photon energy which may cause photo-oxidative damage [32,33] or photoinhibition.[31] This damage is attributed to both the formation of reactive oxygen species (ROS) such as peroxides, superoxide, singlet oxygen [34] and inhibited repair of D1 proteins associated with the photosystem II.[35] Other photoprotective mechanisms include the xanthophyll cycle in algae and higher plants where reversible de-epoxidation of violaxanthin carotenoids results in non-photochemical quenching.[36,37] In cyanobacteria forming the OPG's structural matrix,[20] the orange carotenoid protein performs similar anti-oxidation functions.[38] Photoprotective mechanisms can be defined by energy-related (qE) and state transition (qT) quenching, while longer-lasting photodamage effects are described by photoinhibitory quenching (qI).

The phototrophic production of both microalgal and cyanobacteria cultures has been widely characterized in pure and mixed cultures.[39–44] However, similar characterization in OPGs and other photogranular biomass existing in a commingled moiety with concurrent production and consumption of oxygen in wastewater treatment has not been undertaken. While P-I curves quantify net photosynthesis, RLC indicates the gross photosynthetic activity.[25,44] In the tightly coupled microbial environment of phototrophic granules, concurrent generation and consumption of carbon and oxygen within the granular matrix may impede accurate quantification using P-I curves. Moreover, phototrophic clades present in OPGs have different accessory light-harvesting pigments such as phycobilins in cyanobacteria which interfere with fluorescence emission while generating RLCs.[44] In the present work, we explore the photochemical potential of OPGs applied in wastewater treatment using a modified P-I curve approach and RLC methods. This

characterization will inform the design of scaled-up photogranular wastewater treatment systems with respect to light demand while forestalling its deleterious effects. We also examine the fluorescence response of OPGs to different stress conditions using RLC parameters.

3.3 Materials and methods

3.3.1 Source of oxygenic photogranules (OPGs)

A lab reactor operated in sequencing batches at a 1-day hydraulic retention time (HRT) and fed with wastewater from a local utility was used as a source of OPGs for experimental work. The 8 L lab reactor was operated under two light intensities 200 μmol m^{-2} s^{-1} (LL) (±42) and 460 μmol m^{-2} s^{-1} (HL) (±23), respectively each for 30 days before sampling. The light was provided using daylight mimicking 9 W LEDs (EcoSmart, daylight- 5000 K) with a luminosity of 840 Lumens. The reactor operation was with sequential dark and light cycles every 3 hours and a decanting phase at the end of the light cycle following 10 min settling phase. Both the decanting and filling events were each undertaken for 5 min.

3.3.2 Sample analysis

Biomass characterization of total suspended (TSS) and volatile suspended (VSS) solids were undertaken using Standard Methods 2540D/E [45] and chlorophyll pigments extraction and quantification using Standard Methods 10200H.[45] For phycobilin extraction, the samples were centrifuged at 12000 rpm for 20 min. The clear supernatant was discarded while the pellet was inoculated with an equal volume of 0.025M phosphate buffer at pH 7. The sample was homogenized for 1 min and sonicated (400 W Sonic Dismembrator 500, FISHER Scientific) for 3

min at 20% strength while immersed in an ice bath. Samples were then centrifuged, and the supernatant was analyzed spectrophotometrically (UV-Vis, Thermo scientific). The Bennett and Bogorad equation [46] was used to quantify phycobilins substituting 615 nm with abundant 620 nm peaks.[47–49]

A volume of the sample was also filtered through both 1.5 µm and 0.45 µm filters and used for analysis as total COD and soluble COD fractions respectively using Standard Methods 5220C [45]. The 0.45 µm filtrate was also used for the analysis of soluble fractions of total dissolved nitrogen and dissolved organic carbon using a TN/TOC analyzer (TOC-VCPH, Shimadzu, U.S.A). Dissolved organic nitrogen was determined as the net of inorganic nitrogen species from the total nitrogen concentrations. A Metrohm 850 Professional Ion Chromatograph (IC) (Metrohm, Switzerland) was used to measure phosphate and dissolved inorganic nitrogen species.

3.3.3 Photochemical response to stress

Granules grown under HL were also collected and treated to different stress conditions including temperature (-20^{0}C, 23^{0}C, 50^{0}C), pH (3, 6.2, 7.6), chlorophyll deficiency and phototoxicity using 3-(3,4-dichlorophenyl)-1,1-dimethylurea (DCMU) at concentrations of 0.1 mg/L,10 mg/L, and 100 mg/L. For the low-temperature stress conditions, granule samples were frozen in DI water at -20^{0}C for 8 hours in the dark and thawed just before analysis. Similarly, the high-temperature samples were dark incubated in a water bath (50^{0}C) for 8 hours before analysis. To test the photochemical effect of pH, 0.1N HCl was used to lower the initial pH of the inoculum fluid (Wastewater-WW, Deionized water-DI) to target pH values. Initial pH was 7.6, and 6.2 for the two inoculate fluids, respectively. All samples were then dark-adapted for 8 hours before examining abiotic stress

effects. The chlorophyll deficiency was simulated by first extracting the chlorophyll pigments following the standard methods 10200H.[45] Briefly, a 10 ml sample of OPGs was centrifuged and the supernatant discarded. The pellet was suspended in an equal volume of a magnesium-enriched 90% acetone solution for 16 hours. The extract was discarded, and the pellet washed twice using the extraction solution. This pellet was then dark adapted suspended in deionized water before fluorescence analysis. While chlorophyll extraction eliminates light-harvesting complexes of phototrophs, DCMU inhibits the photosynthetic electron transport chain by blocking the primary electron binding site in photosystem II.[50] This impairs the conversion of harvested light energy into chemical energy-reduced nicotinamide adenine dinucleotide phosphate (NADPH) in photosystem I required for photosynthetic carbon reduction.[51]

3.3.4 Photosynthetic oxygen evolution (POE)

In constructing P-I (hereafter referred to as POE) curves, granules were collected from the reactors and sizes of 0.5 mm to 1 mm in diameter were obtained by sieve analysis. This size class has been reported as being the most abundant and as having the highest oxygen productivity in OPG reactors [18]. The size sorted granules were then dark-adapted for 12 hours [28] to reduce the reaction centers while suspended in nutrient-limited deionized water. In a darkened room, a 1 L glass vessel reactor was then inoculated with the stored granules and topped up with wastewater (primary effluent) from the local wastewater treatment plant. The wastewater was prefiltered through 1.5 µm glass fiber filters. An airtight rubber seal was then used to cap the reactor jar to limit interaction with the atmosphere. A multiparameter probe (Hanna Instruments) matted to this capping seal and calibrated before every test was then used to record dissolved oxygen, temperature, and pH data at 1 min intervals. A 3 mm diameter tubing drilled into the rubber cap

was used to collect analysis samples. A magnetic stirrer bar calibrated at 100 rpm was used for continuous mixing, and a heat sink was used to maintain the temperature between 22-24 ^{0}C.

Light was provided at increasing intensities from 100 µmol m^{-2} s^{-1} to 2000 µmol m^{-2} s^{-1} (±10) using an LED panel (6500 K) and calibrated using a Li-Cor 193S underwater spherical sensor (LI-COR Biosciences) at the surface of the reactor. Initial increase was by 100 µmol m^{-2} s^{-1} and subsequent increases by 200 µmol m^{-2} s^{-1}. Bulk samples were collected at time 0 and subsequently at two 15 min intervals. In the intervening period between light intensities, the reactor was stored in a darkened enclosure for an average of 8 min. Wastewater was added to suppress dissolved oxygen (DO) saturation in the reactor bulk fluid and to prevent gas loss into the headspace. Net photosynthetic oxygen evolution was determined as the sum of differential changes in DO concentration, gross nitrification,[52] and chemical oxygen demand (COD) removal. The oxygen consumption rate of 4.57 mgO_2/NH_3-N for the oxidation of ammonia [52–54] while a ratio of 1 mgO_2/mgCOD was used for biological oxidation of dissolved organics. However, the POE and RLC determinations were not conducted concurrently as commonly practised.[11,25,55]

3.3.5 Fluorescence analysis

Dark-adapted (12 hrs.) granule samples were also analyzed using an imaging pulse amplitude modulation (PAM) fluorometer (M-Series Maxi Version, Walz GmbH, Effeltrich, Germany). Analysis of light induction (Kautsky effect) [25] was followed by rapid light curve measurements for each defined area of interest approximating the granule size. A sample size of n>30 zones was defined for each test. For light induction measurements, the duration of the light pulses was set to 415 s, with a 40 s interval, while intensity was adjusted to the setting 8 and 13, corresponding to

the growth irradiance of 186 μmol m^{-2} s^{-1} and 460 μmol m^{-2} s^{-1}, respectively. Saturating pulses were set at 5000 μmol m^{-2} s^{-1}. The obtained dark-adapted fluorescence (F_o) and maximal fluorescence (F_m) values using dark-adapted granules were utilized to determine maximal PSII quantum yield as,[25] $Fv/Fm = (Fm - Fo)/Fm$. The variable fluorescence (Fv), is the difference between Fm and Fo.

Rapid light curves characterizing the electron transport rate (ETR) were developed via a stepwise increase of saturating pulses from 0 to 1250 μmol m^{-2} s^{-1}. The effective quantum yield (ϕ_{PSII}) evaluated over increasing irradiances was defined as $\phi_{PSII} = (Fm' - Fo')/Fm'$ using light adapted granules,[25,44] The relative electron transport rate (rETR), approximating the electron flow in the photosynthetic reaction chain, was determined by eliminating the absorptance and assumed transmittance fractions of absorbed quanta to PSII from the ETR determination (Eq.1) where PAR is the incident irradiance. This fraction reported for Chlorophyta as 0.5 and Rhodophytes as 0.15 is variable for the mixed clades present in OPGs.[55]

$$\boldsymbol{rETR = \phi_{PSII} * PAR} \qquad \textbf{(Eq 3- 1)}$$

3.3.6 Quenching analysis

Actinic light (AL) equivalent to growth irradiances of 186 μmol m^{-2} s^{-1} and 460 μmol m^{-2} s^{-1} were used to illuminate the sample and modulated measuring light (ML) used to determine fluorescence induction parameters with rapidly changing light conditions. Photochemical quenching (qP) which measures the overall reaction center (RC) openness [56] was determined as (Eq.2),

$$\boldsymbol{qP = (Fm' - F)/(Fm' - Fo')} \qquad \textbf{(Eq 3- 2)}$$

Where Fm' is the light-adapted maximum fluorescence obtained at saturation of reaction centers, F is the average fluorescence at a steady rate, Fo' is the light-adapted fluorescence intensity estimated from Fm' measurements.[57] The coefficient of non-photochemical quenching (qN) describing quenching mechanisms not related to photochemistry was also evaluated (Eq.3).[25] A Stern-Volmer coefficient of non-photochemical quenching (NPQ) which is independent of Fo' and has a higher sensitivity to energy quenching within the antennae matrix [11,25] was also determined (Eq.4).

$$\mathbf{qN} = (\mathbf{Fm} - \mathbf{Fm'})/(\mathbf{Fm} - \mathbf{Fo'}) \quad \textbf{(Eq 3- 3)}$$

$$\boldsymbol{NPQ} = (\boldsymbol{Fm} - \boldsymbol{Fm'})/(\boldsymbol{Fm''}) \quad \textbf{(Eq 3- 4)}$$

3.3.7 Curve fitting

Characteristic photosynthetic parameters were determined by fitting the RLC to a curve. The Platt [58] empirical estimation describing photosynthesis as a single continuous function of incident light was used [25]. The function covers both the initial increasing photosynthetic rates and the diminishing rate due to irradiance driven photoinhibition.[31,59] Adjusted rETR data was exported into origin Pro (v.2020) and processed using the non-linear curve fit function. A double decay exponential function was fitted onto the data using an orthogonal distance regression algorithm (Eq 3-5).

$$\boldsymbol{P = P_s(1 - e^{-(\alpha E_d/Ps)})e^{-(\beta E_d/Ps)}} \quad \textbf{(Eq 3- 5)}$$

Where P is the photosynthetic rate with E_d (μmol m^{-2} s^{-1}) incident radiation, P_s is the light-saturated rETR without photoinhibition, α is the initial slope of the RLC before saturation, and β characterizes the slope of the RLC during photoinhibition. Additionally, the relative maximum electron transport rate ($rETR_{max}$), and minimum saturating irradiance (E_k) were obtained using the

equations described by Ralph et al. [25] A regression coefficient (κ) was determined relating the ETR and POE linear regression in the light-limited region.[11]

$$rETRmax = Ps(\alpha/[\alpha+\beta])\ (\beta/[\alpha+\beta])^{\beta/\alpha} \quad \textbf{(Eq 3- 6)}$$

$$Ek = ETR_{max}/\alpha \quad \textbf{(Eq 3- 7)}$$

A Freundlich regression model in the form $y = E_d X^b$ was fit on non-photochemical quenching coefficients (qN, NPQ) while an exponential decay function ($qP = A\ e^{(-b.\ Ed)}$) was applied to photochemical quenching. The regression analysis was run over 100 iterations to convergence.

3.4 Results

3.4.1 Photosynthetic oxygen evolution (POE) characterization

The average net concentrations of total nitrogen (TN) were 30 (±2.8) and 34 (±10.2) mg/L in LL and HL sample experiments, respectively. Inorganic nitrogen species had net concentrations of 29 (±2.6) and 17 (±4.2) mg/L for the two POE experiments. This suggests that N in the LL set was predominantly inorganic N while the HL bulk samples had, on average, 17 mg/L total organic nitrogen. The phosphorous concentrations were 2.2 (±0.5) mg/ L and 1.3 (±0.5) mg/L during the LL and HL POE determinations. The total COD of the raw wastewater used was on average, 203 (±43) mg/L for the two POE experiments.

The concentration of dissolved oxygen in constant light inoculations increased linearly with time (Figure 3- 1). Moreover, the increase in oxygen evolution increased with irradiance provided up to 1000 μmol m^{-2} s^{-1} for the illumination period while a decrease was observed beyond 40 min for 1500 μmol m^{-2} s^{-1} (Figure 3- 1). A 30 min illumination period for each light intensity was selected

with 15 min sampling intervals for constructing the POE curves. The estimated POE was determined as the sum of changes in DO, and the theoretical oxygen demand for COD removal and nitrification. One potential source of error in this estimation is the inherent low sensitivity of the chemical method determination of COD.[60] Moreover, dark adaptations between sampling were observed to result in photorespiration increasing COD at low light intensities.

POE curves for both OPG growth irradiances exhibited a typical curvilinear trend with increasing light intensity (Figure 3- 2). Granules cultivated under 460 μmol m^{-2} s^{-1} showed higher photosynthetic productivity with a peak (1364 μmol-O_2/mg-chlorophyll a.hr) which was 5.5 times higher than those grown at 200 μmol m^{-2} s^{-1} (Figure 3- 2-a, b). Peak photosynthetic activity was observed at 1000, and 1200 μmol m^{-2} s^{-1} for LL and HL adapted samples, respectively. A photosynthetic curve regression fit using Eq.5 and parameters determined via Eq.6-7 are presented in Table 3- 1. The light saturation coefficient (α) in the LL samples was 2 times lower than that in HL samples. Moreover, the decay coefficient (β) in the LL samples was also 1.6 times lower than in the Hl samples. A minimum saturation irradiances were 250 μmol m^{-2} s^{-1} and 656 μmol m^{-2} s^{-1} for LL and HL samples, respectively (Table 3- 1). These higher values for HL adapted samples allude to photoelasticity of the photosynthetic clades [20] present in OPGs.

.

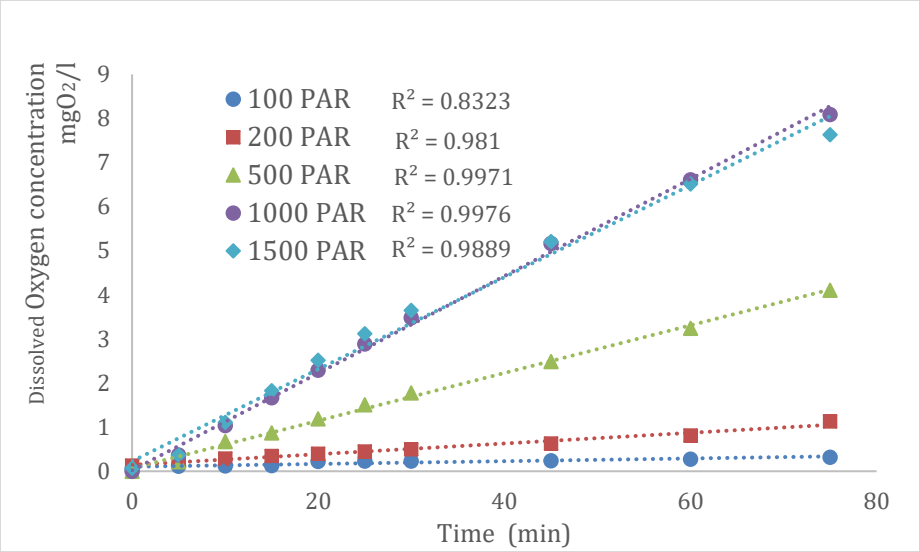

Figure 3- 1: Net photosynthetic oxygen evolution over time for OPGs inoculated in wastewater under different constant light intensities (PAR= µmol m^{-2} s^{-1}) and DO (mg/L) concentration determined at Δt (5 and 15) min intervals. Dotted lines show the linear fits over time while corresponding r- values are indicated for each light intensity.

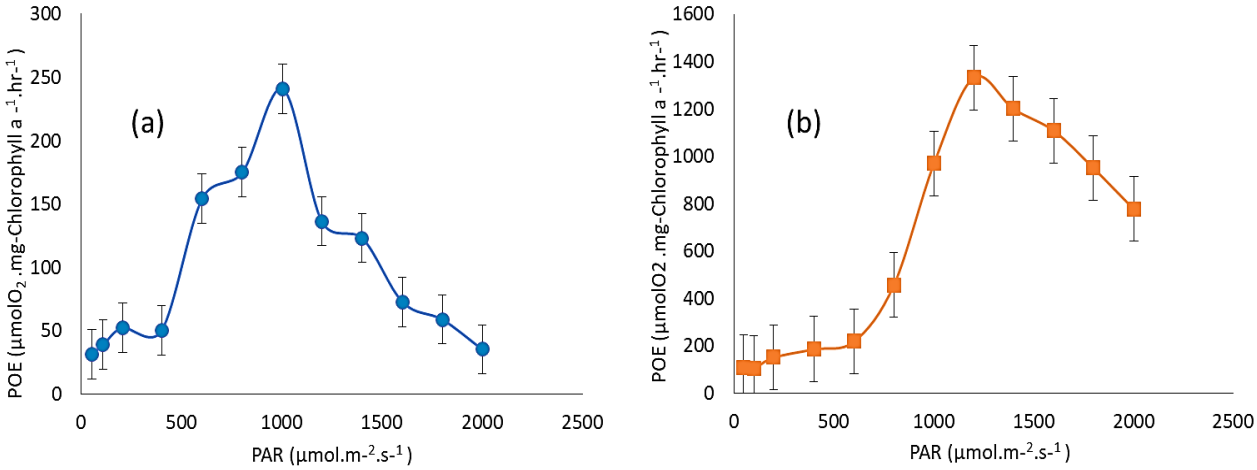

Figure 3- 2: POE determination for samples grown at (a) 220 µmol m^{-2} s^{-1} and (b) 460 µmol m^{-2} s^{-1} with increasing light intensity. Error bars are standard errors of derived oxygen evolution rates.

3.4.2 OPG fluorescence characterization

The light induction fluorescence yields at the growth actinic light are presented in Figure 3- 3 for both (a) 200 µmol m^{-2} s^{-1} and (b) 460 µmol m^{-2} s^{-1} OPG growth irradiances. The curves show no

substantial difference in trends with relatively constant steady-state fluorescence (F) yields of 0.25 and 0.31, respectively (Figure 3- 3). Moreover, LL samples mounted in deionized water (DI) before and after POE experiments (Figure 3- 3-a) showed minimal difference in steady-state fluorescence yields (Figure 3- 3-a). The post-POE samples were dark-adapted for 4 hours compared to 12 hours for the pre-POE samples. Dark-adaptation of phototrophs for long durations can eliminate long-lasting photoinhibition effects (>Hours) [25] explaining the above similarity in F yields. The dark-adapted fluorescence yields (Fo) increased from 0.14 to 0.22 after exposing the LL samples to high irradiances during photosynthetic oxygen evolution (up to 2000 $\mu mol\, m^{-2}\, s^{-1}$) (Figure 3- 3-a). Besides, a 33% decrease in the quantum yield ensued from exposure of OPGs to high light intensity during POE experiments. The fluorescence increase suggests a higher sensitivity of PSII reduction potential for electron transfer even with dark adaptation resulting in higher yields. While repair of the DI protein complex of the PSII is a continuous process, it is inversely responsive to environmental stresses such as temperature and growth irradiance and availability of carbon.[34,35,61]

The different induction (Figure 3- 3-a) and quenching parameters (Figure 3- 4-a, c) observed for pre-POE and post-POE LL samples dark-adapted for 4 and 12 hours respectively can be attributed photochemical recovery kinetics. A component of non-photochemical quenching associated with photoinhibition (qI) [28,62] has been reported to have slower relaxation >30 min to hours. This slow relaxation is also responsible for energy redistribution to PSII.[25] Quenching related to energy-dependent (qE) and state transition (qT) occurs over shorter timescales (<30min).[25,28,31,62,63] Exposing the samples to high light intensities (up to 2000 $\mu mol\, m^{-2}\, s^{-1}$) during POE experiments

resulted in higher photochemical quenching potential (qP). This increase suggests an elasticity in the photochemical capacity of the photosynthetic clades in OPGs.

Similarly, HL samples mounted in DI and wastewater (WW) (Figure 3- 3-b) showed no variability in terminal fluorescence yields, reflecting the light adaptation conditions of phototrophs in the OPG. The comparable steady-state yields observed indicate no limitation in the long-term photosynthetic electron transfer activity utilizing all the available actinic light energy.[25] A 27% higher PSII quantum yield (Fv/Fm) was observed in DI mounted HL samples compared to those in WW (Figure 3- 3-b). Thus, the availability of carbon in wastewater did not increase photosynthetic activity when exposed to light.[64,65] This can be attributed to granular morphology and inorganic carbon limitations for photosynthetic activity. OPG morphology consists of layered microbial niches with the phototrophic zone at their surface.[18] Internally localized heterotrophs respire organic carbon in wastewater generating carbon dioxide [64] available for photosynthesis. Diffusive transfer of these substrates into and out of the different OPG layers may occur at temporal magnitudes higher than that of the fluorescence pulses. This could further explain the short term incongruity and longer-term similarity of fluorescence yields.

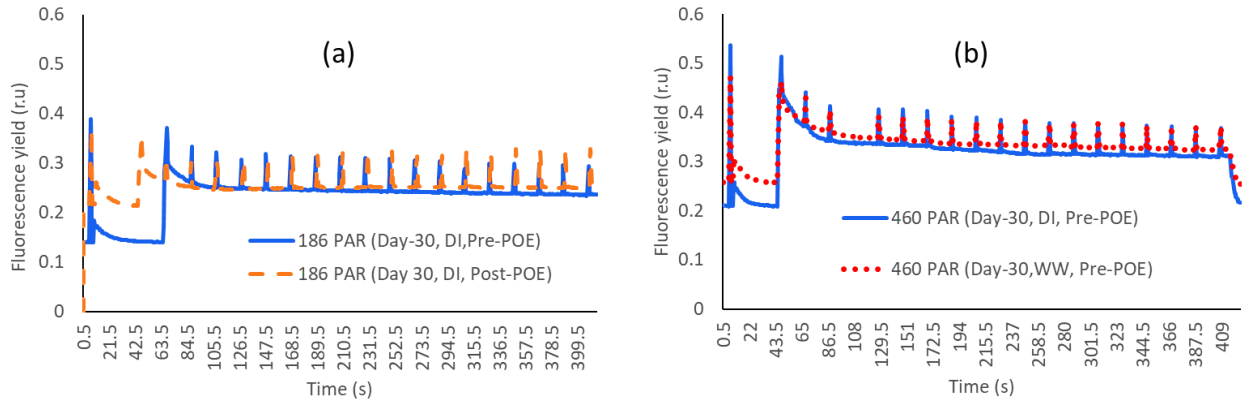

Figure 3- 3: Fluorescence signal charts during light induction (Kautsky effect). (a) OPG biomass adapted at 200 µmol m^{-2} $s^{-1}$with plots taken before (Solid) and after (Dashed) photosynthetic oxygen evolution (POE) experiments. All LL samples were dark-adapted in deionized water (DI). (b) OPG biomass adapted at 460 µmol m^{-2} s^{-1} (Pre-POE) mounted in DI water (dashed lines) and wastewater (solid lines) before oxygen evolution experiments. The vertical axis shows the fluorescence units (arbitrary) with initial maxima (F) and subsequent fluorescence peaks (F') with each saturating pulse. The horizontal axis is in seconds. Each peak represents a saturating pulse (5000 µmol m^{-2} s^{-1}) while actinic light (adapted irradiance) is provided at the intervals. The initial peak (F) is the maximal fluorescence yield for dark-adapted biomass**.**

Excess absorbed photon energy is dissipated via photochemical and non-photochemical pathways characterized by the qP, qN and NPQ coefficients. The plotted quenching coefficients showed an apparent increase in both qN and NPQ, with a corresponding decrease in qP (Figure 3- 4). Under LL conditions, the loss in photochemical quenching capacity diminished to zero at 950 µmol m^{-2} s^{-1} for pre-POE OPGs. In contrast, the qP of LL samples diminished to 0 at 1200 µmol m^{-2} s^{-1} (Figure 3- 4-a) after POE experiments. This higher limiting light alludes to active photoprotection mechanisms [9,31] in post-POE samples hence the ability to function to higher light intensity. Moreover, the heat dissipation coefficients qN and NPQ for the pre-POE samples increased rapidly up to 111 µmol m^{-2} s^{-1} (Figure 3- 4-a, c). Post-POE samples, on the other hand, experienced a lag in the qN and NPQ parameters and a linear trend to 530 µmol m^{-2} s^{-1}. This disparity suggests a higher sensitivity of non-photochemical quenching capacity in the pre-POE samples compared to post-POE samples which had a high irradiance history. The maximum non-photochemical

quenching potential for pre-POE samples was 2 times higher than that of post-POE biomass. Linear regression on the initial linear data points resulted in qN slope coefficients of 0.0007 and 0.0005 (r^2=0.98) for pre and post-POE samples, respectively. Similar fits on the NPQ data resulted in slope coefficients of 0.0003 and 0.00006 (r^2=0.98) equivalent to a rate of 5 times more quenching potential for uncompromised pre-POE biomass.

The qP coefficients in HL adapted OPG biomass decreased to a minimum at 1251 μmol m^{-2} s^{-1}. Samples mounted in wastewater increased the initial qP potential by a 0.15 magnitude compared to HL samples mounted in DI. The qN coefficient for DI mounted OPGs had a sharp linear increase at low PAR up to 0.32 at 21 μmol m^{-2} s^{-1}, subsequently lagging to a maximum of 0.52 at 1251 μmol m^{-2} s^{-1}. On the other hand, wastewater mounted samples experienced a lower qN capacity with a rapid linear increase to 0.28 at a higher intensity of 111 μmol m^{-2} s^{-1} and a maximum of 0.45 at 1251 μmol m^{-2} s^{-1}. The regression coefficient fit on the linear increase was 0.005 for DI mounted samples, and 0.002 for wastewater inoculates (r^2=0.97). In addition, the NPQ potential for HL samples, was higher in DI mounted samples than wastewater mounted samples with a maximum of 0.19 and 0.12, respectively. Regression fit on the linearly increasing data points resulted in slope coefficients of 0.001 for DI and 0.0003 for wastewater mounted samples (r^2=0.97), indicating a 3.3 times higher rate of NPQ increase for DI samples. Despite the long term similarity of fluorescence yields (Figure 3- 3-b), inoculating HL samples in WW confers some quenching resilience compared to DI water. This can be attributed to an extended illumination period in determination of quenching coefficients reflecting amendment of photosynthesis by substrates in WW. NPQ was also higher in HL samples (Figure 3- 4-c) than in LL DI mounted

OPGs (Figure 3- 4-d) indicating a higher sensitivity of HL samples to higher light intensities and was similar to observed fluorescence yield trends (Figure 3- 3).

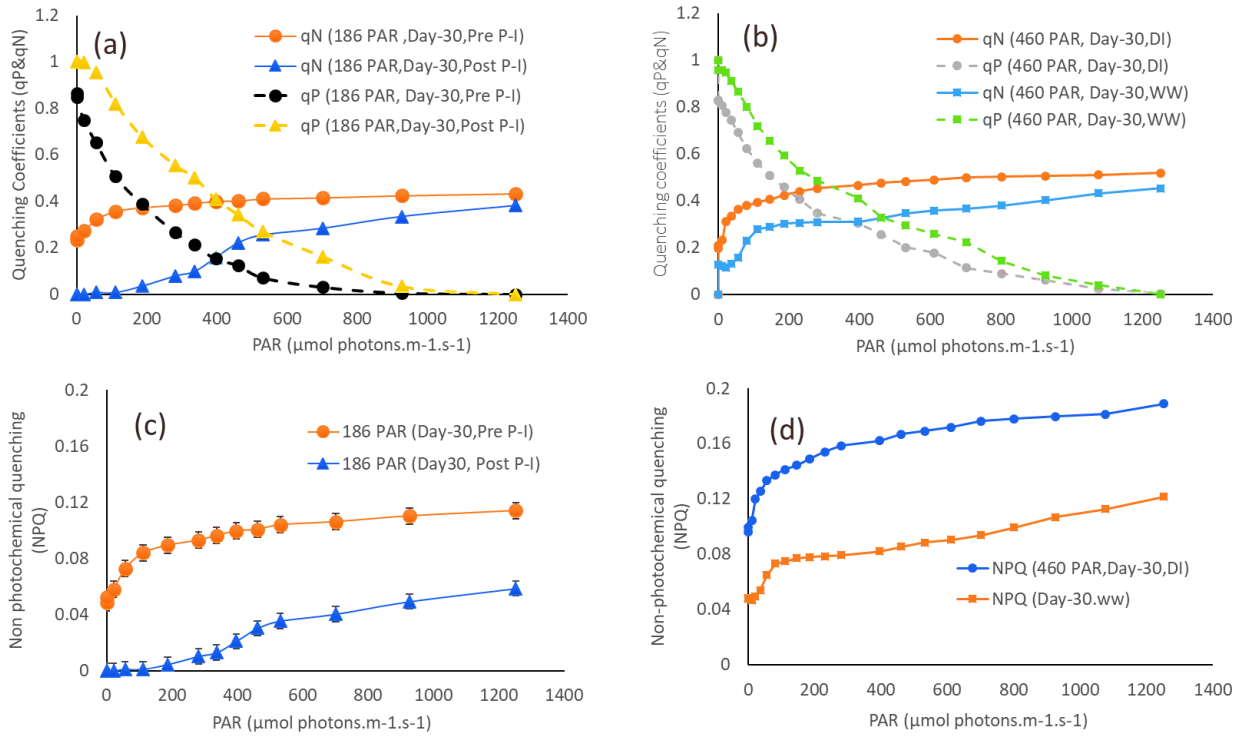

Figure 3- 4: Derived quenching coefficients from rapid light curves applied to light-adapted OPG biomass, photochemical quenching (qP), Non-photochemical quenching (qN) and Stern-Volmer coefficient of non- photochemical quenching (NPQ) expressed as a function of increasing PAR (µmol m^{-2} s^{-1}). (a) qN (solid lines) and qP (dashed lines) for 200 µmol m^{-2} s^{-1} ±20 (LL) adapted OPG pre (○) and post (Δ) photosynthetic oxygen evolution (POE) experiments with samples dark-adapted in DI.(b) qN (solid lines) and qP (dashed lines) parameters for 460 µmol m^{-2} s^{-1} (Pre POE) growth irradiance and dark-adapted in DI (○) and wastewater (WW) (□). (c) and (d) NPQ for 200 and 460 µmol m^{-2} s^{-1} growth irradiances, respectively. HL samples were analyzed pre-POE.

The product of effective quantum yield (ϕ_{PSII}) and PAR gives a relative indication of electron transport [25] since the ϕ_{PSII} is independent of light-harvesting pigment concentrations. The plots of rETR and irradiance showed a curvilinear relationship (Figure 3- 5). A butte followed a monotonic increase in the light-limited zone with a maximum rETR before an rETR limited decrease ensued. OPGs cultivated under low light experienced a 1.4 times increase (55 -75.8) in rETR peaks from exposure to higher light during POE experiments (Figure 3- 5-a). In comparison, OPG biomass

cultivated under 460 μmol m^{-2} s^{-1} had comparable $rETR_{max}$ of 69.6, and 69.3 for DI and WW inoculated samples (Figure 3- 5-b). The HL samples were all processed using pre-POE OPGs, and peak rETR were attained at irradiances of 611 μmol m^{-2} s^{-1} (Figure 3- 5-b). In comparison, LL samples' rETR peaks were 478 μmol m^{-2} s^{-1} (Figure 3- 5-a). The decay observed with RLC can be attributed to downregulation of PSII as opposed to photodamage inherent in POE experiments [25,58].

The parameters from the model fit (Eq 3-5) on the RLC and POE data are presented in Table 3- 1 below. The light saturation coefficient (α) for both LL and HL samples was on average, 0.35 (±0.04) under all conditions (Table 3- 1). This result alludes to a similar photosynthesis response for the OPGs investigated, in light-limited conditions. In contrast, the decay coefficient (β) for LL samples pre-POE was 17.1 and was 3.8 times lower than that of post-POE samples. This RLC decay coefficient for post-POE samples (64.2) was comparable to values obtained for POE determination of LL samples (72.5) (Table 3- 1). In HL samples, a lower β was obtained for DI mounted samples (0.1) compared to WW mounted samples (17.3) indicating a lower sensitivity to saturating light conditions. The higher decay rate could be reflective of elevated microbial activity in substrate laden wastewater compared to DI. A lower minimum saturating irradiance (Ek) was obtained for pre-POE LL samples (145 μmol m^{-2} s^{-1}) compared to 205 μmol m^{-2} s^{-1} for post-POE samples (Table 3- 1). This result parallels the higher qP values in post-POE samples (Figure 3- 4-a) suggesting plasticity of OPG photosynthetic clades. However, the higher Ek in post-POE samples was comparable to that obtained for POE experiments with LL samples (250 μmol m^{-2} s^{-1}). The difference in pre and post-POE minimum saturating irradiances can, therefore, be imputed to structural differences of RLC and POE experiments and OPG morphology.[15,18] The Ek for HL samples was 196 μmol m^{-2} s^{-1}, and 235 μmol m^{-2} s^{-1} for OPGs mounted in DI and WW

respectively (Table 3- 1). These irradiances were lower than those determined from POE experiments with HL samples (656 µmol m^{-2} s^{-1}) (Figure 3- 2).

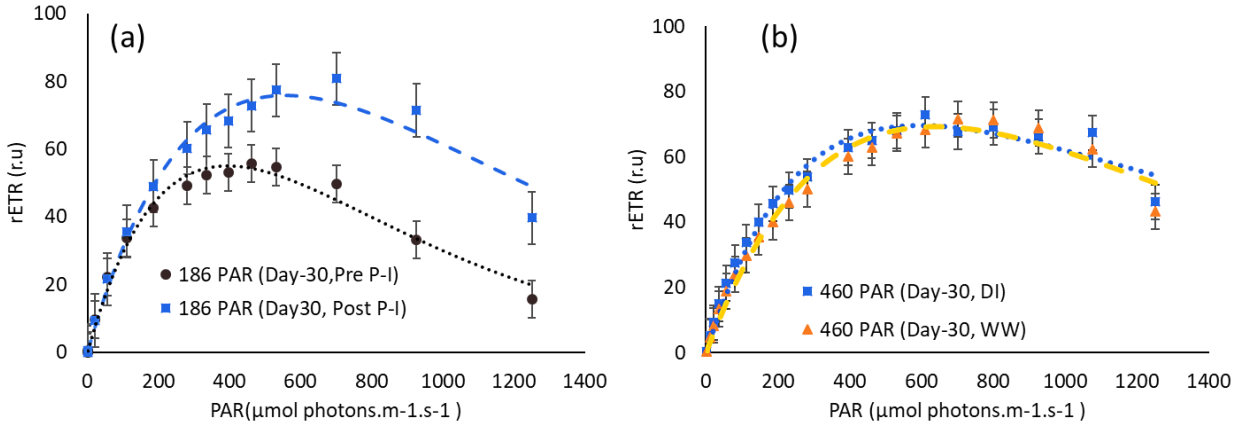

Figure 3- 5: rETR relationship for OPGs grown at different irradiance with increasing light intensity (a) 200 µmol m^{-2} s^{-1} (b) 460 µmol m^{-2} s^{-1}. The PAM setting of 8 was used for chlorophyll fluorescence equivalent to 186 µmol m^{-2} s^{-1} actinic light for the LL cultivation. Dotted lines show the regression fit using the Platt estimation and orthogonal distance regression algorithm.

Table 3- 1: Summary of Photosynthetic parameters from chlorophyll fluorescence experiments. Induction coefficients presented in columns (a)-(c) with respective standard deviations. The effective fluorescence yield(ϕ_{PSII}) for abiotic stress experiments. Rapid light curve parameters are shown in columns (d)-(h) with standard errors where included. The curvilinear double decay function defined in Eq.4-5 was used to estimate growth (α) and decay (β) coefficients which were then used to compute maximum rETR and E_K.

Actinic Light (µmol photons.m^{-1}.s^{-1})			**(a) Fv/FM**	**±Std.Dev**	**(b) Fo**	**±Std.Dev**	**(c) Fm**	**±Std.Dev**	**(d) Ps**	**Std.Error**	**(e) alpha(α)**	**Std.Error**	**(f) Beta(β)**	**Std.Error**	**(g) rETRmax**	**(h) Ek (µmol.m^{-1}.s^{-1})**
	Pre POE	DI	0.612	0.108	0.030	0.007	0.086	0.020	6.81E+03	2.97E+06	0.38	0.020	17.09	7.53E+03	55	145
186	Post POE	DI	0.408	0.331	0.046	0.008	0.077	0.015	3.58E+04	5.14E+06	0.37	0.019	64.21	9.23E+03	76	205
	Pre POE	DI	0.582		0.043	0.005	0.114	0.023	1.26E+02	3.35E+01	0.35	0.023	0.08	4.90E-02	70	196
460	Pre POE	WW	0.464	0.035	0.053	0.008	0.097	0.013	1.11E+04	2.51E+06	0.29	0.012	17.31	3.94E+03	69	235
186±42	POE								4.95E+04	3.34E+08	0.78	0.554	72.48	4.91E+05	196	250
460±23	POE								2.03E+05	4.59E+08	1.59	0.779	112.84	2.58E+05	1044	656
Temp (°C)	**pH**		**ϕ_{PSII}**	**Fv/Fm**	**Fo**	**±Std.Dev**	**Fm**	**±Std.Dev**	**Ps**	**Std.Error**	**alpha(α)**	**Std.Error**	**Beta(β)**	**Std.Error**	**rETRmax**	**Ek**
50°C	pH 6.17	DI	0.000	0.000	0.029	0.004	0.029	0.004	0.00E+00	0.00E+00	0.00	0.00	0.00	0.00E+00	0	0
	pH 7.57	WW	0.000	0.000	0.039	0.004	0.039	0.004	0.00E+00	0.00E+00	0.00	0.00	0.00	0.00E+00	0	0
23°C	pH 6.17	DI	0.594	0.587	0.058	0.007	0.135	0.019	1.91E+04	3.65E+06	0.31	0.02	40.53	7.76E+03	54	173
	pH 7.57	WW	0.583	0.575	0.051	0.007	0.122	0.018	5.53E+03	1.91E+06	0.36	0.02	8.26	2.91E+03	86	241
23°C	pH 3	DI	0.622	0.622	0.051	0.012	0.138	0.031	2.95E+01	2.23E+00	0.37	0.05	0.00	0.00E+00	29	80
	pH 3	WW	0.583	0.568	0.058	0.071	0.116	0.117	8.30E+01	3.72E+01	0.36	0.04	0.13	1.05E-01	37	105
-20°C	pH 6.17	DI	0.000	0.331	0.062	0.006	0.082	0.026	7.04E+00	9.26E-01	0.22	0.05	0.01	3.62E-03	6	29
	pH 7.57	WW	0.000	0.373	0.044	0.008	0.068	0.011	4.53E+03	1.89E+06	0.21	0.02	15.32	6.42E+03	23	108
23°C	pH 6.17	No Chl	0.000	0.000	0.030	0.006	0.030	0.005	0.00E+00	0.00E+00	0.00	0.00	0.00	0.00E+00	0	0
0.1 mg/l DCMU		DI	0.276	0.276	0.051	0.006	0.071	0.009	4.70E+04	1.03E+07	0.36	0.04	136.48	3.01E+04	45	126
10 mg/l DCMU		DI	0.134	0.103	0.072	0.017	0.080	0.020	1.41E+02	1.11E+05	0.01	0.00	0.24	1.93E+02	3	211
100 mg/l DCMU		DI	0.000	0.000	0.064	0.012	0.062	0.013	0.00E+00	0.00E+00	0.00	0.00	0.00	0.00E+00	0	0

The efficiency relation parameter (κ) was significantly higher (P=0.05) [66] for HL samples (1.8) compared to LL samples (0.7) (Figure 3- 6-a, b) with an almost linear relationship observed. A narrow range of this relation has been reported for green algae (1.9-4.9) compared to that of cyanobacteria (2.9-9.2) and diatoms (0.6-6.4) [11] also present in OPGs.[15,20,67]

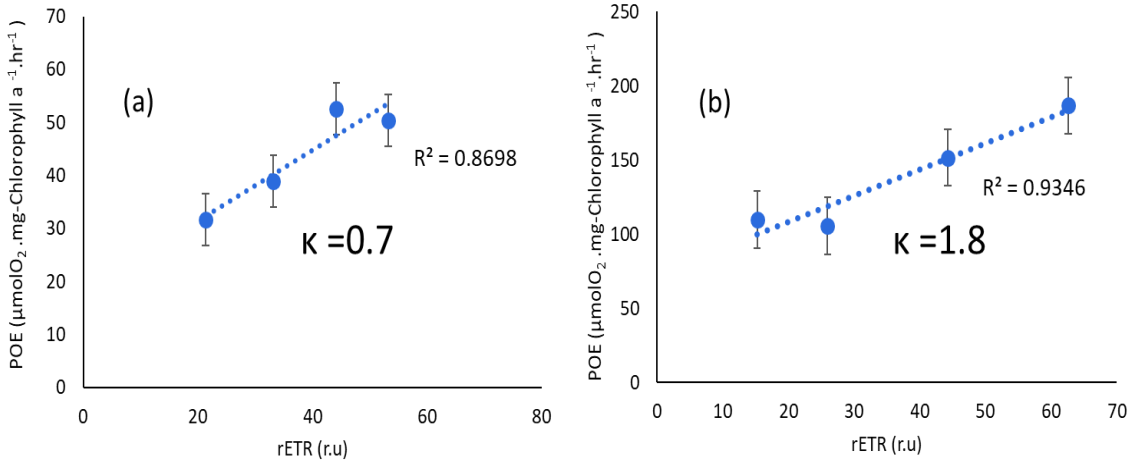

Figure 3- 6: Panels (a) and (b) show the linear regression fit on the first four data points in the light-limited region correlated to equivalent rETR values. (κ) relates the photosynthetic electron transport efficiency to photosynthesis efficiency. Error bars are standard errors of derived POE and rETR relation.

3.4.3 Fluorescence characterization of OPGs with induced stress

3.4.3.1 Evaluation of quenching capacities

The association of microbes in the environment plays a significant role in ensuring their survival by interdependence for trophic needs and protection against abiotic stresses.[68] In doing so, microbes often form structural frameworks such as biofilms and granules.[68,69] Granules, which are self-immobilized biofilms utilized in wastewater treatment confer

process benefits due to both their structure and composition. In addition to their better settlability,[12] granular systems have been reported to have high resilience to shock organic and toxic loadings.[70] The integrity of phototrophic based wastewater treatment process even under various system perturbations relies on the biochemical potential to generate essential oxygen. PAM experiments were used to characterize OPGs' photochemical activity under different toxic shocks.

When OPGs of 0.5-1 mm and grown under HL were exposed to a temperature of 50 ^{0}C, the photochemical quenching and non-photochemical quenching potentials of the granules in DI were extinguished (Figure 3- 7-a). The qP capacity of samples at 23 ^{0}C decreased to zero at 1076 μmol m^{-2} s^{-1} while the qN increased to a maximum of 0.6 (Figure 3- 7-a). When exposed to -20 ^{0}C, the qP coefficient of the OPGs decreased rapidly to a minimum of 231 μmol m^{-2} s^{-1}. These freeze treated samples exhibited a higher qN potential (peak 0.85) (Figure 3- 7-a). The NPQ coefficient similarly had higher maxima 0.32 for -20 ^{0}C compared to 0.19 for 23 ^{0}C OPG samples (Figure 3- 7-b). Rapid saturation of qP potential observed at low temperature translates to a higher non-photochemical quenching with increasing irradiance dissipating the excess energy. The linear increase between 0-81 μmol m^{-2} s^{-1} was defined by a coefficient of 0.003 for qN and 0.0006 for NPQ at 23 ^{0}C (r^2=97). At a temperature of -20 ^{0}C, the linear coefficients were 0.002 and 0.001 for qN and NPQ (r^2=98) with light intensity between 0-36 μmol m^{-2} s^{-1}. These coefficients translate to 0.67 (qN) and 1.7 (NPQ) times higher non-photochemical quenching at the lower temperature compared to room temperature samples. The qN and NPQ coefficients had Freundlich regression fit exponents of 0.18

(±0.08) and 0.30 (±0.01) for 23 ^{0}C temperature conditions. Under -20 ^{0}C, the coefficients had exponents of 0.13 (±0.01) and 0.03 (± 0.001) for qN and NPQ, respectively. All the regression fits had an r^2=0.98.

Figure 3- 7-c shows quenching coefficients qP and qN for samples inoculated in DI at different pH values. The photochemical quenching coefficient (qP) decreased to a minimum at 1076 μmol m^{-2} s^{-1} for both pH-3 and pH 6.2 but had more lag under pH-3, indicating a drastic pH instigated decrease of the photochemical quenching rate. Moreover, the qN (Figure 3- 7-c) and NPQ (Figure 3- 7-d) quenching coefficients had higher peaks at pH-3 (0.60, 0.33) compared to pH 6.2 (0.64, 0.19). The linear increase of qN and NPQ at low intensities had regression fits of 0.004 and 0.002, respectively, at pH-3. This increase represents a 1.3 times higher rate of qN saturation and 3.3 times for NPQ due to lower pH. This pH impact on the quenching coefficients was higher than that of low-temperature conditions induced. It has been reported that the non-photochemical quenching potential increased at low pH for green alga *Chlamydomonas acidophila* with reduced electron transfer between PSII and PSI.[71] Hyperosmotic conditions induce additional respiratory cost on the photochemical electron transport, which could account for the lower qP.[71] A regression fit of the pH-3 data set resulted in Freundlich exponents of 0.08 (±0.01) for qN and 0.15 (±0.02) for NPQ. No quenching capacity in OPGs' without chlorophyll (No Chl) was detected (Figure 3- 7-c,d). This implies that fluorescence of signal irradiance emanates from chlorophyll pigments within the OPGs.

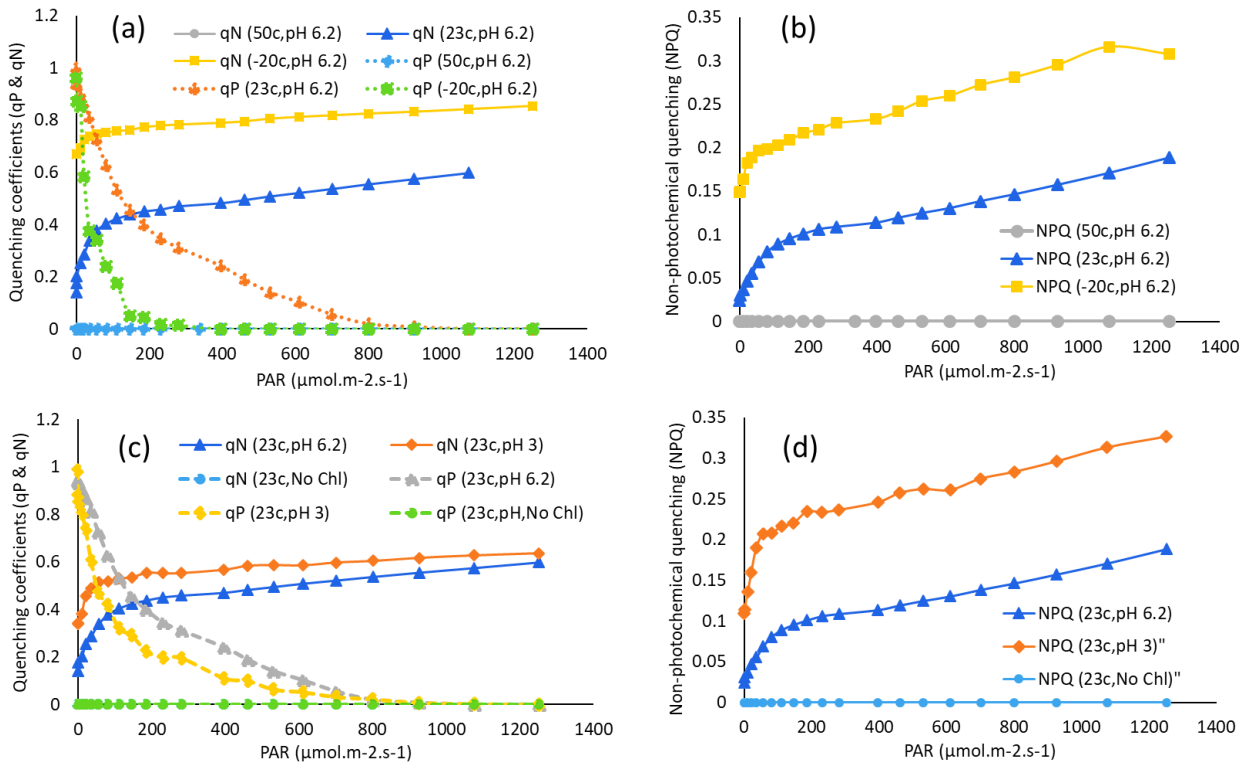

Figure 3- 7: Quenching parameters derived from rapid light curves applied to abiotic stress adapted OPG biomass in deionized water (DI) photochemical quenching (qP), Non-photochemical quenching (qN) and Stern-Volmer coefficient of non-photochemical quenching (NPQ) expressed as a function of increasing PAR (µmol m^{-2} s^{-1}). (a) qN (solid-lines) and qP (dashed lines) for temperature adapted OPGs at (○) 50^{0}C, (Δ) 23^{0}C, and (□)-20^{0}C. (b) NPQ for temperature adapted OPGs at (○) 50^{0}C, (Δ) 23^{0}C, and (□)-20^{0}C. (c) qN and qP for OPGs adapted to different pH at 23^{0}C with (Δ) pH 6.2 and (◊) pH 3 (○) Chlorophyll extracted samples. (d) NPQ for samples adapted to (Δ) pH 6.2 and (◊) pH 3 (○) Chlorophyll extracted samples. All samples were stress adapted for 4 hours before testing.

In wastewater inoculated samples, high temperatures depressed qP signals while freezing resulted in a rapid decrease (0 at 396 µmol m^{-2} s^{-1}) of photochemical potential (Figure 3-8-a) compared to room temperature samples (0 at 1251 µmol m^{-2} s^{-1}). No qN potential was observed with 50 ^{0}C sets while both -20 ^{0}C and 23 ^{0}C had similar trends and comparable peaks 0.5 (Figure 3- 8-a). The NPQ trends were similar for room and freezing temperature conditions and were depressed at high temperature (Figure 3- 8-b). In contrast to the DI mounted samples, the rapid qP saturation did not result in higher qN

at freezing temperatures. Additionally, higher qN peaks resulted in DI (0.85) compared to WW (0.5) mounted samples (Figure 3- 7-a, Figure 3- 8-a). Similarly, peak NPQ values were 0.31 and 0.11 for frozen DI and WW samples, respectively (Figure 3- 7-b, Figure 3- 8-b). Low pH stress in WW samples resulted in repressed qP reducing to 0 at 926 µmol m^{-2} s^{-1}. A plateau followed the rapid increase in both qN and NPQ coefficients up to 281 µmol m^{-2} s^{-1}. In contrast, the coefficients at pH 7.57 increased with light intensity (Figure 3- 8-b). Both DI and WW inoculation had similar qN and NQP trends under low pH stress (Figure 3- 7-c,d, Figure 3- 8-c,d).

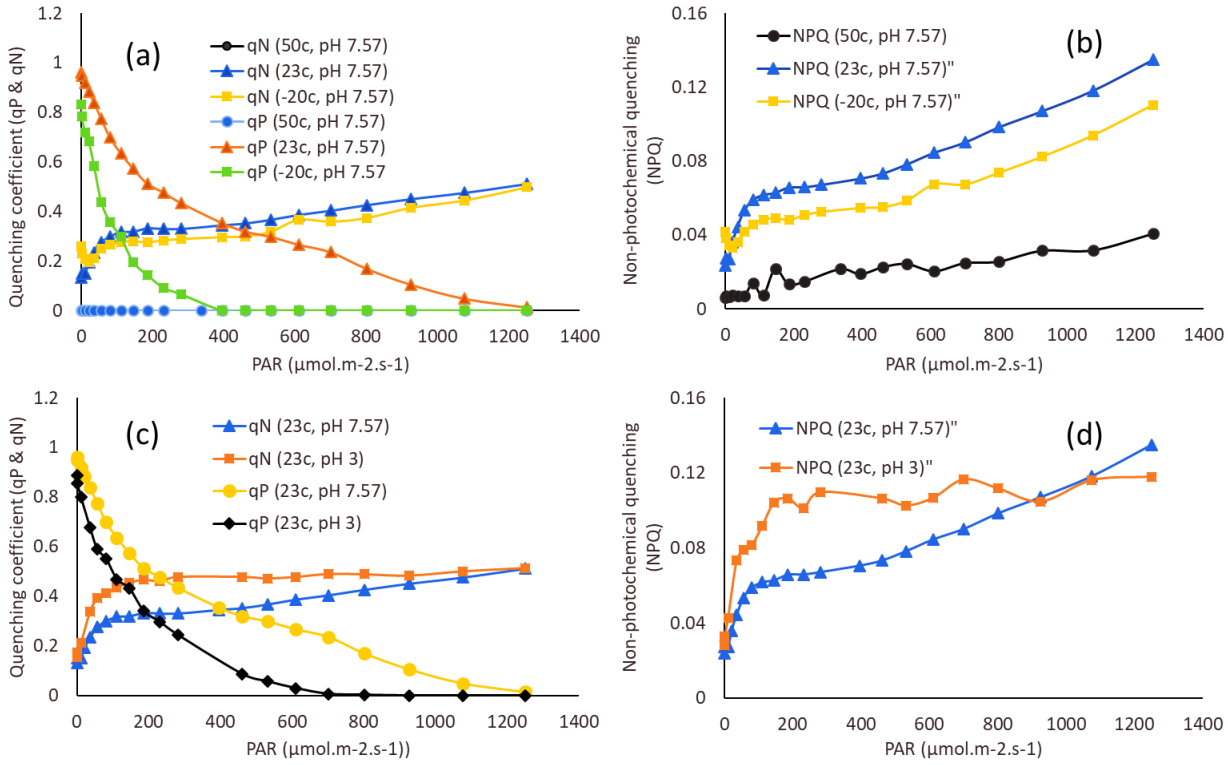

Figure 3- 8: Quenching parameters- derived from rapid light curves applied to abiotic stress adapted OPG biomass in wastewater (WW)-photochemical quenching (qP), Non-photochemical quenching (qN) and Stern-Volmer coefficient of non-photochemical quenching (NPQ) expressed as a function of increasing PAR (µmol m^{-2} s^{-1}). (a) qN and qP for temperature adapted OPGs at (○) 50^0C, (Δ) 23^0C, and (□)-20^0C. (b) NPQ for temperature adapted OPGs at (○) 50^0C, (Δ) 23^0C, and (□)-20^0c. (c) qN and qP for OPGs adapted to different pH at 23^0C with (Δ) pH 7.57 and (○) pH 3. (d) NPQ for samples adapted to (Δ) pH 7.57 and (○) pH 3. All samples were stress adapted for 4 hours before testing.

Photochemical quenching (qP) was inversely proportional to the DCMU concentration. A linear fit on the data points resulted in slopes of -0.002 and -0.025 for 0.1 mg/L and 10 mg/L DCMU, respectively (Figure 3- 9-a). This slope coefficient represents a 12.5 times qP decrease for 100 times increase in DCMU photo inhibitor concentration. A higher initial fluctuation was observed for non-photochemical quenching coefficient qN with maximum levels of qN coefficients of 0.42, 0.20 and 0.15 (Figure 3- 9-a) for 0.1, 10 and 100 mg/L DCMU concentrations, respectively. No qP was detected for 100 mg/L DCMU concentrations. While high peaks (0.52) and NPQ fluctuations were observed with 100 mg/L, the respective maximum NPQ values were 0.053 and 0.013 for 0.1 and 10 mg/L of DCMU (Figure 3- 9-b). A fit on the NPQ linear trend resulted in a slope ratio of 0.17 for 100 times increase in DCMU concentration. DCMU causes phototoxicity by inhibiting electron transfer between the primary (Q_A) and secondary (Q_B) quinone acceptor of PSII. Compromised electron transfer reduces the activity of the oxygen-evolving complex in addition to other cellular processes such as chlorophyll synthesis [72].

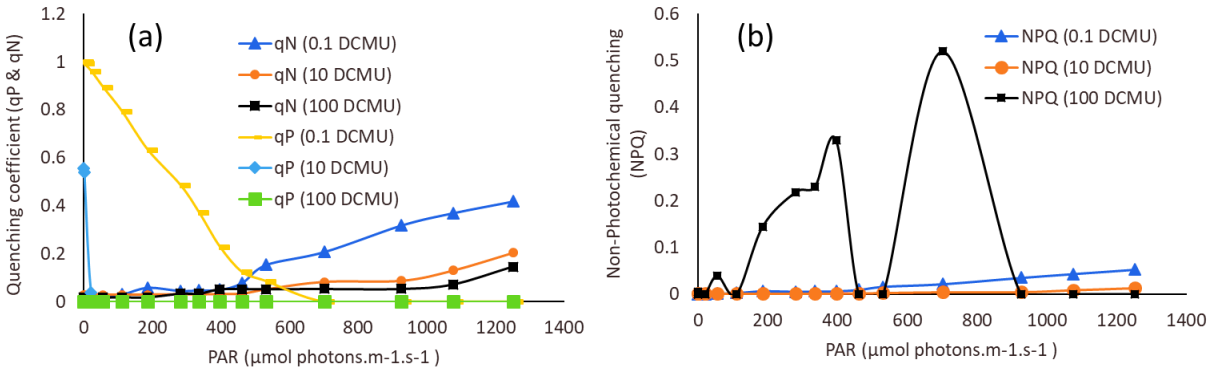

Figure 3- 9: Quenching parameters derived from rapid light curves applied to OPG samples adapted to different concentrations of 3-(3,4-dichlorophenyl)-1,1-dimethylurea(DCMU). Photochemical quenching (qP), Non-photochemical quenching (qN) and Stern-Volmer coefficient of non-photochemical quenching (NPQ). (a) qP and qP for (Δ) 0.1mg/l DCMU, (○) 10mg/l DCMU, and (□) 100mg/l DCMU. (b) NPQ for (Δ) 0.1mg/l DCMU, (○) 10mg/l DCMU, and (□) 100mg/l DCMU.

3.4.3.2 Rapid light curves characterization (RLC)

Both 50 ^{0}C temperature (Figure 3- 10-a, c) and chlorophyll extracted samples (Figure 3- 10-b, d) had no effective quantum yield and consequently no rETR with increasing irradiance. Decreasing the temperature from 23 ^{0}C to -20 ^{0}C (Figure 3- 10-a) on the other hand, resulted in an 8.5 times decrease in $rETR_{max}$ (53.7-6.3) for DI inoculated samples (Table 3- 1). In comparison, a 3.7 times decrease of $rETR_{max}$ ensued for samples mounted in wastewater (86-23) with a similar temperature change (Figure 3- 10-c, Table 3- 1). Samples mounted in WW had higher photochemical quenching coefficients (Figure 3- 8-a) and relative electron transport rates (Figure 3- 10-c) compared to DI mounted samples (Figure 3- 7-a, Figure 3- 10-a). These results can be attributed to either heightened oxygen scavenging by heterotrophic and ammonia oxidizers present in granules or pH differences (7.6 vs 6.2) (Table 3- 1). Similarly, the pH mediated depression of qP in occurred in DI mounted samples (Figure 3- 7-a). Lower $rETR_{max}$ values; 29.5, 37.2 resulted with a pH-3 for DI and WW mounted samples, respectively (Table 3- 1). Maximum rETR values of 45.4, 2.8, and 0 were recorded for 0.1, 10 and 100mg/l of DCMU (Figure 3- 11, Table 3- 1), respectively. The regression analysis had an average r=0.99 for all the stress conditions. Low-temperature treatment (-20^{0}C) in DI (Figure 3- 10-a) and wastewater (Figure 3- 10-b) mounted samples and in 10 mg/l DCMU treatments (Figure 3- 11) resulted in a plateau of the rETR with increasing irradiance with no decaying trend (Figure 3- 10-b).

The corresponding minimum saturation irradiances (E_K) at which downregulation of photosynthesis occurred decreased by an average of 55% (±2) with the decrease in pH to 3 for both DI and WW mounted samples (Table 3- 1). Freezing conditions, on the other hand, resulted in an 83% lower E_K for DI compared to 55% for WW mounted samples. The E_K of 0.1 mg/l DCMU treated samples decreased by 27% while that of 10 mg/l samples increased by 22% (Table 3- 1). Similarly, the alpha values increased by 19% with pH reduction in DI but remained the same (0.36±0.02) for WW mounted samples. The photoinhibition at high irradiances for these low pH samples occurred with a 98% lower decay coefficient (β) in wastewater mounted samples (Table 3- 1). No apparent inhibition occurred for DI mounted samples (Figure 3- 10-a) subjected to pH 3 stress (Table 3- 1). Low temperature (-20^{0}C) decreased the saturation coefficient (α) to an average of 0.22 for both DI and WW sets. On the other hand, a low decay coefficient (0.01) occurred for DI samples subjected to freezing conditions (Figure 3- 10-b) while increasing about 2-fold for wastewater mounted samples (Figure 3- 10-c) in comparison to room temperature values (Table 3- 1).

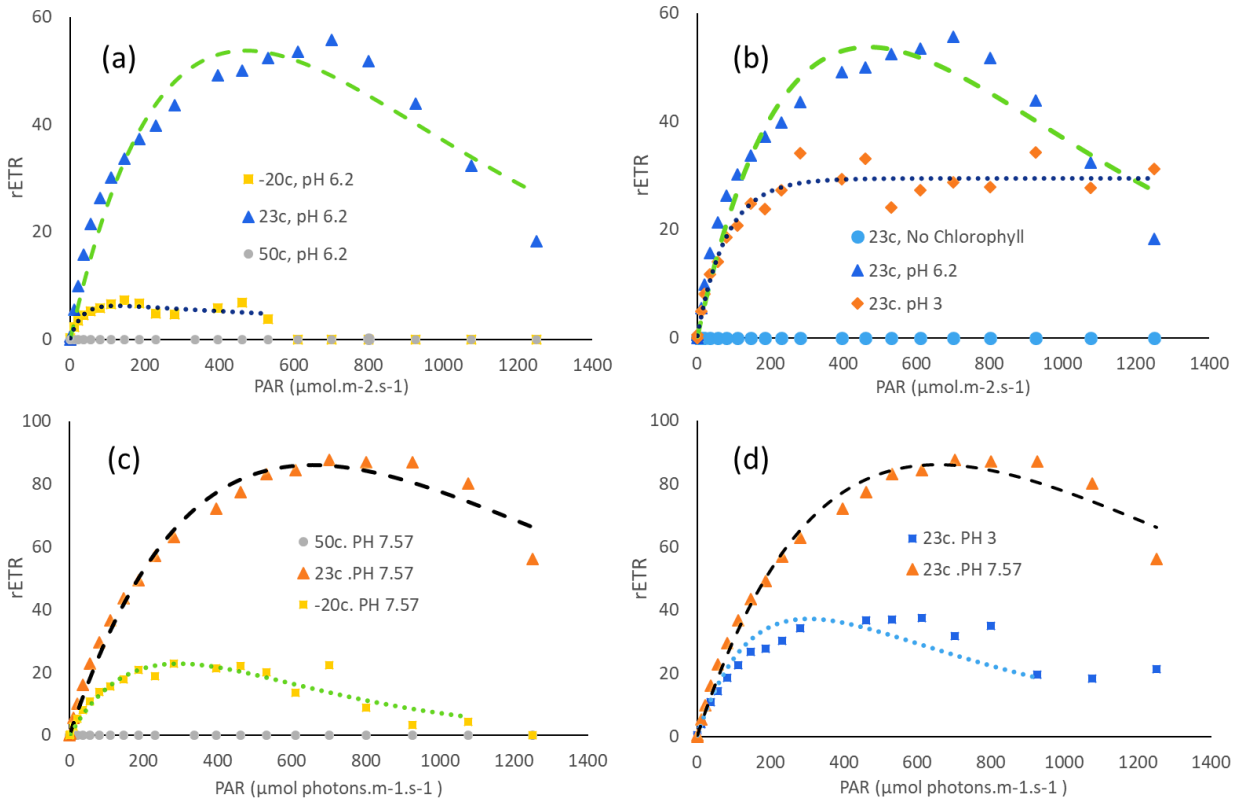

Figure 3- 10: Relative electron transport rates for various stress adapted OPG biomass plotted against increasing PAR (µmol m^{-2} s^{-1}.) (a), Temperature adaptation of DI, (□) -20^0C, (Δ) 23^0C, and (○) 50^0C at pH 6.2. (b) (○) 23^0C chlorophyll extracted samples, (Δ) 23^0C pH 6.2, (◊) 23^0C and pH 3. (c) OPG samples inoculated in wastewater (○) 50^0C (Δ) 23^0C and (□) -20^0C. (d) Wastewater inoculated samples at (□) 23^0C and pH 3 (Δ) 23^0C and pH 7.57. Dotted lines are the regression curve fit of the data points using the Platt double decay equation for curvilinear photosynthesis and convergence using orthogonal distance regression.

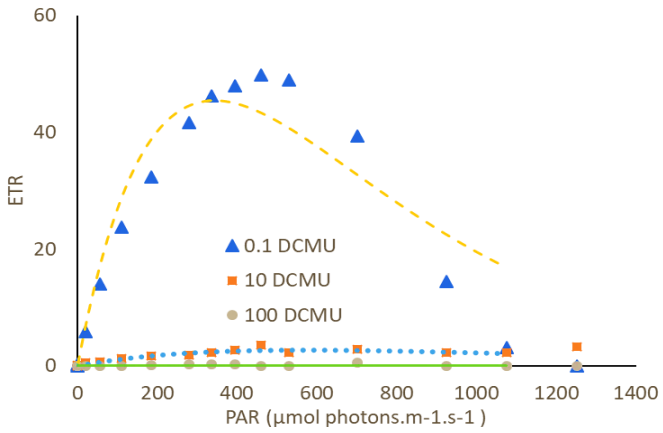

Figure 3- 11: Relative electron transport rates for various stress adapted OPG biomass plotted against increasing PAR (µmol m−2 s−1.). (Δ) 0.1mg/l DCMU, (□) 10mg/l DCMU, and (○) 100mg/l DCMU. Dotted lines are the regression curve fit of the data points using the Platt double decay equation for curvilinear photosynthesis and convergence using orthogonal distance regression.

3.5 Discussion

Biological wastewater treatment cultures microbes in a wastewater stream to uptake dissolved substrates [14,73] through enhanced microbial bioprocesses.[24,74,75] In the activated sludge process, provision and maintaining of dissolved oxygen concentration foster the preferential activity of aerobic microbes to oxidize organics, ammonia and other chemical constituents.[76] Converse to this external addition of oxygen, photosynthetic anchored wastewater systems rely on the biological generation of oxygen [14,67] to satisfy the process oxygen requirement. This photosynthetic process is powered by photon energy harnessed by the light-harvesting antennae [2] of phototrophs. The photosynthetic oxygen evolution increased with light intensity to a maximum (Figure 3- 2) and at a higher incident irradiance for HL than LL adapted samples. These results allude to an inherent photosynthetic versatility of clades in OPGs. The reported POE signals represent the net photosynthetic activity independent of photorespiration.

High photon energy can, however, result in photoinhibition.[31] This inhibiting intensity varied with growth irradiances (Figure 3- 2, Figure 3- 5) and was higher for HL adapted OPG biomass. Light intensity within the photochemical range of the granular biomass, on the other hand, fosters a balance in both the production and consumption of oxygen. Target dissolved oxygen levels can indicate treatment efficacy in batch operations or retention time in continuous flow. When light is limited, the retention times can be increased to reflect the reduced oxygen generation capacity of the system. The saturation rate coefficient (α) increased twofold (Table 3- 1) with HL treatment equivalent to the ratio of HL to LL irradiances for POE experiments. OPGs subjected to HL likewise had a higher decay coefficient (β=112.8) (Table 3- 1) from the POE model fit. The maximum rETR (1044) for POE experiments at the saturating rate was also found to be 5.3 times higher in HL samples with corresponding saturating irradiances (E_k) ratio of 2.6. One theory to explain this high increase of POE_{max} relative to E_k is a higher light penetration into the granular matrix at higher irradiances activating more photoactivity (Table 3- 1). Despite adaptation to higher growth irradiance, a higher decay coefficient indicates a rapid loss of photosynthetic potential (Figure 3- 2).

PAM utilizes fluorescence signals to characterize photochemical activity. The RLC derived from fluorescence experiments resulted in lower peak irradiances (Figure 3- 5) compared to POE (Figure 3- 2). Maximum saturation rates (α) from RLC data for LL and HL adapted OPGs were comparable (0.38 and 0.35) for DI mounted samples (Table 3- 1). However, these rates were 2.1 and 5.4 times lower than corresponding LL and HL

samples, using POE data. Similarly, the decay rates were also 4.2 and 6.5 times lower (Table 3- 1) for RLC experiments. POE experiments induce steady-state conditions at each light intensity while short light pulses utilized in RLC experiments could account for the lower RLC model coefficients.[25]

Moreover, RLCs are dependent on the light pre-history of the phototrophic moiety while POE curves indicate the optimal conditions independent of light history.[25] As both POE and RLC samples were pre-treated similarly, their different coefficient values can also be attributed to the morphology and stratification of the OPGs.[15,18] RLC illumination of the photosynthetic culture is 1-dimensional. The resulting fluorescence and estimations of electron transport rates represent partial light utility in the spheroidal OPG aggregates. In comparison, POE experiments which exhibited higher model coefficients and saturating irradiances reflect overall granule utility. A granular spin resulting from particle-particle interactions and mixing operations in POE determination could expose more photosynthetic apparatus to light. However, variable light penetration in relation to granules stratification could result in shading hence lower the POE activity.[77] This variable interaction impacts light utility within a reactor setting (Chapter 4).

The observed differences in POE and RLC parameters (Table 3- 1) can also be due to the cyanobacterial populations in OPGs.[20] The interpretation of cyanobacteria fluorescence can be compromised by the presence of other fluorescing light-harvesting pigments such as phycobilin's.[44] Moreover, cyanobacteria have evolved energy redistribution mechanisms between the photosystems, eliminating electron transport imbalances.[44]

These rapid state transitions present even in the dark can compromise the determination of non-photochemical quenching (qN).[11] In cyanobacteria, production and consumption pathways intersect in the same thylakoid membranes while also sharing the z-scheme plastoquinone acceptors.[44] At high irradiances, significant electron losses can occur in cyanobacteria with losses of 50-70% of average rates reported in *Synechosystis sp.* PCC 6803.[11] Moreover, oxygen uptake by dark respiration, photorespiration, cyclic electron flow around PSII and Mehler reactions where oxygen becomes reduced, forming superoxide radicals [31,44,78] occurs in cyanobacteria. These competing needs can lead to underestimation of the oxygen generation from cyanobacteria,[44] an integral clade in OPGs. In addition, nitrogen assimilation can cause lower photon yields (ϕ) of both POE and rETR.[55]

The relation of POE and RLC yields characterized by the κ parameter (Figure 3- 6-a,b) for LL (0.7) and HL (1.8) samples are within the range of literature reported values for individual microbial populations.[11] These values reflect the mean activity of the commingled phototrophic consortia in OPGs and are lower than maximum values reported for cyanobacteria (κ =9.2) but within the lower limit reported for diatoms (κ=0.6). RLCs have resulted in higher variability of this correlation for cyanobacteria and diatoms.[11,44] Qualitative use to describe the state of PSII has therefore been recommended.[11,44]

The high light (HL) adapted OPGs had higher photosynthetic quenching capacity than LL adapted OPG biomass (Figure 3- 4-a,b) and had a reduced qP response to increasing light

intensity. Similarly, LL samples exposed to high light intensities during POE experiments exhibited similar qP trend and saturating intensity (1251 μmol m^{-2} s^{-1}) to HL samples (Figure 3- 4-a,b). These results indicate the inherent photochemical elasticity of the OPG biomass. Both the LL and HL adapted reactor granules mounted in DI exhibited a similar trend of non-photosynthetic quenching (qN, NPQ) potential, but HL samples had higher peaks (Figure 3- 4-a,b). The initial rate of qN increase was also 2.9 times higher under 460 μmol m^{-2} s^{-1} than comparable LL conditions. This non-photochemical quenching trend suggests that OPG growth at higher irradiances results in more rapid responses to inhibiting light.

Both POE and RLC, when utilized for photogranular characterization, can have various shortcomings. Typical POE experiments entail strict quantifying of carbon consumption or oxygen evolution from the prototrophic assemblage.[11,25,42] However, granular structures present several challenges for this approach. Granular stratification and variable distribution of phototrophic biomass within the granules of different sizes [14,18] negate the equivalence of bulk and individual granule photochemical capacities. The OPG size class (0.5-1mm) utilized for determination of photochemical capacity were reported to be most abundant within an OPG reactor and as having the highest oxygen generation potential (specific oxygen production rate of 21.9 ± 1.3 mg O_2/g VSS-h).[18,20,67] This oxygen production rate was also 75% higher than of the mixed reactor biomass [18] and approximated to a POE of 60 μmol-O_2/mg-chlorophyll a.hr for a 200 μmol m^{-2} s^{-1} irradiance [67] reactor operation. This generation is 4 times lower than the determined maximum POE value (241 μmol-O_2/mg-chlorophyll a.hr) at equivalent

growth irradiance (Figure 3- 2). Similarly, we can infer a maximum mixed biomass oxygen production as 60 μmol-O_2/mg-chlorophyll a.hr (22 mg O_2/g VSS-h) for the reported reactor.[67] This higher value indicates a maximum oxygen production in ideal reactor operation.

The use of phototrophic markers O_2 and CO_2 in OPGs is also more complicated than in pure cultures or higher plants. In granules, concurrent generation and consumption of oxygen occur with potential transfers out of and into the granule. This can affect the detection of POE signals and function of OPGs in wastewater treatment. The concentration of dissolved oxygen is an essential functional indicator of wastewater treatment processes. High oxygen concentration within the granular matrix can inhibit denitrification [14] while low concentrations can result in reduced COD oxidation rates by aerobic heterotrophs within the granule.[23,67,79] Above saturation concentrations of oxygen in the granules can induce oxidative stress from ROS and increase competition for Ribulose-1, 5-bisphosphate carboxylase/oxygenase (Rubisco) [80] hence decrease the electron transport rates.

Additionally, some oxygen generated within the OPGs dissolves into the bulk fluid. At higher light intensities, the photosynthetic rate can be greater than the rate of oxygen consumption inducing oxidative stress.[80] An oxygen flux into the bulk fluid can result in higher concentrations of dissolved oxygen in the bulk fluid despite high organic loads; hence oxygen consumption (respiration) becomes the rate-limiting process for wastewater treatment. In the design of photobioreactors,[81] maintaining a balance between

oxygen consumption and production should, therefore, be considered in the determination of hydraulic retention time (Chapter 4).

Moreover, carbon transfers within the granule occur via multiple pathways.[40] Organic carbon, which constitutes the highest fraction in wastewater, is oxidized to CO_2 by heterotrophic oxidation. This carbon product can become available for photosynthetic activity resulting in mutualistic associations.[14] Inorganic carbon from the atmosphere can also be available for phototrophic activity via carboxylation in the wastewater stream, a process enhanced by mixing operations. We operated the POE experiments with minimal environmental interaction to limit this external addition of CO_2. Internal cycling of CO_2 was assumed to be a legacy of assimilated organic carbon. Applying carbon tracing for POE curves quantifies photosynthetic targeted inorganic carbon (^{14}C) [25,27] and may not capture this organic source derived carbon. Additionally, phototrophic microbes, including cyanobacteria, present in OPGs have versatile carbon assimilation and concentration mechanisms.[28,82] Members of the genus *Oscillatoria* and *Microcoleus* and chlorophytes genera *Scenedesmus* which are dominant in OPGs [20,83] have reported mixotrophic capacity.[84,85] This metabolic diversity enables microbes to survive in light-limited conditions by the synthesis of organic carbon sources. Hence carbon use within an OPG reactor may be understated due to this uptake in light-limited granule zones affecting POE estimations. This versatility also incurs a metabolic cost that may depress electron transport values for RLC estimations.

In POE evaluation of OPGs, particle morphology results in limited surface area exposure to light compared to pure cultures and plants [11,25,55] a condition that can be exacerbated with RLCs. Moreover, particle spin in POE determination can result in higher surface exposures compared to RLCs, which do not account for the 3-D structure of granules. The saturating irradiances provided [29] may also not penetrate the layered OPG structure [18] hence overestimating fluorescence parameters due to unquantified photochemical quenching. Moreover, it has been reported that chlorophyll quenching consistently understates the efficiency of the photosynthetic production in cyanobacteria. The low values can be attributed to understated yields parameters (F_0 and F_m).[44] Schuurmans et al. hence suggested a qualitative interpretation of this data.[44] In our samples, this error is apparent in the different POE and rETR saturation values (Table 3- 1).

In OPG reactors, the optimal photochemical capacity determined via POE experiments (Figure 3- 2) can be lessened by variable particle flow within the reactor.[86,87] The mixing speed influences the frequency of 'OPG light' events,[88,89] and longer exposures can result in photodamage.[31,32,90] Extended periods in the dark facilitate recovery from photoinhibition but can also lead to elevated photorespiration.[77,91,92] Self-shading effects resulting from particle interaction in relation to the optical path also depend on the size and biomass concentrations.[77] The bulk fluid mixing pattern is a function of reactor size, impeller design, and mixing intensity (Chapter 4). Moreover, particulate interactions and intra-granule substrate transfers depend on their physical permeability and porous characteristics (Chapter 5). Availability of substrates for photosynthesis can impact this optimal photochemical capacity as seen with WW mounted samples (Figure 3- 4).

The oxygenic photogranules were also subjected to various shocks. When subjected to a high temperature of 50 ^{0}C, the OPG biomass showed no photochemical (qP) potential. High temperatures impede the PSII redox reactions, by denaturing of proteins, reducing the plastoquinone acceptor pool and dissociation of ions (Ca^{2+}, Mn^{2+} and Cl^{-}) from the oxygen-evolving complex.[93] In addition, thermal stress enhances state transitions and increases ROS production hence lowering photoactivity.[93] While no non-photochemical quenching capacity (qN, NPQ) was observed in high-temperature conditions for DI mounted samples, WW mounted samples exhibited some quenching capacity as indicated by the NPQ coefficient which was 3.3 times lower than room temperature samples.

Moreover, the NPQ response exhibited an almost linear response to increasing light intensity (Figure 3- 8). Flexible non-photochemical quenching mechanisms in cyanobacteria and algae [63] in addition to alternative carbon sources (inorganic carbon) [85] could be responsible for the dissonance observed in NPQ for high temperature treated, DI and WW mounted sets. In abiotic stress conditions, mixotrophy provides an alternative metabolic pathway.[85] While microbes exhibit various thermal adaptations, cyanobacteria utilize state transitions and regulate the structure of the chlorophyll to withstand thermal stress. Moreover, temperatures above 35 ^{0}C are considered lethal to most algal biomass due to increased respiration and photorespiration rates.[80] Mesophilic bacteria and algae, however, show tolerance to higher temperatures of up to 75 ^{0}C.[80]

Low temperatures, on the other hand, resulted in depressed qP but high NPQ and qN coefficients compared to control samples (Figure 3- 7, Figure 3- 8). In addition, the saturation coefficients decreased by 31% and 46% for DI and wastewater mounted samples with the latter also exhibiting elevated decay sensitivity. The minimum saturation irradiances also decreased by 83% and 55% for cold stressed OPGs mounted in DI and wastewater, respectively (Table 3- 1). Various cyanobacterial and algal species [94] in lakes have reported optimum growth rates at a mean temperature of 29.2^0C with an optimum temperature of 35^0C. The low qP, α and Ek results indicate reduced photochemical activity which can be attributed to slow reaction kinetics.[92,95,96] In addition, cold acclimation has been reported to increase tolerance to photoinhibition.[92] Low (<16 ^{0}C) temperatures limit carbon fixation in microalgae while high temperatures lower the solubility of carbon dioxide in water.[80] Cryoconite granules found in the Arctic and Antarctic regions [97] have a close structural and microbial resemblance to OPGs.[18] Their keystone community- cyanobacteria are adapted to the low temperatures in the polar region.[98]

The pH decay induced decay of the photochemical quenching capacity was on average two times slower than control sets. The effect of pH on non-photochemical quenching coefficients resulted in a higher peak (0.33 vs 0.19) for NPQ, in samples mounted with DI water. The qP coefficient peaks were similar in both cases. However, initial rates of qN increase were higher at this low pH compared to room temperature samples. The pH regulation of inorganic carbon species distribution and availability for algal growth has been reported for neutral to alkaline conditions.[80] Deviations from the optimal 6-8.3 pH

range also affect enzyme activity. At pH between 6.3 and 10.3 carbonic anhydrase reversibly converts abundant bicarbonate for carboxylation of Rubisco maintaining photoactivity.[99] At pH less than 6.3, the bicarbonate substrate is limited with an abundance of aqueous CO_2, which has been reported as a potential hydration substrate.[100] This limitation impacts the photochemical activity evidenced by repressed rETR rates at both lower pH and temperature (Figure 3- 10). This pH adaptability and non-photochemical quenching responses mirrors that reported for *Chlamydomonas acidophila*.[71] The various adaptation strategies to maintain neutral intracellular pH such as active proton pumping incur metabolic energy cost hence decreased phototrophic activity [71] in OPGs.

The addition of DCMU induces phototoxicity by destroying chloroplasts electron transport mechanisms.[101] An erratic qN trend for inhibitor concentrations of 0.1 mg/l ensued. The qP at this low concentration had a decreasing monotonic trend (Figure 3- 9). This could be an indicator of structural resistance [102] to mass transfer into the granules arising from dense EPS structure [15] retaining some phototrophic capacity. At higher irradiances, the non-photochemical quotients increased inversely to the concentration of DCMU (Figure 3- 9). Some limited photosynthetic electron transport occurred with 10 mg/l inhibitor concentrations (Figure 3- 11). We can infer that OPGs have the adaptability to various abiotic stresses due to their microbial composition and adaptation, and granular structure when applied to wastewater treatment.

Granular assemblages confer adaptive benefits to microbial communities living within the self-immobilized biofilm.[103,104] Granules used in wastewater treatment have been reported to have a higher tolerance to shock loadings and toxic wastes.[105] Forming various associative interactions [14] provides protection and a source of substrates for metabolism. In OPGs and other bacterial aggregates, phototrophic microbes generate oxygen which is utilized by other communities within the granule colony.[14,18] Cyanobacteria also generate extracellular polymeric substances (EPS) from their gliding motility [15] while also conferring additional stress protection.[106,107]

3.6 Bibliography

1. Liu, J., Lu, Y., Hua, W. & Last, R. L. A New Light on Photosystem II Maintenance in Oxygenic Photosynthesis. *Front. Plant Sci.* **10**, (2019).

2. Green, B. & Parson, W. W. *Light-Harvesting Antennas in Photosynthesis*. (Springer Science & Business Media, 2003).

3. Saer, R. G. & Blankenship, R. E. Light harvesting in phototrophic bacteria: structure and function. *Biochem. J.* **474**, 2107–2131 (2017).

4. Singh, N. K., Sonani, R. R., Rastogi, R. P. & Madamwar, D. The phycobilisomes: an early requisite for efficient photosynthesis in cyanobacteria. *EXCLI J.* **14**, 268–289 (2015).

5. Young, A. J. Occurrence and distribution of carotenoids in photosynthetic systems. in *Carotenoids in Photosynthesis* (eds. Young, A. J. & Britton, G.) 16–71 (Springer Netherlands, 1993). DOI:10.1007/978-94-011-2124-8_2.

6. Bernstein, H. C. *et al.* Effect of mono- and dichromatic light quality on growth rates and photosynthetic performance of Synechococcus sp. PCC 7002. *Front. Microbiol.* **5**, (2014).

7. Wu, H. Effect of Different Light Qualities on Growth, Pigment Content, Chlorophyll Fluorescence, and Antioxidant Enzyme Activity in the Red Alga Pyropia haitanensis (Bangiales, Rhodophyta). *BioMed Res. Int.* **2016**, (2016).

8. Zhang, B. *et al.* Effect of light intensity on the characteristics of algal-bacterial granular sludge and the role of N-acyl-homoserine lactone in the granulation. *Sci. Total Environ.* (2018) DOI: 10.1016/j.scitotenv.2018.12.250.

9. Bailey, S. & Grossman, A. Photoprotection in cyanobacteria: regulation of light-harvesting. *Photochem. Photobiol.* **84**, 1410–1420 (2008).

10. Berg, M. & Sutula, M. Factors affecting the growth of cyanobacteria with special emphasis on the Sacramento - San Joaquin Delta. (2015).

11. Masojidek, J. Photosystem II Electron Transport Rates and Oxygen Production in Natural Waterblooms of Freshwater Cyanobacteria During a Diel Cycle. *J. Plankton Res.* **23**, 57–66 (2001).

12. Milferstedt, K. *et al.* Biogranules applied in environmental engineering. *Int. J. Hydrog. Energy* **42**, 27801–27811 (2017).

13. Liu, L., Fan, H., Liu, Y., Liu, C. & Huang, X. Development of algae-bacteria granular consortia in a photo-sequencing batch reactor. *Bioresour. Technol.* **232**, 64–71 (2017).

14. Lee, Y.-J. & Lei, Z. Microalgal-bacterial aggregates for wastewater treatment: A mini-review. *Bioresour. Technol. Rep.* 100199 (2019) DOI:10.1016/j.biteb.2019.100199.

15. Kuo-Dahab, W. C. *et al.* Investigation of the Fate and Dynamics of Extracellular Polymeric Substances (EPS) during Sludge-Based Photogranulation under Hydrostatic Conditions. *Environ. Sci. Technol.* **52**, 10462–10471 (2018).

16. Li, D. & Ganczarczyk, J. Advective Transport in Activated Sludge Flocs. *Water Environ. Res.* **64**, 236–240 (1992).

17. Sears K., Alleman J. E., Barnard J. L. & Oleszkiewicz J. A. Density and Activity Characterization of Activated Sludge Flocs. *J. Environ. Eng.* **132**, 1235–1242 (2006).

18. Abouhend, A. S. *et al.* Growth Progression of Oxygenic Photogranules and Its Impact on Bioactivity for Aeration-Free Wastewater Treatment. *Environ. Sci. Technol.* (2019) DOI:10.1021/acs.est.9b04745.

19. Bindhu, B. k. & Madhu, G. Selection pressure theory for aerobic granulation – an overview. *Int. J. Environ. Waste Manag.* **13**, 317–329 (2014).

20. Milferstedt, K. *et al.* The importance of filamentous cyanobacteria in the development of oxygenic photogranules. *Sci. Rep.* **7**, 17944 (2017).

21. Brudvig, G. W. Water oxidation chemistry of photosystem II. *Philos. Trans. R. Soc. B Biol. Sci.* **363**, 1211–1219 (2008).

22. Najafpour, M. M. & Govindjee. Oxygen evolving complex in Photosystem II: Better than excellent. *Dalton Trans.* **40**, 9076 (2011).

23. Park, C. & Dolan, S. (deceased). Patent Algal Sludge Granule OPG Jan 2019. 11, (2019).

24. Giesen, A., Loosdrecht, M. van, Pronk, M., Robertson, S. & Thompson, A. Aerobic Granular Biomass Technology: recent performance data, lessons learnt and retrofitting conventional treatment infrastructure. *Proc. Water Environ. Fed.* **2016**, 1913–1923 (2016).

25. Ralph, P. J. & Gademann, R. Rapid light curves: A powerful tool to assess photosynthetic activity. *Aquat. Bot.* **82**, 222–237 (2005).

26. MacIntyre, H. L., Kana, T. M., Anning, T. & Geider, R. J. Photoacclimation of photosynthesis irradiance response curves and photosynthetic pigments in microalgae and cyanobacteria1. *J. Phycol.* **38**, 17–38 (2002).

27. Macedo, M., Ferreira, J. & Duarte, P. Dynamic behaviour of photosynthesis-irradiance curves determined from oxygen production during variable incubation periods. *Mar. Ecol. Prog. Ser.* **165**, 31–43 (1998).

28. Murchie, E. H. & Lawson, T. Chlorophyll fluorescence analysis: a guide to good practice and understanding some new applications. *J. Exp. Bot.* **64**, 3983–3998 (2013).

29. *Chlorophyll a Fluorescence in Aquatic Sciences: Methods and Applications*. (Springer Netherlands, 2010). DOI:10.1007/978-90-481-9268-7.

30. *Non-Photochemical Quenching and Energy Dissipation in Plants, Algae and Cyanobacteria*. vol. 40 (Springer Netherlands, 2014).

31. Giacometti, G. M. & Morosinotto, T. Photoinhibition and Photoprotection in Plants, Algae, and Cyanobacteria. in *Encyclopedia of Biological Chemistry* (eds. Lennarz, W. J. & Lane, M. D.) 482–487 (Academic Press, 2013). DOI:10.1016/B978-0-12-378630-2.00229-2.

32. da C. A. Alves, P. L., Magalhães, A. C. N. & Barja, P. R. The Phenomenon of Photoinhibition of Photosynthesis and Its Importance in Reforestation. *Bot. Rev.* **68**, 193–208 (2002).

33. Hakkila, K. *et al.* Oxidative stress and photoinhibition can be separated in the cyanobacterium Synechocystis sp. PCC 6803. *Biochim. Biophys. Acta BBA - Bioenerg.* **1837**, 217–225 (2014).

34. Choudhury, F. K., Rivero, R. M., Blumwald, E. & Mittler, R. Reactive oxygen species, abiotic stress and stress combination. *Plant J.* **90**, 856–867 (2017).

35. Nishiyama, Y., Allakhverdiev, S. I. & Murata, N. A new paradigm for the action of reactive oxygen species in the photoinhibition of photosystem II. *Biochim. Biophys. Acta BBA - Bioenerg.* **1757**, 742–749 (2006).

36. Ware, M. A., Dall'Osto, L. & Ruban, A. V. An In Vivo Quantitative Comparison of Photoprotection in Arabidopsis Xanthophyll Mutants. *Front. Plant Sci.* **7**, (2016).

37. Havaux, M. & Niyogi, K. K. The violaxanthin cycle protects plants from photooxidative damage by more than one mechanism. *Proc. Natl. Acad. Sci. U. S. A.* **96**, 8762–8767 (1999).

38. Bao, H., Melnicki, M. R. & Kerfeld, C. A. Structure and functions of Orange Carotenoid Protein homologs in cyanobacteria. *Curr. Opin. Plant Biol.* **37**, 1–9 (2017).

39. Campbell, D., Hurry, V., Clarke, A. K., Gustafsson, P. & Öquist, G. Chlorophyll Fluorescence Analysis of Cyanobacterial Photosynthesis and Acclimation. *Microbiol Mol Biol Rev* **62**, 667–683 (1998).

40. Pastore, M., Santaeufemia, S., Bertucco, A. & Sforza, E. Light intensity affects the mixotrophic carbon exploitation in Chlorella protothecoides: consequences on microalgae-bacteria based wastewater treatment. *Water Sci. Technol.* **78**, 1762–1771 (2018).

41. Malapascua, J., Jerez, C., Sergejevová, M., Figueroa, F. & Masojídek, J. Photosynthesis monitoring to optimize growth of microalgal mass cultures: application of chlorophyll fluorescence techniques. *Aquat. Biol.* **22**, 123–140 (2014).

42. Bouman, H. A. *et al.* Photosynthesis–irradiance parameters of marine phytoplankton: synthesis of a global data set. 16 (2018).

43. Corcoll, N. *et al.* The Use of Photosynthetic Fluorescence Parameters from Autotrophic Biofilms for Monitoring the Effect of Chemicals in River Ecosystems. in *Emerging and Priority Pollutants in Rivers* (eds. Guasch, H., Ginebreda, A. & Geiszinger, A.) vol. 19 85–115 (Springer Berlin Heidelberg, 2012).

44. Schuurmans, R. M., van Alphen, P., Schuurmans, J. M., Matthijs, H. C. P. & Hellingwerf, K. J. Comparison of the Photosynthetic Yield of Cyanobacteria and Green Algae: Different Methods Give Different Answers. *PLOS ONE* **10**, e0139061 (2015).

45. ALPHA. *Standard Methods for the Examination of Water and Wastewater*. (ALPHA,AWWA,WEF, 2012).

46. Bennett, A. & Bogorad, L. Complementary chromatic adaptation in a filamentous blue-green alga. *J. Cell Biol.* **58**, 419–435 (1973).

47. Lawrenz, E., Fedewa, E. J. & Richardson, T. L. Extraction protocols for the quantification of phycobilins in aqueous phytoplankton extracts. *J. Appl. Phycol.* **23**, 865–871 (2011).

48. Sobiechowska-Sasim, M., Stoń-Egiert, J. & Kosakowska, A. Quantitative analysis of extracted phycobilin pigments in cyanobacteria—an assessment of spectrophotometric and spectrofluorometric methods. *J. Appl. Phycol.* **26**, 2065–2074 (2014).

49. Zavřel, T., Chmelík, D., Sinetova, M. A. & Červený, J. Spectrophotometric Determination of Phycobiliprotein Content in Cyanobacterium Synechocystis. *J. Vis. Exp.* (2018) doi:10.3791/58076.

50. Metz, J. G., Pakrasi, H. B., Seibert, M. & Arntzer, C. J. Evidence for a dual function of the herbicide-binding D1 protein in photosystem II. *FEBS Lett.* **205**, 269–274 (1986).

51. Bassham, J. A., Benson, A. A. & Calvin, M. The Path of Carbon in Photosynthesis VIII. The Role of MalicAcid. UCRL--584, 910351 (1950) doi:10.2172/910351.

52. Wezernak, C. T. & Gannon, J. J. Oxygen-Nitrogen Relationships in Autotrophic Nitrification. **15**, 5 (1967).

53. Adams, C. E. & Eckenfelder, W. W. Nitrification Design Approach for High Strength Ammonia Wastewaters. *J. Water Pollut. Control Fed.* **49**, 413–421 (1977).

54. Daigger, G. T. Oxygen and carbon requirements for biological nitrogen removal processes accomplishing nitrification, nitritation, and anammox. *Water Environ. Res. Res. Publ. Water Environ. Fed.* **86**, 204–209 (2014).

55. Figueroa, F. L. Relations between electron transport rates determined by pulse amplitude modulated chlorophyll fluorescence and oxygen evolution in macroalgae under different light conditions. *Photosynth. Res.* **75**, 259–275 (2003).

56. Hofstraat, J. W., Peeters, J. C. H., Snel, J. F. H. & Geel, C. Simple determination of photosynthetic efficiency and photoinhibition of Dunaliella tertiolecta by saturating pulse fluorescence measurements. *Mar. Ecol. Prog. Ser.* **103**, 187–196 (1994).

57. Oxborough, K. & Baker, N. R. Resolving chlorophyll a fluorescence images of photosynthetic efficiency into photochemical and non-photochemical components – calculation of qP and Fv-/Fm-; without measuring Fo-; *Photosynth. Res.* **54**, 135–142 (1997).

58. Platt, T., Harrison, W. G., Irwin, B., Horne, E. P. & Gallegos, C. L. Photosynthesis and photoadaptation of marine phytoplankton in the arctic. *Deep Sea Res. Part Oceanogr. Res. Pap.* **29**, 1159–1170 (1982).

59. Brightman, R. & Smith, W. Photosynthesis-irradiance relationships of Antarctic phytoplankton during austral winter. *Mar. Ecol. Prog. Ser.* **53**, 143–151 (1989).

60. Li, J., Luo, G., He, L., Xu, J. & Lyu, J. Analytical Approaches for Determining Chemical Oxygen Demand in Water Bodies: A Review. *Crit. Rev. Anal. Chem.* **48**, 47–65 (2018).

61. Miyata, K., Ikeda, H., Nakaji, M., Kanel, D. R. & Terashima, I. Rate Constants of PSII Photoinhibition and its Repair, and PSII Fluorescence Parameters in Field Plants in Relation to their Growth Light Environments. *Plant Cell Physiol.* **56**, 1841–1854 (2015).

62. Maxwell, K. & Johnson, G. N. Chlorophyll fluorescence—a practical guide. *J. Exp. Bot.* **51**, 659–668 (2000).

63. Niyogi, K. K. & Truong, T. B. Evolution of flexible non-photochemical quenching mechanisms that regulate light harvesting in oxygenic photosynthesis. *Curr. Opin. Plant Biol.* **16**, 307–314 (2013).

64. Mercado, J. M., Javier, F., Gordillo, L., Xavier Niell, F. & Figueroa, F. L. Effects of different levels of CO2 on photosynthesis and cell components of the red alga Porphyra leucosticta. *J. Appl. Phycol.* **11**, 455–461 (1999).

65. Thompson, M., Gamage, D., Hirotsu, N., Martin, A. & Seneweera, S. Effects of Elevated Carbon Dioxide on Photosynthesis and Carbon Partitioning: A Perspective on Root Sugar Sensing and Hormonal Crosstalk. *Front. Physiol.* **8**, (2017).

66. Pocock, S. J. The simplest statistical test: how to check for a difference between treatments. *BMJ* **332**, 1256–1258 (2006).

67. Abouhend, A. S. *et al.* The Oxygenic Photogranule Process for Aeration-Free Wastewater Treatment. *Environ. Sci. Technol.* **52**, 3503–3511 (2018).

68. Rickard, A. H., Gilbert, P., High, N. J., Kolenbrander, P. E. & Handley, P. S. Bacterial coaggregation: an integral process in the development of multi-species biofilms. *Trends Microbiol.* **11**, 94–100 (2003).

69. Stolz, J. F. Structure of Microbial Mats and Biofilms. *Microb. Sediments* 1–8 (2000) DOI:10.1007/978-3-662-04036-2_1.

70. Giesen, A., van Loosdrecht, M., Robertson, S. & de Buin, B. Aerobic Granular Biomass Technology: further innovation, system development and design optimisation. https://www.ingentaconnect.com/contentone/wef/wefproc/2015/00002015/00000016/art00018 (2015) doi:info:doi/10.2175/193864715819539641.

71. Gerloff-Elias, A., Spijkerman, E. & Pröschold, T. Effect of external pH on the growth, photosynthesis and photosynthetic electron transport of Chlamydomonas acidophila Negoro, isolated from an extremely acidic lake (pH 2.6). *Plant Cell Environ.* **28**, 1218–1229 (2005).

72. Pansook, S., Incharoensakdi, A. & Phunpruch, S. Effects of the Photosystem II Inhibitors CCCP and DCMU on Hydrogen Production by the Unicellular Halotolerant Cyanobacterium Aphanothece halophytica. *The Scientific World Journal* https://www.hindawi.com/journals/tswj/2019/1030236/ (2019) doi:10.1155/2019/1030236.

73. Angelakis, A. N. & Snyder, S. A. Wastewater Treatment and Reuse: Past, Present, and Future. *Water* **7**, 4887–4895 (2015).

74. Etterer, T. Formation, Structure and Function of Aerobic Granular Sludge. (2004).

75. Barr, J. J., Cook, A. E. & Bond, P. L. Granule Formation Mechanisms within an Aerobic Wastewater System for Phosphorus Removal. *Appl Env. Microbiol* **76**, 7588–7597 (2010).

76. Åmand, L. Control of aeration systems in activated sludge processes – a review. /paper/Control-of-aeration-systems-in-activated-sludge-%E2%80%93-a-%C3%85mand/33484777bf4af0743f759899f7bbc520def5b4de (2011).

77. González-Camejo, J. *et al.* Effect of light intensity, light duration and photoperiods in the performance of an outdoor photobioreactor for urban wastewater treatment. *Algal Res.* **40**, 101511 (2019).

78. Babcock, G. T. *et al.* Water oxidation in photosystem II: from radical chemistry to multielectron chemistry. *Biochemistry* **28**, 9557–9565 (1989).

79. Ansari, A. A., Abouhend, A. S. & Park, C. Effects of seeding density on photogranulation and the start-up of the oxygenic photogranule process for aeration-free wastewater treatment. *Algal Res.* **40**, 101495 (2019).

80. Morales, M., Sánchez, L. & Revah, S. The impact of environmental factors on carbon dioxide fixation by microalgae. *FEMS Microbiol. Lett.* **365**, (2018).

81. Yen, H.-W., Hu, I.-C., Chen, C.-Y. & Chang, J.-S. Design of Photobioreactors for Algal Cultivation. in *Biofuels from Algae* 23–45 (Elsevier, 2014). doi:10.1016/B978-0-444-59558-4.00002-4.

82. Tang, K.-H., Tang, Y. J. & Blankenship, R. E. Carbon Metabolic Pathways in Phototrophic Bacteria and Their Broader Evolutionary Implications. *Front. Microbiol.* **2**, (2011).

83. Stauch-White, K., Srinivasan, V. N., Camilla Kuo-Dahab, W., Park, C. & Butler, C. S. The role of inorganic nitrogen in successful formation of granular biofilms for wastewater treatment that support cyanobacteria and bacteria. *AMB Express* **7**, (2017).

84. Subashchandrabose, S. R., Ramakrishnan, B., Megharaj, M., Venkateswarlu, K. & Naidu, R. Mixotrophic cyanobacteria and microalgae as distinctive biological agents for organic pollutant degradation. *Environ. Int.* **51**, 59–72 (2013).

85. Wan, N., Abernathy, M., Tang, J. K.-H., Tang, Y. J. & You, L. Cyanobacterial photo-driven mixotrophic metabolism and its advantages for biosynthesis. *Front. Chem. Sci. Eng.* **9**, 308–316 (2015).

86. Ali, A. *et al.* Just Suspended Speed for Solid Particle Transport in TorusReactor. in *New Trends in Urban Drainage Modelling* (ed. Mannina, G.) 879–885 (Springer International Publishing, 2019). doi:10.1007/978-3-319-99867-1_152.

87. The influence of particles on suspension rheology :: Anton Paar Wiki. *Anton Paar* https://wiki.anton-paar.com/en/the-influence-of-particles-on-suspension-rheology/.

88. Kawase, Y. & Moo-Young, M. Mixing time in bioreactors. *J. Chem. Technol. Biotechnol.* **44**, 63–75 (2007).

89. *Handbook of industrial mixing: science and practice*. (Wiley-Interscience, 2004).

90. Han, B.-P., Virtanen, M., Koponen, J. & Straškraba, M. Effect of photoinhibition on algal photosynthesis: a dynamic model. *J. Plankton Res.* **22**, 865–885 (2000).

91. Takahashi, S. & Badger, M. R. Photoprotection in plants: a new light on photosystem II damage. *Trends Plant Sci.* **16**, 53–60 (2011).

92. Gray, G. R., Hope, B. J., Qin, X., Taylor, B. G. & Whitehead, C. L. The characterization of photoinhibition and recovery during cold acclimation in Arabidopsis thaliana using chlorophyll fluorescence imaging. *Physiol. Plant.* **119**, 365–375 (2003).

93. Mathur, S., Agrawal, D. & Jajoo, A. Photosynthesis: Response to high temperature stress. *J. Photochem. Photobiol. B* **137**, 116–126 (2014).

94. Lürling, M., Eshetu, F., Faassen, E. J., Kosten, S. & Huszar, V. L. M. Comparison of cyanobacterial and green algal growth rates at different temperatures. *Freshw. Biol.* **58**, 552–559 (2013).

95. Gururani, M. A., Venkatesh, J. & Tran, L. S. P. Regulation of Photosynthesis during Abiotic Stress-Induced Photoinhibition. *Mol. Plant* **8**, 1304–1320 (2015).

96. Dechatiwongse, P., Srisamai, S., Maitland, G. & Hellgardt, K. Effects of light and temperature on the photoautotrophic growth and photoinhibition of nitrogen-fixing cyanobacterium Cyanothece sp. ATCC 51142. *Algal Res.* **5**, 103–111 (2014).

97. Takeuchi, N., Kohshima, S. & Seko, K. Structure, Formation, and Darkening Process of Albedo-reducing Material (Cryoconite) on a Himalayan Glacier: A Granular Algal Mat Growing on the Glacier. *Arct. Antarct. Alp. Res.* **33**, 115–122 (2001).

98. Uetake, J. *et al.* Microbial community variation in cryoconite granules on Qaanaaq Glacier, NW Greenland. *FEMS Microbiol. Ecol.* **92**, (2016).

99. Wu, H., Zou, D. & Gao, K. Impacts of increased atmospheric CO2 concentration on photosynthesis and growth of micro- and macro-algae. *Sci. China C Life Sci.* **51**, 1144–1150 (2008).

100. Lindskog, S. & Coleman, J. E. The Catalytic Mechanism of Carbonic Anhydrase. *Proc. Natl. Acad. Sci.* **70**, 2505–2508 (1973).

101. Ridley, S. M. Interaction of Chloroplasts with Inhibitors. *Plant Physiol.* **59**, 724–732 (1977).

102. Figueredo, C. C., Giani, A. & Lemos Filho, J. P. Photosynthetic capacity of three phytoplanktonic species measured by a pulse amplitude fluorometric method. *Braz. J. Plant Physiol.* **21**, 167–174 (2009).

103. Limoli, D. H., Jones, C. J. & Wozniak, D. J. Bacterial Extracellular Polysaccharides in Biofilm Formation and Function. *Microbiol. Spectr.* **3**, (2015).

104. Elias, S. & Banin, E. Multi-species biofilms: living with friendly neighbors. *FEMS Microbiol. Rev.* **36**, 990–1004 (2012).

105. Gao, D., Liu, L., Liang, H. & Wu, W. *Aerobic Granular Sludge: Characterization, Mechanism of Granulation and Application to Wastewater Treatment*. vol. 31 (2010).

106. Flemming, H.-C., Neu, T. R. & Wozniak, D. J. The EPS Matrix: The "House of Biofilm Cells". *J. Bacteriol.* **189**, 7945–7947 (2007).

107. Sheng, G.-P., Yu, H.-Q. & Li, X.-Y. Extracellular polymeric substances (EPS) of microbial aggregates in biological wastewater treatment systems: A review. *Biotechnol. Adv.* **28**, 882–894 (2010).

CHAPTER 4

LIGHT UTILITY IN SCALING UP OXYGENIC PHOTOGRANULE BIOREACTORS

4.1 Abstract

The operational design of photobioreactors can have significant impacts on the interaction of photogranular biomass and light. These interactions determine the productivity of photosynthetic microbes present in these photosystems. Agitation operations distribute the substrate flux and expose granules to the photic zone. The extent of this photic zone depends on biomass concentration, reactor depth, and light intensity, while granular interaction depends on the frequency of exposure due to mixing. We evaluated these entwined interactions in different sizes of oxygenic photogranule (OPG) systems and their effects on the efficiency of wastewater treatment (WWT). Increasing light intensity resulted in disparate nutrient removal trends for the reactor scales examined. Besides, contrasting photosynthetic biomass yields per photon density were observed for the OPG systems with an increase of irradiance and with reactor scale. These differences suggest variable light utility with reactors of different sizes arising from the variable interactions with light. The light utility in the photobioreactor should be an essential design consideration beyond the provision of adequate light for effective WWT.

4.2 Introduction

Wastewater treatment utilizing engineered phototrophic systems exploit the photosynthetic activity of microalgae and cyanobacteria to generate oxygen necessary for

the aerobic transformation of substrates.[1–3] This self-aeration reduces expenditure on energy input into the system [4–6] associated with conventional treatment approaches.[4,5,7] The mechanical aeration accounts for more than 50-60% of the energy used in the activated sludge process (ASP).[3,5,8] In addition, these phototrophic biomes harness solar light energy and store it as biomolecules [9,10] while fixing carbon from both wastewater and the atmosphere hence leading to a negative carbon flux.[2] This has significant impacts on the sustainability of the wastewater treatment processes.[2] The phototrophic biomass in these systems can exist in suspended culture,[11] biofilm [12] and granular morphologies [9] due to adaptive responses [13] from their interaction with various environmental selection pressures.[9,13–15] The biofilm and granular assemblies ease solid and liquid phase separation [1,9] during phototrophic wastewater treatment while also increasing the reactive surface area to volume ratio available for wastewater treatment.[9,16,17] Granular systems additionally have operational versatility due to the potential for higher biomass retentions enabling more loading.[3,18]

In photogranular biomass, such as oxygenic photogranules (OPG),[1,3,9,19] oxygen generated from photosynthesis is utilized by aerobic microbes to consume organic matter in the wastewater [7,20] and for nitrification.[21–23] The provision of oxygen by the OPG's photosynthetic clades,[21,24] therefore, ensures functional integrity of OPG-based wastewater treatment, while constrained photosynthetic activity [9,25,26] could lead to anaerobic conditions [27] and collapse of the granules. This significance renders photosynthesis the limiting process in the OPG process and other phototrophic-based wastewater treatment systems.

The photosynthetic capacity of OPGs and light exposure [15] anchor the design and success of OPG-based wastewater treatment systems.[9,28] The OPG's photosynthetic capacity increases with light intensity to saturation beyond which photoinhibition damages the photosystems of constituent phototrophs [29–31] impairing oxygen production. The photosynthetic clades [32] present in OPGs [21,24] have different photochemical capabilities that can also be impacted by abiotic stresses caused by temperature,[33] carbon concentrations,[34] light, and pH changes. The metabolism of phototrophic clades [35] is also susceptible to photoperiod and wastewater source affecting treatment efficiency.[8] It has been shown that utilizing photoperiods to regulate the accumulation of excess light energy in reactors, increased productivity of microalgae while decreasing overall energy expenditure.[15] Moreover, the carbon and nutrient uptake in wastewater treatment was also reported to have a high correlation to the photoperiod and was optimum with 12h:12h light-dark cycle.[36,37]

The exposure of phototrophic biomass to light in a reactor is a function of both the light supply and reactor mixing operation. The reactor sizing and agitation protocols [38] can be designed towards a light irradiance to achieve a treatment goal(s). Light supply for OPG reactor operation can be from natural [39] or artificial [40,41] sources. Natural light is limited to daylight [25,42,43] with temporal variation within the day and seasonally within the year.[42,44] This variability of light intensity can cause erratic treatment efficiency using phototrophic systems and often necessitates the use of larger surface areas, a hallmark of algal ponds.[45–48] In addition, open natural-light bioreactors may suffer higher

perturbations of the photoactivity related to abiotic stresses. In contrast, artificial light sources can provide modularity [40,49–51] but increase the operational costs for wastewater treatment.

Mixing in activated sludge basins induces aeration to achieve biological wastewater treatment goals.[52] For aerobic granular sludge systems, shear emanating from upflow aeration and mixing [53,54] influences particulate density,[55] settleability, hydrophobicity, bio function, specific oxygen uptake rate (SOUR) and is negatively correlated to granular size.[56] While shear is not the only selection pressure for granulation,[57–59] it is an essential factor driving the granulation process. Moreover, too low or too high shear stress limits granulation.[53,54,56,60] High shear from intensive mixing operations could explain the lack of granulation in activated sludge basins.[61–63] Particle flow dynamics within the reactor are also related to the shear influenced physical characteristics such as density.[64]

In OPG tank reactors with surface lighting, photic activity [65,66] occurs where a light zone persists and varies with reactor depth.[67] Mechanical mixing transports OPG biomass to 'light-rich' photic zone, which impacts the magnitude of photosynthetic activity [68] and resulting oxygen generation. Circulation of granules within this zone is subject to the dissipation of mixing-induced shear stress in a water-particle matrix.[69,70] The resultant flow patterns determine the frequency of granular interactions for light. A reactor turnover rate can characterize the frequency of this exposure, often expressed as the blend time to achieve the desired concentration homogeneity.[38,71,72] In addition, the quantity and quality of light harnessed by OPGs in the photic zone also varies temporally and

spatially due to shading and scattering of light [67] by both the granules and the reactor water column. High attenuation of light in turbid water limits its penetration in the water column [44] as its extinction described by the Beer-lamberts law is linearly proportional to particle concentrations, [73] while shading limits light available to successive granular layers.[15]

Selecting agitation schemes for OPG reactors to support oxygenic photosynthesis for wastewater treatment bears intrinsic design trade-offs. High reactor turnover rate by higher mixing results in not only higher light interactions and oxygen generation, but also higher shear with potential to affect granulation.[56,63] Scaling up mixing operations would also pose both technical and cost challenges.[38,74–76] Producing a higher amount of oxygen for wastewater treatment can likewise be achieved by increasing light intensity. However, this too can result in the deleterious effects of photoinhibition compromising oxygenation potential,[29,31,77] and the OPGs' photosynthetic and structural integrity.[24,78] Balancing light and mixing requirements, therefore, entails relating these trade-offs to sustain functional needs. The trade-offs may also vary based on reactor size due to the scale-dependent energy dissipation and granule-light interactions. This work investigates the utility of light in OPG reactors by evaluating the functional utility of varying light irradiances in reactors of different volumes with comparable turnover rates. A variable OPG performance would indicate fluctuating functional utilization of light provided implying potential trade-off substitution for high mixing needs with more easily scalable light infrastructure.[41,50]

4.3 Materials and methods

4.3.1 Reactor Design and Operation

Three cylindrical reactors of diameters 12.2 cm, 32.2 cm and 54 cm were operated at a 1:1 diameter to height ratio giving an equivalence volume scale of 1: 2.65: 4.43 (Table 4- 1). Reactor R1, which was successfully employed at lab scale for OPG-based wastewater treatment,[3] was utilized as a reference in the design of reactors R2 and R3. Dimensional similitude to R1 parameters was maintained with scaling up (Table 4- 1). Pitched blade impellers were designed using literature [38,79–81] and used to provide reactor bulk axial flow [75,82] with agitation (Table 4- 1). The mixing intensities were selected to achieve comparable theoretical turnover rates for 95% homogeneity [83,84] in R2 and R3 compared to R1 while the reference reactor was operated at 100 rpm resulting in lower turnover times (Table 4-2). The resultant theoretical hydrodynamic parameters [79] are also presented in Table 4- 2. The different impeller Reynolds numbers indicate turbulent conditions >20,000 [81] for R2 and R3. The shear stress increased with reactor size. In R3 the equivalent shear rate was 1.7 times higher than that of R2 despite similar mixing speeds. These two large-volume reactors had the same turnover rates (22 s) while the reference reactor R1 had a lower turnover rate of 16 s. The Kolmogorov length scale decreased with reactor size due to different hydrodynamic characteristics and was inversely collated to increasing shear. This K-scale defines the lower length scale limit of shear energy dissipation before viscous dominance.[85,86] In shear dominated environments absent of microbial amended aggregation, this would be the largest granule size for OPGs.

Table 4- 1: Dimensional parameters of experimental reactors (All dimensions in cm with a tolerance of ±0.05 cm)

Parameter	**1.4 L (R1)**	**26.7 L (R2)**	**123.7 L (R3)**	**Ratios**	
Tank diameter (D, cm)	12.2	32.4	54		
Height (H, cm)	12.2	32.4	54	**H/D**	1.00
Impeller dimeter (d_i, cm)	5.65	15	25	**d_i/D**	0.46
Impeller clearance (C, cm)	4.07	10.8	18	**C/D**	0.33
Width of Impeller (W, cm)	1.13	3	5	**W/d_i**	0.20
Length of Impeller blade (L, cm)	1.41	3.75	6.25	**L/d_i**	0.25
Baffle width (W_B, cm)	1.02	2.7	4.5	**W_B /D**	0.08
Baffle offset (O, cm)	0.17	0.45	0.75	**W_B /6**	0.75
Pitch blade angle (Θ, °)	30	30	30		

Table 4- 2: Estimated hydrodynamic parameters in the three reactors. Furukawa et al. (2012) estimations were used to model flow and power consumption parameters. Post et al. (2010) for mixing time scales and Paul et al. (2004) were used for energy dissipation estimations-K scale. Dimensions indicated for each parameter.

Parameter	**1.4 L (R1)**	**26.7 L (R2)**	**123.7 L (R3)**
Impeller Reynolds Number, N_{Re}	5320	26250	72917
Power Number, Np	0.53	0.52	0.52
Speed (rpm)	100	70	70
Power, P (KW)	0.0000014	0.0001	0.001
Shear Stress, Pa (Kg/ms^2)	0.03	0.05	0.08
Dimensionless time to 95% Homogeneity, N_{mix}	18	26	26
Time to 95% Homogeneity, $Θ_{mix}$ (s)	16	22	22
Rate of Shear, G (s^{-1})	31	49	81
Torque (N.m)	0.00013	0.01	0.11
Tip Speed (m/s)	0.30	0.55	0.92
Kolmogorov length scale (K-scale) (µm)	179	143	111

4.3.2 Operating conditions

All the reactors were fed the same wastewater, primary effluent, from the local utility. The seed granules were first adapted to the operational light intensity for 4 days using the vessel of R3 to obtain consistent initial biomass characteristics. OPG biomass was inoculated into this reactor with a 0.25 volume change undertaken daily, giving 4-day hydraulic retention time (HRT), while a 12h:12h (L:D) light scheme was used for this adaptation period. The biomass was then split into the three reactors by volume fraction. Overhead surface light was provided using LED lighting (5000 K) each rated at 100 W and 12000 lumens. Light intensity measurements were calibrated using a spherical LI-193S underwater sensor (Licor Biosciences) at the reactor water surface level. Average surface light intensities (I_s) of 100 (±12) µmol $m^{-2}s^{-1}$, 250 (±78) µmol $m^{-2}s^{-1}$, and 550 (±53) µmol $m^{-2}s^{-1}$ were provided, each for an operation period of 41 days. Light cycling was undertaken with light: dark (L:D) photoperiods each 3 hours long. The reactors were then operated in sequencing batch mode exchanging a ¼ of the reactor volume at the beginning of each light photoperiod, with 4-periods in a day and 1-day reactor HRT. Mixing was induced at the start of each light photoperiod and turned off at the beginning of the dark period. The effluent was discharged after a 10 min settling period. The influent and effluent phases were undertaken for 15 min each, a 0.083 fraction of the 6 hr reactor operation cycle. Composite samples of both influent and effluent were collected and used for analysis.

4.3.3 Sample analysis

The reactor biomass characterization of mixed liquor suspended solids (MLSS), and volatile suspended solids (VSS) was undertaken following the Standard Methods 2540D/E.[87] Additionally, chlorophyll concentrations were quantified as outlined in Standard Methods 10200H,[87] while phycobilins' extraction was undertaken as previously reported by Abouhend et al., [20] and quantified using the Bennett and Bogorad equation.[88] The influent and effluent samples were analyzed for total chemical oxygen demand (COD) and soluble COD using unfiltered and 0.45 µm pore size filtrates (Millipore) respectively following Standard Methods (5220C).[87] The 0.45 µm pore size filtrate was also used for the analysis of soluble fractions of total dissolved nitrogen and dissolved organic carbon using a TN/TOC analyzer (TOC-VCPH, Shimadzu, U.S.A.). A Metrohm 850 Professional Ion Chromatograph (IC) (Metrohm, Switzerland) was used to measure phosphate, calcium, magnesium, ammonium, nitrite, and nitrate. The absolute concentrations of these substrates, indicating the efficacy of wastewater treatment by OPGs, were utilized in the determination of relative reactor performance. The biomass' settleability was characterized using the sludge volume index (SVI) after 30 minutes settling (SVI_{30}) following the Standard Methods (2710D).[87]

4.3.4 Calculations

The changes in various parameters for each OPG reactor were characterized over 41 days and used to determine derived metrics. These changes were assumed to be correlated to photosynthetic activity in the granules. The sludge retention rate was equivalent to the operation period. The photosynthetic biomass production (PBP) (mg/mol) was calculated

as the ratio of change in photosynthetic pigment concentrations between sampling intervals (mg/l) to the total photon density (mol). This was done for both chlorophyll *a* ($PBP_{Chl.a}$) (Eq 4-1) and phycobilin (PBP_{PBS}) (Eq 4-2) in OPGs.

$$\mathbf{PBP_{Chl.a}} = \frac{\mathbf{\Delta Chl\ a * Vr}}{\mathbf{Is * \Delta t * Sa * 43.2}} \qquad \textbf{(Eq 4-1)}$$

$$\mathbf{PBP_{PBS}} = \frac{\mathbf{\Delta PBS * Vr}}{\mathbf{Is * \Delta t * Sa * 43.2}} \qquad \textbf{(Eq 4-2)}$$

Where V_r is the reactor volume (L), I_S is the average surface light intensity (µmol $m^{-2}s^{-1}$), S_a is the reactor surface area (m^2), Δt represents the diurnal sampling intervals, and 43.2 is a unit conversion factor.

The substrate removal was characterized as removal efficiency (Ø) established as the difference in concentrations (mg/L) of nutrients and soluble chemical oxygen demand (sCOD) in influent (I_{conc}) and effluent (E_{conc}) streams, per HRT (d^{-1}) (Eq 4-3). A net removal factor (NRF) (mg/d: mol), defined as the ratio of change in nutrient removal rate to photon density (mg/mol), was then determined according to Eq 4-4 (modified from Gonzalez-Camejo et al. [1]),

$$\emptyset = \frac{(\mathbf{(Iconc. - Econc.)}(\boldsymbol{mg/l}))}{\mathbf{(HRT)}} \qquad \textbf{(Eq 4-3)}$$

$$\mathbf{NRF_{sCOD}} = \frac{\mathbf{\Delta \emptyset_{COD} * Vr}}{\mathbf{Is * \Delta t * Sa * 43.2}} \qquad \textbf{(Eq 4-4)}$$

Similarly, net removal factors for nitrogen (NRF_N) and phosphorous (NRF_P) were established following Eq 4-4 and Eq 4-5), respectively.

$$\mathbf{NRF_N} = \frac{\mathbf{\Delta \emptyset_N * Vr}}{\mathbf{Is * \Delta t * Sa * 43.2}} \qquad \textbf{(Eq 4- 5)}$$

$$\mathbf{NRF_P} = \frac{\Delta \emptyset_P * Vr}{Is * \Delta t * Sa * 43.2} \qquad \textbf{(Eq 4- 6)}$$

4.3.5 Size analysis

A volume (10 mL) of the biomass sample collected from each reactor was processed for particle size distribution. Petri dish images were acquired and analyzed using Image pro (Media Cybernetics) software. The petri dish diameter was used to scale the image analysis. Particle size data was then exported into Origin Pro (v.2020) software and particle distribution plots were obtained. A Weibull function was used to describe the distribution.

4.3.6 Statistical analysis

A paired student t-test was used to evaluate the changes in mean particle sizes for significance at $p<0.05$. Moreover, ratio means are presented as mean values of duplicate samples. Statistical analysis was conducted using Origin Pro (v.2020) software.

4.4 Results

4.4.1 Evolution of particle size distributions

A decrease in median (d_{50}) sizes from day-2 samples was observed in all reactors under 100 µmol $m^{-2}s^{-1}$ from 300 µm in both R1 and R2. The median size also decreased from 200 µm in reactor R3 to 100 µm by day-41, the end of the experimental period (Table 4-3). Under the same irradiation setting, the mean size of particles in reactors R1, R2, and

R3 decreased by 48%, 57%, and 28%, respectively (Table 4- 3). Under 250 µmol $m^{-2}s^{-1}$ light conditions, the median sizes in R1 increased from 100 µm to 200 µm by day-20 and thereafter decreased to 100 µm by day-41. Median sizes in reactor R2 decreased from 300 µm to 100 µm by day-20 and remained consistent to day-41. The median sizes in reactor R3 decreased from 300 µm to 100 µm by day-20 and increased to 200 µm by day-41. Reactor operation with 250 $\mu mol.m^{-2}.s^{-1}$ photon flux resulted in mean size decrease by 33%, 44% and 31% in reactors R1, R2 and R3, respectively (Table 4- 3). The median sizes with 550 µmol $m^{-2}s^{-1}$ light intensity in R1 increased between day-2 and day-20 from 200 µm to 300 µm and decreased to 200 µm by day-41, a trend concordant to that under 250 µmol $m^{-2}s^{-1}$. In contrast, for R2 and R3, the median size (200 µm) was conserved between day-2 and day-20 but decreased to a terminal value of 100 µm for both reactors. The mean size under this intensity increased by 38% for R1 and decreased by 21% and 29% for R2 and R3, respectively (Table 4- 3). All the changes in mean size were found to be significant ($p=0.05$).

An increase in positive skewness was observed for R1 with 100 and 250 µmol $m^{-2}s^{-1}$ light conditions (Table 4- 3). These increases indicate a higher prevalence of large size particles between consecutive sampling days. However, a decrease of the skewness (4-2-3) was observed with 550 µmol $m^{-2}s^{-1}$ light intensity. In contrast, R2 experienced increasing positive skews for all light conditions (Table 4- 3). The skew in R3 decreased with 100 µmol $m^{-2}s^{-1}$ but slightly increased for both 250 and 550 µmol $m^{-2}s^{-1}$ irradiances. The various increases in skew, median size, and mean sizes can be attributed to both granule-promoting-shear pressure [89–91] and phototrophic enrichment in OPGs.[20,21,24] This

size growth generally exceeded the Kolmogorov length scales, which are 179 µm, 143 µm, and 111 µm for reactors R1, R2, and R3, respectively. However, reactor R1 operation at 100 µmol $m^{-2}s^{-1}$ resulted in a mean size of 179 µm equivalent to the k-scale value. Operating the same reactor with 250 µmol $m^{-2}s^{-1}$, however, resulted in a smaller mean size 146 µm (Table 4- 3).

Table 4- 3: Particle size distribution statistical characteristics for the three reactors under different light conditions. Initial particle size data is presented from day 2.

	Sampling period	N total	Mean (µm)	Standard Deviation	SE of mean	Variance	Skewness	Median (µm)
Reactor R1 (1.43 L)	Day 2-100 PAR	270	343	357	22	127297	3	300
	Day 20-100 PAR	6689	149	137	2	18810	9	100
	Day 41-100 PAR	27132	179	130	1	16939	7	100
	Day 2-250 PAR	973	216	200	6	39915	3	100
	Day 20-250 PAR	10060	196	161	2	25765	7	200
	Day 41-250 PAR	10790	146	103	1	10608	7	100
	Day 2-550 PAR	7810	200	153	2	23551	4	200
	Day 20-550 PAR	8973	319	239	3	57322	2	300
	Day 41-550 PAR	8216	276	214	2	45737	3	200
Reactor R2 (26.7 L)	Day 2-100 PAR	352	424	485	26	235197	4	300
	Day 20-100 PAR	3741	157	180	3	32560	6	100
	Day 41-100 PAR	11485	181	151	1	22888	6	100
	Day 2-250 PAR	438	329	233	11	54348	1	300
	Day 20-250 PAR	2256	215	239	5	56972	4	100
	Day 41-250 PAR	14051	186	140	1	19590	5	100
	Day 2-550 PAR	4213	216	184	3	33917	3	200
	Day 20-550 PAR	5697	243	176	2	30881	3	200
	Day 41-550 PAR	14375	170	105	1	10984	4	100
Reactor R3 (123.7 L)	Day 2-100 PAR	988	293	384	12	147441	5	200
	Day 20-100 PAR	1574	178	238	6	56765	5	100
	Day 41-100 PAR	1573	211	260	7	67723	4	100
	Day 2-250 PAR	333	348	283	15	79972	3	300
	Day 20-250 PAR	907	244	279	9	77675	3	100
	Day 41-250 PAR	1550	241	254	6	64312	4	200
	Day 2-550 PAR	1137	276	262	8	68469	3	200
	Day 20-550 PAR	1314	291	263	7	69293	2	200
	Day 41-550 PAR	5224	196	164	2	26953	4	100

4.4.2 Sludge volume index

The sludge volume index describes the volume occupied by a gram of settled sludge after a 30 min settling interval.87 Low settling sludge indices allude to higher biomass settling velocities associated with particle aggregation.92–94 The SVI can hence be used as a surrogate for flocculation and dense aggregation, a characteristic of granules.9,57,95 Typical well-settled activated sludge biomass has an SVI30 of 150 mL/g 93,96 while OPG granules, on the other hand, have an average SVI30 of 53 mL/g.3

The mean SVI30 index for 100 µmol m-2s-1 light operations in R1 was 77 mL/g (±95). Operation at 250 µmol m-2s-1 and 550 µmol m-2s-1 of R1 had lower mean SVI30 indices of 66 mL/g (±29) and 52 mL/g (±10), respectively for the experimental duration (Figure 4- 1). The SVI30 in reactor R2 operation with 100 µmol m-2s-1 followed a decreasing trend and had a mean SVI30 ratio of 106 mL/g (±68) (Figure 4- 1). A 250 µmol m-2s-1 irradiance, on the other hand, resulted in an initial increase in the SVI30 index, subsequently decreasing with operational time and had mean SVI30 of 70 mL/g (±16). Operation with 550 µmolm-2s-1 did not result in significant undulation with a mean SVI30 of 53 mL/g (±10) (Figure 4- 1).

The variation in SVI30 in R3 under 100 µmol m-2s-1 conditions was less than observed in the other reactors, as seen with lower deviation about the mean SVI30 (118 ml/g ± 50) (Figure 4- 1). However, this mean SVI30 was higher than that in reactor R1 and R2 for comparable (100 µmol m-2s-1) light conditions. The mean SVI30 values for R3

operation with 250 and 550 µmol m-2s-1 light were 88 mL/g (± 24) and 57 mL/g (±19) (Figure 4- 1). The mean SVI30 values decreased with increasing light intensity for all reactors and increased with reactor size for each light condition. Reactor operation 550 µmol m-2s-1 resulted in lowest SVI30 values comparable to OPG reported value (SVI30 53ml/g).3 Limited aggregation can be inferred from the higher SVI30s recorded with 100 and 250 µmol m-2s-1 (Figure 4- 1). Increasing light intensity resulted had a higher reduction in the mean SVI30 for reactor R3 (61%) compared to reactor R2 (53%) and reactor R1(21%).

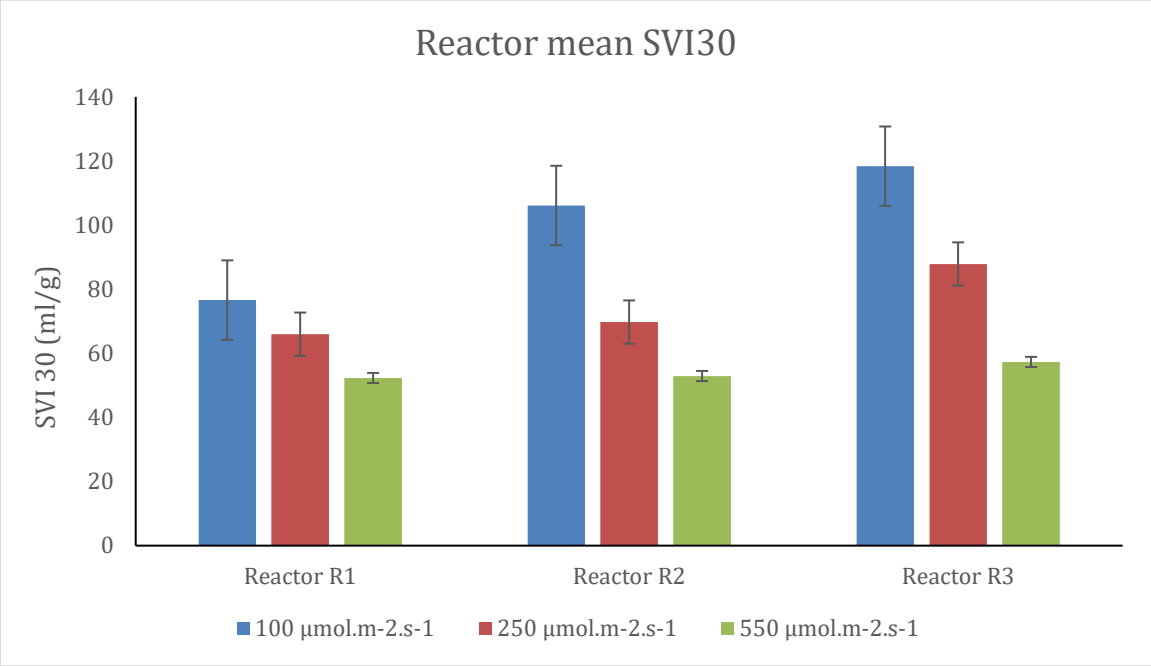

Figure 4- 1: SVI30 values for each reactor and light conditions. The error bars indicate the standard deviation of the mean values.

4.4.3 Changes in biomass concentrations

The biomass expressed as VSS increased proportionately to the increasing light intensity for all reactors (Figure 4- 2). Reactor R1 had the highest biomass increase (Figure 4- 2-a) under all light intensities while reactor R3 had the lowest increase (Figure 4- 2-c). This

alludes to lower light-mediated biomass growth in larger reactors due to limited light conditions. Operation under 100 µmol $m^{-2}s^{-1}$ in reactors R1 and R2 exhibited an almost linear increase in biomass concentrations to day-41 (Figure 4- 2-a, b). The corresponding linear slope coefficient was 13.4 (r^2=0.93) in reactor R1 and 5.2 (r^2=0.9) for R2. For 250 µmol $m^{-2}s^{-1}$, a peak in biomass concentration occurred on day-33 for reactor R1 decreasing thereafter to day-41 (Figure 4- 2-a). In reactor R2, a similar initial trend occurred for volatile suspended solids but increased further (Figure 4- 2-b) by day-41. More perturbations in biomass concentrations occurred with 550 µmol $m^{-2}s^{-1}$ operations, with a peak on day-33 and decreasing to day-41 for reactor R1 and reactor R2.

In reactor R3, higher fluctuation of biomass concentrations occurred under all light intensities (Figure 4- 2-c). The volatile suspended solids concentration for operation under 100 µmol $m^{-2}s^{-1}$ remained stable but followed a general decreasing trend to day-30 for 250 µmol $m^{-2}s^{-1}$ light conditions (Figure 4- 2-c). This period was followed by a sharp increase to day-33 and decrease to day-41 (Figure 4- 2-c). Operation with 550 µmol $m^{-2}s^{-1}$ light intensity resulted in an increase of VSS after day-12 to day-33, decrease to day-37 and increase to day-41 (Figure 4- 2-c). Operation of reactor R3 with 550 µmol$m^{-2}s^{-1}$ exhibited an initial decrease of VSS to day-9, increase to day-30 and was followed by a decrease to day-37 and increase to day-41 (Figure 4- 2-c). The higher fluctuations of biomass concentrations in reactor R3 can be attributed to variable light utility associated with exposure of granules to light. The deviation of flow streamlines from the overall assumed axial paths induced by pitched blade impellers [75,79,82] could be a potential source for this variation. Additionally, particle-particle interactions with higher shear may cause

deviation of OPG granule exposure frequency from the modelled turnover rates (N_{mix}),[79,83] reducing putative exposure time (Table 4- 2) and consequently photo productivity.

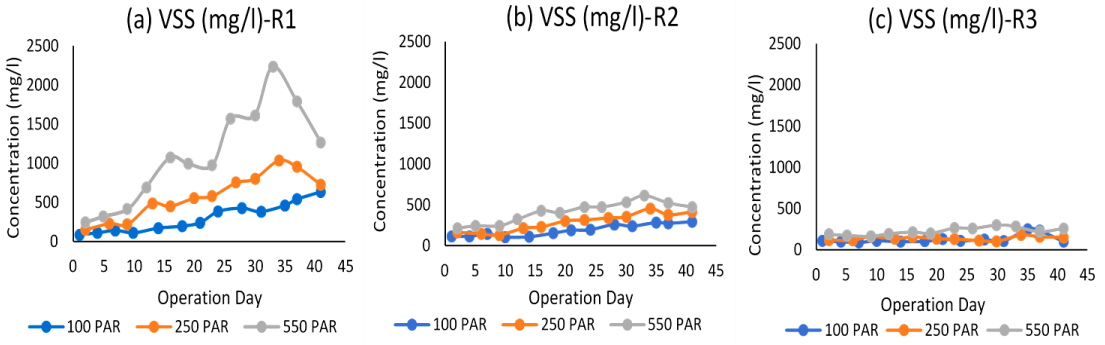

Figure 4- 2: Concentration of volatile suspended solids in the reactors at different light intensities (100 µmol $m^{-2}s^{-1}$,250 µmol $m^{-2}s^{-1}$,550 µmol $m^{-2}s^{-1}$). (a) Reactor R1, (b) Reactor R2, (c) Reactor R3**. (**PAR= µmol $m^{-2}s^{-1}$)

4.4.4 Photosynthetic pigment concentrations

The increase in Chl-*a*/VSS in reactor R1 at 100 µmol $m^{-2}s^{-1}$ had a dual-peak on day-21 and day- 31 but decreased to day-41 (Figure 4- 3-a). A general increasing trend for reactor R1 under 250 µmol $m^{-2}s^{-1}$ with peaks on day-26 and day-41 was observed (Figure 4- 3-a). Under 550 µmol $m^{-2}s^{-1}$, the Chl-*a*/VSS highest peak occurred on day-9 of operation, subsequently decreasing to end of the experiment (Figure 4- 3-a). The peak increase in VSS observed on day-32 (Figure 4- 2-a) for this light condition suggest a significant increase of non-photosynthetic microbes. In reactor R2, Chl *a*/VSS peaks were observed on day-31, day-16 and day-13 for 100 µmol $m^{-2}s^{-1}$, 250 µmol $m^{-2}s^{-1}$ and 550 µmol $m^{-2}s^{-1}$ (Figure 4- 3-b), respectively and decreased to day-41. In reactor R3, the Chl *a*/VSS trend varied minimally from initial value over the experimental period for 100 µmol $m^{-2}s^{-1}$ irradiance operation (Figure 4- 3-c). Further, an initial decreasing trend

ensued under 250 µmol $m^{-2}s^{-1}$ with a subsequent increase from day-13 to day-41. The 550 µmol $m^{-2}s^{-1}$ light conditions induced a rapid increase in the Chl *a*/VSS values to day-9 and a slower increase to day-41 (Figure 4- 3-c). The increases in Chl *a*/VSS allude to progressive phototrophic enrichment [97] of the OPG biome, while the decreases can be attributed to either photic stress at the high irradiances or photolimitation and resultant diminution of photosynthetic clades populations.[20,24,78]

On the other hand, the normalized chlorophyll *b* (Chl-*b*/VSS) concentrations in reactor R1 followed a general undulating trend with an initial increase and characterized by a double peak for 100 µmol $m^{-2}s^{-1}$ and 550 µmol $m^{-2}s^{-1}$ light conditions (Figure 4- 4a). In contrast, an initial decrease in the Chl-*b*/VSS to day-13 was followed by an increase to day-41 under 250 µmol $m^{-2}s^{-1}$ photon density giving the highest ratio peak for reactor R1 (Figure 4- 4). Chlorophyll *b* pigments are accessory light-harvesting pigments found in microalgae.[3,78,97] The Chl *b*/VSS increase can hence be attributed to light enhanced microalgae enrichment, while its decrease may reflect decreasing microalgal populations.[97–99] In reactor R2, the Chl-*b*/VSS trend had an initial plateau to day-9 under all light conditions (Figure 4- 4-b). This initial trend was followed by a rapid increase of the Chl-*b*/VSS proportional to the light intensity (Figure 4- 4-b). Operation of reactor R3 under 100 µmol $m^{-2}s^{-1}$ resulted in a minimal to decreasing trend of Chl-*b*/VSS from initial values. However, under 250 µmol $m^{-2}s^{-1}$ an initial decrease in the ratio was followed by an increasing trend from day-13. Reactor R3 operation under 550 µmol $m^{-2}s^{-1}$ resulted in a rapid increase of Chl *b*/VSS from (day-6) of the experiment (Figure 4- 4-c).

While microalgal enrichment was generally proportional to increasing light intensity for reactors R2 and R3 (Figure 4- 4-b,c), highest enrichment conditions occurred with 250 µmol $m^{-2}s^{-1}$ irradiances in reactor R1 (Figure 4- 4-a). Amongst the three reactors, reactor R2 had the highest chlorophyll *a* (Figure 4- 3-and *b* enrichment ratios suggesting a light utility amenable for microalgal growth. A decreasing chlorophyll *b*/VSS trend coupled with increasing chlorophyll *a*/VSS trend suggests enrichment of photosynthetic clades without chlorophyll *b* light-harvesting pigments, such as cyanobacteria.[3,78,97] This trend was observed in reactor R1 with 100 µmol $m^{-2}s^{-1}$ (Figure 4- 3-a, Figure 4- 4-a). Conversely, a decrease in chlorophyll *a*/VSS with increasing chlorophyll *b*/VSS suggests a decrease in population of these chlorophyll *b* deficient microbes. This latter trend was magnified in reactor R2 after about day-13 with 250 µmol $m^{-2}s^{-1}$ and 550 µmol $m^{-2}s^{-1}$ light conditions (Figure 4- 3-b, Figure 4- 4-b).

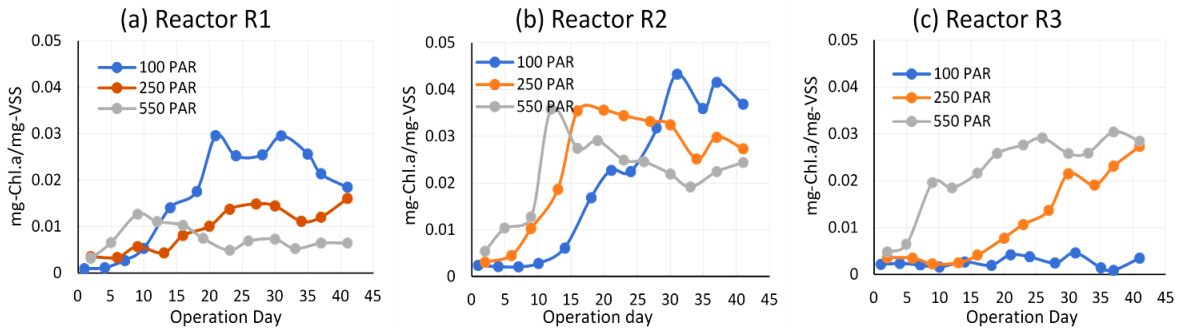

Figure 4- 3: Normalized chlorophyll *a* concentration (mg-Chl *a*/ mg-VSS). (a) Reactor R1 (b) Reactor R2 (c) Reactor R3. (PAR equivalent to µmol $m^{-2}s^{-1}$**)**

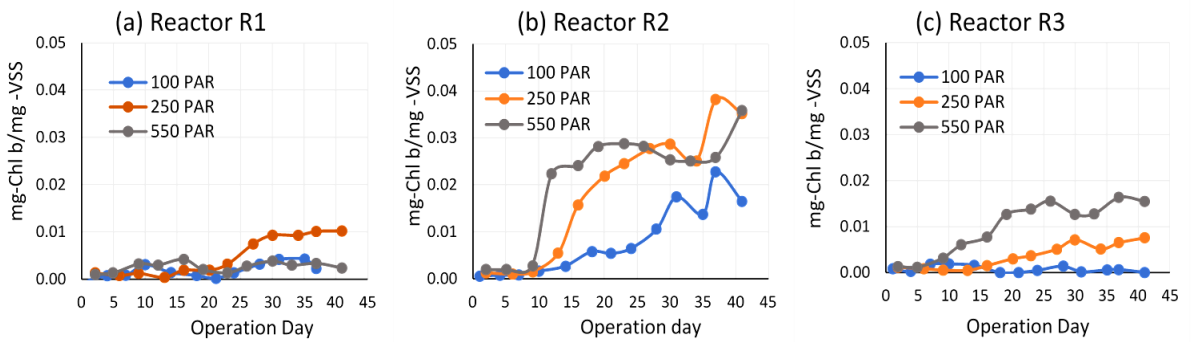

Figure 4- 4: Normalized chlorophyll-b concentration (mg-Chl b/mg-VSS). (a) Reactor R1 (b) Reactor R2 (c) Reactor R3. (PAR equivalent to µmol $m^{-2}s^{-1}$).

Phycobilisomes (PBS) form a significant fraction of the light-harvesting moiety in cyanobacteria.[97,100,101] The concentration of PBS in the bulk biomass describes the transient response of this OPGs keystone community [24] to the reactor conditions. Reactors R1 and R2 had an average initial normalized phycobilin (PBS/VSS) concentration of 0.4 (±0.03) for operation under 100 µmol $m^{-2}s^{-1}$ and 250 µmol $m^{-2}s^{-1}$ light intensities (Figure 4- 5-a, b). In both reactors, operation under 100 µmol$m^{-2}s^{-1}$ increased PBS/VSS to average peaks of 0.9 (±0.04). In contrast, 250 µmol $m^{-2}s^{-1}$ light irradiances resulted in a ratio increase by day-9 and decreased by day-20 (Figure 4- 5-a, b) for reactor R1 and R2. This was followed by a minimal increase to 0.13 and 0.18 for reactor R1 and R2 by day-41. Reactor R3 operation with 100 µmol $m^{-2}s^{-1}$ had higher perturbations of PBS/VSS concentrations with local maxima of 2.2 on day-24 (Figure 4- 5-a). A trend similar to R1 and R2 was observed in reactor R3 operation but with an earlier peak of 0.6 on day-6, and a higher undulation beyond day-15 (Figure 4- 5-c). The decreases mirrored by an inverse chlorophyll *a* and *b* ratio trends (Figure 4- 3-a, Figure 4- 4-a) suggests cyanobacterial depopulation.

Reactor R1 operation with 550 µmol $m^{-2}s^{-1}$ photon density resulted in minimal variation of PBS/VSS ratio around a mean of 0.05 (±0.02) (Figure 4- 5-a). This light intensity in reactor R2 and R3 operations resulted in an increasing trend up to day-20, followed by a constant trend to day-41 (Figure 4- 5-b). The corresponding rapid increases in chlorophyll *a* are therefore largely associated with the population of microalgae rather than cyanobacteria. Microalgae can foster bio-aggregation forming algal-bacterial agglomerations [9,102,102,103] potentially responsible for the increase in modal particle size by day-41 (Table 4- 3). The ratio response with both 250 µmol $m^{-2}s^{-1}$ and 550 µmol $m^{-2}s^{-1}$ operations, alludes to limited opportunity for optimizing cyanobacterial enrichment at higher light intensities in OPG reactors. Cyanobacteria are photophobic to high light intensities.[104]

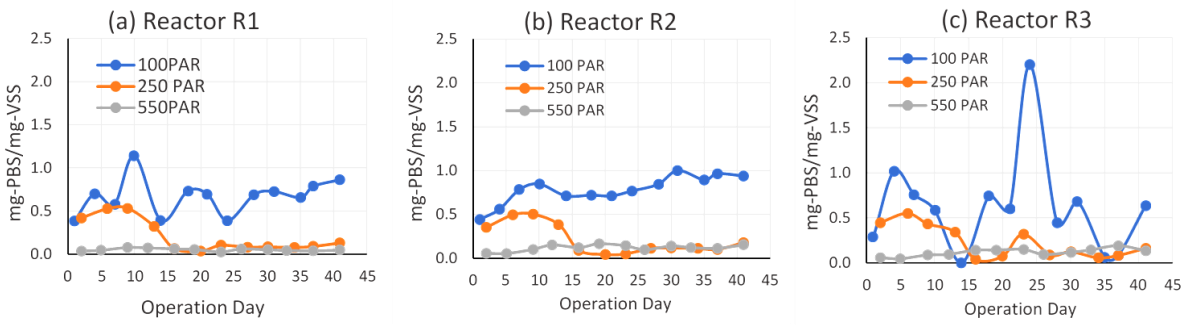

Figure 4- 5: Normalized phycobilisomes concentrations (mg-PBS/mg-VSS). (a) Reactor R1 (b) Reactor R2 (c) Reactor R3. (PAR= µmol$m^{-2}s^{-1}$).

The $PBP_{Chl\text{-}a}$ in reactors R1 and R2 decreased with light intensity (Figure 4- 6-a) while a reverse trend was observed in reactor R3. High $PBP_{Chl\text{-}a}$ mean values were observed in reactor R1 and R2 with 100 µmol $m^{-2}s^{-1}$ and in reactor R3 for operations under 550 µmol $m^{-2}s^{-1}$ (Figure 4- 6-a, Table 4- 4). An increase in the photosynthetic productivity potential suggests increasing light utility. Hence, a higher utility was realized for all phototrophs ($PBP_{Chl\text{-}a}$) with the lower light operation in reactors R1 and reactor R2, and at higher

light for reactor R3 (Figure 4- 6). The deviation of PBP_{Chl-a} potential about the mean decreased with increasing light intensity for reactors R1 and R2 but increased with light for reactor R3 (Figure 4- 6-b). This result alludes to the variability of particle-particle interactions and their impact on light utility at different reactor scales.

The PBP_{PBS} for all reactors decreased with increased irradiance from 100 to 250 µmol $m^{-2}s^{-1}$ (Figure 4- 6-b, Table 4- 4) and increased at a higher light intensity. The operations under 100 µmol $m^{-2}s^{-1}$ had highest PBP_{PBS} deviations about the mean (Figure 4- 6-b). Increased light intensity reduced variability of PBP_{PBS} in all reactors (Figure 4- 6-b). The higher variability at low intensity can hence be attributed to limited light-particle interaction within reactors inducing fluctuating cyanobacterial growth. The operation of reactor R2 with different light intensities had minimal changes in phycobilins productivity (Figure 4- 6-b) while the operation of reactors R1 and R3 indicated comparable cyanobacteria productivity. This result suggests comparable light utility and cyanobacterial growth in these two reactors.

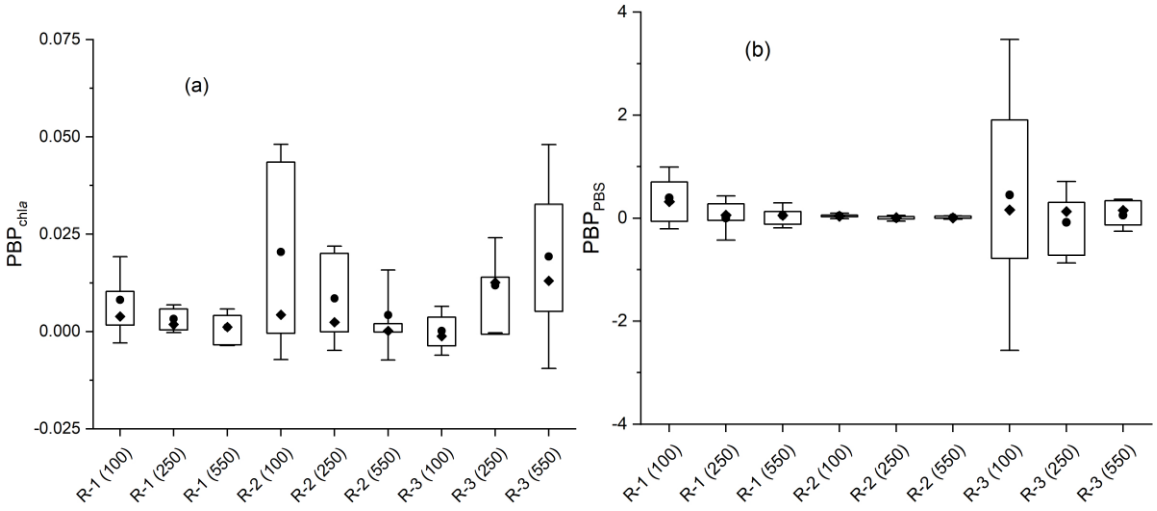

Figure 4- 6: Mean photosynthetic biomass production for reactors R1, R2 and R3 under different light intensities (PAR= µmol $m^{-2}s^{-1}$). (a) PBP-chlorophyll-a (b) PBP-phycobilin. (●) indicate the mean values (Table 8), (♦) indicate the median values, whiskers show the mean ±1 standard deviation, and the boxes are 25 to75 percentiles.

4.4.5 Nutrients removal efficiency

The OPG nutrient removal occurs via oxidation of organic carbon, nitrification, denitrification. [3,21,78] An enhanced phosphorous bioaccumulation similar to agal-bacterial aggregates[105] potentially occurs in OPGs reactor operation. A decrease in the NRF_{COD} ensued with increasing light intensity for all reactors (Table 4- 4). This decrease in tandem with the decreasing phototrophic enrichment, seen with chlorophyll *a* (Figure 4-3) and phycobilins concentration (Figure 4- 5) trends, suggests oxygen deficiency requisite for bacterial respiration.[3,9] A high net removal ratio for nitrogen (NRF_N) resulted from operations at 250 µmol $m^{-2}s^{-1}$ for all reactors with the highest mean value obtained in reactor R2 (Table 4- 4). The removal of nitrogen increased with increasing light intensity from 100 µmol $m^{-2}s^{-1}$ to 250 µmol $m^{-2}s^{-1}$ and decreased with 550 µmol $m^{-2}s^{-1}$ light conditions. Strong coherence between microbial growth rates and nutrient uptake has been reported.[21,22,106] The decreasing chlorophyll and phycobilin's productivity with

light intensity in reactors R1 and R2 (Figure 4- 3, Figure 4- 5) was incongruent to the trend of nitrogen removal. This result suggests nitrogen assimilation by microbes and denitrification within the OPG reactors.[21,22,107]

At the highest light intensity removal of nitrogen was highest in reactor R2 (Table 4- 4). This suggests that reactor R2 had higher light utility for nitrogen removal compared to reactor R3 at high light intensity operations. This result contrasts to the higher chlorophyll *a* productivity observed in reactor R3 with 550 µmol $m^{-2}s^{-1}$ (Table 4- 4). The trend in nitrogen removal for reactor R3 contrasted with the PBP_{PBS} trend (Table 4- 4). Nitrogen depletion has been reported as a growth trigger and transforming exponential to stationary growth phase for cyanobacterium *Cyanothece* sp.[106] However, a negative correlation of phototrophic productivity with nitrogen uptake was observed in all reactors (Figure 4- 7). This alludes to the nutrient replete environment during reactor operations.

The NRFp in all reactors increased with light intensity in contrast to the $PBP_{Chl\text{-}a}$ trend. Negative nutrient removal ratios indicate potential nutrients accumulation within the reactors while a decrease in nutrient removal with increasing light intensity alludes to limited microbial growth.[105,108] The positive correlation observed in reactor R3 between $PBP_{Chl\text{-}a}$: NRFp (Figure 4- 7-a) and negative PBP_{PBS} : NRFp (Figure 4- 7-b) suggests an algal mediated phosphorous nutrients removal. A strongly positive correlation was observed between both chlorophyll and phycobilin productivities and COD removal rates for reactors R1 and R2 (Figure 4- 7). In contrast, the NRF_{COD} in reactor R3 had a strong

negative correlation to chlorophyll productivity and have a weak positive correlation with PBP_{PBS} (Figure 4- 7).

Table 4- 4: Reactor photon utility ratios reported as photosynthetic biomass productivities (PBP_x) and net removal factors (NRF_y). Values shown are the mean for each reactor scale and light intensity.

Reactor	Photon flux ($\mu mol.m^{-2}.s^{-1}$)	PBP_{Chl-a} Mean*10^{-3} (mg/mol)	PBP_{PBS} Mean*10^{-3} (mg/mol)	NRF_{COD} Mean (mg/d)/(mol)	NRF_{N} Mean (mg/d)/(mol)	NRF_{P} Mean (mg/d)/(mol)
Reactor-1	100	8.14	393.43	0.98	0.02	-0.005
	250	3.26	4.29	0.51	0.28	0.001
	550	1.10	54.36	0.09	0.03	0.002
Reactor-2	100	20.44	42.00	1.61	0.04	-0.018
	250	8.51	-1.48	0.43	1.17	-0.001
	550	4.24	11.46	0.04	0.24	0.000
Reactor-3	100	0.20	449.66	0.28	-0.08	-0.041
	250	11.88	-79.95	0.20	0.84	-0.005
	550	19.27	57.03	-0.34	-0.27	0.012

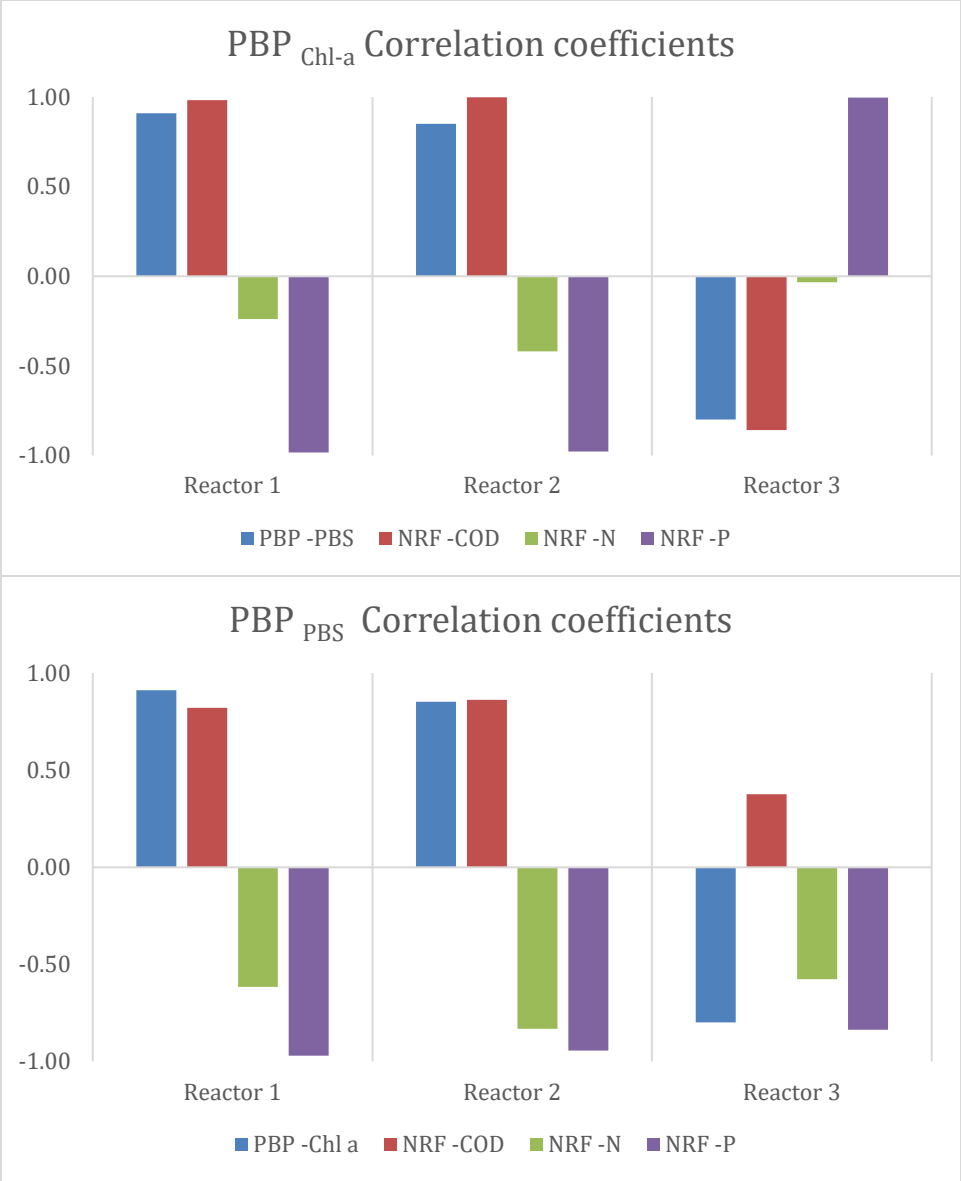

Figure 4- 7: The correlation coefficients of each photosynthetic biomass productivity with each other and with nutrient removal ratios. Each correlation represents the ensemble of light conditions for each reactor.

4.5 Discussion

Selection pressures reported to promote granulation [89–91] were induced in reactor operation. Moreover, various factors reported to impact phototrophic production such as temperature,[33,106] photon flux,[106,109] nutrient loading [15] were similar for all three reactors.

The nutrient replete reactor operation [15] was characterized by an average influent TN of 24 mg-N/L (±9) and phosphorous concentrations of 1.4 mg-P/L (±1). Operation in sequencing batch mode was utilized to induce feast and famine selection pressures reported necessary for granulation.[89] In addition, the rapid settling phase (10 min) before decanting, induced granulation promoting hydraulic selection pressure.[90,110]

However, mixing induced shear selection pressure, [56,63] was not controlled. Higher agitation increases both the frequency of light interaction and shear. As such, the reported variation in particle size distribution reflects the shear heterogeneity and light interaction effects. Both reactor R2 and R3 had homogenous turnover rates (Table 4- 2). Reactor R1, on the other hand, was operated at reported lab-scale OPG reactor operational conditions.[3] Shear stress can have both aggregating and eroding influences [56,60,89] on particles within the OPG reactor. In fluid-solid phase flow systems such as present on OPG reactors, particles increase dissipation of turbulence kinetic energy [111] within the bulk matrix. This causes excess shear on the particles with a lower limit defined by the Kolmogorov length scale.[85,86] Particles that are smaller than this scale experience laminar conditions[112] with viscous dissipation of energy. However, microbial growth can augment aggregation and result in larger particle sizes [56,63] with the capacity to withstand the fracturing influence of shear forces.[112]

An increase in larger particle sizes and improving settling (Figure 4- 1) with increasing light conditions was observed. Across the three reactors, consistent initial decrease (day-2 to day-20) in the mean size (Table 4- 4) was observed at both 100 µmol $m^{-2}s^{-1}$ and 250

µmol $m^{-2}s^{-1}$ experimental conditions, indicating a shear adaptation period (Table 4- 3). In contrast, operation under 550 µmol $m^{-2}s^{-1}$ had moderate initial increases in the mean size for all reactors suggesting enhanced phototrophic amended granulation. This change in particle sizes reflects an equilibrium of granular inducing/degrading pressures within each reactor micro-environment. The observed increase in the number of larger particle sizes, seen with increasing skew (Table 4- 3) also suggests photon pressure enhanced microbial aggregation.[25] While perpetual photoinhibition occurring under all light exposure [113,114] can limit granulation, the size increases suggest the existence of intervening factors to aggregation limitations due to high light. These include amended light interaction due to particle concentrations, shading [15] and reactor depth [15,65,67] enhancing granulation.

Biomass concentrations increased with light intensity for all reactors (Figure 4- 2). For reactor R1, shallower depths (Table 4- 1) led to higher light interactions promoting rapid biomass growth (Figure 4- 2), and hence higher biomass concentrations. A decline in biomass concentrations was observed with 250-550 µmol $m^{-2}s^{-1}$ at the later stages of operation in reactor R1 and R2 and with all light conditions in reactor R3 (Figure 4- 2). This decrease can be related to stagnating and declining chlorophyll concentrations in the same period (Figure 4- 3, Figure 4- 4). This decline can be ascribed to photon stress present with high irradiances inhibiting microbial photoactivity. [29,31,106] Equally, increasing biomass concentrations due to higher light interaction can increase light attenuation limiting light penetration and diminishing photosynthetic production.[67] This attenuation can be exacerbated by smaller particle sizes such as free-floating microalgae

seen with persistent increases on chlorophyll *b* (Figure 4- 4) concentrations. The observed decreases in biomass concentrations, therefore, more likely reflect light-limited conditions in reactors. In reactor R3, a steady increase in biomass concentration was observed with high light intensity (Figure 4- 2). This increase seen with increasing chlorophyll concentrations (Figure 4- 3, Figure 4- 4) allude to a light profile promoting photosynthetic growth and delayed photolimitation potentially due to higher volume (Table 4- 1).

At each light intensity, reactor R2 exhibited higher $PBP_{Chl\text{-}a}$ compared to reactor R1 (Table 4- 4), indicating higher photon yields. Further, the $PBP_{Chl\text{-}a}$ decreased within reactor R1 and R2 with increasing light intensity (Table 4- 4). The concentration of Chlorophyll *a* pigments has been reported to be inversely correlated to increasing light intensity.[98] The PBP_{PBS} in R1 was higher compared to reactor R2 at each light intensity (Table 4- 4). The different trends of $PBP_{Chl\text{-}a}$ and PBP_{PBS} with reactor size can be ascribed to variable light utility within reactors R1 and R2 promoting the growth of different phototrophic microbes. Reactor R1 experienced a higher $PBP_{Chl\text{-}a}$ decrease (86%) compared to reactor R2 (79%) between 100 µmol $m^{-2}s^{-1}$ and 550 µmol $m^{-2}s^{-1}$ photon flux densities Photon stress resulting from shorter optical paths and lower light attenuation in shallow depth [67,115] could account for a higher decrease in $PBP_{Chl\text{-}a}$ in reactor R1.

Moreover, the decrease may be a legacy of higher exposure frequency in reactor R1 (16 sec) compared to R2 (22 sec) (Table 4- 2). Photoinhibition occurs under all light intensities,[114] but at lower rates in the photosynthetic light-limited region.[29] The light-

harvesting moiety in reactor R1 would be exposed to higher photon flux compared to deeper reactors R2 and R3, accounting for the lower $PBP_{Chl\text{-}a}$ in reactor R1. In addition, the decrease in mean phycobilin productivity for reactors R1 and R2 with increasing light intensity to 250 µmol $m^{-2}s^{-1}$ suggests operational conditions inhibiting the growth of cyanobacteria species.[97,104] The higher PBP_{PBS} in reactor R1 compared to reactor R2 (Table 4- 4) on the other hand, can be ascribed to higher biomass concentrations (Figure 4- 2) increasing light attenuation.[65,67] This, in turn, creates low light conditions ideal for the growth of photophobic cyanobacteria.[104]

A higher light attenuation due to depth is expected in reactor R3, compared to reactor R2, resulting in lower light interactions and biomass concentrations (Figure 4- 2-c) despite analogous exposure frequency (Table 4- 2). The $PBP_{Chl\text{-}a}$ in reactor R3 increased with light intensity from 100 µmol $m^{-2}s^{-1}$ to 550 µmol $m^{-2}s^{-1}$ photon flux, a trend contrary to that in reactor R2. The theoretical reactor turnover frequency used to determine the reactor mixing intensity (Table 4- 2) assumes a 95% reactor homogeneity [81,83] with the reactor surface as a reference frame. However, light penetration occurs beyond this reference frame and attenuates exponentially subject to turbidity and depth, per the Beer-Lamberts law.[67] This results in the uneven distribution of light in reactors with increasing depth and biomass concentration. The observed variability in biomass concentrations for reactor R3 (Figure 4- 2-c), could be due to this fluctuating interaction. Moreover, reactor R3 exhibited higher chlorophyll *a* photon yields compared to reactor R2 with operation at 250 µmol $m^{-2}s^{-1}$ and 550 µmol $m^{-2}s^{-1}$ light conditions. This increase of $PBP_{Chl\text{-}a}$ in reactor R3 compared to other reactors indicate the superior utility of light for photosynthetic

function even with a comparable turnover rate to shallower reactor R2 (Table 4- 2). The sustained increase in $PBP_{Chl\text{-}a}$ even at highest light intensities suggest a beneficial influence of depth on light interaction in reactor R3 for photosynthetic production.

Additionally, the PBP_{PBS} in reactor R3 decreased with irradiance from 100 to 250 µmol $m^{-2}s^{-1}$ and increased with 550 µmol $m^{-2}s^{-1}$ (Table 4- 4). The PBP_{PBS} trend suggests optimal light conditions for cyanobacteria growth at 100 µmol $m^{-2}s^{-1}$. The low biomass concentration in reactor R3 (Figure 4- 2) resulting in lower light attenuation suggests potential photon stress at higher irradiances limiting cyanobacterial enrichment. The greater depth and low light conditions within reactor R3 resulted in the highest PBP_{PBS} productivity at 100 µmol $m^{-2}s^{-1}$, among the three reactors (Table 4- 4). Nonetheless, the PBP_{PBS} trend in reactor R3 had a strong negative correlation to $PBP_{Chl\text{-}a}$ (-0.80) (Figure 4-7) alluding to the different light adaptations of microalgae and cyanobacteria.[29,34] Photophobic cyanobacteria [104] utilize phycobilisomes to facilitate light harvesting at low light intensities and constitute on average 50% of their light-harvesting capacity.[116,117] The negative correlation can also be attributed to the contrasting trend of microalgal enrichment seen with the persistent increase of chlorophyll *b* (Figure 4- 4-c) in deeper reactor R3 compared to other reactors.

A decrease in the NRF_{sCOD} was observed with increasing light intensity for all reactors. On the other hand, the NRF_N increased with light intensity from 100 µmol $m^{-2}s^{-1}$ to 250 µmol $m^{-2}s^{-1}$ and decreased at 550 µmol $m^{-2}s^{-1}$ for all reactors. One hypothesis for the reduced nutrient removal efficiency of COD and TDN at higher light intensities is the

effect of reactor depth and self-shading within reactors limiting light-dependent oxygen generation.[15] Moreover, higher particle concentrations (Figure 4- 2) and sizes (Table 4- 3) observed at high irradiance impacts light interaction.[66,67] The lowest NRF_{COD} values recorded in reactor R3 indicates the highest light limitation, which is consistent with depth dependence of light decay.[66,67] While mixing is applied to mitigate these impacts within the reactor,[9,15] the fluid flow streamlines affecting particle interaction vary with reactor size. Consequently, despite homogenous reactor turnover rates between reactors R2 and R3, OPG granules in deeper sections of the reactor R3 experience reduced light due to reduced penetration.[15] Moreover, the longer light-dark pathways achieved with axial flow in deeper reactors promote recovery of induced photoinhibition at higher light intensities.[29,31] This could account for the higher photosynthetic biomass productivities in reactors R2 and reactor R3 with increased light compared to fully light penetrated reactor R1 (Table 4- 4).

Achieving OPG rector operation at large scale can result in significant benefits for wastewater treatment due to their self-aerating potential among other granular incentives.[1,9,15] However, achieving this scale enterprise relies on optimizing light utility within the reactor, beyond the provision of net photon flux.[15] Increasing light intensity at larger reactor scales (Reactor R2 and R3) did not result in increased removal of organics (NRF_{COD}). NRF_N was higher at lower intensities to 250 µmol $m^{-2}s^{-1}$ while NRF_P increased with operational photon flux. Reactor R3 showed differing nutrient removal factors compared to reactor R2 and R1, which had similar trends. Low light is reported to be beneficial to higher nutrients removal in mixed cultures but reduces organic carbon

(NRF_{COD}) exploitation under high light.[8] The photosynthetic biomass productivity in reactor R1 and R2 had consistent trends (Table 4- 4). However, reactor R3 PBP showed variable trends with increasing light intensity, suggesting that environmental conditions within reactors, induce microbial selection. This variable productivity and nutrient removal can be attributed to impacts of (1) reactor depth (2) particle sizes and concentrations and their impact on OPGs light interactions. The frequency of exposure in turn impacts treatment efficiencies due to light utility within the reactor. These differences can be imputed to the variable light interactions with reactor depth, and self-shading effects resulting in different light utility within the reactor. Consequently, OPG scaling up efforts are non-linear and must be tailored to each reactor size within the saturation and wastewater treatment standard limits.

4.6 Bibliography

1. Milferstedt, K. *et al.* Biogranules applied in environmental engineering. *Int. J. Hydrog. Energy* **42**, 27801–27811 (2017).

2. Trebuch, L. M. *et al.* Impact of hydraulic retention time on community assembly and function of photogranules for wastewater treatment. *Water Res.* **173**, 115506 (2020).

3. Abouhend, A. S. *et al.* The Oxygenic Photogranule Process for Aeration-Free Wastewater Treatment. *Environ. Sci. Technol.* **52**, 3503–3511 (2018).

4. Gu, Y. *et al.* Energy Self-sufficient Wastewater Treatment Plants: Feasibilities and Challenges. *Energy Procedia* **105**, 3741–3751 (2017).

5. Managing Energy Costs in Wastewater Treatment Plants - Madison Gas and Electric - Madison, Wisconsin. https://www.mge.com/saving-energy/business/bea/article_detail.htm?nid=%202431.

6. Angelakis, A. N. & Snyder, S. A. Wastewater Treatment and Reuse: Past, Present, and Future. *Water* **7**, 4887–4895 (2015).

7. Park, C. & Dolan, S. (deceased). Patent Algal Sludge Granule OPG Jan 2019. 11 (2019).

8. Pastore, M., Santaeufemia, S., Bertucco, A. & Sforza, E. Light intensity affects the mixotrophic carbon exploitation in Chlorella protothecoides: consequences on microalgae-bacteria based wastewater treatment. *Water Sci. Technol.* **78**, 1762–1771 (2018).

9. Lee, Y.-J. & Lei, Z. Microalgal-bacterial aggregates for wastewater treatment: A mini-review. *Bioresour. Technol. Rep.* 100199 (2019) DOI:10.1016/j.biteb.2019.100199.

10. Tang, K.-H., Tang, Y. J. & Blankenship, R. E. Carbon Metabolic Pathways in Phototrophic Bacteria and Their Broader Evolutionary Implications. *Front. Microbiol.* **2**, (2011).

11. Anderson, D. M., Glibert, P. M. & Burkholder, J. M. Harmful algal blooms and eutrophication: Nutrient sources, composition, and consequences. *Estuaries* **25**, 704–726 (2002).

12. Corcoll, N. *et al.* The Use of Photosynthetic Fluorescence Parameters from Autotrophic Biofilms for Monitoring the Effect of Chemicals in River Ecosystems. in *Emerging and Priority Pollutants in Rivers* (eds. Guasch, H., Ginebreda, A. & Geiszinger, A.) vol. 19 85–115 (Springer Berlin Heidelberg, 2012).

13. Donlan, R. M. Biofilms: Microbial Life on Surfaces. *Emerg. Infect. Dis.* **8**, 881–890 (2002).

14. Kim, B.-H. *et al.* Influence of Water Depth on Microalgal Production, Biomass Harvest, and Energy Consumption in High Rate Algal Pond Using Municipal Wastewater. *J. Microbiol. Biotechnol.* **28**, 630–637 (2018).

15. González-Camejo, J. *et al.* Effect of light intensity, light duration and photoperiods in the performance of an outdoor photobioreactor for urban wastewater treatment. *Algal Res.* **40**, 101511 (2019).

16. Gao, D., Liu, L., Liang, H. & Wu, W. *Aerobic Granular Sludge: Characterization, Mechanism of Granulation and Application to Wastewater Treatment*. vol. 31 (2010).

17. Giesen, A., van Loosdrecht, M., Robertson, S. & de Buin, B. Aerobic Granular Biomass Technology: further innovation, system development and design optimisation. https://www.ingentaconnect.com/contentone/wef/wefproc/2015/00002015/00000016/art00018 (2015) doi:info:doi/10.2175/193864715819539641.

18. Ansari, A. A., Abouhend, A. S. & Park, C. Effects of seeding density on photogranulation and the start-up of the oxygenic photogranule process for aeration-free wastewater treatment. *Algal Res.* **40**, 101495 (2019).

19. Zhao, Z. *et al.* Response of algal-bacterial granular system to low carbon wastewater: Focus on granular stability, nutrients removal and accumulation. *Bioresour. Technol.* **268**, 221–229 (2018).

20. Abouhend, A. S. *et al.* Growth Progression of Oxygenic Photogranules and Its Impact on Bioactivity for Aeration-Free Wastewater Treatment. *Environ. Sci. Technol.* (2019) doi:10.1021/acs.est.9b04745.

21. Stauch-White, K., Srinivasan, V. N., Camilla Kuo-Dahab, W., Park, C. & Butler, C. S. The role of inorganic nitrogen in successful formation of granular biofilms for wastewater treatment that support cyanobacteria and bacteria. *AMB Express* **7**, (2017).

22. Delgadillo-Mirquez, L., Lopes, F., Taidi, B. & Pareau, D. Nitrogen and phosphate removal from wastewater with a mixed microalgae and bacteria culture. *Biotechnol. Rep.* **11**, 18–26 (2016).

23. Schmidt, I. *et al.* New concepts of microbial treatment processes for the nitrogen removal in wastewater. *FEMS Microbiol. Rev.* **27**, 481–492 (2003).

24. Milferstedt, K. *et al.* The importance of filamentous cyanobacteria in the development of oxygenic photogranules. *Sci. Rep.* **7**, 17944 (2017).

25. Arcila, J. S. & Buitrón, G. Influence of solar irradiance levels on the formation of microalgae-bacteria aggregates for municipal wastewater treatment. *Algal Res.* **27**, 190–197 (2017).

26. Lee, K. & Lee, C.-G. Effect of light/dark cycles on wastewater treatments by microalgae. *Biotechnol. Bioprocess Eng.* **6**, 194–199 (2001).

27. Droste, R. L. & Gehr, R. L. *Theory and Practice of Water and Wastewater Treatment*. (John Wiley & Sons, 2018).

28. Yen, H.-W., Hu, I.-C., Chen, C.-Y. & Chang, J.-S. Design of Photobioreactors for Algal Cultivation. in *Biofuels from Algae* 23–45 (Elsevier, 2014). doi:10.1016/B978-0-444-59558-4.00002-4.

29. Giacometti, G. M. & Morosinotto, T. Photoinhibition and Photoprotection in Plants, Algae, and Cyanobacteria. in *Encyclopedia of Biological Chemistry* (eds. Lennarz, W. J. & Lane, M. D.) 482–487 (Academic Press, 2013). DOI:10.1016/B978-0-12-378630-2.00229-2.

30. Bailey, S. & Grossman, A. Photoprotection in cyanobacteria: regulation of light harvesting. *Photochem. Photobiol.* **84**, 1410–1420 (2008).

31. Powles, S. B. Photoinhibition of Photosynthesis Induced by Visible Light. *Annu. Rev. Plant Physiol.* **35**, 15–44 (1984).

32. Schuurmans, R. M., van Alphen, P., Schuurmans, J. M., Matthijs, H. C. P. & Hellingwerf, K. J. Comparison of the Photosynthetic Yield of Cyanobacteria and Green Algae: Different Methods Give Different Answers. *PLOS ONE* **10**, e0139061 (2015).

33. Lürling, M., Eshetu, F., Faassen, E. J., Kosten, S. & Huszar, V. L. M. Comparison of cyanobacterial and green algal growth rates at different temperatures. *Freshw. Biol.* **58**, 552–559 (2013).

34. Beardall, J. & Raven, J. A. Cyanobacteria vs green algae: which group has the edge? *J. Exp. Bot.* **68**, 3697–3699 (2017).

35. Subashchandrabose, S. R., Ramakrishnan, B., Megharaj, M., Venkateswarlu, K. & Naidu, R. Mixotrophic cyanobacteria and microalgae as distinctive biological agents for organic pollutant degradation. *Environ. Int.* **51**, 59–72 (2013).

36. Lee, C. S., Oh, H.-S., Oh, H.-M., Kim, H.-S. & Ahn, C.-Y. Two-phase photoperiodic cultivation of algal–bacterial consortia for high biomass production and efficient nutrient removal from municipal wastewater. *Bioresour. Technol.* **200**, 867–875 (2016).

37. Lee, C. S., Lee, S.-A., Ko, S.-R., Oh, H.-M. & Ahn, C.-Y. Effects of photoperiod on nutrient removal, biomass production, and algal-bacterial population dynamics in lab-scale photobioreactors treating municipal wastewater. *Water Res.* **68**, 680–691 (2015).

38. *Handbook of industrial mixing: science and practice*. (Wiley-Interscience, 2004).

39. He, Q. *et al.* Natural sunlight induced rapid formation of water-born algal-bacterial granules in an aerobic bacterial granular photo-sequencing batch reactor. *J. Hazard. Mater.* **359**, 222–230 (2018).

40. Massa, G. D., Kim, H.-H., Wheeler, R. M. & Mitchell, C. A. Plant Productivity in Response to LED Lighting. *HortScience* **43**, 1951–1956 (2008).

41. Szoradi, C. LED Grow Lights Reshape Agriculture | LED Journal. https://www.ledjournal.com/main/blogs/led-grow-lights-reshape-agriculture/ (2016).

42. Haigh, J. D., Winning, A. R., Toumi, R. & Harder, J. W. An influence of solar spectral variations on radiative forcing of climate. *Nature* **467**, 696–699 (2010).

43. Assemany, P. P. *et al.* Algae/bacteria consortium in high rate ponds: Influence of solar radiation on the phytoplankton community. *Ecol. Eng.* **77**, 154–162 (2015).

44. Sutherland, D. L., Howard-Williams, C., Turnbull, M. H., Broady, P. A. & Craggs, R. J. Seasonal variation in light utilization, biomass production and nutrient removal by wastewater microalgae in a full-scale high-rate algal pond. *J. Appl. Phycol.* **26**, 1317–1329 (2014).

45. Amanatidou, E., Samiotis, G., Trikoilidou, E., Pekridis, G. & Taousanidis, N. Evaluating sedimentation problems in activated sludge treatment plants operating at complete sludge retention time. *Water Res.* **69**, 20–29 (2015).

46. Ellis, K. V. & Mara, D. D. Stabilization ponds: Design and operation. *Crit. Rev. Environ. Sci. Technol.* (2009) doi:10.1080/10643388309381703.

47. Verbyla, von S. Waste Stabilization Ponds. *Global Water Pathogen Project* http://www.waterpathogens.org/book/waste-stabilization-ponds (2017).

48. Hamzeh Ramadan, Waste Stabilization Ponds. http://stabilizationponds.sdsu.edu/.

49. Arrow Electronics. LED application in agricultural lighting can efficiently increase crop yields. *Arrow.com* https://www.arrow.com/en/research-and-events/articles/agriculture-lighting (2017).

50. Nemali, K. Light Quantity and Quality in Controlled Environment Agriculture. 27 (2016).

51. Mahdavian, M. & Wattanapongsakorn, N. Optimizing Greenhouse Lighting for Advanced Agriculture Based on Real Time Electricity Market Price. *Mathematical Problems in Engineering* https://www.hindawi.com/journals/mpe/2017/6862038/ (2017) doi:10.1155/2017/6862038.

52. Åmand, L. Control of aeration systems in activated sludge processes – a review. /paper/Control-of-aeration-systems-in-activated-sludge-%E2%80%93-a-%C3%85mand/33484777bf4af0743f759899f7bbc520def5b4de (2011).

53. Chen, Y., Jiang, W., Liang, D. T. & Tay, J. H. Structure and stability of aerobic granules cultivated under different shear force in sequencing batch reactors. *Appl. Microbiol. Biotechnol.* **76**, 1199–1208 (2007).

54. Zhu, L., Zhou, J., Yu, H. & Xu, X. Optimization of hydraulic shear parameters and reactor configuration in the aerobic granular sludge process. *Environ. Technol.* **36**, 1605–1611 (2015).

55. Winkler, M.-K. H., Kleerebezem, R., Strous, M., Chandran, K. & van Loosdrecht, M. C. M. Factors influencing the density of aerobic granular sludge. *Appl. Microbiol. Biotechnol.* **97**, 7459–7468 (2013).

56. Liu, Y. & Tay, J.-H. The essential role of hydrodynamic shear force in the formation of biofilm and granular sludge. *Water Res.* **36**, 1653–1665 (2002).

57. Liu, Y. Chapter 5 Factors affecting aerobic granulation. in *Waste Management Series* (eds. Tay, J.-H., Tay, S. T.-L., Liu, Y., Show, K.-Y. & Ivanov, V.) vol. 6 99–114 (Elsevier, 2006).

58. Adav, S. S., Lee, D.-J., Show, K.-Y. & Tay, J.-H. Aerobic granular sludge: Recent advances. *Biotechnol. Adv.* **26**, 411–423 (2008).

59. Nancharaiah, Y. V. & Kiran Kumar Reddy, G. Aerobic granular sludge technology: Mechanisms of granulation and biotechnological applications. *Bioresour. Technol.* **247**, 1128–1143 (2018).

60. Tay, J.-H., Liu, Q.-S. & Liu, Y. The effects of shear force on the formation, structure and metabolism of aerobic granules. *Appl. Microbiol. Biotechnol.* **57**, 227–233 (2001).

61. Zheng, Y.-M., Yu, H.-Q. & Sheng, G.-P. Physical and chemical characteristics of granular activated sludge from a sequencing batch airlift reactor. *Process Biochem.* **40**, 645–650 (2005).

62. Li, D. & Ganczarczyk, J. Advective Transport in Activated Sludge Flocs. *Water Environ. Res.* **64**, 236–240 (1992).

63. Nejadnik, M. R., Mei, H. C. van der, Busscher, H. J. & Norde, W. Determination of the Shear Force at the Balance between Bacterial Attachment and Detachment in Weak-Adherence Systems, Using a Flow Displacement Chamber. *Appl Env. Microbiol* **74**, 916–919 (2008).

64. Yeoh, G. H. & Tu, J. Liquid–Particle Flows. in *Computational Techniques for Multiphase Flows* 313–349 (Elsevier, 2010). doi:10.1016/B978-0-08-046733-7.00005-9.

65. Curtis, T. P., Mara, D. D., Dixo, N. G. H. & Silva, S. A. Light penetration in waste stabilization ponds. *Water Res.* **28**, 1031–1038 (1994).

66. Brito, A. C. & Newton, A. Measuring Light Attenuation in Shallow Coastal Systems. *J. Ecosyst. Ecography* **03**, (2013).

67. Gallegos, C. L. & Moore, K. A. Factors contributing to water-column light attenuation. (2000).

68. Falkowski, P. G. & Raven, J. A. *Aquatic Photosynthesis*. (Princeton University Press, 2007).

69. The influence of particles on suspension rheology :: Anton Paar Wiki. *Anton Paar* https://wiki.anton-paar.com/en/the-influence-of-particles-on-suspension-rheology/.

70. Solid-Liquid Mixing In Agitated Vessels (Just Suspended Speed). *Cheresources.com Community* https://www.cheresources.com/invision/blog/4/entry-511-solid-liquid-mixing-in-agitated-vessels-just-suspended-speed/.

71. Bai, G., Armenante, P. M. & Plank, R. V. Experimental and computational determination of blend time in USP Dissolution Testing Apparatus II. *J. Pharm. Sci.* **96**, 3072–3086 (2007).

72. Hall, S. M. Chapter 6 - Blending and Agitation. in *Rules of Thumb for Chemical Engineers (Sixth Edition)* (ed. Hall, S. M.) 99–124 (Elsevier, 2018). DOI:10.1016/B978-0-12-811037-9.00006-0.

73. Kristensen, E. & Suraswadi, P. Carbon, nitrogen and phosphorus dynamics in creek water of a southeast Asian mangrove forest. *Hydrobiologia* **474**, 197–211 (2002).

74. Gubanov, O. & Cortelezzi, L. On the cost efficiency of mixing optimization. *J. Fluid Mech.* **692**, 112–136 (2012).

75. Machado, M. B., Nunhez, J. R., Nobes, D. & Kresta, S. M. Impeller characterization and selection: Balancing efficient hydrodynamics with process mixing requirements. *AIChE J.* **58**, 2573–2588 (2012).

76. Kresta, S. M. Advances in Industrial Mixing. 1034.

77. Han, B.-P., Virtanen, M., Koponen, J. & Straškraba, M. Effect of photoinhibition on algal photosynthesis: a dynamic model. *J. Plankton Res.* **22**, 865–885 (2000).

78. Kuo-Dahab, W. C. *et al.* Investigation of the Fate and Dynamics of Extracellular Polymeric Substances (EPS) during Sludge-Based Photogranulation under Hydrostatic Conditions. *Environ. Sci. Technol.* **52**, 10462–10471 (2018).

79. Furukawa, H. *et al.* Correlation of Power Consumption for Several Kinds of Mixing Impellers. *Int. J. Chem. Eng.* **2012**, 1–6 (2012).

80. Jirout, T. & Rieger, F. Impeller design for mixing of suspensions. *Chem. Eng. Res. Des.* **89**, 1144–1151 (2011).

81. Dickey, D. S. Tackling Difficult Mixing Problems. 8 (2015).

82. Chapple, D., Kresta, S. M., Wall, A. & Afacan, A. The Effect of Impeller and Tank Geometry on Power Number for a Pitched Blade Turbine. *Chem. Eng. Res. Des.* **80**, 364–372 (2002).

83. Post, T. Understand the Real World of Mixing. (2010).

84. van der Lans, R. & Riet, K. Mixing in Bioreactor Vessels. in *Comprehensive Biotechnology* 63–80 (2011). DOI:10.1016/B978-0-08-088504-9.00083-0.

85. Hill, P. S., Nowell, A. R. M. & Jumars, P. A. Encounter rate by turbulent shear of particles similar in diameter to the Kolmogorov scale. *J. Mar. Res.* **50**, 643–668 (1992).

86. Xu, H. & Bodenschatz, E. Motion of inertial particles with size larger than Kolmogorov scale in turbulent flows. *Phys. Nonlinear Phenom.* **237**, 2095–2100 (2008).

87. ALPHA. *Standard Methods for the Examination of Water and Wastewater*. (ALPHA,AWWA,WEF, 2012).

88. Bennett, A. & Bogorad, L. Complementary chromatic adaptation in a filamentous blue-green alga. *J. Cell Biol.* **58**, 419–435 (1973).

89. Bindhu, B. k. & Madhu, G. Selection pressure theory for aerobic granulation – an overview. *Int. J. Environ. Waste Manag.* **13**, 317–329 (2014).

90. Liu, Y.-Q. & Tay, J.-H. Fast formation of aerobic granules by combining strong hydraulic selection pressure with overstressed organic loading rate. *Water Res.* **80**, 256–266 (2015).

91. B K, B. & G, M. Influence of three selection pressures on aerobic granulation in sequencing batch reactor. *Indian J. Chem. Technol. IJCT* **22**, 241–247 (2016).

92. Dyer, K. R. & Manning, A. J. Observation of the size, settling velocity and effective density of flocs, and their fractal dimensions. *J. Sea Res.* **41**, 87–95 (1999).

93. Lee, D. J., Chen, G. W., Liao, Y. C. & Hsieh, C. C. On the free-settling test for estimating activated sludge floc density. *Water Res.* **30**, 541–550 (1996).

94. Adav, S. S., Lee, D.-J. & Lai, J.-Y. Aerobic granulation in sequencing batch reactors at different settling times. *Bioresour. Technol.* **100**, 5359–5361 (2009).

95. Arcila, J. S. & Buitrón, G. Microalgae–bacteria aggregates: effect of the hydraulic retention time on the municipal wastewater treatment, biomass settleability and methane potential. *J. Chem. Technol. Biotechnol.* **91**, 2862–2870 (2016).

96. Sezgin, M. Variation of sludge volume index with activated sludge characteristics. *Water Res.* **16**, 83–88 (1982).

97. Golterman, H. . Chapter 13 Algae and their Pigments. in *Physiological Limnology: An Approach to the Physiology of Lake Ecosystems* vol. 2 233–247 (Elsevier, 1975).

98. Grant, C. & Louda, J. Microalgal pigment ratios in relation to light intensity: implications for chemotaxonomy. *Aquat. Biol.* **11**, 127–138 (2010).

99. Wu, H. Effect of Different Light Qualities on Growth, Pigment Content, Chlorophyll Fluorescence, and Antioxidant Enzyme Activity in the Red Alga Pyropia haitanensis (Bangiales, Rhodophyta). *BioMed Res. Int.* **2016**, (2016).

100. Singh, N. K., Sonani, R. R., Rastogi, R. P. & Madamwar, D. The phycobilisomes: an early requisite for efficient photosynthesis in cyanobacteria. *EXCLI J.* **14**, 268–289 (2015).

101. Khazi, M. I., Demirel, Z. & Dalay, M. C. Evaluation of growth and phycobiliprotein composition of cyanobacteria isolates cultivated in different nitrogen sources. *J. Appl. Phycol.* **30**, 1513–1523 (2018).

102. Ahmad, J. S. M. *et al.* Stability of algal-bacterial granules in continuous-flow reactors to treat varying strength domestic wastewater. *Bioresour. Technol.* **244**, 225–233 (2017).

103. Gutzeit, G., Lorch, D. P., Weber, A., Engels, M. S. & Neis, U. Bioflocculent algal-bacterial biomass improves low-cost wastewater treatment. *Water Sci. Technol. J. Int. Assoc. Water Pollut. Res.* **52**, 9–18 (2005).

104. Castenholz, R. W. Aggregation in a Thermophilic Oscillatoria. *Nature* **215**, 1285–1286 (1967).

105. Liu, Y. Nutrient removal by microbial granules. in *Waste Management Series* (eds. Tay, J.-H., Tay, S. T.-L., Liu, Y., Show, K.-Y. & Ivanov, V.) vol. 6 163–189 (Elsevier, 2006).

106. Dechatiwongse, P., Srisamai, S., Maitland, G. & Hellgardt, K. Effects of light and temperature on the photoautotrophic growth and photoinhibition of nitrogen-fixing cyanobacterium Cyanothece sp. ATCC 51142. *Algal Res.* **5**, 103–111 (2014).

107. Wezernak, C. T. & Gannon, J. J. Oxygen-Nitrogen Relationships in Autotrophic Nitrification. **15**, 5 (1967).

108. Ji, X., Jiang, M., Zhang, J., Jiang, X. & Zheng, Z. The interactions of algae-bacteria symbiotic system and its effects on nutrients removal from synthetic wastewater. *Bioresour. Technol.* **247**, 44–50 (2018).

109. Parkin, T. B. & Brock, T. D. Photosynthetic bacterial production in lakes: The effects of light intensity1: Photosynthetic bacterial production. *Limnol. Oceanogr.* **25**, 711–718 (1980).

110. Tay, J.-H., Yang, S.-F. & Liu, Y. Hydraulic selection pressure-induced nitrifying granulation in sequencing batch reactors. *Appl. Microbiol. Biotechnol.* **59**, 332–337 (2002).

111. Yeoh, G. H. & Tu, J. Gas–Particle Flows. in *Computational Techniques for Multiphase Flows* 243–311 (Elsevier, 2010). doi:10.1016/B978-0-08-046733-7.00004-7.

112. Bowers, D. G. Optical techniques in studying suspended sediments, turbulence and mixing in marine environments. in *Subsea Optics and Imaging* 213–240 (Elsevier, 2013). doi:10.1533/9780857093523.2.213.

113. Aro, E.-M., Virgin, I. & Andersson, B. Photoinhibition of Photosystem II. Inactivation, protein damage and turnover. *Biochim. Biophys. Acta BBA - Bioenerg.* **1143**, 113–134 (1993).

114. Tyystjarvi, E. Photoinhibition of Photosystem II and photodamage of the oxygen evolving manganese cluster. *Coord. Chem. Rev.* **252**, 361–376 (2008).

115. Krause-Jensen, D. & Sand-Jensen, K. Light attenuation and photosynthesis of aquatic plant communities. *Limnol. Oceanogr.* **43**, 396–407 (1998).

116. Saer, R. G. & Blankenship, R. E. Light harvesting in phototrophic bacteria: structure and function. *Biochem. J.* **474**, 2107–2131 (2017).

117. Green, B. & Parson, W. W. *Light-Harvesting Antennas in Photosynthesis*. (Springer Science & Business Media, 2003).

CHAPTER 5

PHYSICAL CHARACTERIZATION OF OXYGENIC PHOTOGRANULES

5.1 Abstract

This study investigated the hydrodynamic properties of oxygenic photogranules (OPGs) generated in a sequencing batch reactor treating wastewater. In addition, we present the properties of OPGs cultivated under hydrostatic conditions and used to seed reactors. An isopycnic centrifugation procedure was applied to determine the density of granules with was on average 1037 kg/m^3 and 1050 kg/m^3 for the reactor and static OPGs respectively. The reactor granules had measured settling velocities in the range of 0.001 m/s, and 0.021 m/s while static OPGs had higher velocities (0.002 m/s -0.07 m/s). This higher settling velocity in larger static granules (0.6 mm-1.4 mm) validates the size effects in free settling tests. The average estimated porosity of reactor granules was 88% while that of static granules was 96%. The porosity and settling velocities of reactor granules showed a general increase with granule size. In contrast, the porosity of the hydrostatically formed OPGs showed low correlations with granular size while their settling velocities decreased with increasing diameter. The densities of reactor granules also showed negative correlations to phototrophic enrichment of the OPG biomass. The granules had high estimated permeabilities of 10^{-5}-10^{-9} for reactor granules and 10^{-4}-10^{-5} for hydrostatic granules which decreased with size.

5.2 Introduction

The application of photogranular technology for wastewater treatment is gaining widespread interest.[1,2] The utility of each granular aggregate as an autonomous reactor in which biotransformation ensues gives many operational benefits compared to canonical

wastewater treatment systems.[2] Compared to other granules, photogranules have the added advantage of self-aerating potential negating the need for energy-intensive aeration.[3] Moreover, microalgal-bacterial aggregates have been reported to have superior nutrients removal efficiency with adequate irradiance compared to aerobic sludge granules.[2]

Oxygenic photogranules (OPGs) have recently been investigated and characterized for aeration free wastewater treatment.[3–8] These photogranules have microbial consortia consisting of phototrophic organisms, predominantly motile filamentous cyanobacteria and algae,[5,9] on their outer surfaces while heterotrophic, nitrifying and denitrifying bacteria colonize their inner regions.[5,7] An oxygen gradient exists into the granular core, due to aerobic conditions at the exterior granular surface and anaerobic or anoxic cores.[9] This stratification results in a spatial functional variation similar to that present in biofilms.[10–12] The generation of oxygen in OPG reactor operations relies on agitation for exposure of photosynthetic microbes to actinic light.[3,13] Consequently, to design an effective OPG wastewater treatment process, the physical characteristics of the granules, including their size, density, permeability and porosity, which affect their hydrodynamic behaviour, are requisite.[14,15] Reactor operational pressures including agitation,[16] light [17,18] and substrate concentrations can affect granular sizes [2,19–21] and subsequently their density [22–24] and function. Moreover, the particles rheology [25,26] continually changes in the shear force field of the bulk fluid and with particle-particle interactions. We hypothesize that OPGs have varying densities and porosities based on assorted sizes.

Characterizing these physical properties can facilitate prediction of OPG movement within the reactor to optimize their interactions with light.

5.3 Materials and methods

5.3.1 Generation of granules

An OPG reactor was operated in sequencing batch mode with wastewater feed (primary effluent) from the local wastewater treatment plant. The glass reactor had an internal diameter of 22.7 cm, a total height of 24 cm and was operated at an 8L working volume. The reactor was run in sequential light-dark photoperiods each 3-hour long with a 180 $\mu mol.m^{-1}.s^{-1}$ light intensity for each treatment cycle, giving 4 treatment cycles per day and 1-day hydraulic retention time (HRT). The feed and decant time were maintained below 0.025 of the total cycle time. Granules were collected and examined on day-95 and day-139 of reactor operation. The influent COD was between 75-130 mg/L during the first period (day-0 to day-95) and 150-210 mg/L during the second period (day-96 to day-135). We also examined OPGs generated from activated sludge inoculum by hydrostatic incubation [7] from the same wastewater treatment plant. The collected reactor and static OPGs were classified into various sizes using sieve analysis (ATSM E-11, ISO 565). The wet sieving method [9] involved sequentially passing the reactor granules through sieves with openings of 0.1 mm, 0.2 mm, 0.3 mm, 0.5 mm, 0.71 mm 1.0 mm,1.7 mm and 3.36 mm. Granules retained between intervening sieve sizes were resuspended in DI water and constituted different size classes for which subsequent characterization was conducted.

Biomass concentrations were evaluated for volatile and total solids fractions according to Standard Methods (2540D).[27] The photosynthetic chlorophyll pigments were extracted and quantified following the standard methods 10200H.[27] Additionally, phycobilin pigments from OPGs were extracted by centrifuging a 10 ml sample volume at 12000 rpm for 10 minutes. The pellet was then resuspended in an equal volume of 0.025 M phosphate buffer solution (pH 7) followed by homogenization at 11000 rpm (IKA T-18, ULTRA-TURRAX) and sonication at 20% strength (M500, Fisher Scientific) for 1 min and 3 min, respectively with a heat sink employed during the extraction. The PBS solution was then centrifuged for 10 min at 12000 rpm. The supernatant absorbances were measured using a spectrophotometer (Genesis 10S UV-VIS) at 280 nm, 495 nm, 566 nm, 620 nm, 652 nm, 675 nm, and 750 nm wavelengths. The Bennett and Bogorad equations were used to quantify phycobilins concentrations.[28,29]

5.3.2 Settling

For the free settling test, we used a vertically mounted transparent plastic cylinder 2.5 m in height and 0.05 m in diameter filled with reactor liquid effluent. Markers were placed at 0.25 m from the cylinder top and capped bottom denoting 2 m and 0 m distances, respectively. Intermediate distances of 0.5 m were also marked out with an accuracy of ±0.5 cm. Before the free settling test, each granule from the various size clusters was photographed for further image analysis (Image Pro v.10, Media cybernetics). The granules were then introduced at the top of the column (2 m), and videos were recorded tracking the movement of granules in the column. The videos were then split into frames

(VLC-videolan.org) and processed to collect time interval details of granules passing each marker between 1.5 m and 0.5 m with an accuracy of ±0.05 sec.

5.3.3 Density measurement

The estimation of OPGs density was undertaken using isopycnic centrifugation. A stock isotonic solution (SIP) was prepared by diluting a Percoll® Plus commercial product with 1.5 M NaCl at 9:1 parts (v/v). The stock solution was further diluted with 0.15 M NaCl to achieve 6 discrete density concentrations in the range of 1.0-1.13 g/mL. A 25 mL volume of each density concentration was pipetted into separate centrifuge tubes. A 50 µL volume of density marker beads (Cospheric™) in the target density range was introduced into 30 mL centrifuge tubes and centrifuged (Sorvall™ RC 5C plus) at 10000 rpm, 12000 rpm, 13000 rpm, 15000 rpm and 17000 rpm each for 15 min. Additional stock dilutions were also centrifuged for 60 min, 90 min at 13000 rpm and 30 min, 45 min at 17000 rpm with a fixed angle rotor (Sorvall SA-600) of 34^0. Calibration curves were prepared, and the resulting density values were then confirmed by correlation with refractive index measured using a digital refractometer (Hanna Instruments). The height of each marker band from the tube bottom was plotted against the density of each band. The experiment was conducted at a temperature of 23±1 ^{0}C. Optimal stock solution dilution (40%) and centrifugation conditions (13000 rpm, 90 min) were selected based on the linearity of this density-depth relation and used for density estimations.

Density estimations were undertaken for granule samples harvested from the reactor on day-95 and day-139 and sorted by sieve analysis into assorted sizes. Centrifuge tubes

with 40% solution of the SIP were centrifuged at 13000 rpm for 90 minutes to create continuous density gradients. Dewatered samples of each granule size class were then introduced in separate centrifuge tubes and centrifuged for 30 minutes at 500 rpm. A separate tube with calibration marker beads was included with each test. The location of both granules and marker beads was measured from the bottom of centrifuge tubes within the nearest 0.5 mm. Hydrostatically-formed OPGs collected from incubation vials [4,5,7] and sized using image analysis were similarly characterized for density but with 17000 rpm centrifugation for 45 min.

5.3.4 Analytical procedure

The free settling test of discrete particles in an infinite fluid medium is described by Stokesian laws that balance the buoyant and drag forces against the particle weight.[30] In general, this relation adjusted for particle porosity (e) and permeability can be expressed as follows,[30–33]

$$V^2 = \frac{4gd_{opg}(\rho_{opg}-\rho_l)(1-e)}{3\rho_l \Omega C_D} \quad \textbf{(Eq 5. 1)}$$

We determined the terminal velocity (v) via free settling test and the diameter of granules (d_{opg}) by image analysis. The parameters ρ_{opg} and ρ_l are the densities of OPGs and liquid, respectively. The flow factor (Ω) describes the flow resistance through the granule body and can be calculated for a porous sphere as [33,34] below (Eq 5.2)

$$\Omega = \frac{2\beta^2 * [1-\frac{\tanh \beta}{\beta}]}{2\beta^2 + 3[1-\frac{\tanh \beta}{\beta}]} \quad \textbf{(Eq 5. 2)}$$

Where β is a normalized particle diameter given by (Eq 5.3),

$$\beta = \frac{d_{opg}}{2\sqrt{k}} \quad \textbf{(Eq 5. 3)}$$

Where k is permeability estimated by the Brinkman model, [32]

$$\boldsymbol{k = \frac{d_{opg}^2}{72}\left(3 + \frac{4}{1-e} - 3\sqrt{\frac{8}{1-e} - 3}\right)} \qquad \textbf{(Eq 5. 4)}$$

Finally, the drag coefficient (C_D) was estimated using the Masliyah and Polikar [35] estimation for permeable porous spheres with a Reynolds number of between 7 and 120.

$$\boldsymbol{C_D = \frac{24\Omega}{Re}[1 + 0.0853Re^{(1.093-0.105w)}]} \qquad \textbf{(Eq 5. 5)}$$

Where $w = log_{10} Re$, and the Reynolds number, $Re = \rho_{opg} v d_p/\mu$ with μ being the fluid viscosity. The solid fraction 1-*e* was calculated as per (Eq.5-1) by minimizing estimated values of porosity (*e*) using excel 2016 Solver. The Pearson correlation coefficient was used to characterize the relation between variables.

5.4 Results

5.4.1 Settling velocity

As shown in Figure 5-1, the average settling velocity of reactor OPGs was 0.0086 m/s (range: 0.0015 m/s-0.021 m/s) for the 0.3 mm-5.9 mm diameter range particles (n=129). The data correspond to Reynolds numbers ranging from 1.3 to 119. The average settling velocity of hydrostatically-formed granules was 0.027 m/s (range: 0.01 m/s-0.05 m/s) (Figure 5-2). Moreover, their larger sizes with a diameter in the range of 6 mm-14 mm (n=17) resulted in higher Reynolds numbers 151-498. In agreement with Stokes law, a general relation of increasing settling velocity with particle sizes was observed for reactor granules. In contrast, we observed a general decline in the settling velocity with increasing size for static granules (Figure 5-2).

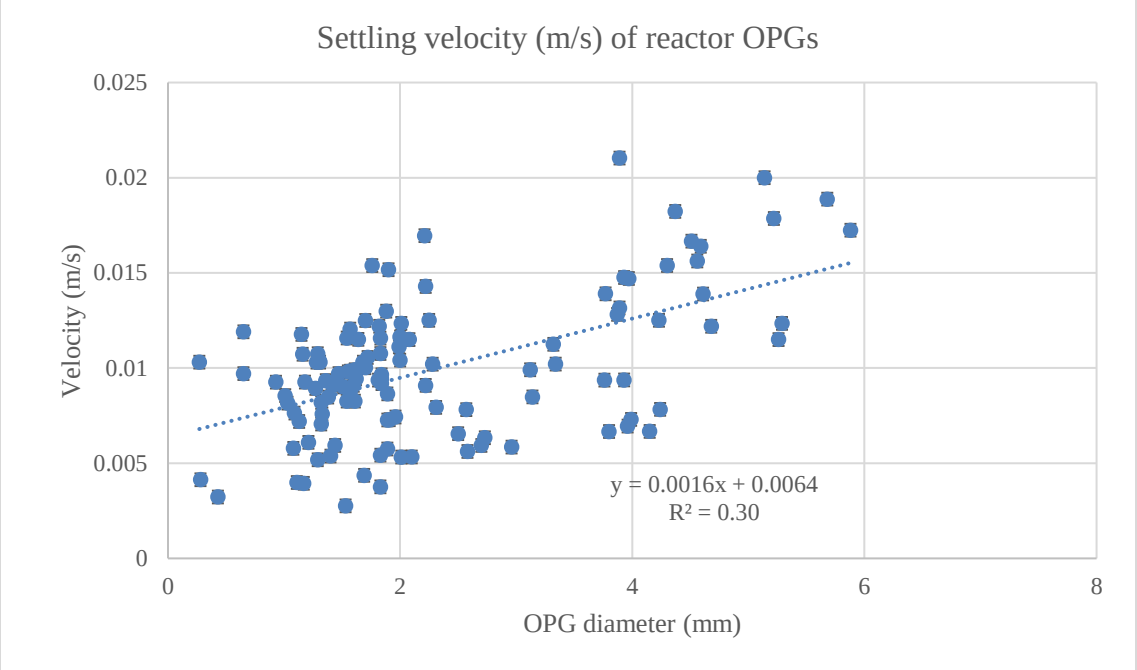

Figure 5-1: Settling velocity of reactor OPGs. Error bars show the standard error of the measured values.

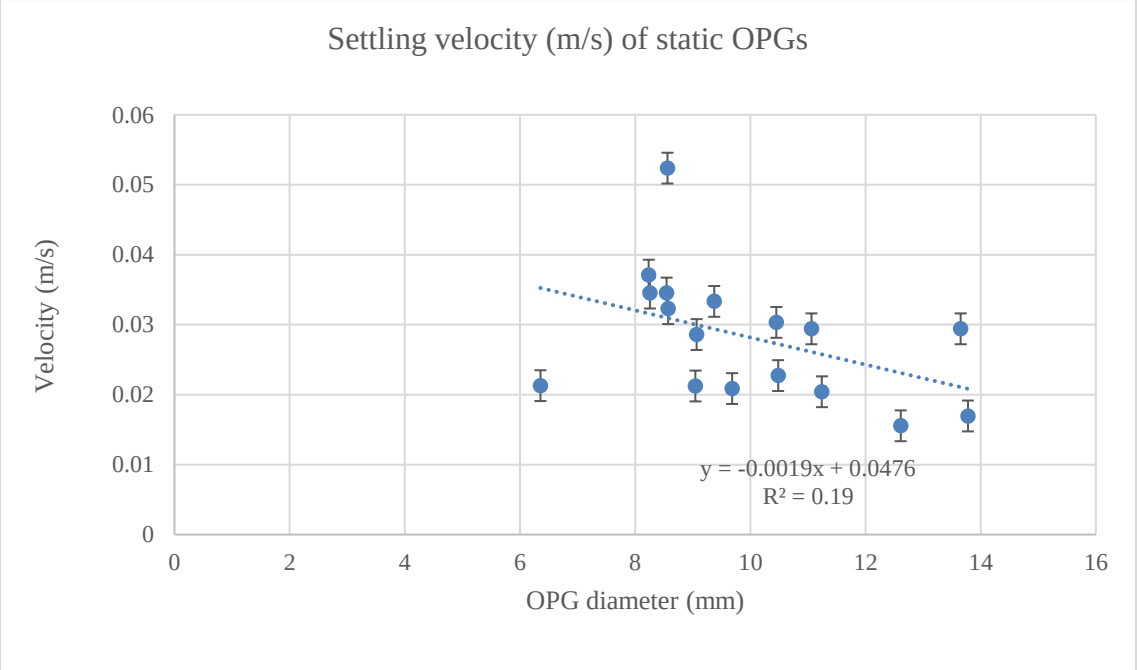

Figure 5-2: Settling velocity of hydrostatically-formed OPGs. Error bars show the standard error of the measured values.

5.4.2 Isopycnic centrifugation for density measurement

Higher centrifugation speeds resulted in steeper gradient curves with a lower concentration of the standard isotonic Percoll (SIP). The vertical section of the calibration curves (Figure 5- 3) was used to model particle density. The 17000 rpm calibration curve was split into two segments for static OPGs settling below and above 2cm from the vial bottom (Figure 5- 3).

For the reactor granules examined, the average density was 1037 kg/m^3 (std. dev 20) with a correlation coefficient of -0.62 between size and density (Figure 5- 4) on day 95. The particles sizes between 0.1 mm-1 mm had higher densities (mean: 1043 kg/m^3) than particles >1 mm size (mean: 1022 kg/m^3). The density decreased for day-139 samples (Figure 5- 4) to a mean of 991 kg/m^3 (std.dev 38) with a Pearson correlation of -0.77 with particle diameter. The mean density decreased to 1005 kg/m^3 and 953 kg/m^3 for particles <1 mm and >1 mm, respectively, by day 139. This decrease can be attributed to higher strength wastewater during this second operation period. For hydrostatically-formed OPGs, three density estimations were conducted. Firstly, granules that settled lower than 2 cm from the vial bottom had an estimated average density of 1056 kg/m^3. Secondly, the density of granules that settled at higher isopycnic gradients had an estimated average density of 1050 kg/m^3 with a range of 1043-1051 kg/m^3 and a correlation coefficient of 0.43 with granule size. Finally, we estimated the density of hydrostatically-formed OPGs using Stokes law (unmodified) and the settling velocities. This estimation resulted in an average density of 998 kg/m^3 (range: 997-999 kg/m^3).

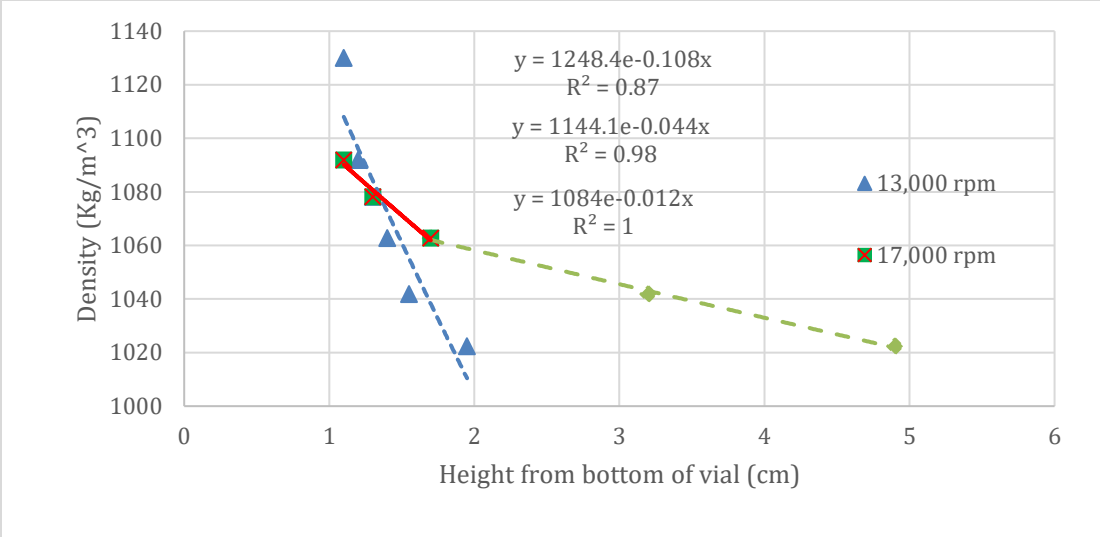

Figure 5- 3: Calibration curve from Isopycnic centrifugation of density marker beads. The exponential model fits for the data are shown (Top) Reactor OPGs, 13000 rpm (Middle) Static OPGs at <2cm height, 17000 rpm (Bottom) Static OPGs >2cm height, 17000 rpm.

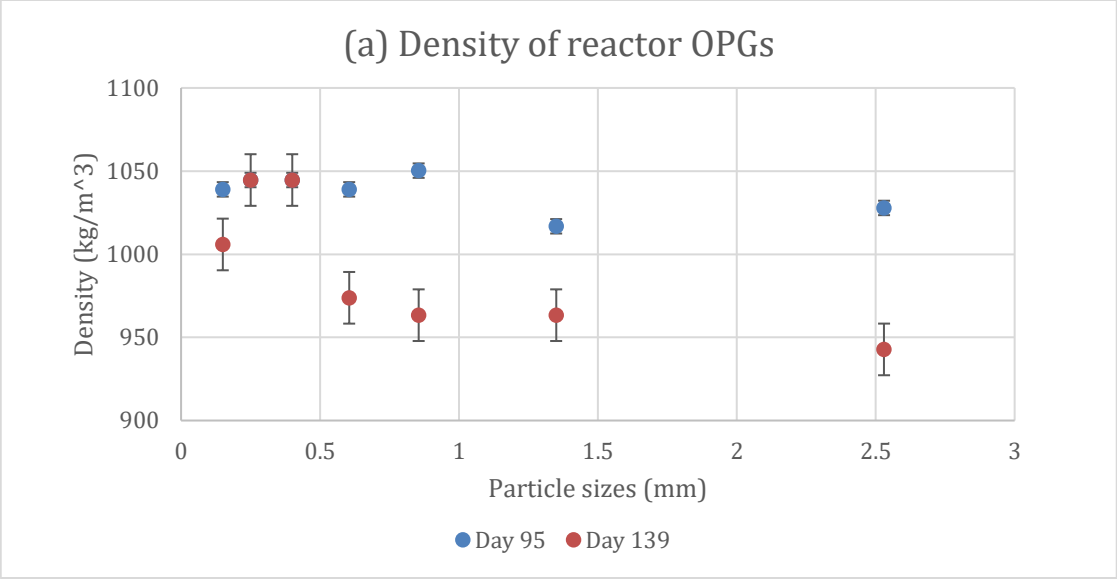

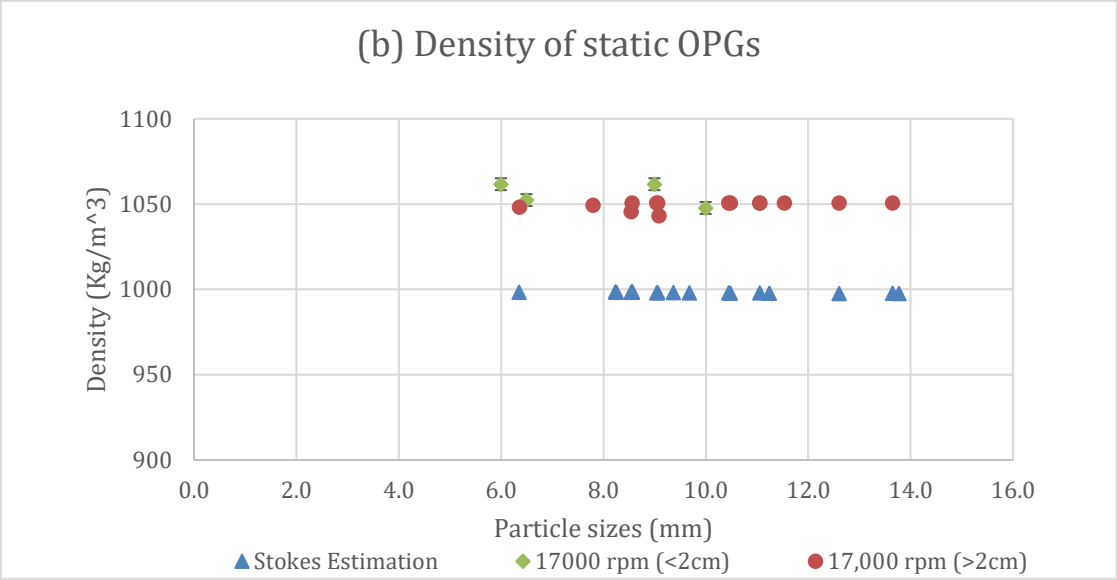

Figure 5- 4: The density of different sized OPGs (a) Reactor OPGs (b) Static OPGs. Size separation was conducted via sieve analysis (ATSM E-11 for size>2.36 and ISO 565 for all smaller sizes). Error bars show the standard error of estimated values.

5.4.3 Determination of porosity and permeability

The measured free settling velocities and average particle densities were substituted in equation 5.1 to estimate the porosities (*e*) of the granules. Reactor OPGs had estimated

porosities between 78% and 94% with an average of 88% (Figure 5- 5) while that of static granules was on average 96%. The estimated permeability (Equation 5.4) decreased with size [22] and was higher for hydrostatic OPGs (Figure 5- 6)

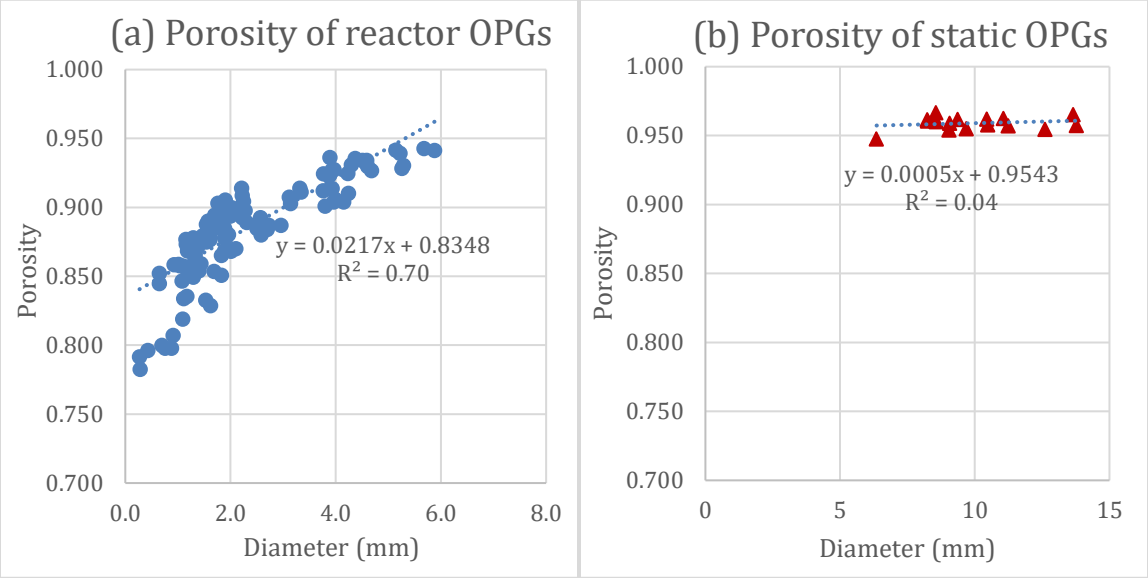

Figure 5- 5: Estimated porosities of different OPG sizes. (a) Reactor OPGs (b) Static OPGs. Dotted lines show the corresponding linear regression fit to the data.

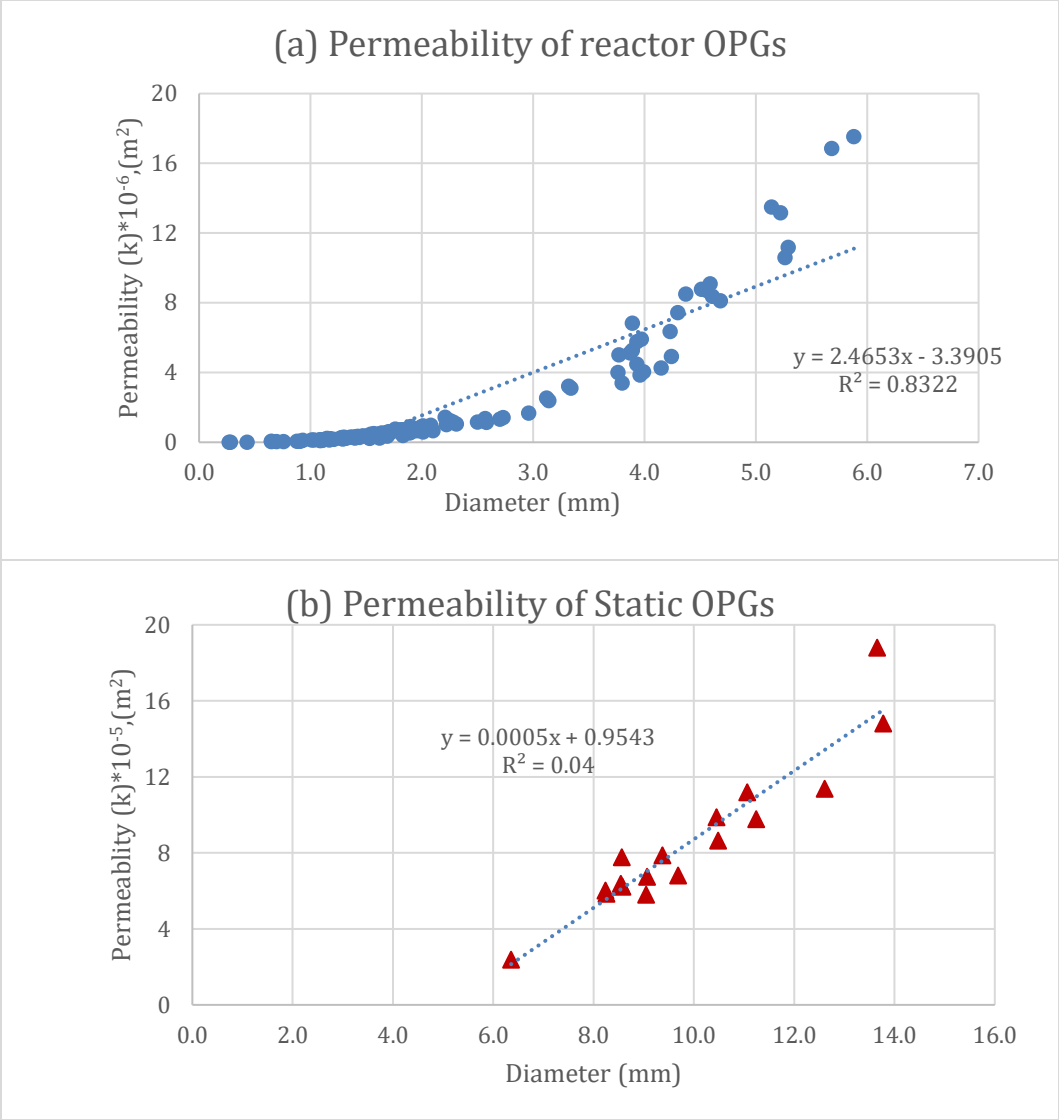

Figure 5- 6: Estimated permeability for different OPG sizes. (a) Reactor OPGs (b) Static OPGs. Dotted lines show the corresponding linear regression fit to the data

5.4.4 Phototrophic characterization of granular biomass

Granular biomass and pigment concentrations were determined for the reactor granules on day-95 and day-139. The ratio of volatile to total biomass solids was on average, 0.86 (std.dev=0.006) for both sampling periods. The 0.2 mm-0.3 mm size class had the highest decrease in biomass concentrations between the two days sampling days (Figure 5-7).

The decrease reflects a lack of biomass of that size class in the day-139 grab samples and is attributable to OPG growth into larger sizes and granular fracture into smaller sizes. Moreover, poor settlability alluded to by lower densities on day-139 (Figure 5- 4) could also result in granular removal with effluent during reactor operation. The changes in density between day-95 and day-139 samples had a negative correlation with both biomass mass fractions with an average of -0.64 for both sampling periods.

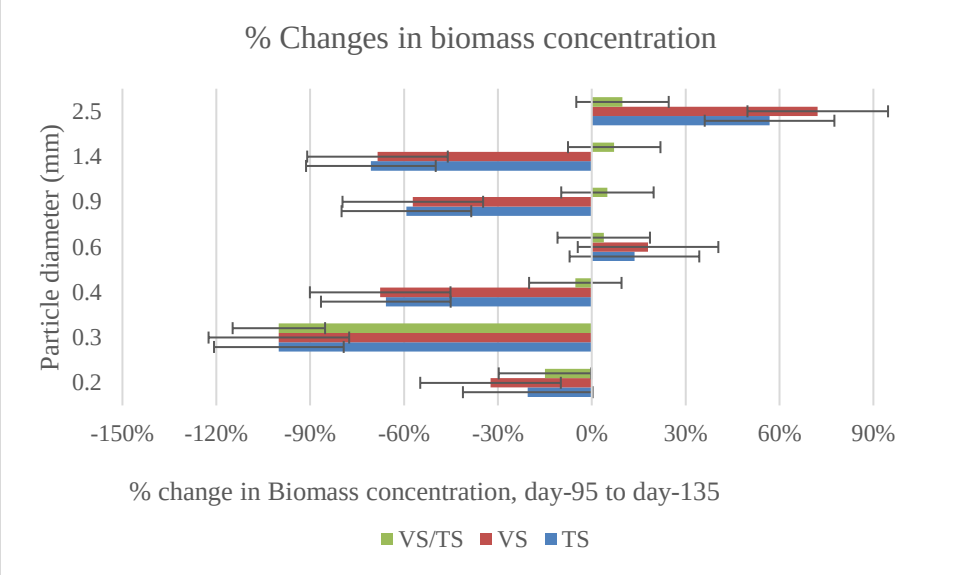

Figure 5- 7: The percentage change in biomass fraction concentrations between sampling day 95 and day 139 for different OPG size classes. The y-axis shows the upper bound of the size class.

Chlorophylls *a* and *b* concentrations increased between day-95 and day-139 for all granular sizes except the 0.2 mm-0.3 mm size class (Figure 5- 8). Chlorophyll *c*, on the other hand, decreased for size classes less than 0.6 mm and in sizes greater than 2.5 mm. In contrast, phycobilin concentrations increased for all size classes other than the 0.2 mm-0.3 mm size class. The average correlation between changes in density and pigment

concentrations for day-95 and day-139 samples was higher for chlorophyll b (-0.51) than chlorophyll a (-0.39) and chlorophyll c (-0.34). This correlation with density changes between the two sampling periods was on average, -0.42 for all chlorophylls and -0.49 for phycobilin.

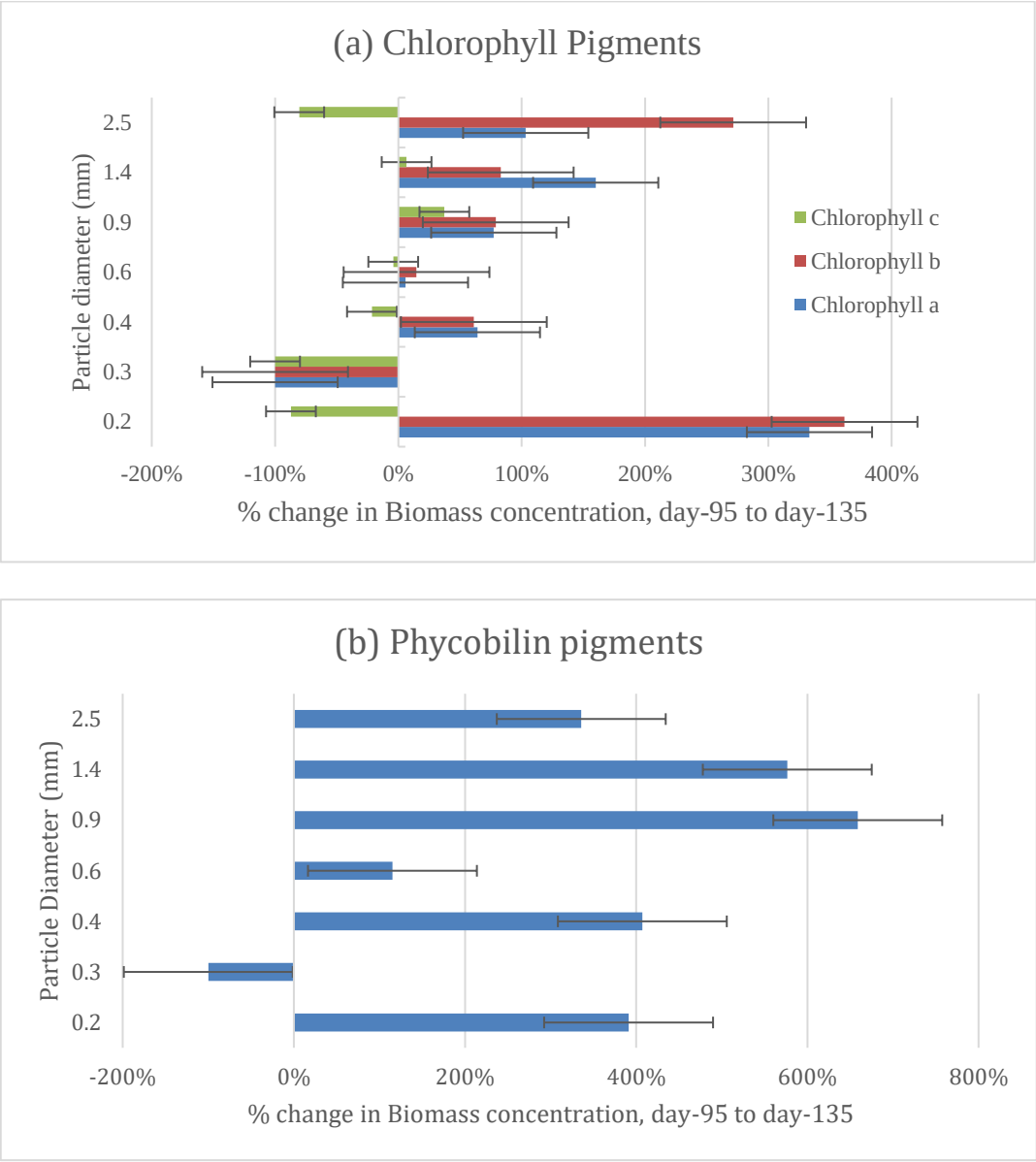

Figure 5- 8: Percentage change in photosynthetic pigments concentration in the granules of different sizes classes between sampling day-95 and day-139. (a) Chlorophyll pigments, (b) Phycobilin pigments. The y-axis shows the upper bound of the size class.

5.5 Discussion

The physical and hydrodynamic properties of granules impact their effectiveness in wastewater treatment applications. Primarily, the lure of a granular system is their better solids settleability, which improves separation from the bulk liquid.[3,6,36] In addition, photogranules require minimal agitation due to their self-aerating potential [1–3] compared to the activated sludge processes which rely on mechanical addition of oxygen.[37–39] Better settlability of granules results in better biomass retention and reduced footprint compared to activated sludge while granules and are also more tolerant to shock loadings.[40] The closely commingled morphology comprising various microbes embedded in an extracellular polymeric matrix [7] alters their density relative to the bulk fluid [41] and changes with granular growth.

The effectiveness of any agitation process with respect to particle suspension depends on the particle density.[14,42] The density of sampled reactor OPGs was found to be in the range of 943 kg/m^3 to 1050 kg/m^3 (Figure 5- 4). The estimated mean density of OPGs (1014 kg/m^3) was slightly lower than values reported for activated sludge [30,43,44] of 1038-1070 kg/m^3, and 1037-1049 kg/m^3 for aerobic granules.[33] Moreover, the porosity (78%-94%) (Figure 5- 5) and settling velocities (0.003 m/s-0.021 m/s) (Figure 5-2) for OPGs were also different to those reported for aerobic granules of 65%-90% and 0.02 m/s-0.07 m/s respectively.[33,41] Hydrostatically-formed OPGs, on the other hand, had settling velocities of 0.02 m/s-0.05 m/s comparable to those of aerobic sludge granules and higher porosities of 94-97%. The similarity of OPG density to that of water eases their

suspension in liquid by agitation. Moreover, while their higher densities are amenable to Stokesian settling, their granular morphologies allude to dominant discrete settling mechanics.[23,45] In addition, their larger sizes result in higher terminal settling velocities compared to smaller activated sludge flocs.[33] In reactor operation, granules of lower density can also be entrapped in flocculant settling biomass. The settling velocities increased with size for reactor granules but decreased with size for static OPGs. The irregularity (sphericity <1) of static OPGs induces higher hydraulic resistance in a Newtons flow regime [46] increasing hydraulic resistance [24] and lowering settling velocities.

Microalgae have both chlorophylls *a* and *b* in their light-harvesting moiety [47] while cyanobacteria have chlorophyll *a* and phycobilin accessory pigments.[47–49] The concentration of light-harvesting pigments in the OPG photosynthetic clades [5,8] increased over time for most sizes of reactor granules. A higher relative increase in chlorophyll *b* pigments for size class 0.1 mm-0.2 mm and 1.7 mm-3.36 mm suggest predominant algal enrichment between the two sampling days (Figure 5-7-a). Additionally, a relative increase in phycobilin concentrations was observed, suggesting cyanobacterial enrichment with growth in all granular sizes between days 95-139 (Figure 5-7-b). This increase in phycobilin concentrations was highest for the 0.71 mm- 1 mm size class (Figure 5-7-b). The 1 mm-1.7 mm size class was also characterized by a higher increase in chlorophyll *a* concentration compared to chlorophyll *b* (Figure 5-7-a), suggesting an increase of cyanobacterial population. Similar cyanobacteria dominated increase has been reported for OPG granules of between 0.5-1 mm diameter.[9] Moreover, a persistent

increase in phycobilin was reported for OPG diameters up to 2.5 mm and decreased in larger sized granules.[9] A relative decrease in chlorophyll *c* over the two sampling days (Figure 5- 8) was also observed for most granule sizes (Figure 5-7-a). This accessory light-harvesting pigment is associated with diatoms,[50] and its decrease could indicate loss of diatoms from the OPG biomass.[9]

The changes in granule density for different size classes of reactor OPGs showed negative correlations with the changes in concentrations of biomass and pigments between the two sampling periods. This relation suggests that phototrophic enrichment and related size increases can result in lower OPG densities and can be related to the increase of granular porosities with larger OPG size (Figure 5-5). Motile filamentous cyanobacteria, essential for OPG development,[5,7] excrete extracellular polymeric substances (EPS) in tubular sheaths.[7] This EPS is composed of polysaccharides, proteins, nucleic acids and lipids [10,51–53] and can amend physical properties of microbial structures including density and porosity.[53] Increasing granule size can induce phototaxis to allow microbes to move to locations with optimal light [54] within the granule.

For OPGs, agitation provides particulate suspension [55] for interaction with a light source in addition to substrate distribution within the reactor. The resulting particle-particle interactions and OPG dynamic behaviour relative to the bulk fluid is influenced by their physical characteristics.[24,56] The use of isopycnic density measurements lends to easy estimation of these hydrodynamic characteristics despite assumptions made in the estimation of porosity using equation 5.1.[30,44] The high estimated permeability and

porosity comparable to that of pervious inorganic materials [57] suggests the existence of substrate advective [31,58,59] and diffusive mass transfers into the granular structure.[33,60] Oxygen liberated from the oxidation of water via photosynthesis is transferred into the core while carbon dioxide from bacterial respiration diffuses towards the granular surface.[1–3] The flow of bulk fluid through the permeable OPG structure [34,59] transfers substrates dissolved in wastewater and reduces the hydraulic resistance during suspension within the reactor.[24] The dry solid density of the granules was not determined but would constitute an upper limit of OPGs density.[31] The density determined can, however, be applied in dynamic models detailing the movement of granules relative to each other and the bulk fluid. These models provide correlations of agitation speeds to rates of granular transition within reactors and can be used to predict frequency of exposure to light zones. This is essential in optimizing the interaction of OPGs with light within reactors to maintain treatment efficacy.

5.6 Bibliography

1. Quijano, G., Arcila, J. S. & Buitrón, G. Microalgal-bacterial aggregates: Applications and perspectives for wastewater treatment. *Biotechnol. Adv.* **35**, 772–781 (2017).

2. Lee, Y.-J. & Lei, Z. Microalgal-bacterial aggregates for wastewater treatment: A mini-review. *Bioresour. Technol. Rep.* 100199 (2019) doi:10.1016/j.biteb.2019.100199.

3. Abouhend, A. S. *et al.* The Oxygenic Photogranule Process for Aeration-Free Wastewater Treatment. *Environ. Sci. Technol.* **52**, 3503–3511 (2018).

4. Park, C. & Dolan, S. (deceased). Patent Algal Sludge Granule OPG Jan 2019. 11 (2019).

5. Milferstedt, K. *et al.* The importance of filamentous cyanobacteria in the development of oxygenic photogranules. *Sci. Rep.* **7**, 17944 (2017).

6. Milferstedt, K. *et al.* Biogranules applied in environmental engineering. *Int. J. Hydrog. Energy* **42**, 27801–27811 (2017).

7. Kuo-Dahab, W. C. *et al.* Investigation of the Fate and Dynamics of Extracellular Polymeric Substances (EPS) during Sludge-Based Photogranulation under Hydrostatic Conditions. *Environ. Sci. Technol.* **52**, 10462–10471 (2018).

8. Stauch-White, K., Srinivasan, V. N., Camilla Kuo-Dahab, W., Park, C. & Butler, C. S. The role of inorganic nitrogen in successful formation of granular biofilms for wastewater treatment that support cyanobacteria and bacteria. *AMB Express* **7**, (2017).

9. Abouhend, A. S. *et al.* Growth Progression of Oxygenic Photogranules and Its Impact on Bioactivity for Aeration-Free Wastewater Treatment. *Environ. Sci. Technol.* (2019) doi:10.1021/acs.est.9b04745.

10. Limoli, D. H., Jones, C. J. & Wozniak, D. J. Bacterial Extracellular Polysaccharides in Biofilm Formation and Function. *Microbiol. Spectr.* **3**, (2015).

11. Spormann, A. M. Physiology of Microbes in Biofilms. in *Bacterial Biofilms* (ed. Romeo, T.) 17–36 (Springer Berlin Heidelberg, 2008). doi:10.1007/978-3-540-75418-3_2.

12. Lewandowski, Z. & Boltz, J. P. Biofilms in Water and Wastewater Treatment. in *Treatise on Water Science* 529–570 (Elsevier, 2011). doi:10.1016/B978-0-444-53199-5.00095-6.

13. McNair, A. Pilot Reactor Operation of the Oxygenic Photogranule (OPG) Wastewater Treatment Process. *Environ. Water Resour. Eng. Masters Proj.* (2017).

14. *Handbook of industrial mixing: science and practice*. (Wiley-Interscience, 2004).

15. Xiao, F., Li, X. Y. & Wang, D. S. Three-dimensional CFD simulation of the flow field around and through particle aggregates. *Colloids Surf. Physicochem. Eng. Asp.* **436**, 1034–1040 (2013).

16. Liu, Y. & Tay, J.-H. The essential role of hydrodynamic shear force in the formation of biofilm and granular sludge. *Water Res.* **36**, 1653–1665 (2002).

17. Dechatiwongse, P., Srisamai, S., Maitland, G. & Hellgardt, K. Effects of light and temperature on the photoautotrophic growth and photoinhibition of nitrogen-fixing cyanobacterium Cyanothece sp. ATCC 51142. *Algal Res.* **5**, 103–111 (2014).

18. Lee, K. & Lee, C.-G. Effect of light/dark cycles on wastewater treatments by microalgae. *Biotechnol. Bioprocess Eng.* **6**, 194–199 (2001).

19. Bindhu, B. k. & Madhu, G. Selection pressure theory for aerobic granulation – an overview. *Int. J. Environ. Waste Manag.* **13**, 317–329 (2014).

20. Liu, Y.-Q. & Tay, J.-H. Fast formation of aerobic granules by combining strong hydraulic selection pressure with overstressed organic loading rate. *Water Res.* **80**, 256–266 (2015).

21. Arcila, J. S. & Buitrón, G. Microalgae–bacteria aggregates: effect of the hydraulic retention time on the municipal wastewater treatment, biomass settleability and methane potential. *J. Chem. Technol. Biotechnol.* **91**, 2862–2870 (2016).

22. Li, X.-Y. & Logan, B. E. Permeability of Fractal Aggregates. *Water Res.* **35**, 3373–3380 (2001).

23. Dyer, K. R. & Manning, A. J. Observation of the size, settling velocity and effective density of flocs, and their fractal dimensions. *J. Sea Res.* **41**, 87–95 (1999).

24. Droppo, I. G., Walling, D. E. & Ongley, E. D. The influence of floe size, density and porosity on sediment and contaminant transport. 8.

25. Datt, C. & Elfring, G. J. Dynamics and rheology of particles in shear-thinning fluids. *J. Non-Newton. Fluid Mech.* **262**, 107–114 (2018).

26. Mikkelsen, L. H. The shear sensitivity of activated sludge: Relations to filterability, rheology and surface chemistry. *Colloids Surf. Physicochem. Eng. Asp.* **182**, 1–14 (2001).

27. ALPHA. *Standard Methods for the Examination of Water and Wastewater*. (ALPHA,AWWA,WEF, 2012).

28. Bennett, A. & Bogorad, L. COMPLEMENTARY CHROMATIC ADAPTATION IN A FILAMENTOUS BLUE-GREEN ALGA. *J. Cell Biol.* **58**, 419–435 (1973).

29. Lauceri, R., Bresciani, M., Lami, A. & Morabito, G. Chlorophyll a interference in phycocyanin and allophycocyanin spectrophotometric quantification. *J. Limnol.* (2017) doi:10.4081/jlimnol.2017.1691.

30. Sears K., Alleman J. E., Barnard J. L. & Oleszkiewicz J. A. Density and Activity Characterization of Activated Sludge Flocs. *J. Environ. Eng.* **132**, 1235–1242 (2006).

31. Li, D. & Ganczarczyk, J. Advective Transport in Activated Sludge Flocs. *Water Environ. Res.* **64**, 236–240 (1992).

32. Huang, H. Porosity-Size Relationship of Drilling Mud Flocs: Fractal Structure. *Clays Clay Miner.* **41**, 373–379 (1993).

33. Etterer, T. & Wilderer, P. A. Generation and properties of aerobic granular sludge. *Water Sci. Technol.* **43**, 19–26 (2001).

34. Neale, G., Epstein, N. & Nader, W. Creeping flow relative to permeable spheres. *Chem. Eng. Sci.* **28**, 1865–1874 (1973).

35. Masliyah, J. H. & Polikar, M. Terminal velocity of porous spheres. *Can. J. Chem. Eng.* **58**, 299–302 (1980).

36. Lee, D.-J., Chen, Y.-Y., Show, K.-Y., Whiteley, C. G. & Tay, J.-H. Advances in aerobic granule formation and granule stability in the course of storage and reactor operation. *Biotechnol. Adv.* **28**, 919–934 (2010).

37. Åmand, L. Control of aeration systems in activated sludge processes – a review. /paper/Control-of-aeration-systems-in-activated-sludge-%E2%80%93-a-%C3%85mand/33484777bf4af0743f759899f7bbc520def5b4de (2011).

38. Amanatidou, E., Samiotis, G., Trikoilidou, E., Pekridis, G. & Taousanidis, N. Evaluating sedimentation problems in activated sludge treatment plants operating at complete sludge retention time. *Water Res.* **69**, 20–29 (2015).

39. Barroso Soares, R. Comparative Analysis of the Energy Consumption of Different Wastewater Treatment Plants. *Int. J. Archit. Arts Appl.* **3**, 79 (2017).

40. Giesen, A., van Loosdrecht, M., Robertson, S. & de Buin, B. Aerobic Granular Biomass Technology: further innovation, system development and design optimisation. https://www.ingentaconnect.com/contentone/wef/wefproc/2015/00002015/00000016/art00018 (2015) doi:info:doi/10.2175/193864715819539641.

41. Basheer, F. & Farooqi, I. H. Hydrodynamic Properties of Aerobic Granules Cultivated on Phenol as Carbon Source. *APCBEE Procedia* **10**, 126–130 (2014).

42. Solid-Liquid Mixing In Agitated Vessels (Just Suspended Speed). *Cheresources.com Community* https://www.cheresources.com/invision/blog/4/entry-511-solid-liquid-mixing-in-agitated-vessels-just-suspended-speed/.

43. Knocke, W. R. Density of activated sludge solids. *Water Res.* **26**, 1559–1561 (1992).

44. Lee, D. J., Chen, G. W., Liao, Y. C. & Hsieh, C. C. On the free-settling test for estimating activated sludge floc density. *Water Res.* **30**, 541–550 (1996).

45. Mancell-Egala, W. A. S. K. *et al.* Limit of stokesian settling concentration characterizes sludge settling velocity. *Water Res.* **90**, 100–110 (2016).

46. Wilén, B. Effect of Different Parameters on Settling Properties of Activated Sludge. 64.

47. Golterman, H. . Chapter 13 Algae and their Pigments. in *Physiological Limnology: An Approach to the Physiology of Lake Ecosystems* vol. 2 233–247 (Elsevier, 1975).

48. Lawrenz, E., Fedewa, E. J. & Richardson, T. L. Extraction protocols for the quantification of phycobilins in aqueous phytoplankton extracts. *J. Appl. Phycol.* **23**, 865–871 (2011).

49. Singh, N. K., Sonani, R. R., Rastogi, R. P. & Madamwar, D. The phycobilisomes: an early requisite for efficient photosynthesis in cyanobacteria. *EXCLI J.* **14**, 268–289 (2015).

50. Zapata, M., Garrido, J. L. & Jeffrey, S. W. Chlorophyll c Pigments: Current Status. in *Chlorophylls and Bacteriochlorophylls: Biochemistry, Biophysics, Functions and Applications* (eds. Grimm, B., Porra, R. J., Rüdiger, W. & Scheer, H.) 39–53 (Springer Netherlands, 2006). doi:10.1007/1-4020-4516-6_3.

51. Thapa, S., Bharti, A. & Prasanna, R. Algal Biofilms and Their Biotechnological Significance. in *Algal Green Chemistry* 285–303 (Elsevier, 2017). doi:10.1016/B978-0-444-63784-0.00014-X.

52. Jiao, Y. *et al.* Characterization of Extracellular Polymeric Substances from Acidophilic Microbial Biofilms. *Appl Env. Microbiol* **76**, 2916–2922 (2010).

53. Flemming, H.-C., Neu, T. R. & Wozniak, D. J. The EPS Matrix: The "House of Biofilm Cells". *J. Bacteriol.* **189**, 7945–7947 (2007).

54. Donkor, V. & Häder, D.-P. Effects of solar and ultraviolet radiation on motility, photomovement and pigmentation in filamentous, gliding cyanobacteria. *FEMS Microbiol. Lett.* **86**, 159–168 (1991).

55. Ali, A. *et al.* Just Suspended Speed for Solid Particle Transport in TorusReactor. in *New Trends in Urban Drainage Modelling* (ed. Mannina, G.) 879–885 (Springer International Publishing, 2019). doi:10.1007/978-3-319-99867-1_152.

56. Yu, W., Gregory, J., Campos, L. & Li, G. The role of mixing conditions on floc growth, breakage and re-growth. *Chem. Eng. J.* **171**, 425–430 (2011).

57. Bear, J. *Dynamics of fluids in porous media*. (Dover, 1988).

58. Lopez-Peña, L. A., Meulenbroek, B. & Vermolen, F. A network model for the biofilm growth in porous media and its effects on permeability and porosity. *Comput. Vis. Sci.* **21**, 11–22 (2019).

59. Selvadurai, A. P. S. On the advective-diffusive transport in porous media in the presence of time-dependent velocities. *Geophys. Res. Lett.* **31**, (2004).

60. Etterer, T. Formation, Structure and Function of Aerobic Granular Sludge. (2004).

BIBLIOGRAPHY

Abouhend, A. S.; McNair, A.; Kuo-Dahab, W. C.; Watt, C.; Butler, C. S.; Milferstedt, K.; Hamelin, J.; Seo, J.; Gikonyo, G. J.; El-Moselhy, K. M.; Park, C. The Oxygenic Photogranule Process for Aeration-Free Wastewater Treatment. *Environmental Science & Technology* **2018**, *52* (6), 3503–3511. https://doi.org/10.1021/acs.est.8b00403.

Abouhend, A. S.; Milferstedt, K.; Hamelin, J.; Ansari, A. A.; Butler, C.; Carbajal-González, B. I.; Park, C. Growth Progression of Oxygenic Photogranules and Its Impact on Bioactivity for Aeration-Free Wastewater Treatment. *Environmental Science & Technology* **2019**. https://doi.org/10.1021/acs.est.9b04745.

Adams, C. E.; Eckenfelder, W. W. Nitrification Design Approach for High Strength Ammonia Wastewaters. *Journal (Water Pollution Control Federation)* **1977**, *49* (3), 413–421.

Adav, S. S.; Lee, D.-J.; Lai, J.-Y. Aerobic Granulation in Sequencing Batch Reactors at Different Settling Times. *Bioresource Technology* **2009**, *100* (21), 5359–5361. https://doi.org/10.1016/j.biortech.2009.05.058.

Ahmad, J. S. M.; Cai, W.; Zhao, Z.; Zhang, Z.; Shimizu, K.; Lei, Z.; Lee, D.-J. Stability of Algal-Bacterial Granules in Continuous-Flow Reactors to Treat Varying Strength Domestic Wastewater. *Bioresource Technology* **2017**, *244*, 225–233. https://doi.org/10.1016/j.biortech.2017.07.134.

Alam, M. A.; Vandamme, D.; Chun, W.; Zhao, X.; Foubert, I.; Wang, Z.; Muylaert, K.; Yuan, Z. Bioflocculation as an Innovative Harvesting Strategy for Microalgae. *Rev Environ Sci Biotechnol* **2016**, *15* (4), 573–583. https://doi.org/10.1007/s11157-016-9408-8.

Ali, A.; Ammar, S.; Farid, H.; Lefkir, A.; Sayah, H. E.; Boubekeur, N. Just Suspended Speed for Solid Particle Transport in TorusReactor. In *New Trends in Urban Drainage Modelling*; Mannina, G., Ed.; Springer International Publishing: Cham, 2019; pp 879–885. https://doi.org/10.1007/978-3-319-99867-1_152.

ALPHA. *Standard Methods for the Examination of Water and Wastewater*; ALPHA,AWWA,WEF: Washington: American Public Health Association, 2012.

Alphenaar, A. Anaerobic granular sludge: **1994**, 214.

Amanatidou, E.; Samiotis, G.; Trikoilidou, E.; Pekridis, G.; Taousanidis, N. Evaluating Sedimentation Problems in Activated Sludge Treatment Plants Operating at Complete Sludge Retention Time. *Water Research* **2015**, *69*, 20–29. https://doi.org/10.1016/j.watres.2014.10.061.

Amanatidou, E.; Samiotis, G.; Trikoilidou, E.; Pekridis, G.; Taousanidis, N. Evaluating Sedimentation Problems in Activated Sludge Treatment Plants Operating at Complete Sludge Retention Time. *Water Research* **2015**, *69*, 20–29. https://doi.org/10.1016/j.watres.2014.10.061.

Åmand, L. Control of aeration systems in activated sludge processes – a review /paper/Control-of-aeration-systems-in-activated-sludge-%E2%80%93-a-%C3%85mand/33484777bf4af0743f759899f7bbc520def5b4de (accessed Dec 6, 2018).

Amin, S.; Barnett, G. V.; Pathak, J. A.; Roberts, C. J.; Sarangapani, P. S. Protein Aggregation, Particle Formation, Characterization & Rheology. *Current Opinion in Colloid & Interface Science* **2014**, *19* (5), 438–449. https://doi.org/10.1016/j.cocis.2014.10.002.

Anderson, D. M.; Glibert, P. M.; Burkholder, J. M. Harmful Algal Blooms and Eutrophication: Nutrient Sources, Composition, and Consequences. *Estuaries* **2002**, *25* (4), 704–726. https://doi.org/10.1007/BF02804901.

Andreas Giesen; Andrew Thompson. Aerobic Granular Biomass: Setting The New Standard For Cost-Effective, Energy Efficient And Sustainable Wastewater Treatment | Request PDF https://www.researchgate.net/publication/323005503_Aerobic_Granular_Biomass_Setting_The_New_Standard_For_Cost-Effective_Energy_Efficient_And_Sustainable_Wastewater_Treatment (accessed Mar 18, 2020).

Angelakis, A. N.; Snyder, S. A. Wastewater Treatment and Reuse: Past, Present, and Future. *Water* **2015**, *7* (9), 4887–4895. https://doi.org/10.3390/w7094887.

Ansari, A. A.; Abouhend, A. S.; Park, C. Effects of Seeding Density on Photogranulation and the Start-up of the Oxygenic Photogranule Process for Aeration-Free Wastewater Treatment. *Algal Research* **2019**, *40*, 101495. https://doi.org/10.1016/j.algal.2019.101495.

Arcila, J. S.; Buitrón, G. Microalgae–Bacteria Aggregates: Effect of the Hydraulic Retention Time on the Municipal Wastewater Treatment, Biomass Settleability and Methane Potential. *Journal of Chemical Technology & Biotechnology* **2016**, *91* (11), 2862–2870. https://doi.org/10.1002/jctb.4901.

Arcila, J. S.; Buitrón, G. Influence of Solar Irradiance Levels on the Formation of Microalgae-Bacteria Aggregates for Municipal Wastewater Treatment. *Algal Research* **2017**, *27*, 190–197. https://doi.org/10.1016/j.algal.2017.09.011.

Aro, E.-M.; Virgin, I.; Andersson, B. Photoinhibition of Photosystem II. Inactivation, Protein Damage and Turnover. *Biochimica et Biophysica Acta (BBA) - Bioenergetics* **1993**, *1143* (2), 113–134. https://doi.org/10.1016/0005-2728(93)90134-2.

Arrow Electronics. LED application in agricultural lighting can efficiently increase crop yields https://www.arrow.com/en/research-and-events/articles/agriculture-lighting (accessed Sep 26, 2018).

Assemany, P. P.; Calijuri, M. L.; Couto, E. de A. do; de Souza, M. H. B.; Silva, N. C.; Santiago, A. da F.; Castro, J. de S. Algae/Bacteria Consortium in High Rate Ponds: Influence of Solar Radiation on the Phytoplankton Community. *Ecological Engineering* **2015**, *77*, 154–162. https://doi.org/10.1016/j.ecoleng.2015.01.026.

B K, B.; G, M. Influence of Three Selection Pressures on Aerobic Granulation in Sequencing Batch Reactor. *Indian Journal of Chemical Technology (IJCT)* **2016**, *22* (5), 241–247.

Babcock, G. T.; Barry, B. A.; Debus, R. J.; Hoganson, C. W.; Atamian, M.; McIntosh, L.; Sithole, I.; Yocum, C. F. Water Oxidation in Photosystem II: From Radical Chemistry to Multielectron Chemistry. *Biochemistry* **1989**, *28* (25), 9557–9565. https://doi.org/10.1021/bi00451a001.

Bai, G.; Armenante, P. M.; Plank, R. V. Experimental and Computational Determination of Blend Time in USP Dissolution Testing Apparatus II. *Journal of Pharmaceutical Sciences* **2007**, *96* (11), 3072–3086. https://doi.org/10.1002/jps.20994.

Bailey, S.; Grossman, A. Photoprotection in Cyanobacteria: Regulation of Light Harvesting. *Photochem. Photobiol.* **2008**, *84* (6), 1410–1420. https://doi.org/10.1111/j.1751-1097.2008.00453.x.

Bao, H.; Melnicki, M. R.; Kerfeld, C. A. Structure and Functions of Orange Carotenoid Protein Homologs in Cyanobacteria. *Current Opinion in Plant Biology* **2017**, *37*, 1–9. https://doi.org/10.1016/j.pbi.2017.03.010.

Trends in Biochemical Sciences **1992**, *17* (2), 61–66. https://doi.org/10.1016/0968-0004(92)90503-2.

Barr, J. J.; Cook, A. E.; Bond, P. L. Granule Formation Mechanisms within an Aerobic Wastewater System for Phosphorus Removal. *Appl. Environ. Microbiol.* **2010**, *76* (22), 7588–7597. https://doi.org/10.1128/AEM.00864-10.

Barroso Soares, R. Comparative Analysis of the Energy Consumption of Different Wastewater Treatment Plants. *International Journal of Architecture, Arts and Applications* **2017**, *3* (6), 79. https://doi.org/10.11648/j.ijaaa.20170306.11.

Basheer, F.; Farooqi, I. H. Hydrodynamic Properties of Aerobic Granules Cultivated on Phenol as Carbon Source. *APCBEE Procedia* **2014**, *10*, 126–130. https://doi.org/10.1016/j.apcbee.2014.10.029.

Bassham, J. A.; Benson, A. A.; Calvin, M. The Path of Carbon in Photosynthesis VIII. The Role of MalicAcid. **1950**, UCRL--584, 910351. https://doi.org/10.2172/910351.

Bathe, S.; Kreuk, M. K. de; McSwain, B. S.; Schwarzenbeck, N. *Aerobic Granular Sludge*; IWA Publishing, 2005.

Bear, J. *Dynamics of Fluids in Porous Media*; Dover: New York, 1988.

Beardall, J.; Raven, J. A. Cyanobacteria vs Green Algae: Which Group Has the Edge? *J Exp Bot* **2017**, *68* (14), 3697–3699. https://doi.org/10.1093/jxb/erx226.

Beck, D. *Technology Development Life Cycle Processes.*; SAND2013-3933, 1089868; 2013. https://doi.org/10.2172/1089868.

Bennett, A.; Bogorad, L. Complementary chromatic adaptation in a filamentous blue-green alga. *J Cell Biol* **1973**, *58* (2), 419–435.

Berg, M.; Sutula, M. Factors Affecting the Growth of Cyanobacteria with Special Emphasis on the Sacramento - San Joaquin Delta. Southern California Coastal Water Research Project Technical Report 869 August 2015.

Bernstein, H. C.; Konopka, A.; Melnicki, M. R.; Hill, E. A.; Kucek, L. A.; Zhang, S.; Shen, G.; Bryant, D. A.; Beliaev, A. S. Effect of Mono- and Dichromatic Light Quality on Growth Rates and Photosynthetic Performance of Synechococcus Sp. PCC 7002. *Frontiers in Microbiology* **2014**, *5*. https://doi.org/10.3389/fmicb.2014.00488.

Bindhu, B. k.; Madhu, G. Selection Pressure Theory for Aerobic Granulation – an Overview. *International Journal of Environment and Waste Management* **2014**, *13* (3), 317–329. https://doi.org/10.1504/IJEWM.2014.059944.

Boller, M. Small Wastewater Treatment Plants — A Challenge to Wastewater Engineers. *Water Science and Technology* **1997**, *35* (6), 1–12. https://doi.org/10.1016/S0273-1223(97)00089-9.

Bouman, H. A.; Platt, T.; Doblin, M.; Figueiras, F. G.; Gudmundsson, K.; Gudfinnsson, H. G.; Huang, B.; Hickman, A.; Hiscock, M.; Jackson, T.; Lutz, V. A.; Mélin, F.; Rey, F.; Pepin, P.; Segura, V.; Tilstone, G. H.; van Dongen-Vogels, V.; Sathyendranath, S. Photosynthesis–Irradiance Parameters of Marine Phytoplankton: Synthesis of a Global Data Set. **2018**, 16.

Bowers, D. G. Optical Techniques in Studying Suspended Sediments, Turbulence and Mixing in Marine Environments. In *Subsea Optics and Imaging*; Elsevier, 2013; pp 213–240. https://doi.org/10.1533/9780857093523.2.213.

Brightman, R.; Smith, W. Photosynthesis-Irradiance Relationships of Antarctic Phytoplankton during Austral Winter. *Mar. Ecol. Prog. Ser.* **1989**, *53*, 143–151. https://doi.org/10.3354/meps053143.

Brito, A. C.; Newton, A. Measuring Light Attenuation in Shallow Coastal Systems. *Journal of Ecosystem & Ecography* **2013**, *03* (01). https://doi.org/10.4172/2157-7625.1000122.

Brudvig, G. W. Water Oxidation Chemistry of Photosystem II. *Philos Trans R Soc Lond B Biol Sci* **2008**, *363* (1494), 1211–1219. https://doi.org/10.1098/rstb.2007.2217.

Bye, C. M.; Dold, P. L. Sludge Volume Index Settleability Measures: Effect of Solids Characteristics and Test Parameters. *Water Environment Research* **1998**, *70* (1), 87–93. https://doi.org/10.2175/106143098X126928.

Caetano, M.; Araujo, C. S.; Amaral, D. C.; Guerrini, F. M. Open Innovation and Technology Development Process: The Gap on Partnership Adoption from a Case Study Perspective. *Product Management & Development* **2011**, *9* (2), 111–120. https://doi.org/10.4322/pmd.2012.003.

Campbell, D.; Hurry, V.; Clarke, A. K.; Gustafsson, P.; Öquist, G. Chlorophyll Fluorescence Analysis of Cyanobacterial Photosynthesis and Acclimation. *Microbiol. Mol. Biol. Rev.* **1998**, *62* (3), 667–683.

Carey, R. O.; Migliaccio, K. W. Contribution of Wastewater Treatment Plant Effluents to Nutrient Dynamics in Aquatic Systems: A Review. *Environmental Management* **2009**, *44* (2), 205–217. https://doi.org/10.1007/s00267-009-9309-5.

Carreira, C.; Staal, M.; Middelboe, M.; Brussaard, C. P. D. Autofluorescence Imaging System to Discriminate and Quantify the Distribution of Benthic Cyanobacteria and Diatoms: Imaging Benthic Photoautotrophs. *Limnology and Oceanography: Methods* **2015**, *13* (4), e10016. https://doi.org/10.1002/lom3.10016.

Castenholz, R. W. Aggregation in a Thermophilic Oscillatoria. *Nature* **1967**, *215* (5107), 1285–1286. https://doi.org/10.1038/2151285a0.

Castenholz, R. W.; Garcia-Pichel, F. Cyanobacterial Responses to UV Radiation. In *Ecology of Cyanobacteria II*; Whitton, B. A., Ed.; Springer Netherlands: Dordrecht, 2012; pp 481–499. https://doi.org/10.1007/978-94-007-3855-3_19.

Chapple, D.; Kresta, S. M.; Wall, A.; Afacan, A. The Effect of Impeller and Tank Geometry on Power Number for a Pitched Blade Turbine. *Chemical Engineering Research and Design* **2002**, *80* (4), 364–372. https://doi.org/10.1205/026387602317446407.

Chen, Y.; Jiang, W.; Liang, D. T.; Tay, J. H. Structure and Stability of Aerobic Granules Cultivated under Different Shear Force in Sequencing Batch Reactors. *Appl Microbiol Biotechnol* **2007**, *76* (5), 1199–1208. https://doi.org/10.1007/s00253-007-1085-7.

Cheremisinoff, N. P. *Handbook of Water and Wastewater Treatment Technologies*; Butterworth-Heinemann, 2001.

Chopra, S.; Thampy, T.; Leahy, J.; Caplin, A.; LeCun, Y. Factor Graphs for Relational Regression. 14.

Choudhury, F. K.; Rivero, R. M.; Blumwald, E.; Mittler, R. Reactive Oxygen Species, Abiotic Stress and Stress Combination. *The Plant Journal* **2017**, *90* (5), 856–867. https://doi.org/10.1111/tpj.13299.

Cohen, S. E.; Erb, M. L.; Pogliano, J.; Golden, S. S. Best Practices for Fluorescence Microscopy of the Cyanobacterial Circadian Clock. *Meth. Enzymol.* **2015**, *551*, 211–221. https://doi.org/10.1016/bs.mie.2014.10.014.

Corcoll, N.; Ricart, M.; Franz, S.; Sans-Piché, F.; Schmitt-Jansen, M.; Guasch, H. The Use of Photosynthetic Fluorescence Parameters from Autotrophic Biofilms for Monitoring the Effect of Chemicals in River Ecosystems. In *Emerging and Priority Pollutants in Rivers*; Guasch, H., Ginebreda, A., Geiszinger, A., Eds.; Springer Berlin Heidelberg: Berlin, Heidelberg, 2012; Vol. 19, pp 85–115. https://doi.org/10.1007/978-3-642-25722-3_4.

Cory, R. M.; Ward, C. P.; Crump, B. C.; Kling, G. W. Sunlight Controls Water Column Processing of Carbon in Arctic Fresh Waters. *Science* **2014**, *345* (6199), 925–928. https://doi.org/10.1126/science.1253119.

Cullen, J. J.; Neale, P. J. Ultraviolet Radiation, Ozone Depletion, and Marine Photosynthesis. *Photosynth Res* **1994**, *39* (3), 303–320. https://doi.org/10.1007/BF00014589.

Curtis, T. P.; Mara, D. D.; Dixo, N. G. H.; Silva, S. A. Light Penetration in Waste Stabilization Ponds. *Water Research* **1994**, *28* (5), 1031–1038. https://doi.org/10.1016/0043-1354(94)90188-0.

da C. A. Alves, P. L.; Magalhães, A. C. N.; Barja, P. R. The Phenomenon of Photoinhibition of Photosynthesis and Its Importance in Reforestation. *The Botanical Review* **2002**, *68* (2), 193–208. https://doi.org/10.1663/0006-8101(2002)068[0193:TPOPOP]2.0.CO;2.

Daigger, G. T. Oxygen and Carbon Requirements for Biological Nitrogen Removal Processes Accomplishing Nitrification, Nitritation, and Anammox. *Water Environ. Res.* **2014**, *86* (3), 204–209. https://doi.org/10.2175/106143013x13807328849459.

Datt, C.; Elfring, G. J. Dynamics and Rheology of Particles in Shear-Thinning Fluids. *Journal of Non-Newtonian Fluid Mechanics* **2018**, *262*, 107–114. https://doi.org/10.1016/j.jnnfm.2018.03.016.

Dechatiwongse, P.; Srisamai, S.; Maitland, G.; Hellgardt, K. Effects of Light and Temperature on the Photoautotrophic Growth and Photoinhibition of Nitrogen-Fixing Cyanobacterium Cyanothece Sp. ATCC 51142. *Algal Research* **2014**, *5*, 103–111. https://doi.org/10.1016/j.algal.2014.06.004.

Delgadillo-Mirquez, L.; Lopes, F.; Taidi, B.; Pareau, D. Nitrogen and Phosphate Removal from Wastewater with a Mixed Microalgae and Bacteria Culture. *Biotechnology Reports* **2016**, *11*, 18–26. https://doi.org/10.1016/j.btre.2016.04.003.

Non-Photochemical Quenching and Energy Dissipation in Plants, Algae and Cyanobacteria; Demmig-Adams, B., Garab, G., Adams III, W., Govindjee, Eds.; Advances in Photosynthesis and Respiration; Springer Netherlands: Dordrecht, 2014; Vol. 40. https://doi.org/10.1007/978-94-017-9032-1.

Deng, S.; Wang, L.; Su, H. Role and Influence of Extracellular Polymeric Substances on the Preparation of Aerobic Granular Sludge. *Journal of Environmental Management* **2016**, *173*, 49–54. https://doi.org/10.1016/j.jenvman.2016.03.008.

Derlon, N.; Wagner, J.; da Costa, R. H. R.; Morgenroth, E. Formation of Aerobic Granules for the Treatment of Real and Low-Strength Municipal Wastewater Using a Sequencing Batch Reactor Operated at Constant Volume. *Water Research* **2016**, *105*, 341–350. https://doi.org/10.1016/j.watres.2016.09.007.

Dickey, D. S. Tackling Difficult Mixing Problems. **2015**, 8.

Donkor, V.; Häder, D.-P. Effects of Solar and Ultraviolet Radiation on Motility, Photomovement and Pigmentation in Filamentous, Gliding Cyanobacteria. *FEMS Microbiology Letters* **1991**, *86* (2), 159–168. https://doi.org/10.1016/0378-1097(91)90661-S.

Donlan, R. M. Biofilms: Microbial Life on Surfaces. *Emerg Infect Dis* **2002**, *8* (9), 881–890. https://doi.org/10.3201/eid0809.020063.

Doran, P. M. Mixing. In *Bioprocess Engineering Principles*; Elsevier, 2013; pp 255–332. https://doi.org/10.1016/B978-0-12-220851-5.00008-3.

Droppo, I. G.; Walling, D. E.; Ongley, E. D. The Influence of Floe Size, Density and Porosity on Sediment and Contaminant Transport. 8.

Droste, R. L.; Gehr, R. L. *Theory and Practice of Water and Wastewater Treatment*; John Wiley & Sons, 2018.

Dyer, K. R.; Manning, A. J. Observation of the Size, Settling Velocity and Effective Density of Flocs, and Their Fractal Dimensions. *Journal of sea research* **1999**, *41* (1), 87–95.

Handbook of Industrial Mixing: Science and Practice; Edward L. Paul, Atiemo-Obeng, V. A., Kresta, S. M., Eds.; Wiley-Interscience: Hoboken, N.J, 2004.

Elias, S.; Banin, E. Multi-Species Biofilms: Living with Friendly Neighbors. *FEMS Microbiol Rev* **2012**, *36* (5), 990–1004. https://doi.org/10.1111/j.1574-6976.2012.00325.x.

Elimelech, M.; Gregory, J.; Jia, X. *Particle Deposition and Aggregation: Measurement, Modelling and Simulation*; Butterworth-Heinemann, 2013.

Ellis, K. V.; Mara, D. D. Stabilization Ponds: Design and Operation. *Critical Reviews in Environmental Science and Technology* **2009**. https://doi.org/10.1080/10643388309381703.

Ellison, C. K.; Kan, J.; Dillard, R. S.; Kysela, D. T.; Ducret, A.; Berne, C.; Hampton, C. M.; Ke, Z.; Wright, E. R.; Biais, N.; Dalia, A. B.; Brun, Y. V. Obstruction of Pilus Retraction Stimulates Bacterial Surface Sensing. *Science* **2017**, *358* (6362), 535–538. https://doi.org/10.1126/science.aan5706.

Esmaeelnejad, L.; Siavashi, F.; Seyedmohammadi, J.; Shabanpour, M. The Best Mathematical Models Describing Particle Size Distribution of Soils. *Model. Earth Syst. Environ.* **2016**, *2* (4), 1–11. https://doi.org/10.1007/s40808-016-0220-9.

Etterer, T.; Wilderer, P. A. Generation and Properties of Aerobic Granular Sludge. *Water Science and Technology* **2001**, *43* (3), 19–26. https://doi.org/10.2166/wst.2001.0114.

Etterer, T. Formation, Structure and Function of Aerobic Granular Sludge. Tec University Munich, Germany December 5, 2004.

Falkowski, P. G.; Raven, J. A. *Aquatic Photosynthesis*; Princeton University Press, 2007.

Figueredo, C. C.; Giani, A.; Lemos Filho, J. P. Photosynthetic Capacity of Three Phytoplanktonic Species Measured by a Pulse Amplitude Fluorometric Method. *Brazilian Journal of Plant Physiology* **2009**, *21* (3), 167–174. https://doi.org/10.1590/S1677-04202009000300001.

Figueroa, F. L. Relations between Electron Transport Rates Determined by Pulse Amplitude Modulated Chlorophyll Fluorescence and Oxygen Evolution in Macroalgae under Different Light Conditions. *Photosynthesis Research* **2003**, *75*, 259–275.

Flemming, H.-C.; Neu, T. R.; Wozniak, D. J. The EPS Matrix: The "House of Biofilm Cells." *J Bacteriol* **2007**, *189* (22), 7945–7947. https://doi.org/10.1128/JB.00858-07.

Ford, T. F. Viscosity-concentration, and fluidity-concentration relationships for suspensions of spherical particles in newtonian liquids. *J. Phys. Chem.* **1960**, *64* (9), 1168–1174. https://doi.org/10.1021/j100838a015.

Furukawa, H.; Kato, Y.; Inoue, Y.; Kato, T.; Tada, Y.; Hashimoto, S. Correlation of Power Consumption for Several Kinds of Mixing Impellers. *International Journal of Chemical Engineering* **2012**, *2012*, 1–6. https://doi.org/10.1155/2012/106496.

Gallegos, C. L.; Moore, K. A. Factors Contributing to Water-Column Light Attenuation. **2000**.

Gao, D.; Liu, L.; Liang, H.; Wu, W. *Aerobic Granular Sludge: Characterization, Mechanism of Granulation and Application to Wastewater Treatment*; 2010; Vol. 31. https://doi.org/10.3109/07388551.2010.497961.

Geider, R. J.; Osborne, B. A. *Algal Photosynthesis*; 1992.

Gerloff-Elias, A.; Spijkerman, E.; Pröschold, T. Effect of External PH on the Growth, Photosynthesis and Photosynthetic Electron Transport of Chlamydomonas Acidophila Negoro, Isolated from an Extremely Acidic Lake (PH 2.6). *Plant, Cell & Environment* **2005**, *28* (10), 1218–1229. https://doi.org/10.1111/j.1365-3040.2005.01357.x.

Giacometti, G. M.; Morosinotto, T. Photoinhibition and Photoprotection in Plants, Algae, and Cyanobacteria. In *Encyclopedia of Biological Chemistry*; Lennarz, W. J., Lane, M. D., Eds.; Academic Press: Waltham, 2013; pp 482–487. https://doi.org/10.1016/B978-0-12-378630-2.00229-2.

Giesen, A.; Loosdrecht, M. van; Pronk, M.; Robertson, S.; Thompson, A. Aerobic Granular Biomass Technology: Recent Performance Data, Lessons Learnt and Retrofitting Conventional Treatment Infrastructure. *proc water environ fed* **2016**, *2016* (11), 1913–1923. https://doi.org/10.2175/193864716819707139.

Giesen, A.; van Loosdrecht, M.; Robertson, S.; de Buin, B. Aerobic Granular Biomass Technology: further innovation, system development and design optimisation https://www.ingentaconnect.com/contentone/wef/wefproc/2015/00002015/00000016/art00018 (accessed Sep 18, 2018). https://doi.org/info:doi/10.2175/193864715819539641.

Gigahertz-Optik. Basics of Light Measurement » Gigahertz-Optik https://www.gigahertz-optik.de/en-us/basics-light-measurement/ (accessed Sep 20, 2018).

Golterman, H. . Chapter 13 Algae and Their Pigments. In *Physiological Limnology: An Approach to the Physiology of Lake Ecosystems*; Developments in Water Science; Elsevier, 1975; Vol. 2, pp 233–247. https://doi.org/10.1016/S0167-5648(08)71070-0.

González-Camejo, J.; Viruela, A.; Ruano, M. V.; Barat, R.; Seco, A.; Ferrer, J. Effect of Light Intensity, Light Duration and Photoperiods in the Performance of an Outdoor Photobioreactor for Urban Wastewater Treatment. *Algal Research* **2019**, *40*, 101511. https://doi.org/10.1016/j.algal.2019.101511.

Gonzalez-Martinez, A.; Sihvonen, M.; Muñoz-Palazon, B.; Rodriguez-Sanchez, A.; Mikola, A.; Vahala, R. Microbial Ecology of Full-Scale Wastewater Treatment Systems in the Polar Arctic Circle: Archaea, Bacteria and Fungi. *Scientific Reports* **2018**, *8* (1). https://doi.org/10.1038/s41598-018-20633-5.

Grant, C.; Louda, J. Microalgal Pigment Ratios in Relation to Light Intensity: Implications for Chemotaxonomy. *Aquatic Biology* **2010**, *11* (2), 127–138. https://doi.org/10.3354/ab00298.

Gray, G. R.; Hope, B. J.; Qin, X.; Taylor, B. G.; Whitehead, C. L. The Characterization of Photoinhibition and Recovery during Cold Acclimation in Arabidopsis Thaliana Using Chlorophyll Fluorescence Imaging. *Physiologia Plantarum* **2003**, *119* (3), 365–375. https://doi.org/10.1034/j.1399-3054.2003.00224.x.

Green, B.; Parson, W. W. *Light-Harvesting Antennas in Photosynthesis*; Springer Science & Business Media, 2003.

Gregory, J. Monitoring Particle Aggregation Processes. *Advances in Colloid and Interface Science* **2009**, *147–148*, 109–123. https://doi.org/10.1016/j.cis.2008.09.003.

Gu, Y.; Li, Y.; Li, X.; Luo, P.; Wang, H.; Wang, X.; Wu, J.; Li, F. Energy Self-Sufficient Wastewater Treatment Plants: Feasibilities and Challenges. *Energy Procedia* **2017**, *105*, 3741–3751. https://doi.org/10.1016/j.egypro.2017.03.868.

Gubanov, O.; Cortelezzi, L. On the Cost Efficiency of Mixing Optimization. *Journal of Fluid Mechanics* **2012**, *692*, 112–136. https://doi.org/10.1017/jfm.2011.498.

Guedes da Silva, L.; Tomás-Martínez, S.; Wahl, A.; van Loosdrecht, M. *The Environment Selects: Modeling Energy Allocation in Microbial Communities under Dynamic Environments*; 2019. https://doi.org/10.1101/689174.

Gururani, M. A.; Venkatesh, J.; Tran, L. S. P. Regulation of Photosynthesis during Abiotic Stress-Induced Photoinhibition. *Molecular Plant* **2015**, *8* (9), 1304–1320. https://doi.org/10.1016/j.molp.2015.05.005.

Gutzeit, G.; Lorch, D. P.; Weber, A.; Engels, M. S.; Neis, U. Bioflocculent Algal-Bacterial Biomass Improves Low-Cost Wastewater Treatment. *Water science and technology : a journal of the International Association on Water Pollution Research* **2005**, *52* (12), 9–18. https://doi.org/10.2166/wst.2005.0415.

Haigh, J. D.; Winning, A. R.; Toumi, R.; Harder, J. W. An Influence of Solar Spectral Variations on Radiative Forcing of Climate. *Nature* **2010**, *467* (7316), 696–699. https://doi.org/10.1038/nature09426.
Hakkila, K.; Antal, T.; Rehman, A. U.; Kurkela, J.; Wada, H.; Vass, I.; Tyystjärvi, E.; Tyystjärvi, T. Oxidative Stress and Photoinhibition Can Be Separated in the Cyanobacterium Synechocystis Sp. PCC 6803. *Biochimica et Biophysica Acta (BBA) - Bioenergetics* **2014**, *1837* (2), 217–225. https://doi.org/10.1016/j.bbabio.2013.11.011.

Hall, S. M. Chapter 6 - Blending and Agitation. In *Rules of Thumb for Chemical Engineers (Sixth Edition)*; Hall, S. M., Ed.; Elsevier, 2018; pp 99–124. https://doi.org/10.1016/B978-0-12-811037-9.00006-0.

Han, B.-P.; Virtanen, M.; Koponen, J.; Straškraba, M. Effect of Photoinhibition on Algal Photosynthesis: A Dynamic Model. *J Plankton Res* **2000**, *22* (5), 865–885. https://doi.org/10.1093/plankt/22.5.865.

Hann, M. Factors Impacting the Cultivation, Structure, and Oxygen Profiles of Oxygenic Photogranules for Aeration-Free Wastewater Treatment. *Environmental & Water Resources Engineering Masters Projects* **2018**.

Haszprunar, G. The Types of Homology and Their Significance for Evolutionary Biology and Phylogenetics. *Journal of Evolutionary Biology* **1992**, *5* (1), 13–24. https://doi.org/10.1046/j.1420-9101.1992.5010013.x.

Hau, K. C.; Sculli, D. Costs of Disposal of Sewage Sludge: A Case Study. *Engineering Costs and Production Economics* **1991**, *21* (2), 133–141. https://doi.org/10.1016/0167-188X(91)90027-Y.

Havaux, M.; Niyogi, K. K. The Violaxanthin Cycle Protects Plants from Photooxidative Damage by More than One Mechanism. *Proc Natl Acad Sci U S A* **1999**, *96* (15), 8762–8767.

He, Q.; Chen, L.; Zhang, S.; Chen, R.; Wang, H.; Zhang, W.; Song, J. Natural Sunlight Induced Rapid Formation of Water-Born Algal-Bacterial Granules in an Aerobic Bacterial Granular Photo-Sequencing Batch Reactor. *Journal of Hazardous Materials* **2018**, *359*, 222–230. https://doi.org/10.1016/j.jhazmat.2018.07.051.

Helbling, E. W.; Villafañe, V.; Ferrario, M.; Holm-Hansen, O. Impact of Natural Ultraviolet Radiation on Rates of Photosynthesis and on Specific Marine Phytoplankton Species. *Marine Ecology Progress Series* **1992**, *80* (1), 89–100.

Hill, P. S.; Nowell, A. R. M.; Jumars, P. A. Encounter Rate by Turbulent Shear of Particles Similar in Diameter to the Kolmogorov Scale. *J Mar Res* **1992**, *50* (4), 643–668. https://doi.org/10.1357/002224092784797539.

Hofstraat, J. W.; Peeters, J. C. H.; Snel, J. F. H.; Geel, C. Simple Determination of Photosynthetic Efficiency and Photoinhibition of Dunaliella Tertiolecta by Saturating Pulse Fluorescence Measurements. *Marine Ecology Progress Series* **1994**, *103* (1/2), 187–196.

Hogg, R. Issues in Particle Size Analysis. *KONA* **2008**, *26* (0), 81–93. https://doi.org/10.14356/kona.2008009.

Huang, H. Porosity-Size Relationship of Drilling Mud Flocs: Fractal Structure. *Clays Clay Miner.* **1993**, *41* (3), 373–379. https://doi.org/10.1346/CCMN.1993.0410314.

Isanta, E.; Suárez-Ojeda, M. E.; Val del Río, Á.; Morales, N.; Pérez, J.; Carrera, J. Long Term Operation of a Granular Sequencing Batch Reactor at Pilot Scale Treating a Low-Strength Wastewater. *Chemical Engineering Journal* **2012**, *198–199*, 163–170. https://doi.org/10.1016/j.cej.2012.05.066.

Jahn, M.; Vialas, V.; Karlsen, J.; Maddalo, G.; Edfors, F.; Forsström, B.; Uhlén, M.; Käll, L.; Hudson, E. P. Growth of Cyanobacteria Is Constrained by the Abundance of Light and Carbon Assimilation Proteins. *Cell Reports* **2018**, *25* (2), 478-486.e8. https://doi.org/10.1016/j.celrep.2018.09.040.

Jasmine, D. A.; Malarmathi, K. B.; Daniel, S. K.; Malathi, S. Natural Algal-Based Processes as Smart Approach for Wastewater Treatment. *Smart Materials for Waste Water Applications* **2016**, 379–398.

Jeffrey, S. W. Photosynthetic pigments of the phytoplankton of some coral reef waters1: pigments of coral reef waters. *Limnol. Oceanogr.* **1968**, *13* (2), 350–355. https://doi.org/10.4319/lo.1968.13.2.0350.

Jensen, H.; Biggs, C. A.; Karunakaran, E. The Importance of Sewer Biofilms. *Wiley Interdisciplinary Reviews: Water* **2016**, *3* (4), 487–494. https://doi.org/10.1002/wat2.1144.

Ji, X.; Jiang, M.; Zhang, J.; Jiang, X.; Zheng, Z. The Interactions of Algae-Bacteria Symbiotic System and Its Effects on Nutrients Removal from Synthetic Wastewater. *Bioresource Technology* **2018**, *247*, 44–50. https://doi.org/10.1016/j.biortech.2017.09.074.

Jiao, Y.; Cody, G. D.; Harding, A. K.; Wilmes, P.; Schrenk, M.; Wheeler, K. E.; Banfield, J. F.; Thelen, M. P. Characterization of Extracellular Polymeric Substances from Acidophilic Microbial Biofilms. *Appl. Environ. Microbiol.* **2010**, *76* (9), 2916–2922. https://doi.org/10.1128/AEM.02289-09.

Jirout, T.; Rieger, F. Impeller Design for Mixing of Suspensions. *Chemical Engineering Research and Design* **2011**, *89* (7), 1144–1151. https://doi.org/10.1016/j.cherd.2010.12.005.

Jørgensen, S. E.; Fath, B. D. Steady-State Models. In *Developments in Environmental Modelling*; Elsevier, 2011; Vol. 23, pp 159–174. https://doi.org/10.1016/B978-0-444-53567-2.00006-5.

June 2015, W. E. F.-W. V.-. WEF - Water Volumes - June 2015 http://wef.org/resources/publications/all-magazines/water-environment-technology/wet-issues/water-environment--technology2/wet-magazine---june-2015/water-volumes---june-2015/ (accessed Jan 28, 2019).

Kalaji, H. M.; Carpentier, R.; Allakhverdiev, S. I.; Bosa, K. Fluorescence Parameters as Early Indicators of Light Stress in Barley. *Journal of Photochemistry and Photobiology B: Biology* **2012**, *112*, 1–6. https://doi.org/10.1016/j.jphotobiol.2012.03.009.

Kalderis, D.; Aivalioti, M.; Gidarakos, E. Options for Sustainable Sewage Sludge Management in Small Wastewater Treatment Plants on Islands: The Case of Crete. *Desalination* **2010**, *260* (1–3), 211–217. https://doi.org/10.1016/j.desal.2010.04.030.

Kang, A. J.; Munz, G.; Yuan, Q. Influence of PH Control on Material Characteristics, Bacterial Community Composition and BNR Performance of Mature Aerobic Granules. *Process Safety and Environmental Protection* **2019**, *124*, 158–166. https://doi.org/10.1016/j.psep.2019.02.014.

Kataria, S.; Jajoo, A.; Guruprasad, K. N. Impact of Increasing Ultraviolet-B (UV-B) Radiation on Photosynthetic Processes. *Journal of Photochemistry and Photobiology B: Biology* **2014**, *137*, 55–66. https://doi.org/10.1016/j.jphotobiol.2014.02.004.

Kawase, Y.; Moo-Young, M. Mixing Time in Bioreactors. *J. Chem. Technol. Biotechnol.* **2007**, *44* (1), 63–75. https://doi.org/10.1002/jctb.280440107.

Khazi, M. I.; Demirel, Z.; Dalay, M. C. Evaluation of Growth and Phycobiliprotein Composition of Cyanobacteria Isolates Cultivated in Different Nitrogen Sources. *J Appl Phycol* **2018**, *30* (3), 1513–1523. https://doi.org/10.1007/s10811-018-1398-1.

Kim, B.-H.; Choi, J.-E.; Cho, K.; Kang, Z.; Ramanan, R.; Moon, D.-G.; Kim, H.-S. Influence of Water Depth on Microalgal Production, Biomass Harvest, and Energy Consumption in High Rate Algal Pond Using Municipal Wastewater. *J. Microbiol. Biotechnol.* **2018**, *28* (4), 630–637. https://doi.org/10.4014/jmb.1801.01014.

Kirilovsky, D. Photoprotection in Cyanobacteria: The Orange Carotenoid Protein (OCP)-Related Non-Photochemical-Quenching Mechanism. *Photosynth Res* **2007**, *93* (1), 7. https://doi.org/10.1007/s11120-007-9168-y.

Kirk, J. T. . *Light and Photosynthesis in Aquatic Ecosystems*, illustrated, reprint, revised.; Cambridge University Press, 1994.

Knocke, W. R. Density of Activated Sludge Solids. *Water Research* **1992**, *26* (11), 1559–1561.

Krause-Jensen, D.; Sand-Jensen, K. Light Attenuation and Photosynthesis of Aquatic Plant Communities. *Limnology and Oceanography* **1998**, *43* (3), 396–407. https://doi.org/10.4319/lo.1998.43.3.0396.

Kristensen, E.; Suraswadi, P. Carbon, Nitrogen and Phosphorus Dynamics in Creek Water of a Southeast Asian Mangrove Forest. *Hydrobiologia* **2002**, *474* (1/3), 197–211. https://doi.org/10.1023/A:1016544006720.

Kuo-Dahab, W. C.; Stauch-White, K.; Butler, C. S.; Gikonyo, G. J.; Carbajal-González, B.; Ivanova, A.; Dolan, S.; Park, C. Investigation of the Fate and Dynamics of Extracellular Polymeric Substances (EPS) during Sludge-Based Photogranulation under Hydrostatic Conditions. *Environmental Science & Technology* **2018**, *52* (18), 10462–10471. https://doi.org/10.1021/acs.est.8b03033.

Lauceri, R.; Bresciani, M.; Lami, A.; Morabito, G. Chlorophyll a Interference in Phycocyanin and Allophycocyanin Spectrophotometric Quantification. *J Limnol* **2017**. https://doi.org/10.4081/jlimnol.2017.1691.

Lawrenz, E.; Fedewa, E. J.; Richardson, T. L. Extraction Protocols for the Quantification of Phycobilins in Aqueous Phytoplankton Extracts. *Journal of Applied Phycology* **2011**, *23* (5), 865–871. https://doi.org/10.1007/s10811-010-9600-0.

Lee, C. S.; Lee, S.-A.; Ko, S.-R.; Oh, H.-M.; Ahn, C.-Y. Effects of Photoperiod on Nutrient Removal, Biomass Production, and Algal-Bacterial Population Dynamics in Lab-Scale Photobioreactors Treating Municipal Wastewater. *Water Research* **2015**, *68*, 680–691. https://doi.org/10.1016/j.watres.2014.10.029.

Lee, C. S.; Oh, H.-S.; Oh, H.-M.; Kim, H.-S.; Ahn, C.-Y. Two-Phase Photoperiodic Cultivation of Algal–Bacterial Consortia for High Biomass Production and Efficient Nutrient Removal from Municipal Wastewater. *Bioresource Technology* **2016**, *200*, 867–875. https://doi.org/10.1016/j.biortech.2015.11.007.

Lee, D. J.; Chen, G. W.; Liao, Y. C.; Hsieh, C. C. On the Free-Settling Test for Estimating Activated Sludge Floc Density. *Water Research* **1996**, *30* (3), 541–550.

Lee, D.-J.; Chen, Y.-Y.; Show, K.-Y.; Whiteley, C. G.; Tay, J.-H. Advances in Aerobic Granule Formation and Granule Stability in the Course of Storage and Reactor Operation. *Biotechnology Advances* **2010**, *28* (6), 919–934. https://doi.org/10.1016/j.biotechadv.2010.08.007.

Lee, K.; Lee, C.-G. Effect of Light/Dark Cycles on Wastewater Treatments by Microalgae. *Biotechnol. Bioprocess Eng.* **2001**, *6* (3), 194–199. https://doi.org/10.1007/BF02932550.

Lee, Y.-J.; Lei, Z. Microalgal-Bacterial Aggregates for Wastewater Treatment: A Mini-Review. *Bioresource Technology Reports* **2019**, 100199. https://doi.org/10.1016/j.biteb.2019.100199.

Lewandowski, Z.; Boltz, J. P. Biofilms in Water and Wastewater Treatment. In *Treatise on Water Science*; Elsevier, 2011; pp 529–570. https://doi.org/10.1016/B978-0-444-53199-5.00095-6.

Li, D.; Ganczarczyk, J. Advective Transport in Activated Sludge Flocs. *Water Environment Research* **1992**, *64* (3), 236–240.

Li, J.; Luo, G.; He, L.; Xu, J.; Lyu, J. Analytical Approaches for Determining Chemical Oxygen Demand in Water Bodies: A Review. *Critical Reviews in Analytical Chemistry* **2018**, *48* (1), 47–65. https://doi.org/10.1080/10408347.2017.1370670.

Li, X.-Y.; Logan, B. E. Permeability of Fractal Aggregates. *Water Research* **2001**, *35* (14), 3373–3380. https://doi.org/10.1016/S0043-1354(01)00061-6.

Li, Y.; Liu, Y. Diffusion of Substrate and Oxygen in Aerobic Granule. *Biochemical Engineering Journal* **2005**, *27* (1), 45–52. https://doi.org/10.1016/j.bej.2005.06.012.

Li, Z.; Lu, P.; Zhang, D.; Chen, G.; Zeng, S.; He, Q. Population Balance Modeling of Activated Sludge Flocculation: Investigating the Influence of Extracellular Polymeric Substances (EPS) Content and Zeta Potential on Flocculation Dynamics. *Separation and Purification Technology* **2016**, *162*, 91–100. https://doi.org/10.1016/j.seppur.2016.02.011.

Li-Cor. Principles of Radiation Measurement. Li-Cor Sciences .;No date.

Limoli, D. H.; Jones, C. J.; Wozniak, D. J. Bacterial Extracellular Polysaccharides in Biofilm Formation and Function. *Microbiol Spectr* **2015**, *3* (3). https://doi.org/10.1128/microbiolspec.MB-0011-2014.

Lindskog, S.; Coleman, J. E. The Catalytic Mechanism of Carbonic Anhydrase. *PNAS* **1973**, *70* (9), 2505–2508. https://doi.org/10.1073/pnas.70.9.2505.

Liu, J.; Lu, Y.; Hua, W.; Last, R. L. A New Light on Photosystem II Maintenance in Oxygenic Photosynthesis. *Front. Plant Sci.* **2019**, *10*. https://doi.org/10.3389/fpls.2019.00975.

Liu, L.; Fan, H.; Liu, Y.; Liu, C.; Huang, X. Development of Algae-Bacteria Granular Consortia in Photo-Sequencing Batch Reactor. *Bioresource Technology* **2017**, *232*, 64–71. https://doi.org/10.1016/j.biortech.2017.02.025.

Liu, X.-W.; Yu, H.-Q.; Ni, B.-J.; Sheng, G.-P. Characterization, Modeling and Application of Aerobic Granular Sludge for Wastewater Treatment. In *Biotechnology in China I*; Advances in Biochemical Engineering / Biotechnology; Springer, Berlin, Heidelberg, 2009; pp 275–303. https://doi.org/10.1007/10_2008_29.

Liu, Y.-Q.; Tay, J.-H. Fast Formation of Aerobic Granules by Combining Strong Hydraulic Selection Pressure with Overstressed Organic Loading Rate. *Water Research* **2015**, *80*, 256–266. https://doi.org/10.1016/j.watres.2015.05.015.

Liu, Y. Chapter 5 Factors Affecting Aerobic Granulation. In *Waste Management Series*; Tay, J.-H., Tay, S. T.-L., Liu, Y., Show, K.-Y., Ivanov, V., Eds.; Biogranulation Technologies for Wastewater Treatment; Elsevier, 2006; Vol. 6, pp 99–114. https://doi.org/10.1016/S0713-2743(06)80107-8.

Liu, Y. Nutrient Removal by Microbial Granules. In *Waste Management Series*; Tay, J.-H., Tay, S. T.-L., Liu, Y., Show, K.-Y., Ivanov, V., Eds.; Biogranulation Technologies for Wastewater Treatment; Elsevier, 2006; Vol. 6, pp 163–189. https://doi.org/10.1016/S0713-2743(06)80110-8.

Liu, Y.; Tay, J.-H. The Essential Role of Hydrodynamic Shear Force in the Formation of Biofilm and Granular Sludge. *Water research* **2002**, *36* (7), 1653–1665.

Liu, Y.; Tay, J.-H. State of the Art of Biogranulation Technology for Wastewater Treatment. *Biotechnology Advances* **2004**, *22* (7), 533–563. https://doi.org/10.1016/j.biotechadv.2004.05.001.

Liu, Y.; Xu, H.-L.; Show, K.-Y.; Tay, J.-H. Anaerobic Granulation Technology for Wastewater Treatment. *World Journal of Microbiology & Biotechnology* **2002**, *18*, 99–113.

Lofrano, G.; Brown, J. Wastewater Management through the Ages: A History of Mankind. *Science of The Total Environment* **2010**, *408* (22), 5254–5264. https://doi.org/10.1016/j.scitotenv.2010.07.062.

Lopez-Peña, L. A.; Meulenbroek, B.; Vermolen, F. A Network Model for the Biofilm Growth in Porous Media and Its Effects on Permeability and Porosity. *Comput. Visual Sci.* **2019**, *21* (1), 11–22. https://doi.org/10.1007/s00791-019-00316-y.

LRC. How can full-spectrum light sources be compared? | Full-Spectrum Light Sources | Lighting Answers | NLPIP https://www.lrc.rpi.edu/programs/nlpip/lightinganswers/fullspectrum/comparisons.asp (accessed Sep 20, 2018).

Lürling, M.; Eshetu, F.; Faassen, E. J.; Kosten, S.; Huszar, V. L. M. Comparison of Cyanobacterial and Green Algal Growth Rates at Different Temperatures. *Freshwater Biology* **2013**, *58* (3), 552–559. https://doi.org/10.1111/j.1365-2427.2012.02866.x.

Macedo, M.; Ferreira, J.; Duarte, P. Dynamic Behaviour of Photosynthesis-Irradiance Curves Determined from Oxygen Production during Variable Incubation Periods. *Mar. Ecol. Prog. Ser.* **1998**, *165*, 31–43. https://doi.org/10.3354/meps165031.

Machado, M. B.; Nunhez, J. R.; Nobes, D.; Kresta, S. M. Impeller Characterization and Selection: Balancing Efficient Hydrodynamics with Process Mixing Requirements. *AIChE J.* **2012**, *58* (8), 2573–2588. https://doi.org/10.1002/aic.12758.

MacIntyre, H. L.; Kana, T. M.; Anning, T.; Geider, R. J. Photoacclimation of Photosynthesis Irradiance Response Curves and Photosynthetic Pigments in Microalgae and Cyanobacteria1. *Journal of Phycology* **2002**, *38* (1), 17–38. https://doi.org/10.1046/j.1529-8817.2002.00094.x.

Mahdavian, M.; Wattanapongsakorn, N. Optimizing Greenhouse Lighting for Advanced Agriculture Based on Real Time Electricity Market Price https://www.hindawi.com/journals/mpe/2017/6862038/ (accessed Sep 26, 2018). https://doi.org/10.1155/2017/6862038.

Malapascua, J.; Jerez, C.; Sergejevová, M.; Figueroa, F.; Masojídek, J. Photosynthesis Monitoring to Optimize Growth of Microalgal Mass Cultures: Application of Chlorophyll Fluorescence Techniques. *Aquat. Biol.* **2014**, *22*, 123–140. https://doi.org/10.3354/ab00597.

Mancell-Egala, W. A. S. K.; Kinnear, D. J.; Jones, K. L.; De Clippeleir, H.; Takács, I.; Murthy, S. N. Limit of Stokesian Settling Concentration Characterizes Sludge Settling Velocity. *Water Research* **2016**, *90*, 100–110. https://doi.org/10.1016/j.watres.2015.12.007.

Masliyah, J. H.; Polikar, M. Terminal Velocity of Porous Spheres. *The Canadian Journal of Chemical Engineering* **1980**, *58* (3), 299–302. https://doi.org/10.1002/cjce.5450580303.

Masojídek, J.; Grobbelaar, J. U.; Pechar, L.; KoblíŽek, M. Photosystem II Electron Transport Rates and Oxygen Production in Natural Waterblooms of Freshwater Cyanobacteria During a Diel Cycle. *J Plankton Res* **2001**, *23* (1), 57–66. https://doi.org/10.1093/plankt/23.1.57.

Massa, G. D.; Kim, H.-H.; Wheeler, R. M.; Mitchell, C. A. Plant Productivity in Response to LED Lighting. *HortScience* **2008**, *43* (7), 1951–1956.

Massoud, M. A.; Tarhini, A.; Nasr, J. A. Decentralized Approaches to Wastewater Treatment and Management: Applicability in Developing Countries. *Journal of*

Environmental Management **2009**, *90* (1), 652–659. https://doi.org/10.1016/j.jenvman.2008.07.001.

Mathur, S.; Agrawal, D.; Jajoo, A. Photosynthesis: Response to High Temperature Stress. *Journal of Photochemistry and Photobiology B: Biology* **2014**, *137*, 116–126. https://doi.org/10.1016/j.jphotobiol.2014.01.010.

Maxwell, K.; Johnson, G. N. Chlorophyll Fluorescence—a Practical Guide. *Journal of Experimental Botany* **2000**, *51* (345), 659–668. https://doi.org/10.1093/jxb/51.345.659.

McHugh, S.; O'Reilly, C.; Mahony, T.; Colleran, E.; O'Flaherty, V. Anaerobic Granular Sludge Bioreactor Technology. *Reviews in Environmental Science and Bio/Technology* **2003**, *2* (2–4), 225–245. https://doi.org/10.1023/B:RESB.0000040465.45300.97.

McNair, A. Pilot Reactor Operation of the Oxygenic Photogranule (OPG) Wastewater Treatment Process. *Environmental & Water Resources Engineering Masters Projects* **2017**.

Mercado, J. M.; Javier, F.; Gordillo, L.; Xavier Niell, F.; Figueroa, F. L. Effects of Different Levels of CO2 on Photosynthesis and Cell Components of the Red Alga Porphyra Leucosticta. *Journal of Applied Phycology* **1999**, *11* (5), 455–461. https://doi.org/10.1023/A:1008194223558.

Mesquita, D. P.; Amaral, A. L.; Ferreira, E. C. Identifying Different Types of Bulking in an Activated Sludge System through Quantitative Image Analysis. *Chemosphere* **2011**, *85* (4), 643–652. https://doi.org/10.1016/j.chemosphere.2011.07.012.

Metz, J. G.; Pakrasi, H. B.; Seibert, M.; Arntzer, C. J. Evidence for a Dual Function of the Herbicide-Binding D1 Protein in Photosystem II. *FEBS Letters* **1986**, *205* (2), 269–274. https://doi.org/10.1016/0014-5793(86)80911-5.

Meyer, R. L.; Saunders, A. M.; Zeng, R. J.; Keller, J.; Blackall, L. L. Microscale Structure and Function of Anaerobic—Aerobic Granules Containing Glycogen Accumulating Organisms. *FEMS Microbiol Ecol* **2003**, *45* (3), 253–261. https://doi.org/10.1016/S0168-6496(03)00159-4.

Michels, M. H. A.; van der Goot, A. J.; Norsker, N.-H.; Wijffels, R. H. Effects of Shear Stress on the Microalgae Chaetoceros Muelleri. *Bioprocess Biosyst Eng* **2010**, *33* (8), 921–927. https://doi.org/10.1007/s00449-010-0415-9.

Mikkelsen, L. H. The Shear Sensitivity of Activated Sludge: Relations to Filterability, Rheology and Surface Chemistry. *Colloids and Surfaces A: Physicochemical and Engineering Aspects* **2001**, *182* (1), 1–14. https://doi.org/10.1016/S0927-7757(00)00772-X.

Milferstedt, K.; Kuo-Dahab, W. C.; Butler, C. S.; Hamelin, J.; Abouhend, A. S.; Stauch-White, K.; McNair, A.; Watt, C.; Carbajal-González, B. I.; Dolan, S.; Park, C. The Importance of Filamentous Cyanobacteria in the Development of Oxygenic Photogranules. *Scientific Reports* **2017**, *7* (1), 17944. https://doi.org/10.1038/s41598-017-16614-9.

Mishima, K.; Nakamura, M. Self-Immobilization of Aerobic Activated Sludge–A Pilot Study of the Aerobic Upflow Sludge Blanket Process in Municipal Sewage Treatment. *Water Science and Technology* **1991**, *23* (4–6), 981–990. https://doi.org/10.2166/wst.1991.0550.

Miyata, K.; Ikeda, H.; Nakaji, M.; Kanel, D. R.; Terashima, I. Rate Constants of PSII Photoinhibition and Its Repair, and PSII Fluorescence Parameters in Field Plants in Relation to Their Growth Light Environments. *Plant Cell Physiol* **2015**, *56* (9), 1841–1854. https://doi.org/10.1093/pcp/pcv107.

Moisander, P. H.; Hench, J. L.; Kononen, K.; Paerl, H. W. Small-Scale Shear Effects on Heterocystous Cyanobacteria. *Limnology and Oceanography* **2002**, *47* (1), 108–119. https://doi.org/10.4319/lo.2002.47.1.0108.

Morales, M.; Sánchez, L.; Revah, S. The Impact of Environmental Factors on Carbon Dioxide Fixation by Microalgae. *FEMS Microbiol Lett* **2018**, *365* (3). https://doi.org/10.1093/femsle/fnx262.

Muga, H. E.; Mihelcic, J. R. Sustainability of Wastewater Treatment Technologies. *Journal of Environmental Management* **2008**, *88* (3), 437–447. https://doi.org/10.1016/j.jenvman.2007.03.008.

Murchie, E. H.; Lawson, T. Chlorophyll Fluorescence Analysis: A Guide to Good Practice and Understanding Some New Applications. *J Exp Bot* **2013**, *64* (13), 3983–3998. https://doi.org/10.1093/jxb/ert208.

Najafpour, M. M.; Govindjee. Oxygen Evolving Complex in Photosystem II: Better than Excellent. *Dalton Transactions* **2011**, *40*, 9076. https://doi.org/10.1039/c1dt10746a.

Nancharaiah, Y. V.; Kiran Kumar Reddy, G. Aerobic Granular Sludge Technology: Mechanisms of Granulation and Biotechnological Applications. *Bioresource Technology* **2018**, *247*, 1128–1143. https://doi.org/10.1016/j.biortech.2017.09.131.

Neale, G.; Epstein, N.; Nader, W. Creeping Flow Relative to Permeable Spheres. *Chemical Engineering Science* **1973**, *28* (10), 1865–1874. https://doi.org/10.1016/0009-2509(73)85070-5.

Nejadnik, M. R.; Mei, H. C. van der; Busscher, H. J.; Norde, W. Determination of the Shear Force at the Balance between Bacterial Attachment and Detachment in Weak-

Adherence Systems, Using a Flow Displacement Chamber. *Appl. Environ. Microbiol.* **2008**, *74* (3), 916–919. https://doi.org/10.1128/AEM.01557-07.

Nemali, K. Light Quantity and Quality in Controlled Environment Agriculture. **2016**, 27.

Neyens, E.; Baeyens, J.; Dewil, R.; De heyder, B. Advanced Sludge Treatment Affects Extracellular Polymeric Substances to Improve Activated Sludge Dewatering. *Journal of Hazardous Materials* **2004**, *106* (2), 83–92. https://doi.org/10.1016/j.jhazmat.2003.11.014.

Niermans, R.; Giesen, A.; Loosdrecht, M. van; Buin, B. de. Full-Scale Experiences with Aerobic Granular Biomass Technology for Treatment of Urban and Industrial Wastewater. *proc water environ fed* **2014**, *2014* (19), 2347–2357. https://doi.org/10.2175/193864714815942512.

Nishiyama, Y.; Allakhverdiev, S. I.; Murata, N. A New Paradigm for the Action of Reactive Oxygen Species in the Photoinhibition of Photosystem II. *Biochimica et Biophysica Acta (BBA) - Bioenergetics* **2006**, *1757* (7), 742–749. https://doi.org/10.1016/j.bbabio.2006.05.013.

Niyogi, K. K.; Truong, T. B. Evolution of Flexible Non-Photochemical Quenching Mechanisms That Regulate Light Harvesting in Oxygenic Photosynthesis. *Current Opinion in Plant Biology* **2013**, *16* (3), 307–314. https://doi.org/10.1016/j.pbi.2013.03.011.

Noppeney, R. About the Nereda Wastewater Treatment Process https://www.royalhaskoningdhv.com/en-gb/nereda/nereda-wastewater-treatment%20technology (accessed Sep 19, 2018).

Oxborough, K.; Baker, N. R. Resolving Chlorophyll a Fluorescence Images of Photosynthetic Efficiency into Photochemical and Non-Photochemical Components – Calculation of QP and Fv-/Fm-; without Measuring Fo-; *Photosynthesis Research* **1997**, *54* (2), 135–142. https://doi.org/10.1023/A:1005936823310.

Oyserman, B. O.; Martirano, J. M.; Wipperfurth, S.; Owen, B. R.; Noguera, D. R.; McMahon, K. D. Community Assembly and Ecology of Activated Sludge under Photosynthetic Feast–Famine Conditions. *Environmental Science & Technology* **2017**, *51* (6), 3165–3175. https://doi.org/10.1021/acs.est.6b03976.

Pansook, S.; Incharoensakdi, A.; Phunpruch, S. Effects of the Photosystem II Inhibitors CCCP and DCMU on Hydrogen Production by the Unicellular Halotolerant Cyanobacterium Aphanothece halophytica https://www.hindawi.com/journals/tswj/2019/1030236/ (accessed Dec 19, 2019). https://doi.org/10.1155/2019/1030236.

Park, C.; Dolan, S. (deceased). Algal-Sludge Granule for Wastewater Treatment and Bioenergy Feedstock Generation. WO/2015/112654, July 31, 2015.

Park, C.; Dolan, S. (deceased). Patent Algal Sludge Granule OPG Jan 2019. US 10189732 B2, January 29, 2019.

Parkin, T. B.; Brock, T. D. The Effects of Light Quality on the Growth of Phototrophic Bacteria in Lakes. *Arch. Microbiol.* **1980**, *125* (1), 19–27. https://doi.org/10.1007/BF00403193.

Parkin, T. B.; Brock, T. D. Photosynthetic Bacterial Production in Lakes: The Effects of Light Intensity1: Photosynthetic Bacterial Production. *Limnology and Oceanography* **1980**, *25* (4), 711–718. https://doi.org/10.4319/lo.1980.25.4.0711.

Pastore, M.; Santaeufemia, S.; Bertucco, A.; Sforza, E. Light Intensity Affects the Mixotrophic Carbon Exploitation in Chlorella Protothecoides: Consequences on Microalgae-Bacteria Based Wastewater Treatment. *Water Sci Technol* **2018**, *78* (8), 1762–1771. https://doi.org/10.2166/wst.2018.462.

Pearsall, W. H.; Ullyott, P. Light Penetration into Fresh Water: I. a Thermionic Potentiometer for Measuring Light Intensity with Photo-Electric Cells. *Journal of Experimental Biology* **1933**, *10* (4), 293–305.

Philo, J.; Arakawa, T. Mechanisms of Protein Aggregation. *Current Pharmaceutical Biotechnology* **2009**, *10* (4), 348–351. https://doi.org/10.2174/138920109788488932.

Photoadaptation of Marine Phytoplankton in the Arctic. *Deep Sea Research Part A. Oceanographic Research Papers* **1982**, *29* (10), 1159–1170. https://doi.org/10.1016/0198-0149(82)90087-5.

Pocock, S. J. The Simplest Statistical Test: How to Check for a Difference between Treatments. *BMJ* **2006**, *332* (7552), 1256–1258.

Post, T. Understand the Real World of Mixing. **2010**.

Powles, S. B. Photoinhibition of Photosynthesis Induced by Visible Light. *Annual Review of Plant Physiology* **1984**, *35* (1), 15–44. https://doi.org/10.1146/annurev.pp.35.060184.000311.

Pronk, M.; de Kreuk, M. K.; de Bruin, B.; Kamminga, P.; Kleerebezem, R.; van Loosdrecht, M. C. M. Full Scale Performance of the Aerobic Granular Sludge Process for Sewage Treatment. *Water Research* **2015**, *84*, 207–217. https://doi.org/10.1016/j.watres.2015.07.011.

Qin, L.; Tay, J.-H.; Liu, Y. Selection Pressure Is a Driving Force of Aerobic Granulation in Sequencing Batch Reactors. *Process Biochemistry* **2004**, *39* (5), 579–584. https://doi.org/10.1016/S0032-9592(03)00125-0.

Quijano, G.; Arcila, J. S.; Buitrón, G. Microalgal-Bacterial Aggregates: Applications and Perspectives for Wastewater Treatment. *Biotechnol. Adv.* **2017**, *35* (6), 772–781. https://doi.org/10.1016/j.biotechadv.2017.07.003.

Ralph, P. J.; Gademann, R. Rapid Light Curves: A Powerful Tool to Assess Photosynthetic Activity. *Aquatic Botany* **2005**, *82* (3), 222–237. https://doi.org/10.1016/j.aquabot.2005.02.006.

Randall, C. W.; Barnard, J. L.; Stensel, H. D. *Design and Retrofit of Wastewater Treatment Plants for Biological Nutritient Removal*; CRC Press, 1998.

Ratkovich, N.; Horn, W.; Helmus, F. P.; Rosenberger, S.; Naessens, W.; Nopens, I.; Bentzen, T. R. Activated Sludge Rheology: A Critical Review on Data Collection and Modelling. *Water Research* **2013**, *47* (2), 463–482. https://doi.org/10.1016/j.watres.2012.11.021.

Richard, M.; Brown, S.; Collins, F., CO. Activated Sludge Microbiology Problems and Their Control; Buffalo, NY, 2003; p 21.

Rickard, A. H.; Gilbert, P.; High, N. J.; Kolenbrander, P. E.; Handley, P. S. Bacterial Coaggregation: An Integral Process in the Development of Multi-Species Biofilms. *Trends in Microbiology* **2003**, *11* (2), 94–100. https://doi.org/10.1016/S0966-842X(02)00034-3.

Ridley, S. M. Interaction of Chloroplasts with Inhibitors. *Plant Physiol* **1977**, *59* (4), 724–732.

Rittmann, B. E.; McCarty, P. L. *Environmental Biotechnology: Principles and Applications*; Tata McGraw Hill Education Private Limited, 2012.

S, P.; Sa, K.; A, P. Characteristics of Photosynthetic Active Radiation (PAR) Through Statistical Analysis at Larnaca, Cyprus. *SM J Biometrics Biostat* **2017**, *2* (2), 1–16. https://doi.org/10.36876/smjbb.1009.

Saer, R. G.; Blankenship, R. E. Light Harvesting in Phototrophic Bacteria: Structure and Function. *Biochemical Journal* **2017**, *474* (13), 2107–2131. https://doi.org/10.1042/BCJ20160753.

Sarma, S. J.; Tay, J. H. Aerobic Granulation for Future Wastewater Treatment Technology: Challenges Ahead. *Environ. Sci.: Water Res. Technol.* **2017**, *4* (1), 9–15. https://doi.org/10.1039/C7EW00148G.

Sarma, S. J.; Tay, J. H.; Chu, A. Finding Knowledge Gaps in Aerobic Granulation Technology. *Trends in Biotechnology* **2017**, *35* (1), 66–78. https://doi.org/10.1016/j.tibtech.2016.07.003.

Schmidt, I.; Sliekers, O.; Schmid, M.; Bock, E.; Fuerst, J.; Kuenen, J. G.; Jetten, M. S. M.; Strous, M. New Concepts of Microbial Treatment Processes for the Nitrogen Removal in Wastewater. *FEMS Microbiology Reviews* **2003**, *27* (4), 481–492. https://doi.org/10.1016/S0168-6445(03)00039-1.

Schubert, H.; Schiewer, U.; Tschirner, E. Fluorescence Characteristics of Cyanobacteria (Blue-Green Algae). *Journal of Plankton Research* **1989**, *11* (2), 353–359. https://doi.org/10.1093/plankt/11.2.353.

Schuurmans, R. M.; van Alphen, P.; Schuurmans, J. M.; Matthijs, H. C. P.; Hellingwerf, K. J. Comparison of the Photosynthetic Yield of Cyanobacteria and Green Algae: Different Methods Give Different Answers. *PLOS ONE* **2015**, *10* (9), e0139061. https://doi.org/10.1371/journal.pone.0139061.

Sears K.; Alleman J. E.; Barnard J. L.; Oleszkiewicz J. A. Density and Activity Characterization of Activated Sludge Flocs. *Journal of Environmental Engineering* **2006**, *132* (10), 1235–1242. https://doi.org/10.1061/(ASCE)0733-9372(2006)132:10(1235).

Selvadurai, A. P. S. On the Advective-Diffusive Transport in Porous Media in the Presence of Time-Dependent Velocities. *Geophysical Research Letters* **2004**, *31* (13). https://doi.org/10.1029/2004GL019646.

Sengar, A.; Basheer, F.; Aziz, A.; Farooqi, I. H. Aerobic Granulation Technology: Laboratory Studies to Full Scale Practices. *Journal of Cleaner Production* **2018**, *197*, 616–632. https://doi.org/10.1016/j.jclepro.2018.06.167.

Seviour, R.; Nielsen, P. H. *Microbial Ecology of Activated Sludge*; IWA Publishing, 2010.

Seynhaeve, L. Anaerobic Digestion of Algal-Sludge Granules. INRA-LBE, France 2014.

Sezgin, M. Variation of Sludge Volume Index with Activated Sludge Characteristics. *Water Research* **1982**, *16* (1), 83–88. https://doi.org/10.1016/0043-1354(82)90056-2.

Sheasley, W. D. Leading the Technology Development Process. *Research-Technology Management* **2016**.

Sheng, G.-P.; Yu, H.-Q.; Li, X.-Y. Extracellular Polymeric Substances (EPS) of Microbial Aggregates in Biological Wastewater Treatment Systems: A Review. *Biotechnology Advances* **2010**, *28* (6), 882–894. https://doi.org/10.1016/j.biotechadv.2010.08.001.

Singh, N. K.; Sonani, R. R.; Rastogi, R. P.; Madamwar, D. The Phycobilisomes: An Early Requisite for Efficient Photosynthesis in Cyanobacteria. *EXCLI J* **2015**, *14*, 268–289. https://doi.org/10.17179/excli2014-723.

Smith, H. Light Quality, Photoperception, and Plant Strategy. *Annual Review of Plant Physiology* **1982**, *33* (1), 481–518. https://doi.org/10.1146/annurev.pp.33.060182.002405.

Snyder, R.; Wyant, D. Training manual for wastewater treatment plant operators. 105.

Sobiechowska-Sasim, M.; Stoń-Egiert, J.; Kosakowska, A. Quantitative Analysis of Extracted Phycobilin Pigments in Cyanobacteria—an Assessment of Spectrophotometric and Spectrofluorometric Methods. *J Appl Phycol* **2014**, *26* (5), 2065–2074. https://doi.org/10.1007/s10811-014-0244-3.

Son, K.-H.; Lee, J.-H.; Oh, Y.; Kim, D.; Oh, M.-M.; In, B.-C. Growth and Bioactive Compound Synthesis in Cultivated Lettuce Subject to Light-Quality Changes. *HortScience* **2017**, *52* (4), 584–591. https://doi.org/10.21273/HORTSCI11592-16.

Spormann, A. M. Physiology of Microbes in Biofilms. In *Bacterial Biofilms*; Romeo, T., Ed.; Current Topics in Microbiology and Immunology; Springer Berlin Heidelberg: Berlin, Heidelberg, 2008; pp 17–36. https://doi.org/10.1007/978-3-540-75418-3_2.

Stauch-White, K.; Srinivasan, V. N.; Camilla Kuo-Dahab, W.; Park, C.; Butler, C. S. The Role of Inorganic Nitrogen in Successful Formation of Granular Biofilms for Wastewater Treatment That Support Cyanobacteria and Bacteria. *AMB Express* **2017**, *7*. https://doi.org/10.1186/s13568-017-0444-8.

Stolz, J. F. Structure of Microbial Mats and Biofilms. *Microbial Sediments* **2000**, 1–8. https://doi.org/10.1007/978-3-662-04036-2_1.

Subashchandrabose, S. R.; Ramakrishnan, B.; Megharaj, M.; Venkateswarlu, K.; Naidu, R. Mixotrophic Cyanobacteria and Microalgae as Distinctive Biological Agents for Organic Pollutant Degradation. *Environment International* **2013**, *51*, 59–72. https://doi.org/10.1016/j.envint.2012.10.007.

Chlorophyll a Fluorescence in Aquatic Sciences: Methods and Applications; Suggett, D. J., Prášil, O., Borowitzka, M. A., Eds.; Springer Netherlands: Dordrecht, 2010. https://doi.org/10.1007/978-90-481-9268-7.

Sutherland, D. L.; Howard-Williams, C.; Turnbull, M. H.; Broady, P. A.; Craggs, R. J. Seasonal Variation in Light Utilisation, Biomass Production and Nutrient Removal by Wastewater Microalgae in a Full-Scale High-Rate Algal Pond. *J Appl Phycol* **2014**, *26* (3), 1317–1329. https://doi.org/10.1007/s10811-013-0142-0.

Szilárd, A.; Sass, L.; Deák, Z.; Vass, I. The Sensitivity of Photosystem II to Damage by UV-B Radiation Depends on the Oxidation State of the Water-Splitting Complex. *Biochimica et Biophysica Acta (BBA) - Bioenergetics* **2007**, *1767* (6), 876–882. https://doi.org/10.1016/j.bbabio.2006.11.020.

Szoradi, C. LED Grow Lights Reshape Agriculture | LED Journal, 2016.

Takahashi, S.; Badger, M. R. Photoprotection in Plants: A New Light on Photosystem II Damage. *Trends in Plant Science* **2011**, *16* (1), 53–60. https://doi.org/10.1016/j.tplants.2010.10.001.

Takeuchi, N.; Kohshima, S.; Seko, K. Structure, Formation, and Darkening Process of Albedo-Reducing Material (Cryoconite) on a Himalayan Glacier: A Granular Algal Mat Growing on the Glacier. *Arctic, Antarctic, and Alpine Research* **2001**, *33* (2), 115–122. https://doi.org/10.1080/15230430.2001.12003413.

Tang, K.-H.; Tang, Y. J.; Blankenship, R. E. Carbon Metabolic Pathways in Phototrophic Bacteria and Their Broader Evolutionary Implications. *Front. Microbiol.* **2011**, *2*. https://doi.org/10.3389/fmicb.2011.00165.

Tay, J.-H.; Liu, Q.-S.; Liu, Y. The Effects of Shear Force on the Formation, Structure and Metabolism of Aerobic Granules. *Appl Microbiol Biotechnol* **2001**, *57* (1), 227–233. https://doi.org/10.1007/s002530100766.

Tay, J.-H.; Yang, S.-F.; Liu, Y. Hydraulic Selection Pressure-Induced Nitrifying Granulation in Sequencing Batch Reactors. *Appl. Microbiol. Biotechnol.* **2002**, *59* (2–3), 332–337. https://doi.org/10.1007/s00253-002-0996-6.

Thapa, S.; Bharti, A.; Prasanna, R. Algal Biofilms and Their Biotechnological Significance. In *Algal Green Chemistry*; Elsevier, 2017; pp 285–303. https://doi.org/10.1016/B978-0-444-63784-0.00014-X.

Thompson, M.; Gamage, D.; Hirotsu, N.; Martin, A.; Seneweera, S. Effects of Elevated Carbon Dioxide on Photosynthesis and Carbon Partitioning: A Perspective on Root Sugar Sensing and Hormonal Crosstalk. *Front Physiol* **2017**, *8*. https://doi.org/10.3389/fphys.2017.00578.

Tiron, O.; Bumbac, C.; Patroescu, I. V.; Badescu, V. R.; Postolache, C. Granular Activated Algae for Wastewater Treatment. *Water Sci. Technol.* **2015**, *71* (6), 832–839. https://doi.org/10.2166/wst.2015.010.

Tixier, N.; Guibaud, G.; Baudu, M. Determination of Some Rheological Parameters for the Characterization of Activated Sludge. *Bioresource Technology* **2003**, *90* (2), 215–220. https://doi.org/10.1016/S0960-8524(03)00109-3.

Trebuch, L. M.; Oyserman, B. O.; Janssen, M.; Wijffels, R. H.; Vet, L. E. M.; Fernandes, T. V. Impact of Hydraulic Retention Time on Community Assembly and Function of Photogranules for Wastewater Treatment. *Water Research* **2020**, *173*, 115506. https://doi.org/10.1016/j.watres.2020.115506.

Tyystjarvi, E. Photoinhibition of Photosystem II and Photodamage of the Oxygen Evolving Manganese Cluster. *Coordination Chemistry Reviews* **2008**, *252* (3–4), 361–376. https://doi.org/10.1016/j.ccr.2007.08.021.

Uetake, J.; Tanaka, S.; Segawa, T.; Takeuchi, N.; Nagatsuka, N.; Motoyama, H.; Aoki, T. Microbial Community Variation in Cryoconite Granules on Qaanaaq Glacier, NW Greenland. *FEMS Microbiol Ecol* **2016**, *92* (9). https://doi.org/10.1093/femsec/fiw127.

Urrestarazu, M.; Nájera, C.; Gea, M. del M. Effect of the Spectral Quality and Intensity of Light-Emitting Diodes on Several Horticultural Crops. *HortScience* **2016**, *51* (3), 268–271.

Valigore, J. M.; Gostomski, P. A.; Wareham, D. G.; O'Sullivan, A. D. Effects of Hydraulic and Solids Retention Times on Productivity and Settleability of Microbial (Microalgal-Bacterial) Biomass Grown on Primary Treated Wastewater as a Biofuel Feedstock. *Water Research* **2012**, *46* (9), 2957–2964. https://doi.org/10.1016/j.watres.2012.03.023.

Van Den Hende, S.; Carré, E.; Cocaud, E.; Beelen, V.; Boon, N.; Vervaeren, H. Treatment of Industrial Wastewaters by Microalgal Bacterial Flocs in Sequencing Batch Reactors. *Bioresource Technology* **2014**, *161*, 245–254. https://doi.org/10.1016/j.biortech.2014.03.057.

van der Lans, R.; Riet, K. Mixing in Bioreactor Vessels. In *Comprehensive Biotechnology*; 2011; pp 63–80. https://doi.org/10.1016/B978-0-08-088504-9.00083-0.

Verbyla, von S. Waste Stabilization Ponds http://www.waterpathogens.org/book/waste-stabilization-ponds (accessed Aug 7, 2018).

Wan, N.; Abernathy, M.; Tang, J. K.-H.; Tang, Y. J.; You, L. Cyanobacterial Photo-Driven Mixotrophic Metabolism and Its Advantages for Biosynthesis. *Front. Chem. Sci. Eng.* **2015**, *9* (3), 308–316. https://doi.org/10.1007/s11705-015-1521-7.

Wang, C.; Lan, C. Q. Effects of Shear Stress on Microalgae - A Review. *Biotechnol. Adv.* **2018**, *36* (4), 986–1002. https://doi.org/10.1016/j.biotechadv.2018.03.001.

Ware, M. A.; Dall'Osto, L.; Ruban, A. V. An In Vivo Quantitative Comparison of Photoprotection in Arabidopsis Xanthophyll Mutants. *Frontiers in Plant Science* **2016**, *7*. https://doi.org/10.3389/fpls.2016.00841.

Wezernak, C. T.; Gannon, J. J. Oxygen-Nitrogen Relationships in Autotrophic Nitrification. **1967**, *15*, 5.

Wilén, B. Effect of Different Parameters on Settling Properties of Activated Sludge. 64.

Wilén, B.-M.; Liébana, R.; Persson, F.; Modin, O.; Hermansson, M. The Mechanisms of Granulation of Activated Sludge in Wastewater Treatment, Its Optimization, and Impact on Effluent Quality. *Appl Microbiol Biotechnol* **2018**, *102* (12), 5005–5020. https://doi.org/10.1007/s00253-018-8990-9.

Winkler, M.-K. H.; Kleerebezem, R.; Strous, M.; Chandran, K.; van Loosdrecht, M. C. M. Factors Influencing the Density of Aerobic Granular Sludge. *Applied Microbiology and Biotechnology* **2013**, *97* (16), 7459–7468. https://doi.org/10.1007/s00253-012-4459-4.

Wood-Black, F. Considerations for Scale-Up – Moving from the Bench to the Pilot Plant to Full Production. In *Academia and Industrial Pilot Plant Operations and Safety*; ACS Symposium Series; American Chemical Society, 2014; Vol. 1163, pp 37–45. https://doi.org/10.1021/bk-2014-1163.ch003.

Wu, H.; Zou, D.; Gao, K. Impacts of Increased Atmospheric CO2 Concentration on Photosynthesis and Growth of Micro- and Macro-Algae. *SCI CHINA SER C* **2008**, *51* (12), 1144–1150. https://doi.org/10.1007/s11427-008-0142-5.

Wu, H. Effect of Different Light Qualities on Growth, Pigment Content, Chlorophyll Fluorescence, and Antioxidant Enzyme Activity in the Red Alga Pyropia Haitanensis (Bangiales, Rhodophyta). *Biomed Res Int* **2016**, *2016*. https://doi.org/10.1155/2016/7383918.

Xia, J.; Ye, L.; Ren, H.; Zhang, X.-X. Microbial Community Structure and Function in Aerobic Granular Sludge. *Appl Microbiol Biotechnol* **2018**, *102* (9), 3967–3979. https://doi.org/10.1007/s00253-018-8905-9.

Xiao, F.; Li, X. Y.; Wang, D. S. Three-Dimensional CFD Simulation of the Flow Field around and through Particle Aggregates. *Colloids and Surfaces A: Physicochemical and Engineering Aspects* **2013**, *436*, 1034–1040. https://doi.org/10.1016/j.colsurfa.2013.08.046.

Xu, C.; Sullivan, J. H. Reviewing the Technical Designs for Experiments with Ultraviolet-B Radiation and Impact on Photosynthesis, DNA and Secondary Metabolism. *Journal of Integrative Plant Biology* **2010**, *52* (4), 377–387. https://doi.org/10.1111/j.1744-7909.2010.00939.x.

Xu, H.; Bodenschatz, E. Motion of Inertial Particles with Size Larger than Kolmogorov Scale in Turbulent Flows. *Physica D: Nonlinear Phenomena* **2008**, *237* (14), 2095–2100. https://doi.org/10.1016/j.physd.2008.04.022.

Yen, H.-W.; Hu, I.-C.; Chen, C.-Y.; Chang, J.-S. Design of Photobioreactors for Algal Cultivation. In *Biofuels from Algae*; Elsevier, 2014; pp 23–45. https://doi.org/10.1016/B978-0-444-59558-4.00002-4.

Yeoh, G. H.; Tu, J. Gas–Particle Flows. In *Computational Techniques for Multiphase Flows*; Elsevier, 2010; pp 243–311. https://doi.org/10.1016/B978-0-08-046733-7.00004-7.

Yeoh, G. H.; Tu, J. Liquid–Particle Flows. In *Computational Techniques for Multiphase Flows*; Elsevier, 2010; pp 313–349. https://doi.org/10.1016/B978-0-08-046733-7.00005-9.

Young, A. J. Occurrence and Distribution of Carotenoids in Photosynthetic Systems. In *Carotenoids in Photosynthesis*; Young, A. J., Britton, G., Eds.; Springer Netherlands: Dordrecht, 1993; pp 16–71. https://doi.org/10.1007/978-94-011-2124-8_2.

Yu, W.; Gregory, J.; Campos, L.; Li, G. The Role of Mixing Conditions on Floc Growth, Breakage and Re-Growth. *Chemical Engineering Journal* **2011**, *171* (2), 425–430. https://doi.org/10.1016/j.cej.2011.03.098.

Yuanyuan, Z.; Xuehong, Z.; Wenjie, Z. Research Advances in Anammox Granular Sludge. In *Proceedings of the AASRI International Conference on Industrial Electronics and Applications (2015)*; Atlantis Press: London, UK, 2015. https://doi.org/10.2991/iea-15.2015.113.

Zapata, M.; Garrido, J. L.; Jeffrey, S. W. Chlorophyll c Pigments: Current Status. In *Chlorophylls and Bacteriochlorophylls: Biochemistry, Biophysics, Functions and Applications*; Grimm, B., Porra, R. J., Rüdiger, W., Scheer, H., Eds.; Advances in Photosynthesis and Respiration; Springer Netherlands: Dordrecht, 2006; pp 39–53. https://doi.org/10.1007/1-4020-4516-6_3.

Zavřel, T.; Chmelík, D.; Sinetova, M. A.; Červený, J. Spectrophotometric Determination of Phycobiliprotein Content in Cyanobacterium Synechocystis. *Journal of Visualized Experiments* **2018**, No. 139. https://doi.org/10.3791/58076.

Zhang, B.; Guo, Y.; Lens, P. N. L.; Zhang, Z.; Shi, W.; Cui, F.; Tay, J. H. Effect of Light Intensity on the Characteristics of Algal-Bacterial Granular Sludge and the Role of N-Acyl-Homoserine Lactone in the Granulation. *Science of The Total Environment* **2018**. https://doi.org/10.1016/j.scitotenv.2018.12.250.

Zhang, B.; Lens, P. N. L.; Shi, W.; Zhang, R.; Zhang, Z.; Guo, Y.; Bao, X.; Cui, F. Enhancement of Aerobic Granulation and Nutrient Removal by an Algal–Bacterial Consortium in a Lab-Scale Photobioreactor. *Chemical Engineering Journal* **2018**, *334*, 2373–2382. https://doi.org/10.1016/j.cej.2017.11.151.

Zhang, C.; Sun, S.; Liu, X.; Wan, C.; Lee, D.-J. Influence of Operational Conditions on the Stability of Aerobic Granules from the Perspective of Quorum Sensing. *Environ Sci Pollut Res* **2017**, *24* (8), 7640–7649. https://doi.org/10.1007/s11356-017-8417-7.

Zhang, Q.; Hu, J.; Lee, D.-J. Aerobic Granular Processes: Current Research Trends. *Bioresource Technology* **2016**, *210*, 74–80. https://doi.org/10.1016/j.biortech.2016.01.098.

Zhao, Z.; Yang, X.; Cai, W.; Lei, Z.; Shimizu, K.; Zhang, Z.; Utsumi, M.; Lee, D.-J. Response of Algal-Bacterial Granular System to Low Carbon Wastewater: Focus on Granular Stability, Nutrients Removal and Accumulation. *Bioresource Technology* **2018**, *268*, 221–229. https://doi.org/10.1016/j.biortech.2018.07.114.

Zheng, Y.-M.; Yu, H.-Q.; Sheng, G.-P. Physical and Chemical Characteristics of Granular Activated Sludge from a Sequencing Batch Airlift Reactor. *Process Biochemistry* **2005**, *40* (2), 645–650. https://doi.org/10.1016/j.procbio.2004.01.056.

Zhou, D.; Niu, S.; Xiong, Y.; Yang, Y.; Dong, S. Microbial Selection Pressure Is Not a Prerequisite for Granulation: Dynamic Granulation and Microbial Community Study in a Complete Mixing Bioreactor. *Bioresource Technology* **2014**, *161*, 102–108. https://doi.org/10.1016/j.biortech.2014.03.001.

Zhu, L.; Zhou, J.; Yu, H.; Xu, X. Optimization of Hydraulic Shear Parameters and Reactor Configuration in the Aerobic Granular Sludge Process. *Environmental Technology* **2015**, *36* (13), 1605–1611. https://doi.org/10.1080/09593330.2014.998717.

Hamzeh Ramadan, Waste Stabilization Ponds http://stabilizationponds.sdsu.edu/ (accessed Aug 8, 2018).

Managing Energy Costs in Wastewater Treatment Plants - Madison Gas and Electric - Madison, Wisconsin https://www.mge.com/saving-energy/business/bea/article_detail.htm?nid=%202431 (accessed Oct 4, 2018).

Sanitation https://www.who.int/news-room/fact-sheets/detail/sanitation (accessed Nov 26, 2019).

Solid-Liquid Mixing In Agitated Vessels (Just Suspended Speed) https://www.cheresources.com/invision/blog/4/entry-511-solid-liquid-mixing-in-agitated-vessels-just-suspended-speed/ (accessed Jun 7, 2019).

The influence of particles on suspension rheology :: Anton Paar Wiki https://wiki.anton-paar.com/en/the-influence-of-particles-on-suspension-rheology/ (accessed May 26, 2019).

The Reuse Opportunity https://iwa-network.org/publications/the-reuse-opportunity/ (accessed Nov 26, 2019).

Biological Wastewater Treatment: Principles, Modelling and Design; Henze, M., Ed.; IWA Pub: London, 2008.